The Dissertation Committee for Andrea Robin Holthouse Putz Certifies that this is the approved version of the following dissertation:

Biological Activated Carbon: The Relative Role of Metabolism and Cometabolism in Extending Service Life and Improving Process Performance

Committee:

Gerald E. Speitel Jr., Supervisor

Lynn E. Katz

Desmond F. Lawler

Kerry A. Kinney

George Georgiou

Biological Activated Carbon: The Relative Role of Metabolism and Cometabolism in Extending Service Life and Improving Process Performance

by

Andrea Robin Holthouse Putz, B.S., M.S.

Dissertation

Presented to the Faculty of the Graduate School of

The University of Texas at Austin

in Partial Fulfillment

of the Requirements

for the Degree of

Doctor of Philosophy

The University of Texas at Austin

May, 2004

Dedication

To my husband, Karl, who has always encouraged me.

To my mother, who inspired my love of science and my interest in the environment.

To the memory of my father, for always telling me I could do anything boys could do.

Acknowledgements

I would like to thank my advisor Dr. Gerald E. Speitel Jr. for his mentoring, patience, and encouragement for these past six years. Working with him has taught me so much. I will forever be grateful. I would also like to thank Dr. Lynn Katz for her expertise in dealing with my new arch nemesis, ferric hydroxide. In addition, I would like to thank the rest of my committee members, Dr. Desmond Lawler, Dr. Kerry Kinney, and Dr. George Georgiou for helping to guide me in my research. I also thank Dr. Hillary Hart for helping me wade through the mire that is my writing style. I am grateful to the United States Environmental Protection Agency for providing funding with an EPA STAR Fellowship.

Many people in the lab, past and present, have provided companionship as well as assistance with research problems: Dr. Jonathan Pressman, Dr. Matt Morley, Derek Losh, Dr. Dustin Poppendieck, Dave Wahman, Dr. Caroline Gerwe, Greg Pope, and Jennifer Warren. In addition, Charlie Perego was always around to help in an equipment emergency, and it seemed there was one at least once a week. I would also like to thank Dr. Aiza José Sánchez and Josefina Rodgriguez for all our wonderful conversations both in english and in spanish.

Of course, these past six years would have been much more difficult without the love and support of my family.

Biological Activated Carbon: The Relative Role of Metabolism and Cometabolism in Extending Service Life and Improving Process Performance

Publication No._____

Andrea Robin Holthouse Putz, Ph.D.

The University of Texas at Austin, 2004

Supervisor: Gerald E. Speitel Jr.

Granular activated carbon (GAC) is commonly used to remove synthetic organic chemicals (SOCs) from contaminated water. Replacement and subsequent disposal of spent GAC is expensive. By increasing the service life of the GAC, costs can be decreased. Encouragement of biodegradation (metabolism and cometabolism) where one or more of the SOCs are biodegradable can lengthen the GAC service life for some SOC mixtures. The service life increases because a biofilm that forms on the GAC can biodegrade SOCs, thereby reducing competition for GAC adsorption sites and allowing any remaining SOCs to adsorb onto the GAC to a greater extent than in the absence of biodegradation. SOCs in both the aqueous phase and adsorbed on the GAC are available to the microorganisms. Biodegradation of adsorbed SOCs (termed bioregeneration)

renews the GAC's capacity for SOC adsorption, while aqueous phase biodegradation slows the rate of GAC exhaustion, thereby lengthening the GAC service life and decreasing operation and maintenance costs. Adsorption isotherms and biological kinetic studies were performed to describe GAC column performance. Continuous-flow GAC bioregeneration experiments (pre-equilibrated and virgin) were conducted using a mixture of biodegradable (toluene) and either nonbiodegradable (perchloroethylene, PCE) or traditionally nonbiodegradable (trichloroethylene, TCE) SOCs. In the pre-equilibrated experiments, the GAC was saturated with respect to toluene and PCE or TCE to observe the biggest effect on bioregeneration performance. If no dissolved oxygen limitations occurred, the biodegradable SOC effluent concentration decreased over time and remained low, after which the nonbiodegradable or traditionally nonbiodegradable SOC effluent concentration also decreased because of the increased availability of adsorption sites on the GAC as well as the cometabolism of TCE, if present, by enzymes produced via toluene metabolism. Virgin column experiments were also run and allowed for direct measurement of the service life increase due to biodegradation. Toluene-and TCE-based bioregeneration ranged from 26 - 53% and 2.2 - 7.4%, respectively, of the initial loading after 11 to 20 days. Pre and post-experimental GAC loadings showed a decrease in the biodegradable SOC loading as well as an increase in the nonbiodegradable SOC loading. Greater degrees of bioregeneration were found for higher SOC concentrations and longer EBCTs.

Table of Contents

List of Tables xii

List of Figures xvii

Chapter 1: Introduction and Objectives 1

1.1 Problem Description 1

1.2 Objectives 3

Chapter 2: Literature Review 7

2.1 Chemical Selection 7

2.2 Chemical Properties, Usage, and Regulation 8

2.3 Adsorption Equilibrium 13

2.4 GAC Adsorption Kinetics 17

2.5 Microbial Kinetics 21

2.5.1 Toluene and TCE Biodegradation 21

2.5.2 Factors Affecting the Rate of Cometabolism 28

2.5.3 Enzyme Activity 31

2.6 Bioreactors 33

2.7 Biological Activated Carbon 36

2.8 Fenton's Oxidation 42

2.9 BAC Column Modeling 47

2.10 Cometabolism Modeling 52

2.11 Summary 56

Chapter 3: Materials and Methods 57

3.1 Experimental Procedures 57

3.1.1 Activated Carbon Adsorption and Desorption 57

3.1.2 Biodegradation Kinetic Parameters Methodology 58

3.1.3 Exhausted and Virgin GAC Column Methodology 62

3.1.4 GAC Extraction and Cell Detachment Procedures....70
3.2 Materials....73
3.3 Chemical and Biological Analyses....74
3.3.1 Gas Chromatograph Analyses....74
3.3.2 Radiochemical Analysis....77
3.3.3 Iron and H_2O_2 Measurement....79
3.3.4 Biological Analyses....82
Chapter 4: Background Results....87
4.1 PAC Adsorption Isotherms....87
4.2 GAC Column Kinetics....93
4.3 Batch Biodegradation Kinetics....100
4.3.1 Enzyme Competition....100
4.3.2 Effect of Iron on Biodegradation....102
4.3.3 Toluene Metabolism Kinetic Parameters....104
4.3.4 TCE Cometabolism Kinetic Parameters....111
4.3.5 Biological Activity Baseline....116
4.3.6 Enzyme Location....119
4.4 Summary....120
Chapter 5: Bioregeneration Column Results....121
5.1 Metabolism-Only Exhausted Column Experiments....121
5.1.1 SOC Concentrations and Loadings....121
5.1.2 Bioregeneration Calculations....130
5.2 Combined Metabolism-Cometabolism Exhausted Column Experiments....134
5.2.1 Effect of Equilibrium Exchange on Bioregeneration....134
5.2.2 Effect of Fenton's Oxidation on Bioregeneration....138
5.2.3 Effect of EBCT and Enzyme Activity on TCE-based Bioregeneration....145
5.2.4 Simultaneous Toluene- and TCE-based Bioregeneration....151

5.2.5 Effect of Toluene to TCE Ratio on Bioregeneration 155
5.3 Combined Metabolism-Cometabolism Virgin Column Experiments .. 162
5.3.1 Metabolism and Cometabolism without Adsorption 163
5.3.2 Adsorption without Metabolism or Cometabolism 166
5.3.3 Effect of Biological Activity on Service Life 169
5.3.4 Effect of Biological Activity on SOC Loading and Bioregeneration 171
5.3.5 Effect of Fenton's Oxidation on Bioregeneration 178
5.4 Summary 183
Chapter 6: Mathematical Modeling Results 186
6.1 Metabolism-Only Exhausted Column Experiment 186
6.2 Metabolism-Cometabolism Exhausted Column Experiment 191
6.3 Metabolism-Cometabolism Virgin Column Experiments 200
6.4 Full-Scale Model Predictions 211
6.4.1 Effect of EBCT on Column Performance 213
6.4.2 Effect of SOC Adsorbability and Concentration on Column Performance 216
6.4.3 Effect of Bacterial Seeding and Culture Kinetics on Column Performance 221
6.5 Summary 224
Chapter 7: Conclusions and Recommendations 227
7.1 Conclusions 227
7.2 Future Recommendations 234
Appendix A – Bioregeneration Analysis Method 237
Appendix B – Additional Analytical Methods 241
Appendix C - Raw Batch Kinetic Data 260
Appendix D – Raw Column Experiment Data 266
D.1 Effluent SOC and DO Concentrations 266

D.2 Bioregeneration Rate and Extent 275
D.3 GAC Loadings 283
D.4 Biological Measurements at End of Experiment 287
Glossary 290
References 291
Vita… 304

List of Tables

Table 2.1 Chemical Properties of BTEX Compounds and Chlorinated Solvents 9

Table 2.2 National Primary Drinking Water Standards for BTEX Compounds and Selected Chlorinated Solvents (Pontius, 1998) 12

Table 2.3 Freundlich Parameters for Toluene and TCE on F400 (Speth and Miltner, 1990) 15

Table 2.4 Characteristics of Reviewed Cometabolism Models 53

Table 3.1 Nutrient Concentrations for Batch Microbial Growth 59

Table 3.2 Nutrient Concentrations for Column Studies 63

Table 4.1 Summary of Adsorption Parameters from Single Component Studies 88

Table 4.2 Calculated PSDM Kinetic Coefficients for Adsorption and Desorption 97

Table 4.3 Monod Kinetic Parameters for Toluene 111

Table 4.4 Kinetic Parameters for TCE Cometabolism 114

Table 5.1 Summary of Toluene-PCE Bioregeneration Experimental Conditions 123

Table 5.2 Summary of Toluene-PCE Bioregeneration Experiment Results 131

Table 5.3 Summary of Toluene-TCE Exhausted Bioregeneration Experimental Conditions 134

Table 5.4 Summary of Toluene-TCE Exhausted Bioregeneration Experiment Results 162
Table 5.5 Summary of Toluene-TCE Virgin Bioregeneration Experimental Conditions 163
Table 5.6 Summary of Toluene-TCE Virgin Bioregeneration Experiment Results 182
Table 5.7 Summary of Bioregeneration Experiment Conditions and Results 185
Table 6.1 MDBA Model Inputs for Exp. 1, 6.9-min. EBCT, Iron Free 187
Table 6.2 MDBA Model Inputs for Exp. 3, 10.3-min. EBCT, Column A 192
Table 6.3 MDBA Model Inputs for Exp. 7, 1.1-min. EBCT, Iron Free 201
Table 6.4 MDBA Model Inputs for Virgin BAC Column, 1.0-min. EBCT 212
Table 6.5 Column Dimensions for Virgin BAC Column Modeling 212
Table B.1 Sequential Methanol Extraction Data, Toluene and PCE 241
Table B.2 Sequential Methanol Extraction Data, Toluene and TCE 243
Table B.3 Extraction Correction Factor Summary 244
Table B.4 Headspace Analyzer User Program 244
Table B.5 GC Peak Times 245
Table B.6 Standard Curve Preparation 245
Table B.7 GC-FID Standard Curve Example, Toluene and PCE 246
Table B.8 GC-FID Standard Curve Example, Toluene and TCE 247
Table B.9 GC-ECD Standard Curve Example, PCE 249
Table B.10 GC-ECD Standard Curve Example, TCE 250
Table B.11 Liquid Scintillation Counter User Program 251

Table B.12 ^{14}C-Toluene Radioactive Background Tests, Toluene/PCE Experiments 253
Table B.13 ^{14}C-Toluene Radioactive Background Tests, Toluene/TCE Experiments 254
Table B.14 ^{14}C-TCE Radioactive Background Tests 254
Table B.15 Phenanthroline Iron Standard Data Example 255
Table B.16 OD_{600}/TSS/VSS Standard Data 255
Table B.17 Protein Standard Data Example 256
Table B.18 NADH Standard Data Example 257
Table B.19 Enzyme Activity Analysis Example 258
Table B.20 Enzyme Activity Slope Example 259
Table C.1 Data for Toluene Monod Kinetic Parameter Determination with and without Iron Present 260
Table C.2 Data for TCE Monod Kinetic Parameter Determ. with & without Iron 261
Table C.3 Data for Toluene Endogenous Decay Coefficients Determination 262
Table C.4 Data for TCE Transformation Capacity Determination 263
Table C.5 Data for Culture Baseline Determination 264
Table C.6 Data for Toluene Dioxygenase Enzyme Location Determination 265
Table D.1 Effluent SOC and DO Concentrations, Experiment 1 266
Table D.2 Effluent SOC and DO Concentrations, Experiment 2 267
Table D.3 Effluent SOC and DO Concentrations, ^{14}C-TCE Pre-Equilibrated Sterile Column 268

Table D.4 Effluent SOC and DO Concentrations, Experiment 3 269
Table D.5 Effluent SOC and DO Concentrations, Experiment 4 269
Table D.6 Effluent SOC and DO Concentrations, Experiment 5 270
Table D.7 Effluent SOC and DO Concentrations, Experiment 6 270
Table D.8 Effluent SOC and DO Concentrations, Anthracite Control Experiment 271
Table D.9 Effluent SOC and DO Concentrations, Virgin Sterile Column 272
Table D.10 Effluent SOC and DO Concentrations, Experiment 7 273
Table D.11 Effluent SOC and DO Concentrations, Experiment 8 274
Table D.12 Bioregeneration Rate and Extent, Experiment 2 275
Table D.13 Bioregeneration Rate and Extent, ^{14}C-TCE Pre-Equilibrated Sterile Column 276
Table D.14 Bioregeneration Rate and Extent, Experiment 3 277
Table D.15 Bioregeneration Rate and Extent, Experiment 4 278
Table D.16 Bioregeneration Rate and Extent, Experiment 5 279
Table D.17 Bioregeneration Rate and Extent, Experiment 6 280
Table D.18 Bioregeneration Rate and Extent, Experiment 7 281
Table D.19 Bioregeneration Rate and Extent, Experiment 8 282
Table D.20 GAC Loadings, Experiment 1 283
Table D.21 GAC Loadings, Experiment 2 283
Table D.22 GAC Loadings, ^{14}C-TCE Pre-Equilibrated Sterile Column 283
Table D.23 GAC Loadings, Experiment 3 284
Table D.24 GAC Loadings, Experiment 4 284

Table D.25 GAC Loadings, Experiment 5 284
Table D.26 GAC Loadings, Experiment 6 285
Table D.27 GAC Loadings, Anthracite Control Experiment 285
Table D.28 GAC Loadings, Virgin Sterile Control 285
Table D.29 GAC Loadings, Experiment 7 285
Table D.30 GAC Loadings, Experiment 8 286
Table D.31 Biological Measurements, Experiment 3 287
Table D.32 Biological Measurements, Experiment 4 287
Table D.33 Biological Measurements, Experiment 5 287
Table D.34 Biological Measurements, Experiment 6 288
Table D.35 Biological Measurements, Anthracite Control Experiment 288
Table D.36 Biological Measurements, Experiment 7 288
Table D.37 Biological Measurements, Experiment 8 289

List of Figures

Figure 2.1 The Chromatographic Effect for Toluene & TCE (C = Concentration) 19

Figure 2.2 Structure of an Activated Carbon Particle (Crittenden *et al*., 1987) 20

Figure 2.3 Toluene Degradation Pathways for *Pseudomonas* and Related Species (1) *P. putida* mt-2, (2) *P. mendocina* KR1 (Wackett, 2000) 23

Figure 2.4 Toluene Degradation Pathways for *Pseudomonas* and Related species (3) *B. cepacia* G4, (4) *P. picketti* PKO1, (5*) P. putida* F1 (Wackett, 2000) 24

Figure 2.5 Toluene Degradation Pathways for *Rhodococcus rhodochrous* (Vanderberg *et al*., 2000) 25

Figure 2.6 TCE Degradation Pathways using (1) toluene 2-monooxygenase and (2) toluene dioxygenase (Oh *et al*., 2001) 27

Figure 2.7 The Oxidation of Indole to Indigo (Jenkins and Dalton, 1985) 33

Figure 2.8 Diffusion of Substrate Into a Microorganism-Covered GAC Particle (Zhu, 1987) 49

Figure 3.1 Experimental Column Setup 65

Figure 4.1 Individual Adsorption Isotherms for Toluene, C_o = 58 (1) and 62 (2) mg/L 89

Figure 4.2 Individual Adsorption Isotherms for TCE, C_o = 85 (1) and 79 (2) mg/L 89

Figure 4.3 Individual Adsorption Isotherm for PCE, C_o = 26 mg/L 90
Figure 4.4 Toluene and TCE Competitive Isotherm 1, Toluene C_o = 61 mg/L, TCE C_o = 48 mg/L, P = 1 for both.....91
Figure 4.5 Toluene and TCE Competitive Isotherm 2, Toluene C_o = 62 mg/L, TCE C_o = 74 mg/L, P = 1 for both.....91
Figure 4.6 Toluene and PCE Competitive Isotherm, Toluene C_o = 15 mg/L, PCE C_o = 26 mg/L.....92
Figure 4.7 Measured and PSDM-Fitted Toluene and TCE Adsorption, Toluene C_o = 1570 µg/L, TCE C_o = 87 µg/L, 0.9-min. EBCT.....96
Figure 4.8 Measured and PSDM-Predicted Toluene and TCE Desorption, Toluene Equilibrium Conc. = 474 µg/L, TCE Equilibrium Conc. = 858 µg/L, 0.08-min. EBCT 99
Figure 4.9 Simultaneous Toluene and TCE Batch Degradation, X_o = 36 mg/L .101
Figure 4.10 TCE Batch Cometabolism in the Presence of Increasing Initial Toluene Concentrations, X_o = 19 - 26 mg/L.....102
Figure 4.11 Toluene and TCE Batch Degradation With and Without Iron, X_o = 80 – 93 mg/L 103
Figure 4.12 ^{14}C-Radiochemical Toluene Batch Metabolism With Iron, X_o = 40 mg/L.....105
Figure 4.13 Determination of Biomass Carbon Fraction Converted to CO_2 (K_c) With and Without Iron.....105
Figure 4.14 Determination of Endogenous Decay Coefficient (b) With and Without Iron.....106

Figure 4.15 Example Runge-Kutta Monod Fits of Toluene Batch Degradation Data, X_o = 28 (iron) and 12 (no iron) mg/L.....108
Figure 4.16 95% Joint Confidence Interval for Toluene Metabolism Without Iron.....109
Figure 4.17 95% Joint Confidence Interval for Toluene Metabolism With Iron 110
Figure 4.18 ^{14}C-Radiochemical TCE Batch Cometabolism With Iron, Xo = 105 mg/L.....113
Figure 4.19 Example Pseudo First Order Equation Fits of TCE Batch Degradation Data, X_o = 249 (iron) and 29 (no iron) mg/L.....116
Figure 4.20 Baseline TSS and Protein Levels During Growth.....117
Figure 4.21 Baseline Enzyme Activity and NADH Levels During Growth 119
Figure 5.1 Effluent Toluene and PCE Concentrations, Exp. 1, 6.9-min. EBCT, No Iron, Avg. C_o = 610 (toluene) and 845 (PCE) µg/L.....123
Figure 5.2 Effluent Toluene and PCE Concentrations and D.O., Exp. 1, 11-min. EBCT, No Iron, Avg. C_o = 610 (toluene) and 845 (PCE) µg/L 125
Figure 5.3 Final SOC Loading on GAC Column, Exp. 1, No Iron, Avg. C_o = 610 (toluene) and 845 (PCE) µg/L 126
Figure 5.4 Effluent Concentrations and Toluene Bioregeneration Rate, Exp. 2, 2.5-min. EBCT, No Iron, Avg. C_o = 1000 (toluene) and 501 (PCE) µg/L 128

Figure 5.5 Effluent Concentrations and Toluene Bioregeneration Rate, Exp. 2, 12-min. EBCT, No Iron, Avg. C_o = 1000 (toluene) and 501 (PCE) µg/L 128

Figure 5.6 Effect of Toluene Equilibrium Concentration and EBCT on Toluene-Based Bioregeneration 133

Figure 5.7 Total Radioactivity Profile for the Sterile Column (^{14}C-TCE, No Iron, 0.9-min. EBCT), Column A (biologically-active, ^{14}C-toluene, Iron, 3.0-min. EBCT), and Column B (biologically-active, ^{14}C-TCE, Iron, 3.0-min. EBCT) of Exp. 6 136

Figure 5.8 Fraction Radioactivity Desorbed for the Sterile Column (^{14}C-TCE, No Iron, 0.9-min. EBCT), Column A (biologically-active, ^{14}C-toluene, Iron, 3.0-min. EBCT), Column B (biologically-active, ^{14}C-TCE, Iron, 3.0-min. EBCT) of Exp. 6, and the Less Biologically Active Column (^{14}C-toluene, No Iron, 5.0-min. EBCT) 137

Figure 5.9 Effluent Toluene and TCE Concentrations and D.O., Exp. 3, Iron-Free Influent, 10.3-min. EBCT, Avg. C_o = 1740 (toluene) and 179 (TCE) µg/L 140

Figure 5.10 TCE Effluent Concentrations, Exp. 3, Avg. C_o = 1740 (toluene) and 179 (TCE) µg/L 141

Figure 5.11 TCE Radioactivity Profile, Exp. 3, Iron-Free Influent, 10.3-min. EBCT, Avg. C_o = 1740 (toluene) and 179 (TCE) µg/L 143

Figure 5.12 TCE Radioactivity Profile, Exp. 3, Iron-Containing Influent, 10.4-min. EBCT, Avg. C_o = 1740 (toluene) and 179 (TCE) µg/L 143
Figure 5.13 Effluent Concentrations, Exp. 4, Metabolism-Tracking Column, Iron, 3.4-min. EBCT, Avg. C_o = 6500 (toluene) and 266 (TCE) µg/L 146
Figure 5.14 Final SOC Loadings, Exp. 4, Column A (metabolism-tracking, 3.4-min. EBCT) and Column B (cometabolism-tracking, 3.5-min. EBCT), Iron, Avg. C_o = 6500 (toluene) and 266 (TCE) µg/L147
Figure 5.15 Enzyme Activity Across the Column, Exps. 3 – 5 (with H_2O_2) 148
Figure 5.16 Enzyme Activity Across the Column, Exps. 3 (with H_2O_2) and 6 (very little H_2O_2).....148
Figure 5.17 Cumulative Cometabolism-Based Bioregeneration and Bioregeneration Rate, Exps. 3 (10.4-min. EBCT, Iron, Avg. C_o = 1740 (toluene) and 179 (TCE) µg/L) and 4 (3.5-min. EBCT, Iron, Avg. C_o = 6500 (toluene) and 266 (TCE) µg/L).....151
Figure 5.18 Effluent Toluene and TCE Concentrations, Exp. 5, ^{14}C-Toluene-Tracking Column, 2.3-min. EBCT, Iron, Avg. C_o = 3320 (toluene) and 200 (TCE) µg/L.....152
Figure 5.19 Toluene Radioactivity Profile, Exp. 5, ^{14}C-Toluene-Tracking Column, 2.3-min. EBCT, Iron, Avg. C_o = 3320 (toluene) and 200 (TCE) µg/L 153

Figure 5.20 Toluene and TCE Bioregeneration Rates, Exp. 5, 2.3 (Toluene) and 1.7-min. (TCE) EBCTs, Iron, Avg. C_o = 3320 (toluene) and 200 (TCE) µg/L 154
Figure 5.21 Final SOC Loadings, Exp. 5, 2.3 (Col A) and 1.7-min. (Col B) EBCTs, Iron, Avg. C_o = 3320 (toluene) and 200 (TCE) µg/L 155
Figure 5.22 Effect of Equilibrium Toluene:TCE Concentration Ratio and EBCT on TCE-Based Bioregeneration.....157
Figure 5.23 Effluent Toluene Concentrations, Exp. 6 (2.3 (A) and 1.7-min. (B) EBCTs, Iron, Avg. Toluene C_o = 1420 µg/L) and Sterile Column (0.9-min. EBCT, No Iron, Avg. Toluene C_o = 1490 µg/L) 159
Figure 5.24 Effluent TCE Concentrations, Exp. 6 (2.3 (A) and 1.7-min. (B) EBCTs, Iron, Avg. TCE C_o = 721 µg/L) and Sterile Column (0.9-min. EBCT, No Iron, Avg. TCE C_o = 916 µg/L).....159
Figure 5.25 Final SOC Loadings, Exp. 6 (2.3 (A) and 1.7-min. (B) EBCTs, Iron, Avg. TCE C_o = 721 µg/L) and Sterile Column (0.9-min. EBCT, No Iron, Avg. TCE C_o = 916 µg/L).....161
Figure 5.26 Toluene Effluent Concentrations, Anthracite Control Experiment, 1.0 (A), 0.9 (B), and 1.0-min. (C) EBCTs, Avg. Toluene C_o = 623 µg/L 165
Figure 5.27 TCE Effluent Concentrations, Anthracite Control Experiment, 1.0 (A), 0.9 (B), and 1.0-min. (C) EBCTs, Avg. TCE C_o = 62 µg/L ...165

Figure 5.28 Toluene and TCE Effluent Concentrations, Sterile Column, No Iron, Toluene C_o = 1570 µg/L, TCE C_o = 87 µg/L, 0.9-min. EBCT 167
Figure 5.29 Measured and PSDM-Fitted Toluene and TCE Effluent Concentrations, Sterile Column, Toluene C_o = 1570 µg/L, TCE C_o = 87 µg/L, 0.9-min. EBCT 169
Figure 5.30 Toluene Effluent Concentrations, Exp. 7 Column B (No Iron, 1.1-min. EBCT), Exp. 7 Column C (Iron, 1.2-min. EBCT), and Sterile Column (No Iron, 0.9-min. EBCT), Avg. Toluene C_o = 1500 µg/L 170
Figure 5.31 TCE Effluent Concentrations, Exp. 7 Column B (No Iron, 1.1-min. EBCT), Exp. 7 Column C (Iron, 1.2-min. EBCT), and Sterile Column (No Iron, 0.9-min. EBCT), Avg. TCE C_o = 88 µg/L 170
Figure 5.32 Final SOC Loadings for Exp. 7 Col B (No Iron, 1.1-min. EBCT), Exp. 7 Col C (Iron, 1.2-min. EBCT), and Sterile Column (No Iron, 0.9-min. EBCT)..... 173
Figure 5.33 Radioactivity Profile, Exp. 7, Column B, Iron-Free Influent, 1.1-min. EBCT, Avg. C_o = 1500 (toluene) and 88 (TCE) µg/L 175
Figure 5.34 Bioregeneration Rate, Exp. 7, Column B (No Iron, 1.1-min. EBCT), and Exp. 7, Col C (Iron, 1.2-min. EBCT), Avg. C_o = 1500 (toluene) and 88 (TCE) µg/L 176

Figure 5.35 Cumulative Metabolism-Based Bioregeneration, Exp. 7, Col B (No Iron, 1.1-min. EBCT), and Exp. 7, Col C (Iron, 1.2-min. EBCT), Avg. C_o = 1500 (toluene) and 88 (TCE) µg/L 177
Figure 5.36 Toluene Effluent Concentrations, Exp. 8, 1.0-min. EBCTs, Avg. C_o = 741 (toluene) and 65 (TCE) µg/L.....179
Figure 5.37 TCE Effluent Concentrations, Exp. 8, 1.0-min. EBCTs, Avg. C_o = 741 (toluene) and 65 (TCE) µg/L.....179
Figure 5.38 Toluene Bioregeneration Rate, Exp. 8, 1.0-min. EBCTs, Avg. C_o = 741 (toluene) and 65 (TCE) µg/L.....181
Figure 5.39 Effect of Toluene Concentration and EBCT on Toluene-Based Bioregeneration in both Exhausted and Virgin Column Exps. 183
Figure 6.1 Effluent Toluene and PCE Concentration and Toluene Bioregeneration Rate Simulations for Exp. 1, 6.9-min. EBCT, No Iron, Avg. C_o = 607 (toluene) and 845 (PCE) µg/L 189
Figure 6.2 Measured and Simulated Final SOC Loadings for Exp. 1, 6.9-min. EBCT, No Iron, Avg. C_o = 607 (toluene) and 845 (PCE) µg/L 190
Figure 6.3 Effluent Toluene and TCE Concentration Simulations for Exp. 3, 10.3-min. EBCT, Column A, Iron-Free Influent, Avg. C_o = 1730 (toluene) and 179 (TCE) µg/L.....193
Figure 6.4 TCE Bioregeneration Rate Simulation for Exp. 3, 10.3-min. EBCT, Column A, Iron-Free Influent, Avg. C_o = 1730 (toluene) and 179 (TCE) µg/L 194

Figure 6.5 Measured and Simulated Final SOC Loadings for Exp. 3, 10.3-min. EBCT, Column A, Iron-Free Influent, Avg. C_o = 1730 (toluene) and 179 (TCE) µg/L 195
Figure 6.6 Bulk Toluene Concentration Simulations Over Time for a Variation of Exp. 3, 10.3-min. EBCT, Column A, Iron-Free Influent, Avg. C_o = 1730 (toluene) and 179 (TCE) µg/L 197
Figure 6.7 Bulk TCE Concentration Simulations Over Time for a Variation of Exp. 3, 10.3-min. EBCT, Column A, Iron-Free Influent, Avg. C_o = 1740 (toluene) and 179 (TCE) µg/L 197
Figure 6.8 Toluene Loading Simulations Over Time for a Variation of Exp. 3, 10.3-min. EBCT, Column A, Iron-Free Influent, Avg. C_o = 1740 (toluene) and 179 (TCE) µg/L 199
Figure 6.9 TCE Loading Simulations Over Time for a Variation of Exp. 3, 10.3-min. EBCT, Column A, Iron-Free Influent, Avg. C_o = 1740 (toluene) and 179 (TCE) µg/L 199
Figure 6.10 Effluent Toluene and TCE Concentration Simulations for Exp. 7, 1.1-min. EBCT, Iron-Free, Toluene C_o = 1540 µg/L, TCE C_o = 91 µg/L 203
Figure 6.11 Toluene Adsorption and Bioregeneration Rate Simulation for Exp. 7, 1.1-min. EBCT, Iron-Free, Toluene C_o = 1540 µg/L, TCE C_o = 91 µg/L 204
Figure 6.12 Simulated Final SOC Loadings (697 hrs.) for Exp. 7, 1.1-min. EBCT, Iron-Free, Toluene C_o = 1540 µg/L, TCE C_o = 91 µg/L 205

Figure 6.13 Toluene Concentration Simulations for Exp. 7, 1.1-min. EBCT, Iron-Free, Toluene C_o = 1540 µg/L, TCE C_o = 91 µg/L 208
Figure 6.14 Toluene Loading Simulations Over Time for Exp. 7, 1.1-min. EBCT, Iron-Free, Toluene C_o = 1540 µg/L, TCE C_o = 91 µg/L 208
Figure 6.15 TCE Concentration Simulations for Exp. 7, 1.1-min. EBCT, Iron-Free, Toluene C_o = 1540 µg/L, TCE C_o = 91 µg/L 210
Figure 6.16 TCE Loading Simulations Over Time for Exp. 7, 1.1-min. EBCT, Iron-Free, Toluene C_o = 1540 µg/L, TCE C_o = 91 µg/L 210
Figure 6.17 Predicted Effluent Toluene Concentration in Biologically-Active GAC Columns, Toluene C_o = 2000 µg/L, TCE C_o = 100 µg/L.....214
Figure 6.18 Predicted Biologically-Active Toluene Bioregeneration Rate at the Influent and Effluent Ends of the Column, Toluene C_o = 2000 µg/L, TCE C_o = 100 µg/L.....215
Figure 6.19 Predicted Biologically-Active Effluent TCE Concentrations, Toluene C_o = 2000 µg/L, TCE C_o = 100 µg/L 216
Figure 6.20 Predicted Reduction in Normalized Effluent Toluene Concentration due to Metabolism & Cometabolism 217
Figure 6.21 Predicted Reduction in Normalized Effluent Toluene Concentration due to Metabolism & Cometabolism, Toluene C_o = 2000 µg/L, TCE C_o = 100 µg/L.....219
Figure 6.22 Predicted Reduction in Normalized Effluent TCE Concentration due to Metabolism & Cometabolism, Toluene C_o = 2000 µg/L, TCE C_o = 100 µg/L.....220

Figure 6.23 Predicted Reduction in Normalized Effluent TCE Concentration due to Cometabolism Only, Toluene C_o = 2000 µg/L, TCE C_o = 100 µg/L 221
Figure 6.24 Predicted Biologically-Active Effluent Toluene Concentrations, 1-min. EBCT, Toluene C_o = 2000 µg/L, TCE C_o = 100 µg/L..... 222
Figure 6.25 Predicted Biologically-Active Effluent TCE Concentrations, 1-min. EBCT, Toluene C_o = 2000 µg/L, TCE C_o = 100 µg/L..... 223
Figure 6.26 Predicted Reduction in Normalized Effluent TCE Concentration from Cometabolism due to an Increase in the TCE k_1 224
Figure B.1 0 – 100 µg/L Standard Curve Example, Toluene and PCE..... 246
Figure B.2 100 – 1000 µg/L Standard Curve Example, Toluene and PCE..... 247
Figure B.3 0 – 100 µg/L Standard Curve Example, Toluene and TCE..... 248
Figure B.4 100 – 1000 µg/L Standard Curve Example, Toluene and TCE..... 248
Figure B.5 Standard Curve Example, PCE..... 249
Figure B.6 Standard Curve Example, TCE 251
Figure B.7 Phenanthroline Iron Standard Curve Example 255
Figure B.8 OD_{600}/TSS/VSS Standard Curve..... 256
Figure B.9 Protein Standard Curve Example 257
Figure B.10 NADH Standard Curve Example 258
Figure B.11 Enzyme Activity Curve Example..... 259

Chapter 1: Introduction and Objectives

1.1 PROBLEM DESCRIPTION

Granular activated carbon (GAC) is often used in drinking water and ground water treatment to adsorb synthetic organic chemicals (SOCs). SOCs in the environment may result from such things as gasoline spills or improper disposal of dry cleaning solvents. Much research has been done on the adsorption of mixtures of SOCs and on the biodegradation and adsorption of mixtures of biodegradable SOCs. In this research, biodegradation is defined as the sum of metabolism and cometabolism, where metabolism is the use of an SOC as a carbon and energy source, and cometabolism is the fortuitous degradation of a traditionally nonbiodegradable SOC with a non-specific enzyme (*i.e.*, degradation without benefit to the cell). The term "traditionally nonbiodegradable" is used here to denote a compound that has historically been considered nonbiodegradable under normal conditions but can, in fact, be cometabolized. Very little work has been done on the biodegradation *and* adsorption of mixtures of biodegradable and nonbiodegradable SOCs. Furthermore, virtually no work has been done on simultaneous metabolism and cometabolism of such mixtures. The absence of such research is particularly problematic since many practical applications involve mixtures of biodegradable and nonbiodegradable SOCs as a result of their widespread occurrence in the environment.

Once a GAC column is exhausted, the GAC must be replaced and disposed of or recycled in some way (*i.e.*, landfilling, incineration, thermal

reactivation). Replacement and disposal of exhausted GAC is quite expensive. Encouragement of biodegradation (in the form of metabolism and cometabolism) where one or more of the SOCs are biodegradable is one way to lengthen the GAC service life for some SOC mixtures. The GAC service life increases because a biofilm that forms on the GAC can metabolize or cometabolize SOCs, thereby reducing competition for GAC adsorption sites and allowing any remaining SOCs to adsorb onto the GAC to a greater extent than in the absence of biodegradation. SOCs present both in the aqueous phase and desorbed off the GAC are available to the microorganisms. Biodegradation of adsorbed SOCs (termed bioregeneration) renews the GAC's capacity for SOC adsorption, while biodegradation of SOCs in the aqueous phase slows the rate of GAC exhaustion. Biodegradation of SOCs present in either phase can lengthen the GAC service life, thereby decreasing operation and maintenance costs. Furthermore, if biodegradation of the SOC is complete, the SOC is broken down into harmless by-products, thereby removing any health threat.

The dissolved oxygen level in biologically-active GAC columns can be limiting when vigorous biodegradation occurs; thus, the addition of an oxygen source may be beneficial in maximizing the bioregeneration rate and extending the GAC column service life. One way to increase the dissolved oxygen level is by encouraging Fenton's oxidation, an abiotic reaction between ferrous iron and hydrogen peroxide that produces hydroxyl radicals and oxygen. In addition, Fenton's oxidation may further increase the GAC column service life because the hydroxyl radicals abiotically degrade sorbed or aqueous SOCs, thereby reducing

competition for GAC adsorption sites, as in the case of biologically-active GAC columns. The encouragement of Fenton's oxidation in a biologically-active GAC column should, therefore, increase the service life beyond that achieved by either treatment alone. Hydroxyl radicals will also react with (*i.e.*, disinfect) biomass, however, so the effect of combining Fenton's oxidation and biodegradation is not completely additive.

1.2 OBJECTIVES

Given the lack of research on simultaneous metabolism and cometabolism in biologically-active GAC columns, many research questions about the treatment process remain unanswered. The following research objectives serve to address the most critical of these.

1. Determine the relative significance of metabolism and cometabolism as mechanisms for increasing GAC service life. Consider for simplicity a two-component mixture of one biodegradable and one "nonbiodegradable" SOC. As the biodegradable SOC is degraded, the competition for GAC adsorption sites between the two SOCs decreases. Furthermore, if the "nonbiodegradable" SOC is also cometabolized, additional lengthening of the GAC service life may result because only a fraction of the "nonbiodegradable" SOC has to be treated via adsorption. The relative increase in GAC service life in comparison to metabolism of the biodegradable SOC alone, as well as compared to GAC adsorption alone (*i.e.*, no biodegradation), must be carefully quantified. Understanding the relative contribution of cometabolism and documenting the

conditions under which this contribution is significant are the primary goals of this research.

2. Explore how relative chemical adsorbability and column penetration influence the extent of cometabolism. Again considering the simplest case of a two-component mixture of one biodegradable and one nonbiodegradable SOC, the relative adsorbability of the two SOCs determines the proximity of the two chemicals within the GAC column. Cometabolism can only occur in that portion of the GAC column where both SOCs are present, because the presence of the biodegradable SOC is necessary to support microbial growth. Relative adsorbability determines the extent of the overlap between the two SOCs and, thus, should be an important indicator of the significance of cometabolism. *A priori*, cometabolism was expected to have the largest effect on process performance when the two chemicals have similar adsorption characteristics. Likewise, the extent of SOC penetration into the GAC column prior to the onset of significant biodegradation should significantly affect the improvement in GAC service life realized. Encouragement of a rapid onset of biodegradation is expected to provide the best results in this regard, but experimental proof in the literature is lacking.

3. Determine the significance of enzyme competition and intermediate toxicity in limiting the rate of cometabolism. Because the primary substrate (*i.e.*, the SOC supporting microbial growth) and the SOC undergoing cometabolism are both degraded by the same enzyme (usually an oxygenase), the two SOCs compete for the enzyme, which may adversely affect the rate of cometabolism. If

the primary substrate is present at too high a concentration, enzyme competition will become large, and the cometabolism rate may become negligible. If the concentration of the primary substrate is too low, however, the bacterial culture will not be able to grow sufficiently, and again the cometabolism rate may decrease. To some extent, the concentration effects on cometabolism are organism and SOC specific; however, with detailed study some generalizations may be possible about typical ranges of SOC concentration where cometabolism can significantly affect process performance. Furthermore, other research has found intermediates of chlorinated solvent cometabolism to be toxic or to inactivate the enzymes in biodegradation. If intermediate toxicity is occurring, the rate of cometabolism decreases.

4. Determine the significance of adding Fenton's oxidation as a mechanism for increasing GAC service life. With the addition of Fenton's oxidation, the degradation of both biodegradable and nonbiodegradable SOCs is possible, leading to regeneration as well as a decreased usage rate of the GAC. Since only a fraction of the SOCs has to be treated via adsorption, the service life of the GAC column should increase. The increase in GAC service life relative to the combined biodegradation and adsorption of the SOCs, as well as to GAC adsorption alone (*i.e.*, no biodegradation), needs to be carefully quantified. The effect of hydroxyl radical destruction of biomass within the column needs to be identified as well.

5. Refine existing metabolism-based models of adsorption/biodegradation systems to account for cometabolism. Existing equilibrium and kinetic models for

simultaneous adsorption and biodegradation do not account for cometabolism. Modification of these mathematical models to include cometabolism was expected to be essential for experimental design, data analysis and interpretation, and ultimately process design. Simultaneous adsorption and biodegradation in GAC columns is complex, and mathematical models provide a conceptual framework for thinking about the process.

Chapter 2: Literature Review

2.1 CHEMICAL SELECTION

For this research, four criteria had to be met in the selection of chemicals for cometabolism batch and column studies.

1. There was one biodegradable and one traditionally nonbiodegradable chemical.
2. The degradation pathway of the biodegradable chemical produced a non-specific enzyme that also degraded the traditionally nonbiodegradable chemical, thereby supporting cometabolism.
3. The biodegradable chemical could be biodegraded aerobically by an existing mixed culture of *Pseudomonas* species and *Rhodococcus rhodochrous*.
4. Both chemicals were of similar activated carbon adsorbability because cometabolism was expected to have the largest effect on process performance when the two chemicals had similar adsorption characteristics.

Given these criteria, the biodegradable and traditionally nonbiodegradable SOCs chosen for cometabolism studies were toluene and trichloroethylene (TCE), respectively. For metabolism studies, the biodegradable and nonbiodegradable SOCs chosen were toluene and perchloroethylene (PCE). These chemicals were chosen based on TCE's ability to be cometabolized; toluene, PCE, and TCE's similar activated carbon adsorbability (see Section 2.3 Adsorption Equilibrium);

and toluene's ability to serve as a primary substrate for TCE cometabolism using the previously studied mixed culture. Chloroform and 1,2-dichloroethane were also explored as weakly adsorbable cometabolites; however, they cannot be cometabolized by toluene or phenol oxidizers (such as the existing mixed culture). Instead, they can only be cometabolized by methane or propane oxidizers (Chang and Alvarez-Cohen, 1995b). Biodegradable SOCs other than toluene were investigated (phenol, benzene, xylenes) but either had an activated carbon adsorbability that differed too much from that of TCE or would not be degraded via a pathway that would produce a non-specific enzyme suitable for TCE cometabolism (see Section 2.5 Microbial Kinetics).

2.2 CHEMICAL PROPERTIES, USAGE, AND REGULATION

Toluene is one of the BTEX compounds (benzene, toluene, ethylbenzene, and xylenes), and TCE and PCE are chlorinated solvents. Chemical properties of BTEX compounds and chlorinated solvents are shown in Table 2.1. The data in Table 2.1 originate from Software to Estimate Physical Properties (National Center for Clean Industrial and Treatment Technologies, CenCITT) as well as literature sources (Verschueren, 1983; USEPA, 1999). Because of low sorption onto soil and sediments, toluene, PCE, and TCE that is spilled is readily transported through soil and into groundwater and surface water (USEPA, 1998; USEPA, 1999). Table 2.1 suggests that, once in these water sources, chlorinated solvents sink, whereas BTEX compounds float when present as separate phases. Dilution and turbulence in the environment, however, often result in mixing of

both chemical types. BTEX compounds and chlorinated solvents are volatile and thus will partition into the air from contaminated water sources.

Table 2.1 Chemical Properties of BTEX Compounds and Chlorinated Solvents

Compound	**Molecular Weight** (g/mol)	**Density** (g/mL)	**Solubility at 20°C** (mg/L)	**Boiling Point** (°C)	**Vapor Pressure (1 atm., 20°C)** (mm Hg)
Toluene	92.15	0.867	515	110.8	22
Benzene	78.11	0.878	1780	80.1	76
Ethyl-benzene	106.17	0.869	152	136	7.1
o-Xylene	106.17	0.88	175	144.4	5
m-Xylene	106.17	0.86	175	139	6
p-Xylene	106.17	0.86	198	138.4	6.5
TCE	131.39	1.47	1100	87	57.8
PCE	165.83	1.62	162	121	14.2
Carbon Tetrachloride	153.82	1.59	800	76.6	91.3

The major source of toluene is refining from petroleum crude oil. Some of the toluene is then added directly to gasoline (also produced from crude oil), because it acts as an octane booster (USEPA, 1994). The remaining toluene is used for other purposes, including chemical manufacturing, solvent operations, manufacturing of paints, lacquers, adhesives, and rubber, printing, leather tanning, metal degreasing, and electroplating (Environmental Defense, 2003a). It is also

used in nail polish, rubber cement, cosmetics, stain removers, fabric dyes, and antifreeze and is found in cigarette smoke (ATSDR, 1994).

A large amount of TCE is used as a solvent for metal degreasing due to its cleaning properties, low flammability, and lack of measurable flashpoint (ATSDR, 1997; HSIA, 2001). TCE is also used in the production of fluorochemicals and polyvinyl chloride, dry cleaning solvents and other solvent operations, and the oxidation of wafers in semiconductors (Environmental Defense 2003b; HSIA, 2001). Typewriter correction fluids, paint removers, adhesives, refrigerants, and spot removers also contain TCE (ATSDR, 1997).

Both toluene and TCE are considered high volume chemicals, since the production of each exceeds 1 million pounds annually. In 1994, annual production of toluene in the US was 6.8 billion pounds, and the US capacity for toluene production was between 10.8 and 12.3 billion pounds (USEPA, 1994). TCE production is slightly lower. In 1998, the US demand for TCE was 171 million pounds. That same year 15 million pounds of TCE were imported, and 84 million pounds were exported (HSIA, 2001).

In the US between 1987 and 1993, over 4 million pounds of toluene were released into the environment. Of that, 3,670,000 pounds were released onto land and 730,000 pounds were released into water (USEPA, 1998). The major sources of toluene pollution are petroleum refining industries, gasoline spills from underground storage tanks, run off from gas station pumps, and motor vehicle exhaust (ATSDR, 1994). Despite its biodegradability, toluene releases into the environment have contaminated many water sources. Federal and state surveys

show more toluene contamination in surface water than groundwater. In a 1988 survey of hazardous waste sites, the EPA found toluene contamination in 29% of the groundwater, surface water, and soil samples. Average concentrations in the non-zero groundwater, surface water, and soil samples were 21 ppb, 7.5 ppb, and 77 ppb, respectively (ATSDR, 1994). In addition, toluene is flammable, increasing its hazard potential (USEPA, 1998).

In the US between 1987 and 1993, 190,000 pounds of TCE were released onto land and 100,000 pounds were released into water (USEPA, 1999). Major sources of TCE pollution are evaporation from metal degreasing operations and TCE migration from hazardous waste disposal facilities (ATSDR, 1997). Many TCE spills have occurred in the past 70 years of its industrial use. Of 1179 hazardous waste sites on the National Priorities list, 460 were found to have TCE contamination. TCE pollution is significant, as can be seen by the fact that between 9 and 34% of US water supply sources are contaminated with TCE, with an average TCE concentration of 1 to 2 ppb in contaminated samples and maximum concentrations in the mid-ppm range. In addition, outdoor air samples were found to contain a background TCE concentration of 30 to 460 ppt (ATSDR, 1997).

Given the ubiquitous presence of these SOCs in the environment, the Environmental Protection Agency has taken steps to regulate their presence in water. Toluene, PCE, and TCE are all regulated under the Safe Drinking Water Act and the Clean Water Act. Table 2.2 shows current drinking water legislation for BTEX and selected chlorinated solvents (Pontius, 1998). The selected

chlorinated solvents in Table 2.2 have maximum contaminant level goals (MCLGs) and maximum contaminant levels (MCLs) that are lower than or equal to those for BTEX.

Table 2.2 National Primary Drinking Water Standards for BTEX Compounds and Selected Chlorinated Solvents (Pontius, 1998)

Compound	**MCLG** (mg/L)	**MCL** (mg/L)	**Potential Health Effects**
Toluene	1	1	Liver, kidney, nervous system and circulatory system effects
Benzene	0	0.005	Cancer
Ethylbenzene	0.7	0.7	Liver, kidney, nervous system effects
Xylenes (total)	10	10	Liver, kidney, nervous system effects
TCE	0	0.005	Cancer
PCE	0	0.005	Cancer
Carbon Tetrachloride	0	0.005	Cancer

Clearly, these SOCs present a health hazard. If they are found in water sources, they need to be removed. The best available treatment technology for toluene and TCE is considered to be either GAC adsorption or packed tower aeration (USEPA, 1998; USEPA, 1999). Because of more stringent air pollution regulations, however, packed tower aeration alone is not permissible in many areas since it simply transfers the SOCs from the water into the air. The

following sections discuss batch GAC adsorption as well as three other SOC treatment technologies: flow-through GAC adsorption, batch biodegradation, and biologically-activated GAC columns.

2.3 ADSORPTION EQUILIBRIUM

Activated carbon adsorption is a common way to treat a broad spectrum of organic pollutants. In order to determine the adsorbability of chemicals on activated carbon, adsorption isotherms are often performed. This technique was first used in gas adsorption studies, where temperature has a large effect on the amount of gas adsorbed; thus, the term isotherm (constant temperature) was used to describe adsorption experiments where the temperature was held constant but varying amounts of adsorbent or chemical were used. Temperature has a very small effect on liquid adsorption isotherms (Snoeyink *et al.*, 1969). The time needed for an isotherm to reach equilibrium, however, is very important. Failure to reach equilibrium between the activated carbon and adsorbate may result in the underestimation of an activated carbon's long term capacity (Peel and Benedek, 1980). To ensure equilibration has been reached in isotherm studies, powdered activated carbon (PAC) is recommended instead of GAC because the small particle size reduces the time needed to reach equilibrium.

A common way to model activated carbon adsorption isotherms is to use the Freundlich isotherm equation as seen in equation 2.1 (Freundlich, 1926).

$$q_e = K C_e^{1/n} \qquad \text{(Eq. 2.1)}$$

where:

q_e is the adsorptive capacity at equilibrium (µg adsorbate /g GAC)

K is the adsorption capacity at unit concentration (µg/g $(L/\mu g)^{1/n}$)

C_e is the equilibrium adsorbate concentration in solution (µg/L)

1/n is the adsorption intensity (dimensionless)

The values for adsorption intensity range between zero and one for single chemicals. Other isotherm equations, such as a linear equation or the Langmuir equation, do not model activated carbon adsorption as well as the Freundlich equation, because the Freundlich equation is better for heterogeneous surfaces (Weber and DiGiano, 1996). The Freundlich equation makes the same assumptions as in the Langmuir isotherm (a fixed amount of adsorption sites, monolayer adsorption) except that it assumes each site varies in its energy of adsorption (Weber and DiGiano, 1996). This site variability means that some adsorption sites are preferable to others and thus are occupied first. For ease of analysis, the Freundlich equation is often linearized using a log scale as seen in equation 2.2. Equation 2.2 has a slope of 1/n and an intercept of log K.

$$\log q_e = \log (K) + (1/n) \log C_e \qquad \text{(Eq. 2.2)}$$

A large K and small 1/n indicate a highly adsorbable chemical (Weber and DiGiano, 1996). Table 2.3 presents published literature values for the Freundlich parameters. These Freundlich parameter values indicate toluene and TCE are both moderately adsorbable. Their closeness in adsorbability indicates potential for extensive competition for adsorption sites on activated carbon.

Table 2.3 Freundlich Parameters for Toluene and TCE on F400 (Speth and Miltner, 1990)

SOC	**K** $\mu g/g\ (L/\mu g)^{1/n}$	**1/n** (-)	**Equilibrium Conc.** (µg/L)	**Initial Conc.** (µg/L)
Toluene	5,010	0.429	2.3 – 104	361 - 394
PCE	4,050	0.516	3.6 – 421	534 – 1,010
TCE	2,000	0.482	7.7 – 442	766 – 1,100

As mentioned above, SOCs often are present in mixtures, not individually. Some SOC mixtures may also contain background natural organic matter (NOM). Mixtures of SOCs are more difficult to treat since each SOC may vary in its ability to be biodegraded or adsorbed. Multi-chemical GAC adsorption is often described by the Ideal Adsorbed Solution Theory (IAST). IAST was originally developed by Myers and Prausnitz (1965) for gas mixtures but was then adapted for aqueous mixtures by Radke and Prausnitz (1972). When GAC is used to treat mixtures of chemicals, competition for adsorption sites occurs. Competition results in a lowered GAC loading for each chemical in comparison to that for the individual chemical alone. IAST predicts this competitive behavior given single component isotherm parameters.

IAST is based on the concept of spreading pressure (π), which is defined as the difference in surface tension between water on a clean surface and water on a surface covered with the compound of interest. As the concentration of SOCs increases, the surface tension of the mixture tends to decrease; thus the spreading pressure tends to increase. Equation 2.3 demonstrates this relationship, where the

single component spreading pressure is equal to the spreading pressure of the mixture of compounds (π_m).

$$\pi_i = \frac{RT}{A}\int_0^{q_i^o} \frac{d\ln C_i^o}{d\ln q_i^o}\, dq_i^o = \pi_m \qquad \text{for i = 1 to N} \qquad \text{(Eq. 2.3)}$$

where R is the ideal gas constant, T is temperature, A is the surface area available for adsorption, q_i^o is the single component, solid phase loading of component i in equilibrium with concentration C_i^o. Additional relationships between single component and mixture parameters are shown in equations 2.4, 2.5, and 2.6.

$$q_T = \sum_{i=1}^{N} q_i \qquad \text{(Eq. 2.4)}$$

$$C_i = z_i C_i^o \quad \textit{where } z_i = \frac{q_i}{q_T} \qquad \text{(Eq. 2.5)}$$

$$\frac{1}{q_T} = \sum_{i=1}^{N} \frac{z_i}{q^o{}_i} \qquad \text{(Eq. 2.6)}$$

where q_T is the total molar surface loading, q_i is the competitive solid phase loading in equilibrium with concentration C_i, z_i is the mole fraction of the solid phase loading for component i, and N is the number of components in solution.

Crittenden *et al.* (1985a) combined IAST equations 2.3 through 2.6 with the Freundlich equation (equation 2.1) to predict multiple component equilibrium with heterogeneous adsorbents such as GAC. Equation 2.7 shows the final result.

$$C_{io} = \frac{M\, q_i}{V} + \frac{q_i}{\sum_{j=1}^{N} q_j}\left(\frac{\sum_{j=1}^{N} n_j\, q_j}{n_i K_i}\right)^{n_i} \qquad \text{for i = 1 to N} \qquad \text{(Eq. 2.7)}$$

where C_{io} is the initial concentration of component i, M is the mass of adsorbent, and V is the volume of the isotherm bottle. Often, a correction factor, P, is

applied to the IAST equation (as a multiplier to q_i) in order to account for differences between predicted and measured equilibrium due to nonideal mixing in real aqueous systems (Thacker *et al.*, 1984; Smith and Weber, 1988).

2.4 GAC ADSORPTION KINETICS

Depending upon the point in its service life, a GAC column contains three zones of varying length: exhausted GAC, partially exhausted GAC (also known as the mass transfer zone (MTZ)), and virgin GAC. As time goes on, the length of the exhausted zone increases because more GAC becomes exhausted by the incoming SOC. Accordingly, the constant length MTZ moves through the column at a constant velocity (assuming a constant influent concentration). The length of the virgin GAC zone, therefore, decreases in a manner that is inversely proportional to the increase in the exhausted GAC zone (Weber and Smith, 1987). Since breakthrough occurs when the MTZ reaches the end of the column, the length and velocity of the MTZ determine the service life of a GAC column.

In addition, the GAC column service life decreases with increasing GAC particle size, increasing SOC influent concentration, and decreasing empty bed contact time (EBCT) (Clark and Lykins, 1989). A larger GAC particle size results in a slower adsorption rate (see discussion in Section 2.3 on time needed for isotherm equilibrium) and thus a longer MTZ. However using a small activated carbon particle size, such as PAC, can result in significant headloss; thus, a balance between headloss and MTZ length must be struck. Also, an increased SOC influent concentration results in a faster MTZ velocity, since it

takes less time for a fixed number of adsorption sites to be exhausted by a larger SOC concentration than by a smaller SOC concentration (assuming that 1/n is less than one, as is usually the case except for group characteristics such as chemical oxygen demand). Furthermore, in the case of a small EBCT, the MTZ length may be longer than the length of the column, resulting in instantaneous SOC breakthrough.

GAC column service life is also affected by what is known as "the chromatographic effect" in columns treating multiple components (Sontheimer *et al.*, 1988). In the chromatographic effect, the effluent concentration of a less adsorbable chemical is temporarily higher than its influent concentration. This phenomenon occurs because GAC columns treating multiple chemicals have separate MTZs for each chemical, which may or may not overlap with each other, because each chemical has a different adsorbability and thus has a different velocity through the column (Weber and Smith, 1987). The less adsorbable chemical breaks through first, followed by the more adsorbable chemical. However, when the more adsorbable chemical breaks through, it displaces the less adsorbable chemical, resulting in the increased effluent concentration of the less adsorbable chemical. Figure 2.1 demonstrates a simulated chromatographic effect. The predicted simultaneous adsorption of toluene and TCE is shown along with the predicted single-component adsorption of toluene and TCE for comparison. The TCE effluent to influent ratio is greater than one as the toluene starts to break through because the TCE that had been adsorbed in the absence of toluene is displaced by the more adsorbable toluene (Weber and DiGiano, 1996).

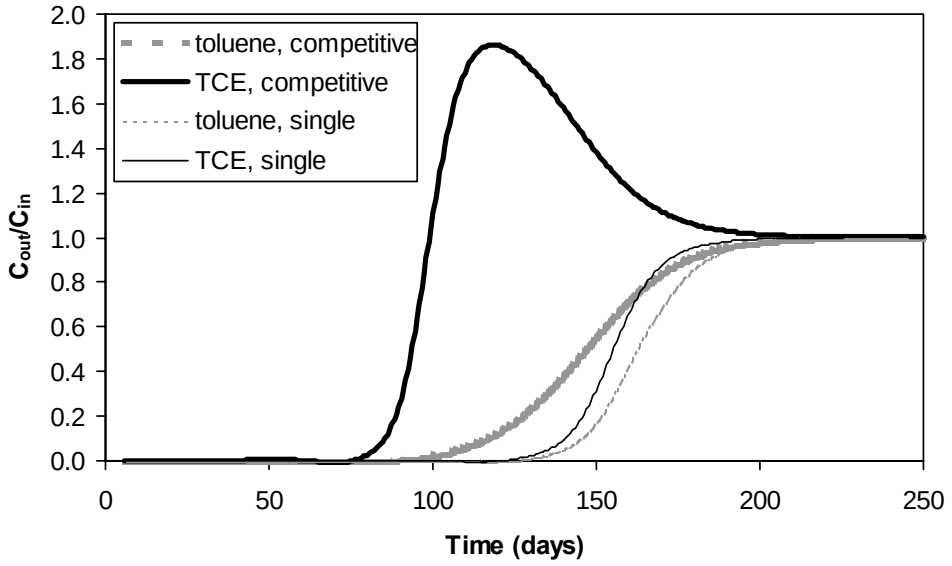

Figure 2.1 The Chromatographic Effect for Toluene & TCE (C = Concentration)

Several mathematical models have been used to describe adsorption behavior in GAC columns. One model that is often used is the Homogeneous Surface Diffusion Model (HSDM). The HSDM assumes the GAC particle is a homogenous solid in which an SOC adsorbs radially by surface diffusion, thus pore diffusion contributes negligibly to mass transport. Equilibrium is assumed to exist only at the outer surface of the GAC particle. Another model that is often used is the Pore Surface Diffusion Model (PSDM). The PSDM assumes that there are homogeneously distributed pores within a GAC particle (see Figure 2.2). These pores are assumed to contain liquid or air that is in equilibrium with the activated carbon surface with respect to the SOC that is adsorbed. Since these pores are distributed throughout the GAC particle, both a liquid or air SOC

concentration and a SOC surface loading exist at all radial positions within the GAC particle. Furthermore, both intraparticle pore and surface diffusion are assumed to be potentially significant mass transport mechanisms and to occur in only the radial direction (Hand *et al.*, 1989). In addition, the PSDM uses the Freundlich equation to describe adsorption of single components and IAST to describe adsorption of multiple components. AdDesignS© (Adsorption Design Software, CenCITT), an implementation of the PSDM, is used to predict individual and competitive GAC column runs.

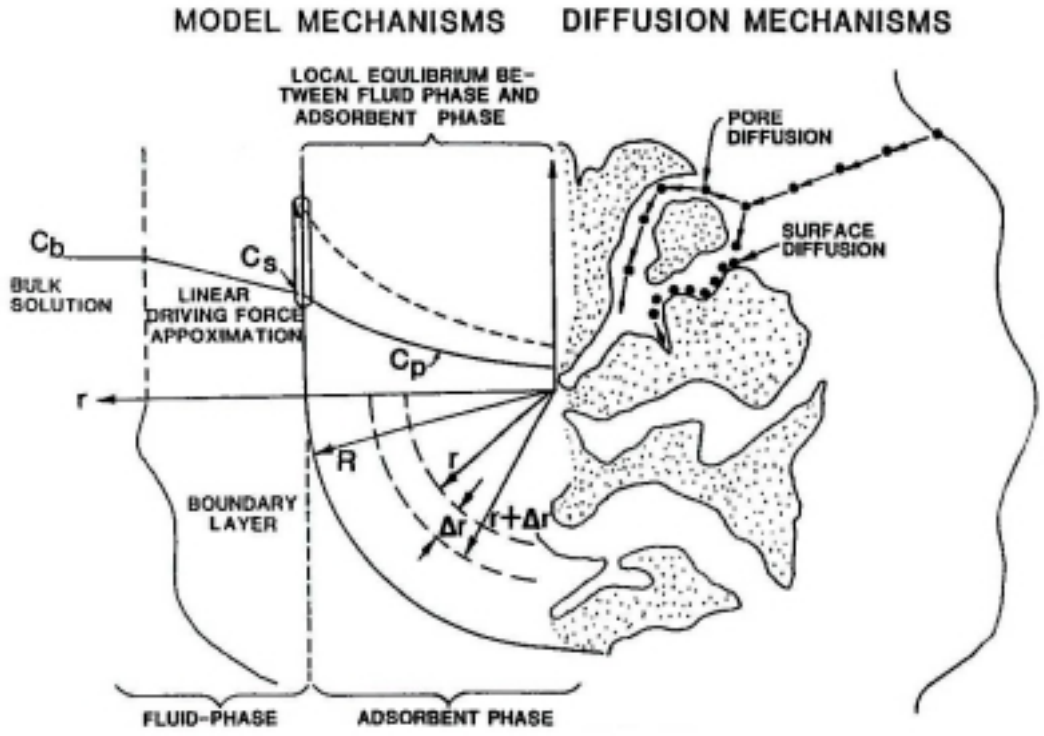

Figure 2.2 Structure of an Activated Carbon Particle (Crittenden *et al.*, 1987)

There are some key disadvantages, however, to GAC adsorption alone. In essence, GAC adsorption only results in a transfer of SOCs from one phase to another, instead of resulting in their destruction. Then the exhausted GAC must be disposed of or regenerated, which can be costly. In addition, GAC adsorption can be expensive if the chemical to be adsorbed is not very adsorbable, resulting in a short GAC column service life. Furthermore, effluent concentrations may be higher than influent concentrations if strongly adsorbed chemicals displace weakly adsorbed chemicals from the GAC (as is seen for TCE in Figure 2.2).

2.5 MICROBIAL KINETICS

2.5.1 Toluene and TCE Biodegradation

Aerobic biodegradation allows biodegradable SOCs to be converted to CO_2 through a series of enzymatic reactions, thereby destroying the SOC instead of merely transferring it from one phase to another. This research used a mixed culture of *Pseudomonas sp.* and *Rhodococcus rhodochrous* donated from Micro-Bac International, Inc., and Dr. Kerry Kinney in the Civil Engineering Department at the University of Texas at Austin, respectively.

Figures 2.3 and 2.4 show the toluene degradation pathways for some common *Pseudomonas* and related species that use either the toluene dioxygenase enzyme or one of the toluene monooxygenase enzymes (Wackett, 2000). Under aerobic conditions, toluene induces the *Tod* operon in *P. putida* F1 to produce toluene dioxygenase enzymes that, along with NADH, add one mole of oxygen across a carbon-carbon bond within the ring of toluene, thereby initiating the

biodegradation process (Wackett and Gibson, 1988). In other *Pseudomonas* species that use monooxygenases, only 0.5 moles of oxygen are used per reaction and NADH is not needed except in the case of toluene 2-monooxygenase (Wackett, 2000).

Possible toluene degradation pathways for *Rhodococcus rhodochrous* strain OFS are shown in Figure 2.5 (Vanderberg *et al.*, 2000). Figure 2.5 is based on degradation intermediates that were identified in a pure culture degrading toluene. Solid arrows indicate the involvement of *R. rhodochrous*, open arrows indicate known pathways in *Pseudomonas* species, and dashed arrows indicate abiotic pathways. The *R. rhodochrous* toluene degradation pathways result in the same chemical intermediates as pathways number one, four, and five shown in Figures 2.3 and 2.4 for the *Pseudomonas* species.

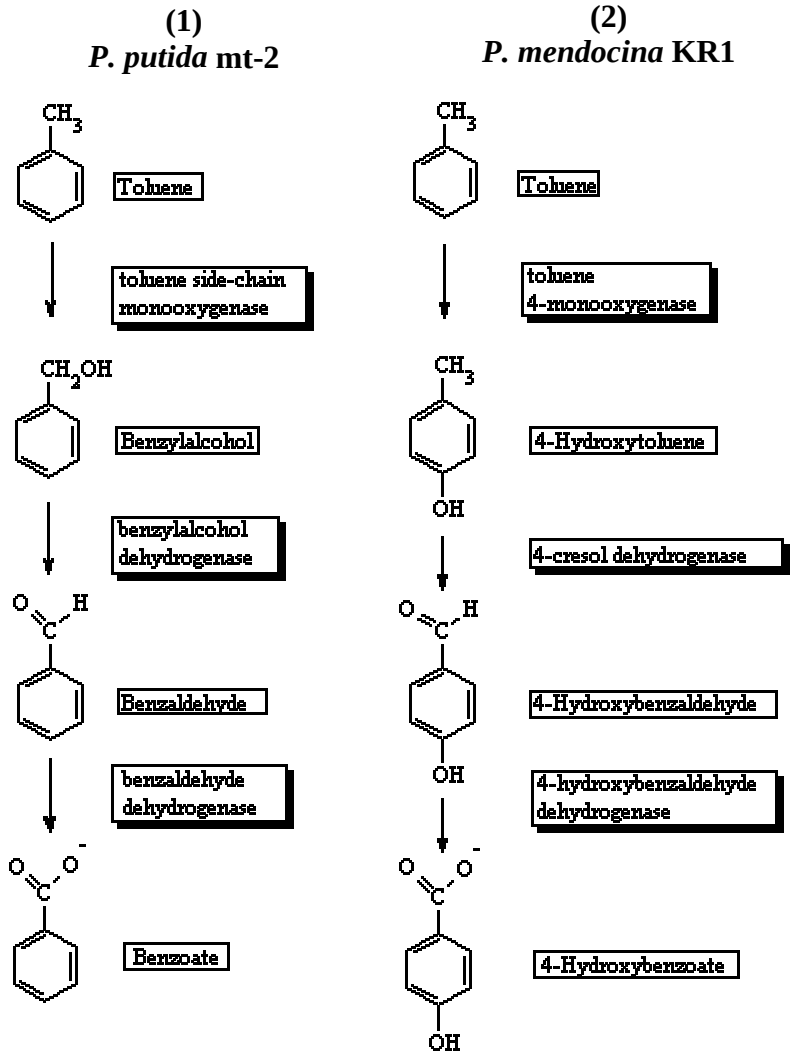

Figure 2.3 Toluene Degradation Pathways for *Pseudomonas* and Related Species (1) *P. putida* mt-2, (2) *P. mendocina* KR1 (Wackett, 2000)

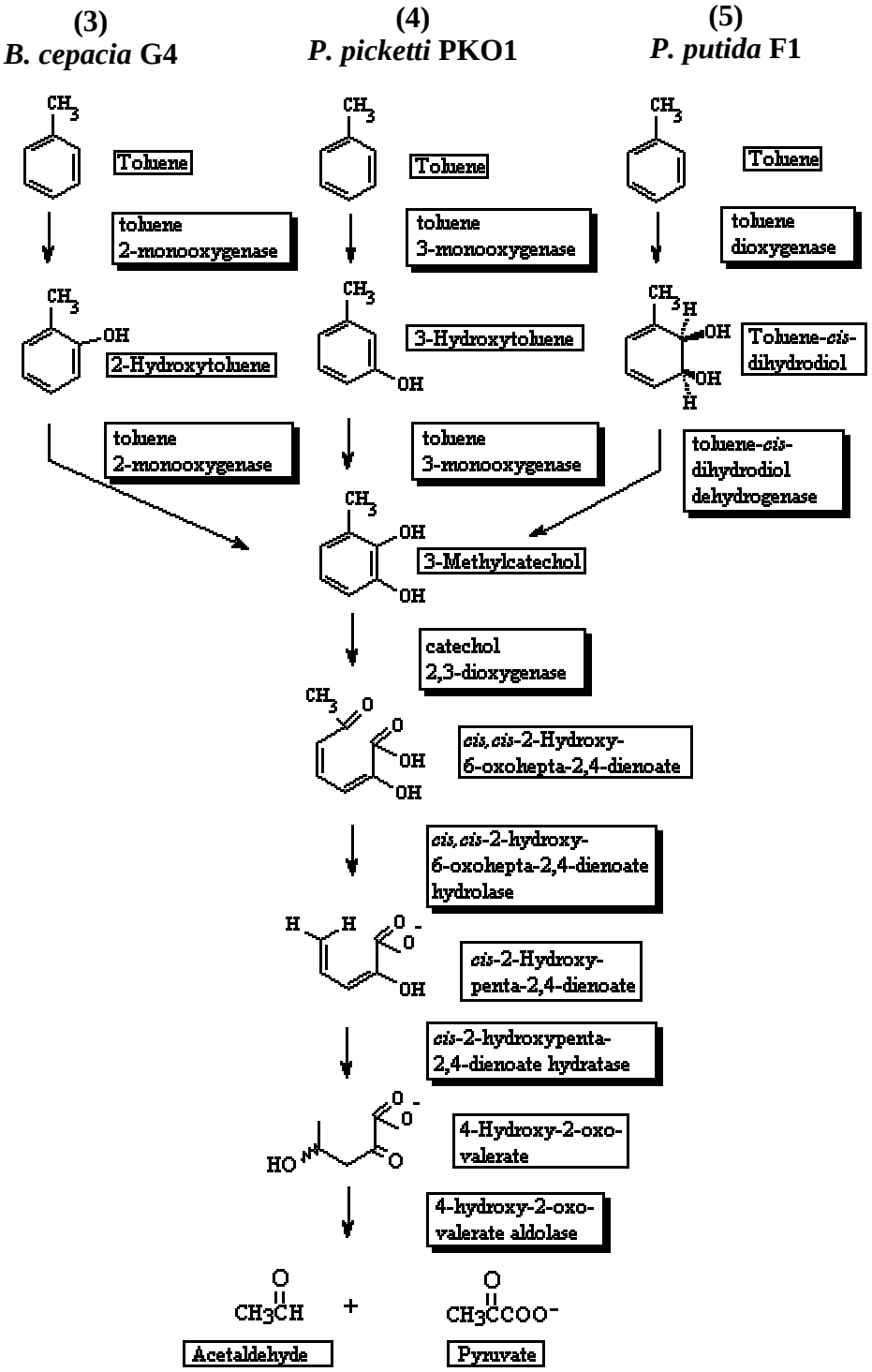

Figure 2.4 Toluene Degradation Pathways for *Pseudomonas* and Related species (3) *B. cepacia* G4, (4) *P. picketti* PKO1, (5*) P. putida* F1 (Wackett, 2000)

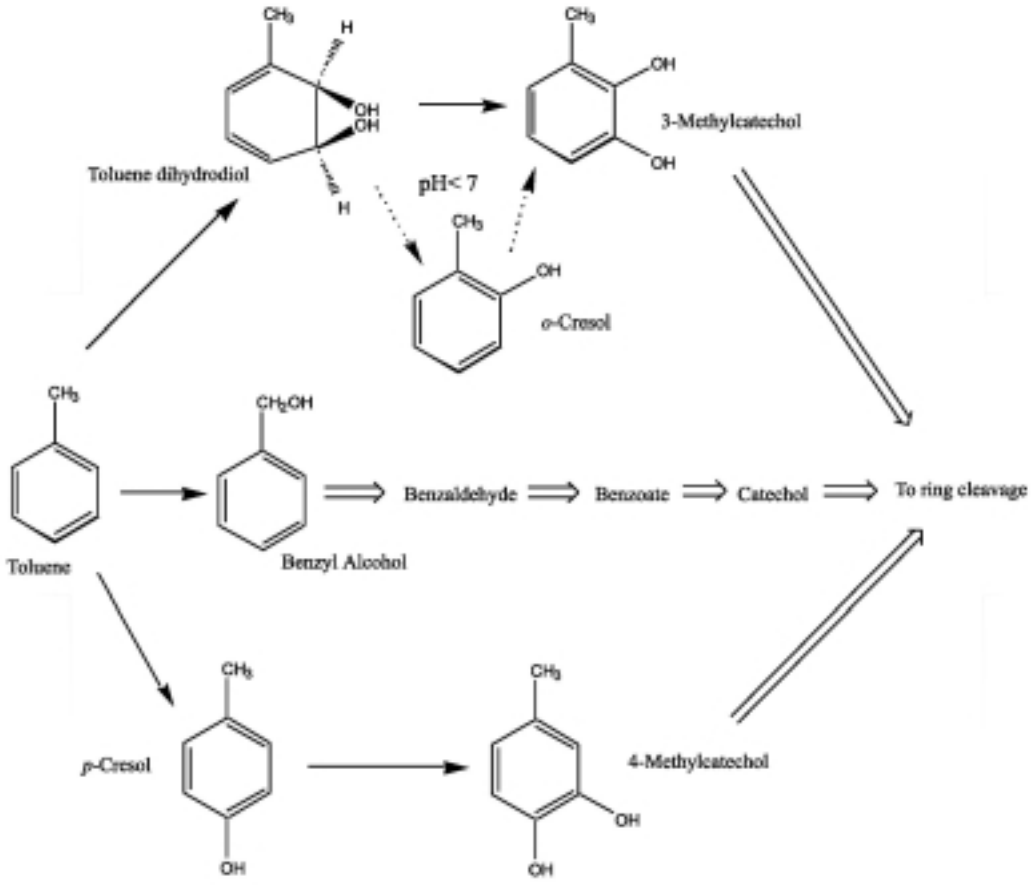

Figure 2.5 Toluene Degradation Pathways for *Rhodococcus rhodochrous* (Vanderberg *et al*., 2000)

TCE is considered nonbiodegradable under most typical environmental conditions, as are most other chlorinated solvents. This designation makes sense, since thermodynamically, little use can be made of most chlorinated pollutants as carbon and energy sources. That is where cometabolism comes into play. In cometabolism, a primary substrate is used as a carbon and energy source for microorganisms while another substrate, the cometabolite, is fortuitously degraded by non-specific enzymes. The microorganism produces these non-

specific enzymes in order to oxidize the growth chemical, but the enzymes also happen to oxidize the cometabolite. No regeneration of NADH occurs with the oxidation of cometabolite, so the microorganism reaps no benefits from cometabolism (Chang and Alvarez-Cohen, 1995a). Figure 2.6 shows a fortuitous TCE degradation pathway with toluene dioxygenase as the non-specific enzyme (Oh *et al*., 2001). Toluene monooxygenase-producing cultures have also been found to fortuitously degrade TCE (Leahy *et al*., 1996). The toluene 2-monooxygenase enzyme reaction with TCE requires NADH as a co-factor, however, although this is not shown in Figure 2.6.

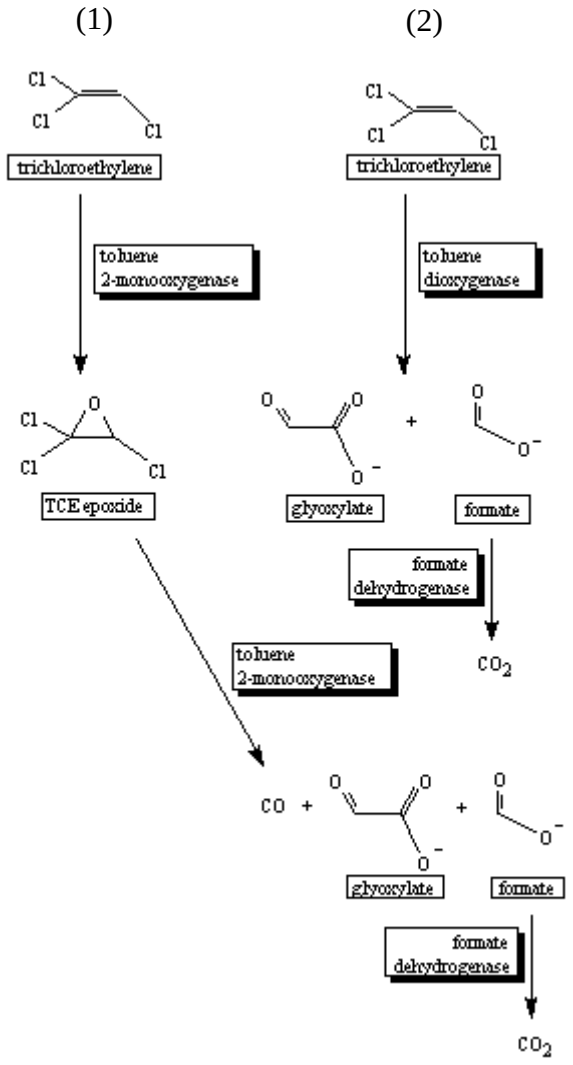

Figure 2.6 TCE Degradation Pathways using (1) toluene 2-monooxygenase and (2) toluene dioxygenase (Oh *et al*., 2001)

Under anaerobic conditions, TCE and other highly chlorinated compounds such as PCE or carbon tetrachloride can be biodegraded by reductive dehalogenation instead of by oxygenase enzymes. During reductive dehalogenation, chlorine molecules are removed one at a time in a series of reactions. Intermediates in the TCE reductive dehalogenation reaction, such as

vinyl chloride, can be more toxic than TCE itself (Ensley, 1991). In order to avoid reductive dehalogenation in this research, keeping the dissolved oxygen (D.O.) above 2 mg/L was important so that aerobic conditions are maintained (Lu *et al*., 1995). Furthermore, Bae and Rittmann (1995) found that maximizing the oxygen concentration was important to increase the cometabolism rate for a reaction involving an oxygenase enzyme.

2.5.2 Factors Affecting the Rate of Cometabolism

In addition to the D.O. concentration, several factors may affect the extent of TCE cometabolism. The effect of the type of primary substrate used for TCE cometabolism was researched by Lu *et al.* (1998). Phenol-degrading microorganisms were found to cometabolize TCE the fastest. With equal carbon concentrations of each substrate, the initial TCE removal rates were 1.5, 30, and 100 μg/L-hr for methane, toluene, and phenol, respectively. Enzyme type also affects the extent of TCE cometabolism. Leahy *et al*. (1996) found that pathways utilizing toluene monooxygenases degraded more TCE (36 to 67%) than those using toluene dioxygenase (12%). In addition, some questions have been raised as to whether or not TCE induces the production of toluene oxygenases in the absence of toluene. Historically, it has been found that TCE cannot be degraded in the absence of a primary substrate and thus cannot induce oxygenase enzymes on its own (Nelson *et al.*, 1987; Fan and Scow, 1993; McClay *et al*., 1995; Applegate *et al.*, 1997; Cox and Robinson, 1998; Lu *et al*., 1998). Some researchers, however, have presented bioluminescence and RNA transcription level measurements to show TCE induces oxygenase production (Heald and

Jenkins, 1994; Leahy *et al*., 1996; Shingleton *et al*., 1998). It has been suggested that bioluminescence, however, may be artificially increased in the presence of TCE. TCE and other chlorinated solvents are theorized to perturb the cell membrane, thereby increasing cell cycling of fatty acids and thus bioluminescence, but not actually increasing the transcription of toluene oxygenases (Heitzer *et al*., 1994).

Furthermore, 10 to 23% growth inhibition and biotoxicity in the presence of TCE and TCE metabolites have been cited by some researchers (Wackett and Householder, 1989; Cox *et al*., 1998; Shingleton *et al*., 1998). TCE and TCE metabolites have been cited as being toxic to both the whole cell and the enzyme, but there appears to be more evidence for whole cell toxicity. Wackett and Householder (1989) found TCE that had been activated by toluene dioxygenase inhibited cellular growth and covalently modified cellular molecules. Tetrachloroethylene, another chlorinated solvent with similar properties to TCE, did not inhibit growth, suggesting that it is only the toluene dioxygenase activated form of TCE (*i.e.*, a TCE metabolite) that is toxic to the cell. Further testing with a toluene dioxygenase mutant (defective in toluene dioxygenase production) showed no growth inhibition or modification of cellular components, further supporting the idea of TCE metabolite toxicity. Similar results were also found by Chang and Alvarez-Cohen (1995b).

Toluene-to-TCE concentration ratios may also affect the extent of cometabolism. Since toluene induction of the *tod* operon is probably the source of toluene oxygenases that degrade TCE, the mass of toluene determines the

amount of toluene oxygenase enzymes that will be produced. If enzyme levels are insufficient for complete TCE degradation, some TCE will remain in solution. Thus, it is not only the absolute mass of each SOC that matters, but also its relative mass. As long as sufficient D.O. is available, the higher the toluene to TCE ratio, the more toluene dioxygenase available, and the more TCE removed. Lu *et al*. (1998) found optimal toluene to TCE ratios to be between 14 and 24 mg toluene per mg TCE. For toluene to TCE initial concentration ratios ranging from 6.8 to 1022 mg toluene per mg TCE, TCE degradation ranged from 60 to 97% (not respectively) with 100% removal of toluene (Nelson *et al*., 1987; Fan and Scow, 1993; Lu *et al*., 1998). Because NADH (reducing power) is not regenerated by TCE cometabolism reactions (as it is in toluene metabolism), NADH levels may be limiting and therefore reduce the extent of TCE removal (Chang and Alvarez-Cohen, 1995a).

Furthermore, both toluene and TCE compete for active sites on the oxygenase enzymes, resulting in competitive inhibition of the degradation kinetics. Toluene has been shown to outcompete TCE for these sites (Robinson *et al*., 1998). In some studies, competitive inhibition has been quite significant, resulting in TCE not being cometabolized until toluene was nearly completely degraded (Robinson *et al*., 1998; Cox *et al*., 1998). In other studies, very little competitive inhibition was noted, and toluene and TCE were degraded simultaneously (Nelson *et al*., 1987; Fan and Scow, 1993; Lu *et al*., 1998). The variation in the extent of competitive inhibition seen in the literature is most likely explained by different ratios of initial concentrations of toluene and TCE. A

greater amount of competition can occur in cases of high ratios, resulting in a decreased *rate* of TCE degradation, although still an increased *extent* of TCE degradation (as in Robinson *et al*., 1998 and Cox *et al*., 1998). In a study of TCE degradation with phenol as a primary substrate, a 50% decrease in the phenol degradation rate occurred with a phenol-to-TCE initial concentration of only 0.51 mg phenol per mg TCE (Folsom *et al.*, 1990).

It has also been found (Aziz *et al*., 1999; Anderson and McCarty, 1994) that the rate of TCE cometabolism depends on the ratio of the primary substrate concentration to its half-saturation coefficient. If the ratio is low, the primary substrate degrades quickly, thereby presenting little competition with TCE for enzyme reaction sites. If the ratio was high, competitive inhibition occurred. Thus, a balance must be struck in having sufficient toluene for enzyme induction but not having so much that competitive inhibition delays TCE degradation.

2.5.3 Enzyme Activity

Delays in TCE degradation due to competitive inhibition bring up the question of the half-life of oxygenase enzymes. Researchers have found degradation of TCE to occur well (up to 10 days) after toluene has been fully metabolized, although at a much slower rate than when toluene is present, which indicates a relatively long half-life of the enzymes (Cox *et al*., 1998; Lu *et al*., 1998). Woo *et al*. (2000), however, estimated the half-life of the toluene dioxygenase enzyme to be 5.5 to 8 hours, which is relatively short. If the lifetime of the enzyme is not long enough, it will deactivate before completely degrading any remaining TCE.

The level of toluene oxygenase enzyme activity is, therefore, another piece of information that aids in the evaluation of TCE degradation performance in biological activated carbon (BAC) columns. Measurement of toluene dioxygenase in cells extracted from biofilm-covered GAC at the end of BAC experiments serves to normalize TCE degradation results between different columns, since a higher level of enzyme activity should result in more TCE degradation.

To measure toluene dioxygenase enzyme activity, several sources used variations of the original method by Jenkins and Dalton (1985). In this method, indole is added to samples of interest and the absorbency over time is measured at 400 nm. The reaction is as follows: indole is oxidized by toluene dioxygenase to form cis-indole 2,3-dihydrodiol, water is eliminated spontaneously to form indoxyl, and further air oxidation produces indigo (See Figure 2.7). Indoxyl is a bright yellow compound that absorbs at 400nm. The rate of indole oxidation to indoxyl was found to correlate with the level of toluene dioxygenase activity. It does not appear, however, that toluene monooxygenases oxidize indole in the same manner as toluene dioxygenase does (Nelson *et al*., 1987). If a mixed culture does not contain a large portion of microorganisms producing toluene dioxygenase as opposed to other oxygenases, enzyme activity may be greatly underestimated. Gram stains done on the mixed culture of *Pseudomonas sp.* and *Rhodococcus rhodochrous* have shown that the *Pseudomonas* species dominate the culture, and thus toluene dioxygenase enzymes dominated the total enzymes produced.

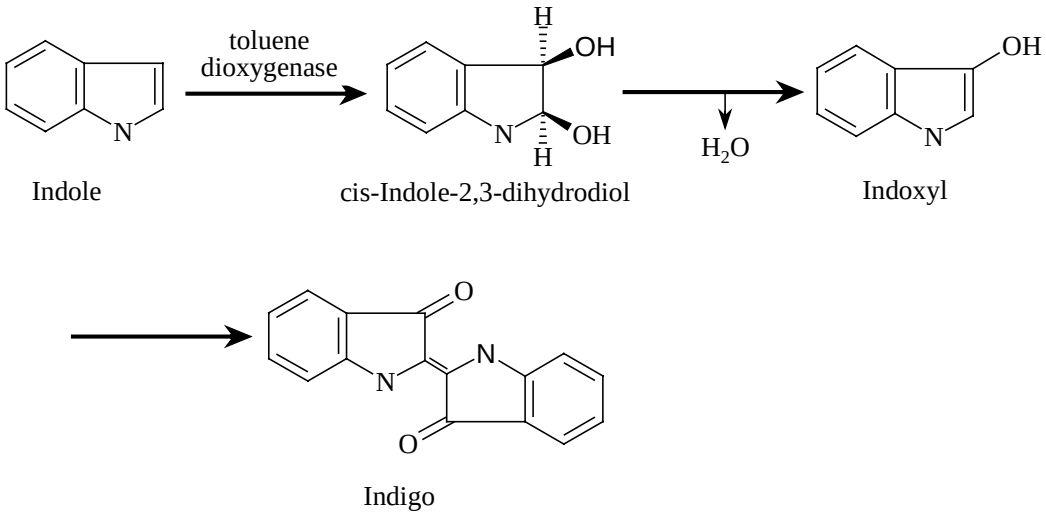

Figure 2.7 The Oxidation of Indole to Indigo (Jenkins and Dalton, 1985)

2.6 BIOREACTORS

In an ideal continuous flow application, a constant source of substrate is available. If a sufficiently sized bioreactor is degrading only biodegradable SOCs, all of the waste will be converted to carbon dioxide (assuming aerobic conditions) or biomass after an initial start up period where biomass acclimates to the SOC and forms a biofilm. The service life of a bioreactor treating only biodegradable SOCs, therefore, would theoretically be infinite. A bioreactor (packed with non-adsorbent media) being fed a mixture of biodegradable and nonbiodegradable SOCs will, by definition, not be able to treat the nonbiodegradable SOC.

If the nonbiodegradable SOC can be cometabolized, however, both metabolism and cometabolism may take place. Segar *et al*. (1995) found some

difficulty in effectively employing both metabolism and cometabolism simultaneously. As a preliminary experiment, a biologically-active glass bead column was fed with phenol and TCE simultaneously; however, TCE removals only ranged between 0 to 20% and were sporadic, resulting in pseudo first order rate constants between 3 and 17 L/g TSS-d. Using computer modeling, it was estimated that the TCE rate constant needed for a reasonably sized reactor would be 100 L/g TSS-d. The low TCE removals in the glass bead column were attributed to competitive inhibition between phenol and TCE because when the same test was repeated without phenol present, TCE removal reached 40%. Low TCE removals in the glass bead column were also attributed to differences in metabolism and cometabolism rates. It was calculated that in order to achieve high TCE removals given its slow rate of cometabolism, the TCE flow rate should be 10 to 20 times slower than the phenol flow rate.

Competitive inhibition has a greater effect in continuous-flow applications than in batch applications (Anderson and McCarty, 1994). A greater inhibition effect occurs because there is a constant flux of chemical entering the column, so if competitive inhibition occurs, the TCE may never get cometabolized, compared to batch systems where TCE degradation would occur after toluene was significantly degraded.

An enhanced competitive inhibition effect or lack of enzyme production was seen in the findings of Cox *et al*. (1998). An influent concentration ratio of 3 mg toluene per mg TCE resulted in an insignificant amount of TCE degradation, despite the fact that a well-mixed, batch reactor system (Lu *et al*., 1998) with only

a slightly larger ratio (6.8 mg toluene per mg TCE) resulted in 96% TCE degradation. In addition, it has been theorized that biofilms in continuous-flow applications may contain less active biomass than in dispersed growth reactors (Arvin, 1991). The small amount of active biomass results from D.O. limitations in deeper layers of the biofilm whereas in batch systems both bacteria and D.O. are dispersed, avoiding the D.O. limiting conditions (Champagne *et al*., 1998).

To avoid competitive inhibition, Segar *et al*. (1995) used a sequencing biofilm reactor. In this setup, during two to three hours per day, rejuvenation occurred. During rejuvenation, a large concentration of phenol was fed to the bioreactor. After the rejuvenation period, the phenol influent concentration was dropped to zero, and only TCE degradation took place. Much better TCE removal was achieved using this setup: 70 to 90% at a hydraulic retention time of 14 minutes. This technology is only viable, however, if the water to be treated does not already contain the primary substrate.

In studies done by Folsom and Chapman (1991), some success was found with consistent TCE degradation. The maximum TCE degradation rate using phenol as a primary substrate was found to be 1.1 g /g protein-d (4.9×10^{-7} L/mg cells-d assuming protein to be 65% of cell weight) for a chemostat setup and 0.7 g/g protein-d (3.1×10^{-7} L/mg cells-d assuming protein to be 65% of cell weight) for a recirculating bioreactor. High ratios of influent phenol to TCE concentrations were used in these studies, but there was little evidence of competitive inhibition with the culture used. The kinetics of cometabolism can be on the order of 10 times slower than that for metabolism (Speitel and Segar,

1995), so it makes sense that the extent of TCE removal was found to increase with increasing reaction time (*i.e.*, recirculation), since long exposure times accommodate the slow kinetics of cometabolism. TCE removal also increased with increasing biomass.

There are several disadvantages, however, to treatment using biodegradation alone. The first is that it does not treat nonbiodegradable chemicals in any way. Furthermore, it does not give a back up treatment method during any startup or acclimation periods or during spikes of SOC concentrations when microorganisms may not be able to degrade a large amount of the incoming SOC mass (Shi *et al.*, 1995).

2.7 BIOLOGICAL ACTIVATED CARBON

GAC is often used in drinking water and ground water treatment to adsorb SOCs. Frequently, this GAC is home to an ecosystem of bacteria and protozoans due to its well-suited surface and macropores. The rough, pitted surface of GAC provides shelter from fluid shear forces; enriches substrates, nutrients, and oxygen concentrations; and contains functional groups that enhance the attachment of microorganisms (Weber *et al.*, 1978; Voice *et al.*, 1992). The microorganisms growing on the GAC surface can be used in the combined adsorption and biodegradation of SOCs.

There is a difference between simply *tolerating* bacteria inhabiting a GAC column and *encouraging* them to grow there in order to take full advantage of biodegradation as a treatment process (as in BAC columns). Speitel (1985)

presented five major design variables that affect bacterial growth in GAC columns. Contact time is an important parameter in that as it increases, there is more time for bacterial growth to occur before saturation of the GAC can occur. As discussed in Section 2.5, it is also important to keep the dissolved oxygen level high enough to maintain aerobic conditions so that growth is not hindered. Furthermore, it is advisable to adjust the temperature, pH, and nutrient (including metals) level to whatever is needed for the type of bacteria being encouraged to grow. Treatment processes that occur upstream, such as chlorination or ozonation, may have an effect on the biological growth within the GAC column. Chlorination may produce chlorinated chemicals that are more recalcitrant than the organic acids that tend to be produced by ozonation. Lastly, seeding a GAC column may be necessary if the goal is to treat recalcitrant chemicals or to hasten the onset time of biodegradation.

Much research has been done in recent years on bioregeneration (biodegradation of adsorbed SOCs) of GAC using only biodegradable chemicals (Chudyk & Snoeyink, 1984; Speitel & DiGiano, 1987; Speitel *et al*., 1987; Voice *et al*., 1992; Zhao *et al*., 1999). In this situation, only biodegradable chemicals are being adsorbed and biodegraded. After steady state has been reached, very little adsorption occurs due to biodegradation of the majority of the incoming chemical. Depending on the adsorption characteristics of the chemical, therefore, the service life of the GAC column could be indefinite.

In some instances, researchers have observed slower adsorption kinetics and decreased capacity due to biofilm development in GAC columns. Slower

adsorption kinetics may occur in BAC columns due to an increase in the mass-transfer resistance resulting from biofilm growth (Hutchinson and Robinson, 1990). In addition, microbial end products (MEPs) excreted from bacteria may irreversibly sorb to GAC, thereby decreasing the adsorption capacity over long periods of time (Zhao *et al*., 1999; Schultz and Keinath, 1984). Specifically, Olmstead (1989) found that as the biomass in a BAC column increased the Freundlich adsorption capacity, K, decreased; however, the Freundlich adsorption intensity, 1/n, was stable. If the GAC adsorption capacity is only used as a buffer during startup periods when microorganisms may not be able to degrade large amounts of the incoming SOC, this remaining GAC capacity may be sufficient without GAC replacement.

In investigations by Shi *et al*. (1995) and Voice *et al*. (1992) using fluidized bed reactors to degrade toluene, BAC columns were preferred to columns employing adsorption or biodegradation alone. During startup of a column, BACs employed adsorption as a back up treatment while the microorganisms acclimated to the substrate and attached to the GAC. In the case of columns using only biodegradation, there was no back up treatment, and so breakthrough occurred rapidly until a sufficient biofilm was formed. After the start up period, when steady state was reached, biodegradation became the main removal mechanism. In practice, variable influent concentrations may occur, including slugs of concentrated SOCs. Several studies (Voice *et al*., 1992; Shi *et al*., 1995; Chudyk and Snoeyink, 1984) have shown that BAC columns can handle these transient loading conditions more reliably and efficiently than

columns using either adsorption or biodegradation alone. Excess SOC is adsorbed during a pulse of concentrated SOC. When the influent concentration decreases again, the SOC is desorbed and biodegraded.

Previous studies on biologically-active GAC (BAC) columns treating only biodegradable chemicals have sought to describe the many factors that affect the rate and extent of bioregeneration. Bioregeneration can depend on the biodegradability of the SOC, the dissolved oxygen (D.O.) concentration, the SOC loading on the GAC, SOC adsorption characteristics, and location within the GAC column (Thacker *et al*. 1984, Chudyk and Snoeyink 1984, Speitel and DiGiano 1987, Speitel 1985, Lu 1989). Sufficient D.O. must be available to degrade not only the substrate present in the influent but also the substrate that desorbs off the GAC, or biodegradation may cease.

The SOC loading on the GAC and the Freundlich isotherm slope and sorption capacity also play important roles in bioregeneration. In general, as the loading and isotherm parameters increase, the driving force for SOC desorption off the GAC will increase, as will the rate and extent of bioregeneration. The driving force for desorption as manifested by concentration gradients within the GAC particles is critical, because beyond a short period after the onset of biodegradation, diffusive transport within the GAC controls the movement of SOCs to the bacteria on the external surface of the GAC. Conversely, small values of the Freundlich isotherm slope present the possibility of small concentration gradients and significant irreversible adsorption to the GAC, especially at low concentrations (Lu 1989, Li and DiGiano 1983, Speitel *et al*.

1989b). Obviously, bioregeneration would be impeded under such conditions. Bioregeneration may also vary temporally and spatially within a GAC column. Depending upon the point in its service life, a GAC column contains three zones of varying length: exhausted GAC, partially exhausted GAC (i.e., the mass transfer zone), and virgin GAC. Biological activity in the exhausted GAC zone holds by far the most promise for bioregeneration because the exhausted zone has the most potential for desorption and subsequent biodegradation of the sorbed, biodegradable SOC.

Speitel *et al*. (1987) presented research showing that the bioregeneration rate is also dependent upon the diffusive transport resistance in the GAC. A BAC column was used to treat low concentrations of phenol and paranitrophenol (PNP). The long-term bioregeneration rates were found to decrease according to homogeneous surface diffusion model predictions, which shows that diffusive transport in the GAC controls the substrate supply rate to the biofilm. Furthermore, findings by Li and DiGiano (1983), who used three different GAC particle sizes in infinite batch recycle, fluidized bed reactors, show the extent of GAC diffusive transport increases with decreasing particle size, as expected from mass transfer fundamentals.

Previous experimental and mathematical modeling research provides some limited insights into the behavior of BAC columns treating mixtures of biodegradable and nonbiodegradable SOCs. Mixtures of SOCs are more difficult to treat since each SOC may vary in its ability to be biodegraded or adsorbed. De Laat *et al.* (1985) compared BAC and sterile GAC columns treating two different

sets of biodegradable and nonbiodegradable chemicals. Findings were similar to that found for single chemical BAC columns. The key difference, however, was that as the biodegradable chemical was desorbed and biodegraded, the renewed adsorption sites became available for the nonbiodegradable chemical. This resulted in a reduction of both the biodegradable and nonbiodegradable chemical effluent concentrations. Because of the increased adsorption capacity for the nonbiodegradable chemical, complete breakthrough of the nonbiodegradable chemical occurred later than that for the sterile GAC column. Some breakthrough of the biodegradable chemical occurred in the BAC column during the startup period, when biomass was still acclimating and growing, but soon after the effluent concentration decreased to near zero as a stable biofilm was formed.

Similar results were found in another study by Speitel *et al.* (1989) in which biodegradable PNP and nonbiodegradable trichloroethylene (TCE) were treated using a BAC column. Pre-exhausted GAC columns were used along with radiochemical techniques for measuring $^{14}CO_2$ production from biological activity. PNP is much more adsorbable than TCE, however, thus TCE did not provide very much competition for adsorption sites. To realize the benefit of bioregeneration, it is important that the chemical(s) undergoing biodegradation provide a degree of competition for adsorption sites with non-biodegradable chemicals. Since competition tends to increase with increasing concentration, the very low solute concentrations used in this research probably provided a small degree of interaction between biodegradable and non-biodegradable chemicals.

Another condition that may affect the service life of a BAC column is the location of the non-specific enzymes along the length of the column. Since metabolism and cometabolism can only occur in the presence of the non-specific enzyme, their location indicates the zone of greatest SOC removal. The location of the non-specific enzymes within the column depends on their association with respect to the cell itself. The enzyme may be excreted by the cell, located in the cytoplasm, or located in the cell membrane. If the enzyme is excreted, it may adsorb onto the GAC or wash out of the column. If the enzyme is membrane-bound, the enzyme will only be available where there is biomass on the GAC. Given the amino acid sequence of toluene dioxygenase (Zylstra and Gibson, 1989), a predicted hydropathy plot was constructed which showed the toluene dioxygenase surface to be overall hydrophobic. Hydrophobic surfaces generally indicate a membrane-bound protein. However, toluene dioxygenase is composed of four subunits (tod A, tod B, todC1, tod C2), and only three of these subunits have overall hydrophobic surfaces. This fact may indicate a peripherally-associated membrane protein as opposed to an integral membrane protein.

2.8 FENTON'S OXIDATION

Another process that can be used to destroy SOCs is Fenton's oxidation, an abiotic reaction of ferrous iron and hydrogen peroxide. The chemistry of this reaction is complex in that several unstable oxidizing radicals are formed and some species are involved in subsequent propagation and termination reactions. Detailed reaction mechanisms and kinetics can be found in Tekin *et al.* (2002) and

Chen *et al*. (2001). A summary of the reactions that occur once ferrous iron and hydrogen peroxide react is shown in equation 2.8 through 2.13 (Kuo, 1992).

$$Fe^{2+} + H_2O_2 \rightarrow Fe^{3+} + OH^- + OH^\bullet \quad \text{(Eq. 2.8)}$$

$$Fe^{2+} + OH^\bullet \rightarrow Fe^{3+} + OH^- \quad \text{(Eq. 2.9)}$$

$$H_2O_2 + OH^\bullet \rightarrow H_2O + HO_2^\bullet \quad \text{(Eq. 2.10)}$$

$$Fe^{2+} + HO_2^\bullet \rightarrow Fe^{3+} + HO_2^- \leftrightarrow H_2O_2 \quad \text{(Eq. 2.11)}$$

$$Fe^{3+} + HO_2^\bullet \rightarrow Fe^{2+} + H^+ + O_2 \quad \text{(Eq. 2.12)}$$

$$Fe^{3+} + H_2O_2 \rightarrow Fe^{2+} + HO_2^\bullet + H^+ \quad \text{(Eq. 2.13)}$$

The hydroxyl radical, formed in equation 2.8, has the strongest oxidation capacity (Walling, 1975). Scavenging of the hydroxyl radical occurs with both the original reactants, ferrous iron and hydrogen peroxide, as shown in equations 2.9 and 2.10, so a balance must be struck between production and scavenging of hydroxyl radicals (Tang and Huang, 1996). The formation of oxygen as shown in equation 2.12 results in an increase of the D.O. content of the solution, which is often advantageous. The overall stoichiometry of Fenton's oxidation is shown in equation 2.14 (Turney, 1965).

$$2\ Fe^{2+} + H_2O_2 + 2\ H^+ \rightarrow 2\ Fe^{3+} + 2\ H_2O \quad \text{(Eq. 2.14)}$$

An important fact about the stoichiometry of equation 2.8 is that lowering the pH of the solution increases the production of hydroxyl radicals. Hydrogen ions will also scavenge hydroxyl radicals to form water, though, so once again care must be taken to balance production and scavenging of hydroxyl radicals (Tang and Huang, 1996).

Fenton's oxidation has been used to degrade a variety of organic chemicals, either as a treatment method in itself or as a treatment upstream of a biological process. Fenton's oxidation has been shown to have a preference for reaction with certain organic chemicals more than others. Augusti *et al*. (1998) researched degradation of benzene derivatives with Fenton's oxidation. The authors found toluene was less reactive than chlorobenzene and bromobenzene, but more reactive than nitrobenzene and phenol; having a rate constant of 3.1 x 10^{-2} min^{-1} at a pH of 3. The order of reactivity of the benzene derivatives indicated strong electron-withdrawing substitutions (such as OH) had a negative effect whereas strong electron donating substitutions (Cl, Br) had a positive effect. Tang and Huang (1996), however, found that increasing the chlorine content of unsaturated chlorinated compounds decreased their reactivity in Fenton's oxidation. Chen *et al*. (2001) researched the in situ application of Fenton's oxidation for TCE degradation. The TCE reaction rate at pH of 3 was found to be between 5.7 x 10^{-3} for aqueous solutions to 0.033 min^{-1} for soil slurries. Comparing the reaction rates for toluene and TCE found in these literature, it appears that toluene should be preferentially degraded over TCE, despite the strong electron donating nature of the chlorine substitutions on TCE.

Chen *et al*. (2001) also found in situ remediation using Fenton's oxidation problematic due to the soil-induced decomposition of hydrogen peroxide into oxygen gas. Furthermore, since Fenton's oxidation is an exothermic reaction, the temperature of the soil slurry was increased. The heat and gas resulted in

stripping of the TCE into the vapor phase, thus preventing oxidation of the TCE from occurring in the slurry.

The combination of batch GAC adsorption and Fenton's oxidation was researched by Huling *et al*. (2000) for above ground treatment. In this study, the GAC was pre-coated with iron oxide; hydrogen peroxide was then added which reacted with the iron on the GAC to induce Fenton's oxidation. Although hydrogen peroxide decomposed rapidly to oxygen gas in the presence of GAC, as was the case with soil, there was a larger driving force for adsorption of the contaminant onto the GAC than for stripping into the vapor phase. The authors found that the GAC acted to concentrate the contaminant in the vicinity of the production of the hydroxyl radical, an improvement over in-situ remediation. Oxidation of both sorbed and soluble 2-chlorophenol occurred in the GAC slurry, resulting in a regeneration of the GAC adsorption sites. Treatment efficiency of the 2-chlorophenol increased with increasing amounts of iron oxide and 2-chlorophenol sorbed on the GAC. Furthermore, sequential adsorption/oxidation cycles were not found to alter the GAC adsorption capacity.

Much research has been done utilizing Fenton’s oxidation (sometimes combined with UV radiation) as an above ground pretreatment to decrease the concentration and increase the biodegradability of recalcitrant chemicals being fed to biological treatment processes downstream (Lee and Carberry, 1991; Bin *et al*., 2000). This increase in biodegradability of treated wastes was evidenced by an increase in the ratio of biological oxygen demand to chemical oxygen demand (Ben Abderrazik *et al.*, 2002). Lee and Carberry (1991) found biodegradation

rates of TCE to be very slow with both a pre-selected culture and activated sludge. With pretreatment using Fenton's oxidation, however, biodegradation increased, with the highest biodegradation rates being realized at a molar ratio of 1:1 for hydrogen peroxide to TCE. Lin *et al*. (1998) reversed the order of treatment and used a biologically-active GAC column followed by treatment with Fenton's oxidation for photo processing waste. This reverse scheme allowed for the adjustment of pH after the biological process had occurred and for less hydrogen peroxide to be used; however, the advantage of the increase in biodegradability of the feed chemicals was lost.

Much Fenton's oxidation research has been done at a pH of 3 to balance the production and scavenging of hydroxyl radicals; however, a pH that low would inhibit surrounding microbial populations. Kastner *et al*. (2000) researched in-situ pre-treatment with Fenton's oxidation followed by biodegradation in a TCE and PCE-contaminated aquifer. After pre-treatment with Fenton's oxidation, the pH of the groundwater in the aquifer decreased from 5 to 2.4. The groundwater pH then gradually rose again to 3.4 after approximately 1.5 years due to the buffering capacity of the surrounding soil. Microbial growth was then stimulated in-situ by adding either methane or phenol as a carbon substrate; however, this addition resulted in only limited growth compared to control cultures at a pH of 4.9. The authors concluded that microbial growth was inhibited by the low pH created by the Fenton's reactions and suggested that to minimize detrimental microbial effects, a higher pH and a lower hydrogen peroxide concentration should be used. For optimum microbial growth, a neutral

pH and hydrogen peroxide to TCE molar ratios of 22 to 878:1 (1.5 – 5.6 mg/L H_2O_2) were used in the current research.

2.9 BAC COLUMN MODELING

Computer models have been created to predict bioregeneration in BAC columns treating mixtures of biodegradable and nonbiodegradable chemicals. One such model is the biodegradation/adsorption screening model (BASM); a two-component equilibrium-based model developed by Erlanson *et al*. (1997). By considering only equilibrium situations in BAC columns, the modeling becomes much simpler compared to that of kinetic models. BASM is based on the Equilibrium Column Model (Crittenden *et al*., 1987) which describes equilibrium conditions for competitive adsorption. The BASM model was verified using data from DeLaat *et al*. (1985). The model successfully predicted the timing and duration of peaks and dips in the effluent concentration profiles of both sterile and BAC columns treating a mixture of biodegradable and nonbiodegradable chemicals. To determine which adsorption-only situations could possibly benefit by employing simultaneous biodegradation and adsorption, several hundred hypothetical situations were modeled. With respect to the nonbiodegradable chemical, significant increases in the GAC service life, up to 1.5 times that for adsorption alone, occurred when both the biodegradable and nonbiodegradable chemicals were of similar adsorbabilities. The similar adsorbability of the two chemicals led to competition for adsorption sites on the GAC; thus, when the biodegradable chemical was removed via biodegradation,

less competition existed for the adsorption of the nonbiodegradable chemical. For the case where the nonbiodegradable chemical is less adsorbable than the nonbiodegradable chemical, and thus controls the service life of a GAC column, significant gains in the service life, 1.2 – 7 times that for adsorption alone, were predicted.

A kinetic model was developed by Speitel *et al*. (1989a) that describes both adsorption and biodegradation in multi-component GAC columns. This model is referred to as the MDBA (Multiple component, biofilm Diffusion, Biodegradation, and Adsorption) model. The MDBA model combines a single-component adsorption and biodegradation model developed by Speitel *et al*. (1987) with IAST to account for multi-component adsorption. The IAST equation was adjusted using a correction factor, P, to account for differences between predicted and measured equilibrium (Thacker *et al.*, 1984; Smith and Weber, 1988).

In the model, mass balances are done for three phases: GAC, biofilm, and liquid. Figure 2.8 illustrates these phases and shows diffusion of substrate into a microorganism-covered GAC particle (Zhu, 1987). In the model, homogeneous surface diffusion is assumed, so the pore diffusion shown in Figure 2.8 is considered insignificant. The mass balance on a GAC particle is shown in equation 2.15.

$$\frac{\partial q_i(r,x,t)}{\partial t} = \frac{D_{s,i}}{r^2}\frac{\partial}{\partial r}\left[r^2\frac{\partial q_i(r,x,t)}{\partial t}\right] \qquad \text{(Eq. 2.15)}$$

where x is the axial coordinate along the GAC column, t is time, $D_{s,i}$ is the surface diffusivity for component i in the GAC particle, r is the radial coordinate across

the GAC particle, and the remainder of the variables are defined in the IAST discussion in section 2.3.

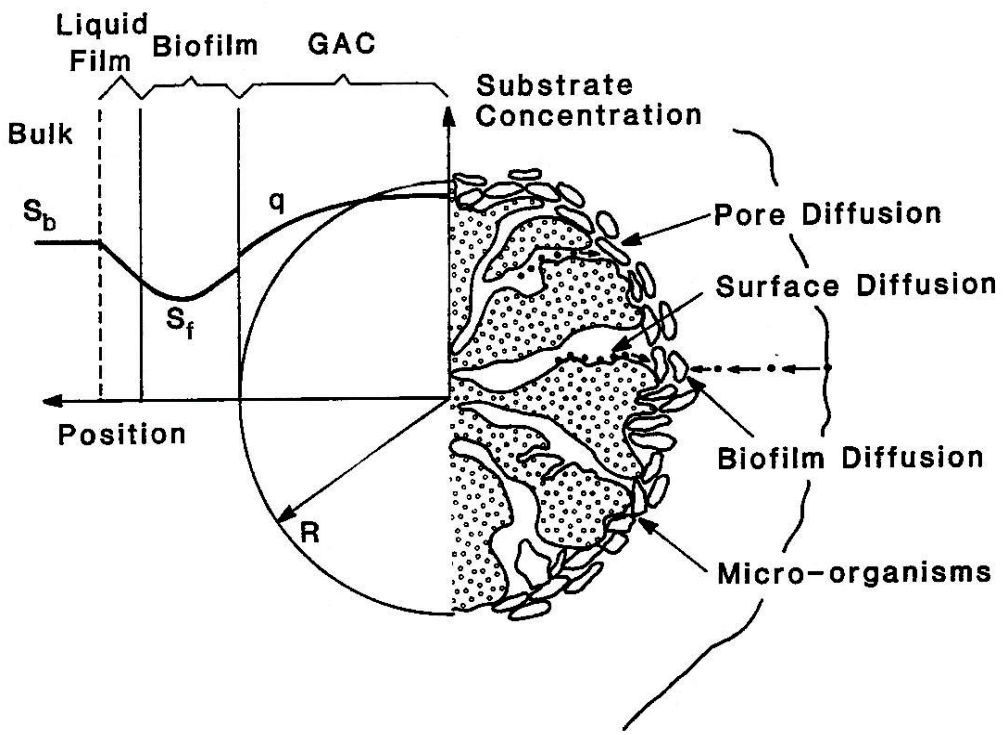

Figure 2.8 Diffusion of Substrate Into a Microorganism-Covered GAC Particle (Zhu, 1987)

Boundary conditions for the GAC mass balance are (1) symmetry of the concentration profile around the GAC particle midpoint (equation 2.16) and (2) equality of the biofilm and GAC interface mass transport rates (equation 2.17). Equation 2.18 presents the initial condition.

$$\frac{\partial}{\partial r} q_i(r=0, x, t) = 0 \qquad \text{(Eq. 2.16)}$$

$$D_{f,i} \frac{\partial}{\partial z} C_{f,i}(z=0,\ x,\ t) = \frac{\rho_a}{R^2} \frac{\partial}{\partial t} \int_0^R q_i(r, x, t)\, r^2\, dr \qquad \text{(Eq. 2.17)}$$

$$q_i\,(r,\ x,\ t=0) = q_{io} \qquad \text{(Eq. 2.18)}$$

where $D_{f,i}$ is the diffusivity for component i in the biofilm, $C_{f,i}$ is the concentration of component i in the biofilm, z is the position coordinate across the biofilm thickness and z = 0 at the GAC interface, ρ_a is the apparent density of the GAC, and R is the GAC particle radius.

This model also assumes (1) Monod kinetics and (2) that biodegradation of more than one substrate occurs simultaneously, which aids in simplifying the model. The biofilm mass balance is shown in equation 2.19.

$$\frac{\partial C_{f,i}(z,\ x,\ t)}{\partial t} = D_{f,i}\ \frac{\partial^2 C_{f,i}(z,\ x,\ t)}{\partial z^2} - \frac{k_i\ X_f\ C_{f,i}(z,\ x,\ t)}{K_{s,i}\ + C_{f,i}(z,\ x,\ t)} \qquad \text{(Eq. 2.19)}$$

where k_i is the maximum specific substrate utilization rate for component i, X_f is the biomass concentration in the biofilm, and $K_{s,i}$ is the half-saturation coefficient. For nonbiodegradable components, k_i is set to zero, resulting in equation 2.19 accounting solely for diffusion. The boundary conditions for the biofilm mass balance are shown in equation 2.17 and equation 2.20. Equation 2.21 presents the initial condition.

$$D_{f,i}\ \frac{\partial}{\partial z}\, C_{f,i}(z = L_f\,,\ x,\ t) = k_{f,i}\ \left[C_{b,i}(x,\ t) - C_{f,i}(z = L_f\,,\ x,\ t)\right] \qquad \text{(Eq. 2.20)}$$

$$C_{f,i}(z,\ x,\ t = 0) = C_{b,io} \qquad \text{(Eq. 2.21)}$$

where L_f is the biofilm thickness, $k_{f,i}$ is the liquid film transfer coefficient for component i, $C_{b,i}$ is the concentration of component i in the bulk liquid phase, and $C_{b,io}$ is the initial concentration of component i in the bulk liquid phase. Furthermore, the equation describing the biofilm thickness along the column as a function of time is shown in equation 2.22.

$$\frac{\partial L_f(x,t)}{\partial t} = (1 - b'_s)\sum_{i=1}^{N}\left[k_i Y_i \int_0^{L_f} \frac{C_{f,i}(z,x,t)}{K_{s,i} + C_{f,i}(z,x,t)}\,dz\right] - k_d L_f(x,t) \qquad \text{(Eq. 2.22)}$$

where b'_s is the biological biofilm shearing coefficient, Y_i is the yield coefficient for component i, and k_d is the overall biofilm loss coefficient.

The mass balance for the bulk liquid phase is shown in equation 2.23.

$$\frac{\partial C_{b,i}(x,t)}{\partial t} = -\upsilon\frac{\partial C_{b,i}(x,t)}{\partial x} - \frac{3k_{f,i}(1-\varepsilon_b)}{\varepsilon_b R}\left[C_{b,i}(x,t) - C_{f,i}(z = L_f, x, t)\right] \qquad \text{(Eq. 2.23)}$$

where ε_b is the GAC column porosity and υ is the interstitial fluid velocity. The boundary and initial conditions are shown in equation 2.24 and 2.25, respectively.

$$C_{b,i}(x = 0, t) = C_{io} \qquad \text{(Eq. 2.24)}$$

$$C_{b,i}(x, t = 0) = C_{b,io} \qquad \text{(Eq. 2.25)}$$

where C_{io} is the influent concentration of component i.

Model predictions were tested using exhausted BAC columns simultaneously treating PNP (biodegradable) and TCE (assumed to be nonbiodegradable under the experimental conditions). Fairly good correlation was found between predicted and measured effluent concentrations, although 3 of the 24 input parameters were assigned a value based on goodness-of-fit of the model predictions to the measured concentrations. The remaining input parameters were measured in the laboratory or calculated.

2.10 COMETABOLISM MODELING

To extend the multi-component adsorption and biodegradation model to account for cometabolism instead of just metabolism, it may be necessary to account for enzyme competition and intermediate toxicity, although incorporating the latter concept may make the model too complex to be of practical use. To account for enzyme competition, it is necessary to alter the independence of the chemical degradation rates from one another. This assumption is not valid in the case of enzyme competition since there is interaction between the biodegradable and traditionally nonbiodegradable chemical for the non-specific enzymes that initiate biodegradation, commonly resulting in the biodegradable chemical being degraded before the traditionally nonbiodegradable chemical. A rate expression would have to be created that accounted for this delay in cometabolism.

In order to explore mathematical modifications that may be necessary to properly model cometabolism in multi-component BAC columns, cometabolism-only models were investigated. Many cometabolism models have been developed, and the characteristics of several selected models are shown in Table 2.4. The major factors to be considered to model cometabolism are the reactor type (*i.e*. batch or continuous-flow), enzyme competition, intermediate toxicity, reducing power availability, and endogenous cell decay. If the reactor is continuous-flow, such things as the biofilm thickness, biofilm diffusion, and external diffusion (between bulk liquid and the biofilm) also become important. Inclusion of reducing power availability or intermediate toxicity add complexity

Table 2.4 Characteristics of Reviewed Cometabolism Models

	Model					
Component	1	2	3	4	5	6
Biofilm Thickness	N/A	N/A	N/A	N/A	Fixed	Variable
Biofilm Diffusion	N/A	N/A	N/A	N/A	Yes	Yes-pseudo-steady state
External Diffusion	N/A	N/A	N/A	N/A	Yes	Yes
Competitive Inhibition	No	Yes	Yes	Yes	Yes	Yes
Product Toxicity to Cell	Yes	Yes	Product toxicity to enzyme	Yes	Yes	Yes
Endogenous Decay	Yes	Yes	No	Yes	Yes	Yes
Reducing Power	No	Enhanced deg. rate w/ NADH	No	Limiting NADH condition	Yes	No
Reactor Description	Batch, resting cells	Batch, resting & growing cells	Fed-batch, resting & growing cells	Batch, resting & growing cells	CSTR-biofilm, resting & growing	Biofilm, resting & growing cells
Verification of Model	TCE	*Resting cells**: Toluene & p-xylene *Growing cells*: TCE & methane	TCE & NH_3	TCE, methane, propane, toluene, & phenol	None	Compared to published data**

1: Alvarez-Cohen and McCarty (1991)
2: Criddle (1993) & Chang & Criddle (1997), *data from Chang *et al*. (1993)
3: Ely *et al*. (1995)
4: Chang and Alvarez-Cohen (1995a)
5: Champagne *et al*. (1998)
6: Anderson and McCarty (1994), **published data from Arvin (1991)
N/A = not applicable

to cometabolism models. For purposes of creating a multi-component biodegradation and adsorption model that includes cometabolism, it appears that model 6 (Anderson and McCarty, 1994) is the best to combine with the previous multi-component biodegradation and adsorption kinetic model from Speitel *et al*. (1989a). Model 6 includes all the major components except reducing power availability and has been structured to simulate a continuous-flow reactor. Model 6 assumes there are three types of biomass (but does not include a sloughing coefficient, unlike the multi-component biodegradation and adsorption kinetic model):

X_m = active biomass

X_s = secondary biomass; includes biomass that has been made inactive due to intermediate toxicity from cometabolism, other species that might be present in the mixed culture but do not degrade the chemicals of interest, and cellular decay products

X_i = inert cell material; includes any nonbiodegradable cell decay material

Only X_m plays a role in cometabolism. The equations describing substrate and cometabolite concentrations as a function of time are based on the Monod equation but include enzyme competition:

$$\frac{dS}{dt} = -\frac{k_s\ X_m\ S}{S + K_s\left(1 + \frac{C}{K_c}\right)} \qquad \text{(Eq 2.26)}$$

$$\frac{dC}{dt} = -\frac{k_c\ X_m\ C}{C + K_c\left(1 + \frac{S}{K_s}\right)} \qquad \text{(Eq 2.27)}$$

where S is the primary substrate concentration, C is the cometabolite concentration, k_s and k_c are the substrate maximum utilization rates for the primary substrate and cometabolite, respectively, and K_s and K_c are the half-saturation coefficients for the primary substrate and cometabolite, respectively. To account for intermediate toxicity in Model 6, the transformation capacity (T_c) was measured. The transformation capacity is the maximum mass of TCE that can be cometabolized per mass of biomass inactivated, and thus measures the capacity of cells for TCE cometabolism before intermediate toxicity becomes overwhelming. X_m depends on the amount of cell growth from metabolism, the amount of inactivation from intermediate toxicity (incorporating T_c), the amount of secondary biomass growth at the expense of active biomass, and the endogenous decay rate. X_s increases with intermediate toxicity inactivation of X_m and with growth at the expense X_m, and decreases with endogenous decay. X_i depends on the nonbiodegradable fraction of endogenous decay products of X_m and X_s.

$$\frac{dX_m}{dt} = Y\left(-\frac{dS}{dt}\right) - \frac{1}{T_c}\left(-\frac{dC}{dt}\right) - b_i X_m - b_d X_m \qquad \text{(Eq. 2.28)}$$

$$\frac{dX_s}{dt} = \frac{1}{T_c}\left(-\frac{dC}{dt}\right) + b_i X_m - b_d X_s \qquad \text{(Eq. 2.29)}$$

$$\frac{dX_i}{dt} = (1 - f_d) b_d (X_m + X_s) \qquad \text{(Eq. 2.30)}$$

where Y is the yield, b_i is the fraction of the secondary biomass that is produced at the expense of the active biomass (may be more applicable in with methanotrophs than with *Pseudomonas* sp.), b_d is the endogenous decay coefficient, and f_d is the

degradable fraction of the cellular decay products (usually equal to 0.8 in real systems).

Equations 2.26 through 2.30 are the key equations that should be substituted into the biomass mass balances in the multi-component biodegradation and adsorption kinetic model (the GAC mass balance would remain the same) in order to account for cometabolism in BAC columns. The overall biomass density is assumed to be constant in Model 6, so that any changes in biomass concentration are translated into changes in biofilm thickness.

2.11 SUMMARY

Given the background material presented in this chapter, it is apparent that a gap in the knowledge exists regarding simultaneous metabolism and cometabolism in BAC columns. This research addresses the significance of both metabolism and cometabolism for increasing GAC service life, the influence of chemical adsorbability and column penetration on cometabolism, the significance of enzyme competition and intermediate toxicity in limiting the rate of cometabolism, the significance of adding Fenton's oxidation for increasing GAC service life, and the ability of metabolism-based BAC models to account for cometabolism. The next chapter presents the materials and methods used in conducting this research. Following the materials and methods chapter, experimental background and column results are presented along with a discussion of trends and significance. The last chapter presents MDBA modeling results for pre-equilibrated and virgin BAC column experiments.

Chapter 3: Materials and Methods

3.1 EXPERIMENTAL PROCEDURES

This section describes the experimental procedures used in activated carbon adsorption experiments, biodegradation experiments, and biological activated carbon columns treating either toluene and perchloroethylene (PCE) or toluene and trichloroethylene (TCE). As explained in the previous chapter, toluene is biodegradable, PCE is nonbiodegradable, and TCE is traditionally nonbiodegradable SOC. Procedures for GAC extractions are also presented.

3.1.1 Activated Carbon Adsorption and Desorption

Individual activated carbon adsorption isotherms were measured for each SOC. Competitive adsorption isotherms were also run for each pair of biodegradable and traditionally nonbiodegradable SOCs. Competitive adsorption isotherms were measured in order to compare IAST predicted competitive behavior to actual experimental behavior. All isotherms used Calgon F-400 granular activated carbon ground to 200 x 350 mesh (powdered activated carbon, PAC) and were conducted using the bottle-point method (Randtke and Snoeyink, 1983). Each bottle was injected with identical amounts of SOC stock solutions but contained varying masses of activated carbon. This procedure resulted in a different equilibrium concentration in each bottle. Bottles were agitated end-over-end for two weeks on a rotary mixer to achieve equilibrium. The equilibration time was chosen to balance the time needed for adsorption with the prevention of bacterial contamination. An equation combining both the surface

and pore diffusion control of adsorption estimated that less than two days was needed for both toluene and TCE to reach equilibrium, depending on the initial concentration (Sontheimer *et al*., 1988). Thus, 14 days was used to ensure adsorption equilibrium. Equilibrium concentrations were then measured with a gas chromatograph (GC) after filtration with a 0.45-µm Osmonics cellulose nitrate filter.

In addition, GAC desorption and adsorption continuous-flow column experiments were run with toluene and TCE. The ability for toluene and TCE to be desorbed from activated carbon is important, because if the SOC is irreversibly adsorbed, bioregeneration of adsorption sites cannot take place. To run the desorption experiment, Calgon F-400 activated carbon (30 x 40 mesh) was first exhausted by mixing the GAC with the appropriate concentration of toluene and TCE in a headspace-free bottle that was agitated end over end for two weeks until equilibrium was reached. This exhausted GAC was then packed into a glass column and fed sterile, buffered water. Subsequently, effluent toluene and TCE concentrations were measured.

3.1.2 Biodegradation Kinetic Parameters Methodology

Toluene-degrading bacteria used in this research consisted of a mixed culture of *Pseudomonas sp.* and *Rhodococcus rhodochrous* donated from Micro-Bac International, Inc. (Round Rock, TX), and Dr. Kerry Kinney in the Civil Engineering Department at the University of Texas at Austin, respectively. Two batches of this culture were maintained: one free of iron, and one containing 40 µM total iron. Each batch was fed 15 mg/L toluene every four days. The batches

were kept at room temperature on a New Brunswick Scientific R2 platform shaker. Both batches were fed nutrients resulting in final concentrations as shown in Table 3.1. When used in an experiment, the cultures were harvested between 13.6 and 14.5 hours after feeding, approximately at the end of the exponential growth phase. The harvested culture was then purged with air to volatilize any remaining toluene from solution.

Table 3.1 Nutrient Concentrations for Batch Microbial Growth

Nutrient	**Concentration (mg/L)**
KH_2PO_4	360
K_2HPO_4	450
KNO_3	200
$CaCl_2$	23
$MgSO_4$	8.6

Batch biodegradation experiments utilizing ^{14}C-radiolabeled substrates were conducted in a stirred, 250-mL, headspace-free, gas-tight syringe using the toluene-acclimated mixed culture. Either ^{14}C-toluene or ^{14}C-TCE was used as the substrate, depending on the experiment. Radioactive toluene was uniformly ring-labeled to assure that $^{14}CO_2$ produced was from degradation of the whole compound as opposed to just the attached methyl group. Radioactivity in disintegrations per minute (dpm) was measured using a liquid scintillation counter (Beckman LS 5000TD) using the method described in Section 3.3.2. Samples were taken to measure the $^{14}CO_2$, ^{14}C-biomass, ^{14}C-non-purgeable degradation products (NPPs), and ^{14}C-substrate over time. Four, 5-mL effluent samples were

taken and placed in 20-mL borosilicate glass scintillation vials (Fisher Scientific) during each sampling time:

1. Total: sample injected into 10 mL of either ScintiVerse II or ScintiSafe 50% scintillation cocktail (Fisher Scientific). Both cocktails were designed for samples with high water content.
2. Acid: sample injected into 20 µL of 6N HCl (to reach a sample pH of ≤ 2 so that any inorganic carbon was in the volatile form), then purged with N_2 gas at 65 mL/min for 6 min to remove the inorganic carbon as well as any remaining substrate, then mixed with 10 mL of scintillation cocktail.
3. Base: sample injected into 300 µL of pH 12 CarboSorb II (Packard Instrument) solution (to reach a sample pH of 10.5 -11 so that any inorganic carbon was in the nonvolatile form (CO_3^{2-})), then purged with N_2 gas at 65 mL/min for 6 min, then mixed with 10 mL of scintillation cocktail. CarboSorb II is an organic amine that reduces chemiluminescence during scintillation counting.
4. Filter: sample expelled onto a 0.45-µm Osmonics cellulose nitrate filter in a vacuum flask, then the filter was rinsed with 15 mL of 50% ethanol solution (which removed any residual substrate or intermediates), then the filter was removed and placed in 10 mL of scintillation cocktail

These samples then were run with a blank vial containing only 10 mL of scintillation cocktail to correct for background radiation. This method allowed for the determination of the yield coefficient, the half saturation coefficient, and the maximum substrate utilization rate as described in Speitel (1985) and Speitel and DiGiano (1988).

In addition, endogenous decay experiments were run with both the iron-free and iron-containing batches. Endogenous decay occurs when, due to a lack of growth substrate, the cells in a culture die off and are metabolized by the surviving cells. Endogenous metabolism produces CO_2 as an end product. This CO_2 production must be distinguished from the CO_2 production from growth substrate metabolism in order to properly compute the extent of bioregeneration in column studies. Endogenous decay was measured by first feeding ^{14}C-toluene to both the iron-free and iron-containing batches of the mixed culture. The ^{14}C-toluene was then metabolized and the radiolabeled carbon was incorporated into the cell components, resulting in ^{14}C-cells. After a sufficient mass of ^{14}C-cells was grown, the cells were harvested and purged of any remaining toluene. Subsequently, the endogenous decay experiments were conducted in the same manner as the batch biodegradation experiments except that no substrate was provided, thus resulting in starvation of the culture. This method allowed for the determination of the endogenous decay coefficient and the biomass carbon fraction converted to CO_2, as described in Speitel (1985) and Speitel and DiGiano (1988).

Another biodegradation parameter, the transformation capacity (T_c), was measured to account for possible intermediate toxicity. The transformation capacity is the maximum mass of TCE (or other traditionally nonbiodegradable chemical) that can be cometabolized per mass of biomass inactivated, and thus measures a microbial culture's capacity for TCE cometabolism before toxic degradation intermediates become overwhelming. The experimental setup for

transformation capacity experiments was the same as for batch TCE biodegradation experiments (with no toluene present) except that much larger initial concentrations were used. Samples were taken to measure the remaining TCE concentration until the TCE concentration no longer decreased, indicating inactivation of the cells or enzymes. The difference between the initial and final TCE concentrations was divided by the concentration of cells to arrive at the transformation capacity. The use of a large initial concentration was necessary to avoid transformation of all the TCE in solution, because total TCE transformation does not allow for determination of culture inactivation. The cometabolism rate can decrease from other causes besides intermediate toxicity; therefore, it was also necessary to measure the dissolved oxygen and NADH concentrations to make sure that neither was limiting. The duration of transformation capacity experiments was minimized as much as possible to avoid significant cell inactivation due to endogenous decay.

3.1.3 Exhausted and Virgin GAC Column Methodology

For column studies, a large amount of sterilized, buffered, nutrient water was needed to maintain the desired flow rate. Although autoclaving provides an easy means to this end, precipitation of some nutrients can occur under the high temperature and pressure environment. In addition, the autoclave was not capable of autoclaving the required volume of water in the time needed. Thus, sterilization was achieved by ozonation using the methods of Lu (1989). Before ozonation, a 45-L glass carboy was filled with distilled, deionized water combined with a nutrient stock, resulting in the final concentrations shown in

Table 3.2. These nutrient concentrations differ from those in Table 3.1 for microbial growth only in the amount of nitrate added. The amount of nitrate was reduced for column studies to avoid excessive microbial growth and subsequent plugging of the columns. After the nutrient solution was prepared, a Welsbach T-816 ozonator was used to feed approximately 1 L/min of ozone to the solution via a stainless steel diffuser. Given the hazardous nature of ozone, effluent gases from the carboy were fed to a solution of potassium iodide, which reacted with the ozone to form potassium iodate and oxygen. Ozonation of the nearly full 45-L carboy occurred for 8 hours, followed by 8 hours of purging of remaining ozone using GAC/cotton-filtered air. Purging was an important step because any ozone remaining in solution may react with SOCs in the feed water.

Table 3.2 Nutrient Concentrations for Column Studies

Nutrient	**Concentration (mg/L)**
KH_2PO_4	360
K_2HPO_4	450
KNO_3	20
$CaCl_2$	23
$MgSO_4$	8.6

For simplicity, each exhausted BAC column experiment involved one biodegradable (toluene) and either one nonbiodegradable SOC (PCE) or one traditionally nonbiodegradable SOC (TCE). A diagram of the experimental setup is shown in Figure 3.1. Adsorptive and volatile losses were minimized by using only glass, stainless steel, and Teflon throughout the system as described in Losh

(2001). The 1.5-cm diameter glass columns were packed with pre-exhausted 30x40 mesh Calgon F400 GAC (0.52-mm average diameter) and seeded with the toluene-acclimated culture. The column diameter divided by the GAC particle diameter resulted in a ratio of 30, which was larger then the minimum needed to avoid wall effects (Rose, 1951). The GAC used to pack the column was exhausted in the same manner as the GAC used in the desorption column study described in Section 3.1.1.

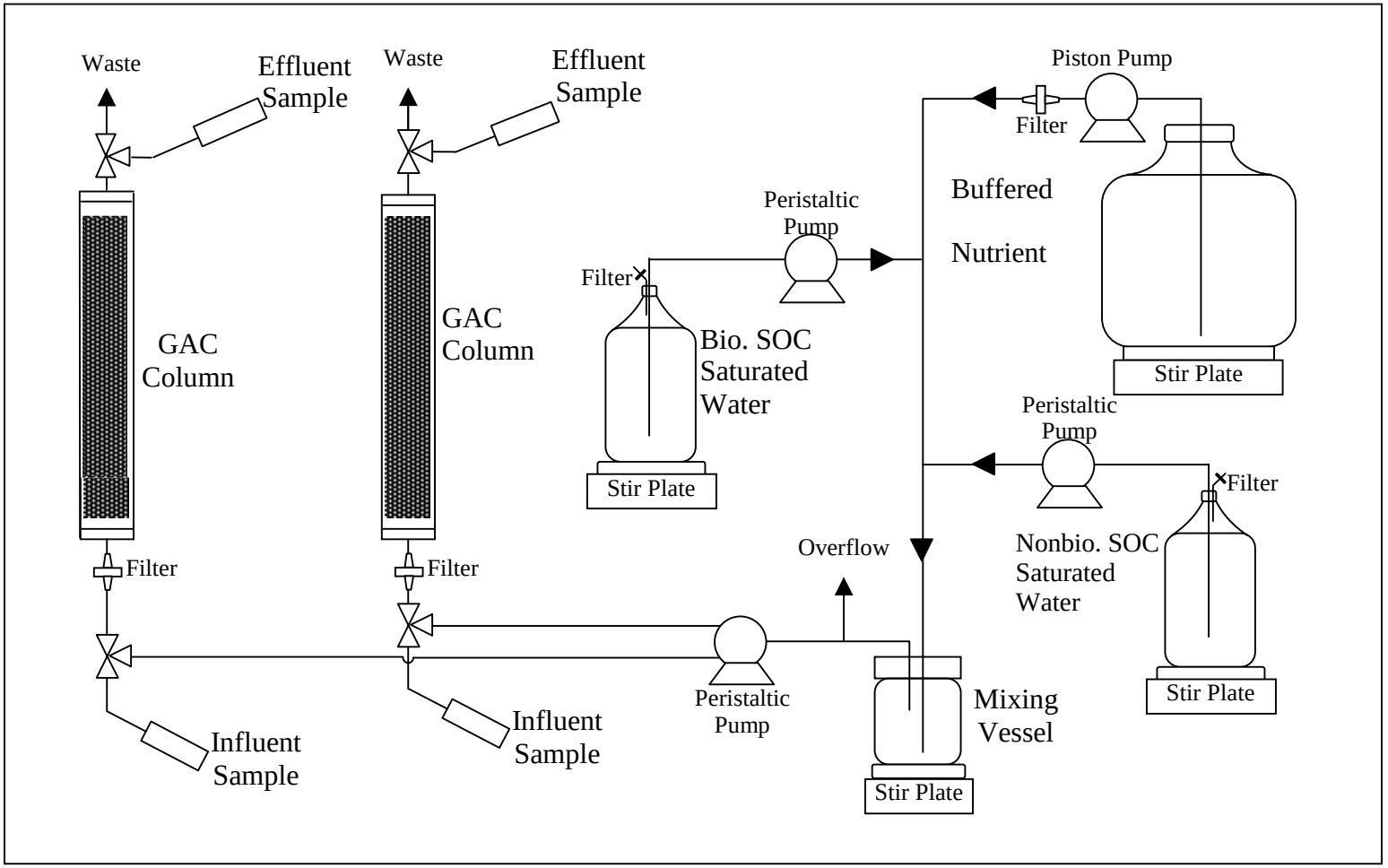

Figure 3.1 Experimental Column Setup

In addition, in-line 0.2-µm filters (Whatman polydisc AS, 50-mm diameter) were used at two locations to help maintain sterility in the influent system. Either hydrogen peroxide (less than 0.1% by volume) or oxygen gas was then added to the ozone-sterilized, buffered, nutrient water to maintain a sufficiently high dissolved oxygen level in the GAC columns. Toluene and TCE were pumped from bottles containing water saturated with toluene or TCE (with a neat layer still visible), respectively, and mixed with the buffered nutrient water in the mixing vessel. In some experiments, iron sulfate dissolved in 1 mM sulfuric acid was then added (at 0.3% of the total flow rate) using a peristaltic pump prior to entering the packed column. The overall flow rate pumped to the column was usually 2.0 to 2.5 mL/min. Furthermore, in most exhausted GAC experiments, the traditionally nonbiodegradable SOC influent concentration was maintained at or above the equilibrium concentration of the exhausted GAC; thus, any decrease in traditionally nonbiodegradable SOC effluent concentrations could only be due to metabolism or cometabolism-based bioregeneration.

In some exhausted GAC column experiments, a portion of either the toluene or TCE adsorbed at the effluent end of the GAC column was ^{14}C-radiolabeled to allow measurement of bioregeneration through the production of $^{14}CO_2$ from either metabolism or cometabolism of the adsorbed SOC. As either metabolism or cometabolism decreased the liquid phase SOC concentration, a driving force occurred for desorption of the radiolabeled SOC off the GAC, and degradation of the desorbed SOC ensued. Metabolism or cometabolism of the

radiolabeled SOC resulted in $^{14}CO_2$ production that was measured using a liquid scintillation counter.

The location of the radiolabeled GAC element within the column has an effect on the extent of bioregeneration that is measured (Speitel, 1985). The radiolabeled element was placed at the effluent end of the column so that effluent sample concentrations would be representative of the liquid phase concentration in the radiolabeled element and so that the maximum possible bioregeneration rate could be determined (the liquid phase concentration should be lowest at the column end). Placement of the radiolabeled element upstream of the column end could have resulted in sorption of the radiolabeled SOC downstream, thus confounding the interpretation of radioactive measurements. During these experiments, effluent samples containing radioactive toluene and TCE were taken over time. Four, 5-mL effluent samples were taken during each sampling time using the same procedure as for batch kinetic experiments in Section 3.1.2. With a detailed mass balance analysis of the radiochemical data, the rate and extent of metabolism or cometabolism-based bioregeneration over time was estimated for the portion of the GAC column containing the radiolabeled element (Speitel, 1985; Speitel and DiGiano, 1987; Lu, 1989). $^{14}CO_2$ formation is the principal input to these calculations, but consideration of cell production, endogenous metabolism, and radiolabeled substrate leaving the GAC column is required to develop an accurate estimate of bioregeneration (see Appendix A).

In the case of the virgin BAC columns, the experimental set up was the same as in Figure 3.1, except that fresh (unspent) GAC was used to pack the

column and the experiments were run for a longer period. Also, due to the high level of molecular exchange of sorbed radiolabeled TCE with unlabeled TCE in the bulk liquid observed in the exhausted GAC experiments, only radiolabeled toluene was used in virgin BAC columns. High levels of equilibrium exchange are problematic because they confound the interpretation of bioregeneration data. The GAC in the virgin columns was not pre-equilibrated; thus the radioactive SOC had to be provided in a manner other than pre-equilibration. Instead, radiolabeled toluene was fed in the column influent for a short period at the beginning of the experiment until $^{14}CO_2$ was measurable in the effluent. The presence of $^{14}CO_2$ in the effluent indicated that cell growth, and thus toluene biodegradation, had become significant in the column. The column was fed radiolabeled toluene at the beginning of the experiment; therefore, the main portion of the column that had radiolabeled toluene sorbed to the GAC was the influent end, not the effluent end as in the exhausted column experiments.

In all but one virgin BAC experiment, the GAC was pre-loaded with iron in one column and acid washed (to remove any iron that naturally occurred in the GAC) in a second column. Pre-loading the GAC with iron was an alternate method to feeding iron to the column, because iron feeding often resulted in precipitation of iron as $Fe(OH)_3$ which plugged the column. Pre-loading iron onto the GAC was achieved using a modification of the method presented in Huling *et al*. (2000): 0.35 g of $FeCl_3 \bullet 6H_20$ was added to a phosphate buffered solution in a sterile 40-mL glass screw-cap septum vial (Pierce Chemical Co.) at a ratio of 0.35 g of $FeCl_3 \bullet 6H_20$ to 20 mL of solution. 3 N NaOH was then added to bring the pH

to neutral and pure O_2 gas was added to the headspace to maintain an oxygen-rich environment so that Fe(III) (greenish color) rapidly precipitated as the orange-red colored $Fe(OH)_3$. Subsequently, 1 g of GAC was added to the solution followed by more pure O_2 gas. This mixture was then shaken on a New Brunswick Scientific R2 platform shaker for 24 hours and rinsed with sterile phosphate buffer. A small amount of Fe-loaded GAC was sampled in order to measure the resulting iron loading (see Section 3.3.3) and the rest of the GAC was used to pack the column. The mass of GAC used for iron analysis was dried and weighed afterwards to determine by difference the total amount of GAC used to pack the column.

This pre-loading method maintained a neutral pH and high D.O. environment, allowing for $Fe(OH)_3$ adsorption. Maintenance of iron in the $Fe(OH)_3$ form was important because Fe(II) and Fe(III) ions could undergo redox reactions with the functional groups on the surface of the GAC (Uchida *et al*., 2000; Ahumada *et al*., 2002) such that the ability of the GAC to adsorb organic chemicals was changed. Fe(II) and Fe(III) ions, however, may adsorb onto the GAC to a higher extent than $Fe(OH)_3$. A combination of low pH and low D.O. results in a stable environment for Fe^{2+} ions, instead of driving a reaction with OH^- ions to form $Fe(OH)_{3(s)}$. It is important to follow all the steps of the iron pre-loading method to avoid the creation of a stable environment for Fe^{2+} ions. The addition of GAC to the phosphate buffer without pure O_2 gas in the headspace lowers the D.O. level of the solution, creating an environment for Fe^{2+} ions. The

addition of iron salts to this slurry without adding a base decreases the pH to an acidic range, also creating an environment for Fe^{2+} ions.

Some Fe-loading methods also involve baking the iron-GAC mixture between 90 and 105°C to better adhere the iron onto the GAC (Edwards and Benjamin, 1989; Reddy, 1994; Na *et al*., 2002). Baking was not done in this case due to the desire to maintain relatively similar conditions compared to columns that had iron fed in the influent.

The method for acid-washing GAC to desorb iron was similar to the Fe-loading method. Uranowski *et al*. (1998) found no impact on GAC adsorption due to acid washing. A sterile 40-mL glass screw-cap septum vial was filled with a pre-weighed amount of GAC and 30 mL of 1 N HCl. This mixture was then shaken for 40 minutes and then rinsed with sterile phosphate buffer. This method removed iron that was easily accessible to the microorganisms, but not iron that may be part of the structural make-up of the GAC (Uranowski *et al*., 1998).

3.1.4 GAC Extraction and Cell Detachment Procedures

Two different analyses were performed on the GAC from each column experiment. The SOC loading on the GAC was measured before (if pre-equilibrated) and after the column experiments by methanol desorption using the method of Shi *et al.* (1995). In this method, small samples of GAC were taken before and after each bioregeneration experiment, blotted with a Kimwipe to remove excess liquid, placed in a headspace-free vial containing methanol, and mixed on a rotary mixer for 4 days. Samples of this methanol solution were then diluted and analyzed. Extraction correction factors were measured by

equilibrating GAC with a known SOC loading and then doing sequential methanol extractions until insignificant amounts of SOC were desorbed. The measured SOC loading was then compared with the known SOC loading to arrive at a correction factor for each SOC. The data used to determine the correction factors for toluene, TCE, and PCE are presented in Appendix B.

Cells were detached from the GAC after the column experiment was over, using the methods of DeWaters (1987) with modifications. The first step of this modified method was to push out the spent GAC with a rod onto a plastic sheet. Due to the cohesiveness of the bacteria, the GAC column maintained its cylindrical shape. Next, approximately 0.5 g (dry weight) of GAC was removed in slices from measured lengths along the column. Each sample was then put into a 50-mL plastic culture tube filled with 8 mL of 0.1% polyvinyl pyrrolidone (PVP)/1% sodium pyrophosphate (PPi) solution made with sterile, buffered water. This polymeric solution helped detach the cells from the GAC surface without lysing them. The culture tubes were then shaken horizontally on the previously-described platform shaker for 30 minutes.

The second step was to separate the GAC from the desorbed cells. Being careful not to remove any GAC, but maintaining the bacteria in suspension, 6.6 mL of supernatant were drawn up with a 10-mL gas-tight syringe. This step left approximately 2.5 mL of solution and GAC in the culture tube. Contrary to the DeWaters method, any amount of sonication was found to powder the GAC, making it very difficult to draw up bacteria without drawing up PAC as well. Furthermore, centrifuging the GAC solution pelleted down the bacteria along with

the GAC, making separation more difficult. When the GAC was simply left to settle for a few seconds, however, the bacteria was still suspended but the GAC was in the bottom of the culture tube, allowing for ease of separation. In addition, just one wash of the GAC with the PVP/PPi solution was found to be sufficient to remove enough cells for the subsequent analyses.

The third step in the cell extraction method was to remove the PVP/PPi from solution, as these compounds interfered with the subsequent analyses. To this end, the 6.6 mL of supernatant drawn up in the second step were expelled into a new 50-mL culture tube. The tubes were then centrifuged at 14,000 rpm for 10 minutes at room temperature, resulting in the bacteria pelleting out at the bottom of the tube. Next, 5 mL of supernatant was removed without disturbing the pellet and the total volume was decreased to 5 mL (allowing for some concentration of the cells) by adding 3.4 mL with sterile buffer solution. The tubes were then mixed by inversion, centrifuged again (14,000 rpm for 10min), and 3.4 mL of supernatant was removed and replaced with sterile buffer solution. Mixing of the pellet of bacteria was accomplished by vortexing followed by sonicating (Branson 3510 Sonicator) the tubes for 10-15 seconds. The last step was to perform analyses on the detatched cells using the methods of Woo *et al*. (2000). Analyses included measurement of OD_{600} (to measure suspended solids), protein, NADH, and enzyme activity (via indole oxidization measurement) as described in Section 3.3.4.

3.2 MATERIALS

Calgon Filtrasorb 400 granular activated carbon was used for all the adsorption experiments in this research. To achieve the desired size for PAC (200 x 325-mesh) or GAC (30 x 40-mesh), the F-400 was ground in a Waring laboratory blender and passed through the appropriately sized set of sieves. These sieves were rinsed with distilled, deionized water and then each mesh size was placed in a beaker where subsequent rinsing took place until all fines and oil were removed. The activated carbon was then baked at 95°C and stored in a glass container.

Variously sized gas-tight syringes were used throughout the research and were obtained from either Hamilton or Fisher Scientific. The exception to this was the gas-tight, 250-mL syringes used in standard curve preparation and kinetic biodegradation studies, which were obtained from VICI Precision Sampling, Inc. (Baton Rouge, LA).

The SOCs used in this research and as internal standards were toluene, TCE, PCE, benzene, and bromoform. Toluene (99.8% purity) and TCE (99.9%) were obtained from Fisher Scientific whereas PCE (99.9+%), TCE (99.9%), benzene (min. 99.9%), and bromoform (min. 99%) were obtained from Sigma-Aldrich. ^{14}C-radiolabeled versions of the toluene and TCE were obtained from Sigma Chemical Company and had specific activities of 2.8 and 5.4 mCi/mmol, respectively.

Additional materials used in column studies included hydrogen peroxide, in-line filters, and reagent powder for nitrate measurement. The hydrogen

peroxide was obtained from Fisher Scientific and was 30% by volume. The sterile 0.2-µm, in-line filters were Whatman brand polydisc AS filters, with a 50-mm diameter (Fisher Scientific). NitraVer 5 nitrate reagent powder pillows were obtained from Hach Chemicals and used to measure nitrate concentrations in the column feed.

Bacto agar and petri dishes (100 mm diameter, sterile, plastic) were purchased from Fisher Scientific for enumeration of bacteria in biological experiments. Bacto agar contained no carbon sources, which allowed for bacteria to be incubated with only toluene as the sole carbon source. Other materials used in biological analyses included bicinchoninic acid (BCA) protein assay kits which were purchased from Pierce Chemical Company and 98% pure beta-NADH which was purchased from Aldrich Chemical. The NADH was stored in a desiccated container at 4°C. To measure enzyme activity in biological experiments, indole (99% purity) dissolved in N,N-dimethylformamide (ACS reagent grade) was used as a reagent. Both chemicals were purchased from Sigma Chemical Company.

3.3 CHEMICAL AND BIOLOGICAL ANALYSES

3.3.1 Gas Chromatograph Analyses

A GC was used to measure all the liquid-phase SOC concentrations in this research. SOC samples taken from columns, GAC extractions, kinetic experiments, and most isotherms were analyzed using headspace analysis. To prepare a sample, 10 mL of the liquid to be tested was injected using a 10-mL

gas-tight syringe into an acidified 20-mL glass headspace GC vial (Agilent Technologies) and sealed with a 20-mm, teflon-faced, molded black butyl septum and a 20-mm, aluminum crimp cap (both from Agilent Technologies). Acidification of the sample ensured termination of biodegradation at the sampling time. Continuation of Fenton's oxidation in samples taken from GAC column experiments did not occur because any H_2O_2 in the influent reacted with the GAC to form O_2 and any hydroxyl radicals formed were highly reactive and not likely to remain in the effluent. Samples were stored upside-down at 4°C for a maximum of two weeks to minimize volatilization. Before GC analysis, the sealed sample was injected with 10 µL of a 1-g/L benzene internal standard through the septum. The GC used was a Hewlett-Packard 5890A with a Tekmar-Dohrmann 7000 Headspace Autosampler, RTX-624 column (0.53-mm ID, 30-m, Restek Corporation), and flame ionization detector (FID). The headspace analyzer program method is presented in Appendix B. The GC temperature programming method for toluene and PCE mixtures was 40°C for 1 min. and 20°C/min. to 120°C whereas for toluene and TCE mixtures it was 40°C for 4 min. and 20°C/min. to 100°C. The injector and detector temperatures were 250°C and 275°C, respectively. The overall flow rate was 36 mL/min with a column head pressure of 12 psi. The helium and hydrogen gas line pressures were 40 psi and the nitrogen gas and air line pressures were 44 psi. Method detection limits (MDLs) for toluene and TCE were 0.68 and 0.75 µg/L, respectively (the PCE MDL was not determined on the FID). The MDLs were determined using Method 1030E from Standard Methods for the Examination of Water and

Wastewater (18th ed., 1992). GC data were analyzed by calculating the ratio of the SOC chromatogram peak area to that of the internal standard. A two-part linear standard curve (0-100 µg/L; 100-1000 µg/L) was used to convert the area ratios to SOC concentrations. Example GC-FID standard curves from this procedure are shown in Appendix B.

SOC samples taken from some isotherms were analyzed on a GC equipped with an electron capture detector (ECD) when greater sensitivity was required for PCE or TCE. To prepare a sample, a 25-mL glass screw-cap septum vial (Pierce Chemical Co.) was filled headspace-free with the liquid to be tested and sealed with a 22-mm Teflon-coated silicone septa (Sun Brokers). Then the upside-down vial was injected with 3 mL of pentane solution spiked with 1.5 mg/L bromoform (the internal standard) so that the pentane solution floated to the top (and the pentane did not contact the pierced septum) while the displaced liquid sample exited the vial via an open needle outlet. The vial was subsequently shaken (septum-side down) on a horizontal table shaker for 1 hr. to allow for SOC extraction into the pentane, followed by removal of the floating pentane layer to a 1.5-mL, 11-mm diameter, glass GC auto-sampler vial (Sun Brokers) sealed with a rubber-lined aluminum cap. The samples were then analyzed on a Hewlett-Packard 5890A with a Hewlett-Packard 7673A automatic injector, a DB-5 column (0.25-mm ID, 30-m), and ECD. The temperature programming method for PCE was 50°C for 5 min. and 10°C/min. to 100°C. The method for TCE was modified from Cobb and Bouwer (1991): 35°C for 2 min., 2.5°C/min. to 57°C, and 4°C/min. to 64°C. The injector and detector temperatures were 150°C and

300°C, respectively. The overall flow rate was 32 mL/min with a column head pressure of 16.5 psi. The helium and P-5 argon gas line pressures were 16.5 and 40 psi, respectively. The MDL for PCE was 5.61 µg/L (the TCE MDL was not determined on the ECD). Standard curves were prepared in the same manner as for the GC-FID. Example GC-ECD standard curves from this process are shown in Appendix B.

3.3.2 Radiochemical Analysis

When possible, scintillation counting was preferred to gas chromatography due to the increased sensitivity of the measurements as well as the quickness with which analysis can be performed. The user program for the Beckman LS 5000TD liquid scintillation counter for counting ^{14}C-containing samples is shown in Appendix B. Quench correction was done by the H number technique using the instrument's internal cesium-137 source. For the radioactive samples prepared as described in Section 3.1.2, three background experiments were done to determine the correction factors to account for process efficiency. These correction factors were used in all radioactive calculation spreadsheets. The first experiment tested the amount of chemiluminescence of the "base" sample during scintillation counting. Chemiluminescence can be a significant problem at pHs that are too high, and results in photons being released from the sample that are not associated with radioactive decay. These photons can be picked up by the photomultiplier tubes and thus artificially increase the radioactivity count. To determine the level of chemiluminescence, two samples with 5 mL of the same ^{14}C-substrate solution were measured on the scintillation

counter, except one was near neutral and one was at a pH of 11. Each of these samples was measured 6 times over a 24-hr. period to determine the time dependence of chemiluminescence. Depending on the results, samples would be stored until chemiluminescence had ceased before being run on the scintillation counter.

The second radioactive background experiment tested ^{14}C-substrate uptake on filters containing radioactive biomass. Not all of the ^{14}C-substrate sorbed to the filter after sample filtration was removed by the 50% ethanol rinse, so a correction factor accounting for the resulting increase in measured radioactivity was necessary. To find the correction factor, three samples were run for each substrate (^{14}C-tolune or ^{14}C-TCE): (1) 5 mL of a ^{14}C-substrate solution, (2) an unrinsed 0.45-µm Osmonics cellulose nitrate filter after filtration of 5 mL of the same ^{14}C-substrate solution, and (3) a filter rinsed with 15 mL of 50% ethanol after filtration of 5 mL of the same ^{14}C-substrate solution. The correction factor was then calculated by dividing the count for sample 3 by that for sample 1. The correction factor was also compared to the count for sample 2 divided by that for sample 1 to evaluate the use of the ethanol rinse. When used in the radioactive calculations spreadsheet, this correction factor was multiplied by the net "total" sample count and then subtracted from the net "filter" count.

The third radioactive background experiment tested the nitrogen purging efficiency of the pH-adjusted radioactive samples. To test this, three samples were prepared for each ^{14}C-substrate: (1) 5 mL of a ^{14}C-substrate solution, (2) 5 mL of the same ^{14}C-substrate solution acidified to pH ~1.5, and (3) 5 mL of the

same ^{14}C-substrate solution adjusted to pH ~10.5. These samples were then purged at 65 mL/min. of N_2 gas for 6 min. each and measured on the scintillation counter. Correction factors for the "acid" and "base" samples were determined by divided the counts for samples 2 and 3 by that for sample 1. When used in the radioactive calculations spreadsheet, these correction factors were multiplied by the net "total" sample count and then subtracted from the net "acid" or "base" count. Results of these background tests are shown in Appendix B.

3.3.3 Iron and H_2O_2 Measurement

Samples containing iron were analyzed using either the phenanthroline method (based on Method 3500-Fe D from Standard Methods, 18th ed., 1992) or the inductively coupled plasma (ICP) method. The phenanthroline method measures Fe(II) only, so all other forms of iron to be measured must first be converted to Fe(II). To measure iron via the phenanthroline method, first a 20-mL sample was placed in a 50-mL acid-washed (to make iron-free) plastic culture tube (Corning) along with 100 µL of 6 N HCl to maintain iron in the Fe(II) state and stored at 4°C. This solution was then poured into an acid washed 125-mL Erlenmeyer flask along with 1.5-mm.-diameter glass beads. Next, 0.8 mL of concentrated HCl and 0.4 mL of hydroxylamine solution (10 g $NH_2OH \bullet HCl$ in 100 mL DDI water) were added to the flask and the solution was boiled until less than half of the original volume remained. The samples were cooled to room temperature and 4 mL of ammonium acetate buffer (250 g of $NH_4C_2H_3O_2$ in 150 mL DDI water, followed by adding 700 mL concentrated acetic acid) was added. Next, 1.6 mL of phenanthroline solution (100 mg of 1,10-phenanthroline

monohydrate in 100 mL DDI water heated to 80°C) was added causing pink color development in the presence of Fe(II). The samples were then poured back into the 50-mL plastic tubes, diluted to 20 mL with DDI water, and mixed. After 15 minutes, the samples were measured on a spectrophotometer (Agilent 8453 UV-Visible Spectroscopy System) at 510 nm after blanking with a sample prepared in the same manner but using iron-free water. An example standard curve for the phenanthroline method is shown in Appendix B.

The ICP method measured total iron instead of only Fe(II). Thus, it was not as important to maintain iron in the Fe(II) state other than to minimize iron adhesion to the plastic culture tube. To minimize iron adhesion, a 20 to 50-mL sample was placed in a 50-mL acid-washed plastic culture tube (Corning) along with 100 µL of 6 N HCl and stored at 4°C. Next, the calibration standards were prepared for the ICP (Spectro Ciros CCD Spectrophotometer). A 10-ppm Fe(II) standard was prepared using $FeSO_4$ in a 1-mM H_2SO_4 solution to keep the iron reduced so that precipitates did not form and settle to the bottom of the tube. A 0-ppm standard consisted of iron-free, 1.5% nitric acid solution. Argon gas was fed at 60 psi to the ICP with a plasma power of 1400 W, a coolant flow of 14 L/min, an auxiliary flow of 1 L/min, and a nebulizer flow of 0.8 L/min. The resulting spectrum was measured on an atomic emission spectrophotometer. Values measured at 259.9 nm represented iron and were recorded and averaged. The typical detection limit for iron was 1 µg/L.

Hydrogen peroxide was used in various columns to raise the D.O. and react with iron as Fenton's oxidation. The method presented by Belhateche and

Symons (1991) was used to measure hydrogen peroxide on a spectrophotometer. First, 4 mL of saturated sodium bicarbonate solution (25 g of $NaHCO_3$ in 250 mL of DDI water) was added to a 25-mL acid-washed glass volumetric flask. Then, 0.25 mL of cobalt solution (19 g of $CoSO_4 \bullet 7H_2O$ in 1 L of DDI water) was added to the volumetric flask. Next, grab samples containing hydrogen peroxide, bacteria, and organics were collected in a 50-mL acid-washed (to make iron-free) plastic culture tube. Subsequently, 20 mL of sample (or DDI water for blanking the spectrophotometer) was transferred to the volumetric flask followed by additional bicarbonate solution to fill the flask to the 25-mL mark. The volumetric flask was then allowed to sit for 15 min. for color development (green indicated the presence of H_2O_2). If the sample contained significant bacterial counts, it was filtered through a 0.45-µm syringe filter before analysis at an absorbance of 310 nm. The author's standard curves for TCE and benzene-contaminated H_2O_2 samples were then used to determine the H_2O_2 concentration. The benzene standard curve was used instead of one for toluene because it was the closest chemical to toluene used in the study. The toluene and TCE concentrations were inputs to the H_2O_2 standard curves to account for the increased absorbance measured with their presence. No PCE standard curve was necessary because H_2O_2 measurements were not taken during toluene-PCE experiments. The H_2O_2 concentration was calculated by multiplying the micromoles of H_2O_2 measured by its molecular weight, 34.02 g/mol, and dividing by the sample volume.

3.3.4 Biological Analyses

To enumerate bacteria, carbon-free Bacto agar was used. Bacto agar contained no carbon sources, which allowed for bacteria to be incubated with only toluene as the sole carbon source. To make the carbon-free agar, 6.9 g of Bacto agar powder was stirred into 300 mL of 5 times the normal growth nutrients concentration shown in Table 3.1. The mixture was then heated until boiling and autoclaved at 121°C and 17 psi for 15 minutes. After autoclaving, the mixture was cooled and poured into 100-mm diameter plastic petri dishes in a laminar-flow hood to minimize contamination. Cooled petri dishes were stored upside-down in sterile sleeves at 4°C for up to 3 months. When enumerating a sample, 0.1 mL of liquid was dropped onto the agar plate and smeared with a sterile bent glass rod. After the liquid had soaked into the agar, the petri dishes were put upside-down in an incubator filled with vapor phase toluene (the source was a small beaker of liquid toluene) to select for toluene degraders.

To differentiate between gram positive and gram negative bacteria, gram stains were performed. First, a glass microscope slide was cleaned with alcohol, rinsed with DDI water, and blotted with paper. Then the slide was sterilized over a flame and cooled. A sterile loop of the bacterial sample was then spread across the middle of the slide and dried at room temperature. To affix the cells to the slide, the bottom of the slide was passed through a flame 2 – 3 times. Next, crystal violet (VWR) was poured on top of the cells. After letting the solution saturate for 1 minute, the slide was rinsed with DDI water and blotted with paper. This saturating process was repeated separately with iodine, decolorizer, and

safranin O stain (VWR). The glass slide was then observed under a microscope. Purple-stained bacteria were gram positive, while red-stained bacteria were gram negative. The overall process was repeated several times to get a range of values.

When measuring the concentration of biomass, two methods were available: (1) total suspended solids (TSS) / volatile suspended solids (VSS) (Methods 2540 D and E from Standard Methods, 18th ed., 1992) or (2) optical density at 600 nm (OD_{600}). TSS was measured by baking a glass fiber filter (0.5-µm, 47-mm diameter, Metrigard) at 550°C in an aluminum pan to volatilize any contaminants. The filter and aluminum pan were then cooled in a dessicator and weighed. Next, a well-stirred sample containing cells was vacuum-filtered through the glass fiber filter and the funnel setup was rinsed with DDI water to rinse off any remaining cells. The filter was then transferred back to the aluminum pan, baked at 100°C overnight, and re-weighed. The TSS was then calculated by the difference in filter weight divided by the sample volume. TSS only represents the concentration of solids not volatilized at 100°C, however, which may include solids other than cells. A truer measure of cell concentration is VSS. VSS was measured by the same method as TSS, except that after the 100°C-dried filter and pan were measured, they were baked at 550°C for 1 hour and re-weighed. The VSS was calculated as the difference between the 100°C weight and the 550°C weight divided by the sample volume. The OD_{600} method consisted of taking a well-mixed sample and measuring the absorbance on the spectrophotometer blanked with DDI water. The OD_{600} method was the preferred method used in this research due to the small sample size and quick analysis, thus

a standard curve for conversion between OD_{600} and TSS/VSS was created and is shown in Appendix B.

A modification of the Pierce BCA (Bicinchoninic Acid) Protein Assay method was used to measure protein. First, a protein standard curve was created using BSA (Bovine Serum Albumin) stock. The BSA (in a dried disc form) was reconstituted with DDI water to make a 2000-mg/L stock. A 0 - 250-mg/L BSA protein standard curve was prepared in 3 M NaOH. Then, 200 µL of each standard was transferred to an acid-washed, 10-mL glass test tube. Sodium hydroxide was used instead of DDI water to maintain the same basic pH as in the actual lysed cell samples. Next, 200-µL samples (or more if necessary) were pipetted into 1.5-mL polypropylene Eppendorf tubes (Brinkmann Instruments, Inc.) and spun on a microcentrifuge (Eppendorf Centrifuge 5410) at 14,000 rpm for 5 minutes to pellet down the cells. The supernatant was removed and 3 M NaOH solution was added to the 200-µL mark. The tubes were mixed and placed in a 65°C water bath for 30 min. to lyse the cells and solubilize the proteins (Stein, 1998). Then the tubes were cooled and centrifuged again at 14,000 rpm for 5 min. to pellet out insoluble material. From each Eppendorf tube, 200 µL of supernatant was pipetted into an acid-washed, 10-mL glass test tube. Next, the working reagent was mixed from 50 parts BCA Protein Reagent A (Pierce) and 1 part BCA Protein Reagent B (Pierce). To each sample or standard curve test tube, 4 mL of the working reagent was added and mixed. The test tubes were then placed in a rack and heated in a 60°C water bath (Lab-Line Instruments, Inc.) for 30 minutes. After heating in the water bath, the test tubes were cooled to room

temperature and measured at 562 nm in a 1-cm quartz cell on a spectrophotometer blanked with the 0-mg/L standard. An example protein standard curve is shown in Appendix B.

NADH and enzyme activity were measured at the end of biological activated carbon column experiments via the methods of Woo *et al*. (2000). After desorption of cells off the GAC as described in Section 3.1.4, the next step was to blank a fluorescence spectrophotometer (Perkin-Elmer LS-5) with DDI water at 340 nm (excitation) and 425 nm (emission) to measure NADH. The side slot dials on the fluorescence spectrophotometer were set to 10. A 1-cm quartz cell was used that had no frosted sides so that light could pass through one side and out at a 90° angle. After blanking, the cuvette was emptied and 300 µL of the 5 mL sample described in Section 3.1.4 was injected. Then, 2.7 mL of DDI water was injected into the cuvette to lyse the cells by osmotic difference. The cuvette was covered with a plastic cap and mixed by inversion three times. After waiting one minute for lysing to take place, the cuvette was mixed again and placed in the fluorescent spectrophotometer for measurement. This process was repeated two more times to get an average value. An example NADH standard curve is shown in Appendix B.

To measure the enzyme activity using the methods of Jenkins and Dalton (1985), the solution in the cuvette was disposed of and the cuvette was rinsed. The cuvette was filled with fresh suspended sample, covered with a plastic cap, and mixed by inversion three times. After quickly checking for water droplets on the sides of the cuvette, 20 seconds were allowed to pass and the fluorescence

spectrophotometer was re-blanked with the suspended sample at 365 nm (excitation) and 470 nm (emission). In this method, indole was added to samples of interest and the absorbance over time was measured at 400 nm as indole was oxidized to indigo. Next, the sample was transferred from the cuvette to the 50-mL plastic culture tube and 20 µL of indole stock (100 mM in N,N-dimethylformamide) was added. Immediately a timer was started and the sample was vortexed. Then, the sample and indole mixture was poured into the cuvette, mixed by inversion, and placed in the spectrophotometer. After 40 seconds, the absorbance was recorded. This process was repeated every 2 - 5 minutes, depending on how fast the absorbance increased. Only the initial portion of the absorbance slope is needed for analysis (~4 to 6 points). The enzyme activity was quantified by the slope of the initial portion of the absorbance increase. The absorbance slope was used because indigo was not commercially available; therefore, no standard curve for indigo was available. An example analysis of raw enzyme activity data is shown in Appendix B.

Chapter 4: Background Results

The main focus of this research was studying the relative effect of metabolism and cometabolism on granular activated carbon (GAC) bioregeneration. To this end, there were two main research phases. The first phase, as discussed in this chapter, involved determining batch adsorption equilibrium, GAC column kinetic parameters, and batch microbial kinetic parameters for each synthetic organic chemical (SOC). These parameters were estimated or measured in preparation for running the second phase of the research, which consisted of dual-component exhausted and virgin GAC column experiments. The second phase of the research is discussed in Chapter 5.

4.1 PAC Adsorption Isotherms

Individual adsorption isotherms were performed on powdered activated carbon (PAC) for toluene, PCE, and TCE, from which the Freundlich adsorption parameters, K and 1/n, were estimated. The isotherms for toluene and TCE were performed in duplicate to ensure the accuracy of the measured Freundlich parameters. The resulting adsorption parameters are presented in Table 4.1 along with their 95% confidence intervals (CI). Toluene, PCE, and TCE are all moderately adsorbable. Furthermore, good agreement was seen between the duplicate isotherm Freundlich parameters. Some overlapping was seen between 95% CI values for the TCE 1/n value as well as the toluene K value. The 95% CI values were very close for the toluene 1/n value and the TCE K value; however, they did not overlap.

Table 4.1 Summary of Adsorption Parameters from Single Component Studies

Chemical	Equil. Conc. µg/L	Freundlich Parameters 1/n -	95% CI -	K µg/g (L/µg)$^{1/n}$	95% CI µg/g (L/µg)$^{1/n}$
Biodegradable					
Toluene	9 – 5,180	0.3641	0.3600 - 0.3682	10,230	9,937 – 10,500
	29 – 11,900	0.3528	0.3460 - 0.3597	9,706	9,188 – 10,211
Cometabolite					
TCE	5 – 416	0.4447	0.4388 - 0.4529	3,576	3,387 – 3,701
	36 – 15,050	0.4375	0.4323 - 0.4429	4,021	3,844 – 4,181
Nonbiodegradable					
PCE	7 – 953	0.4660	0.4400 - 0.4983	14,000	13,130 – 14,680

The results of the individual adsorption isotherm studies are presented in Figures 4.1 through 4.3. The isotherm lines plotted over the experimental data are the best-fit Freundlich isotherms, determined by simple linear regression on a log-log plot, where C_e is the liquid-phase equilibrium concentration and q_e is the solid-phase equilibrium loading.

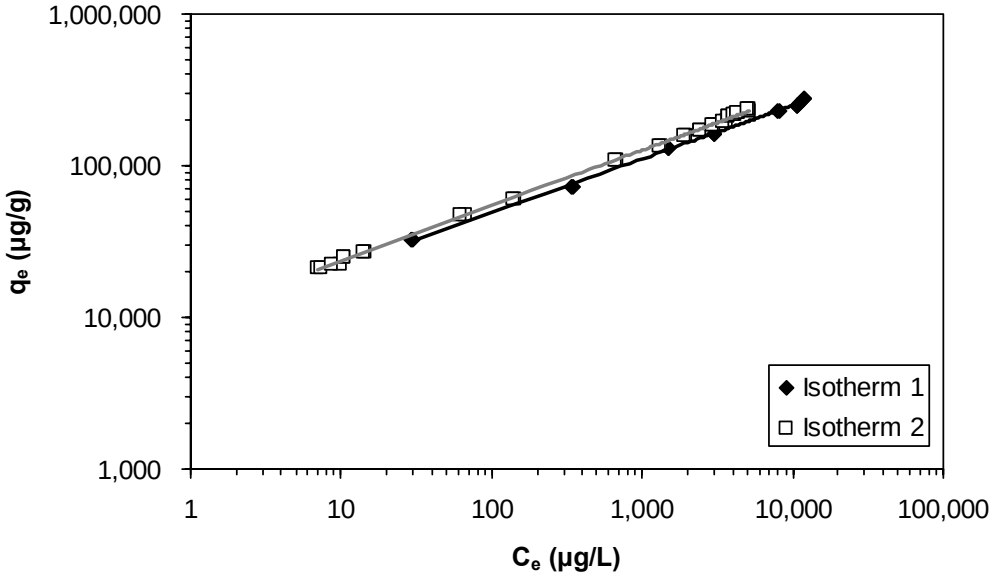

Figure 4.1 Individual Adsorption Isotherms for Toluene, C_o = 58 (1) and 62 (2) mg/L

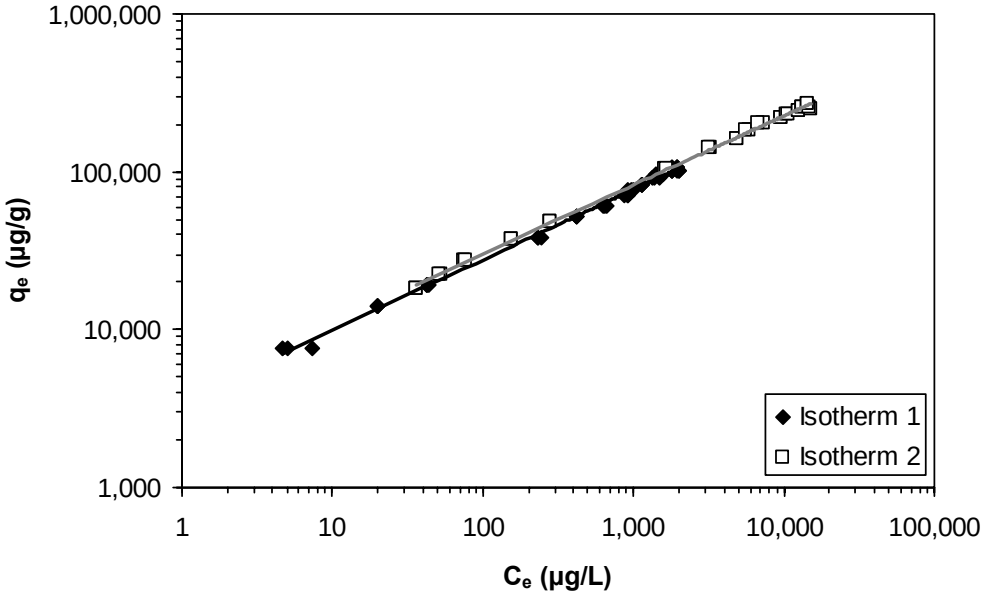

Figure 4.2 Individual Adsorption Isotherms for TCE, C_o = 85 (1) and 79 (2) mg/L

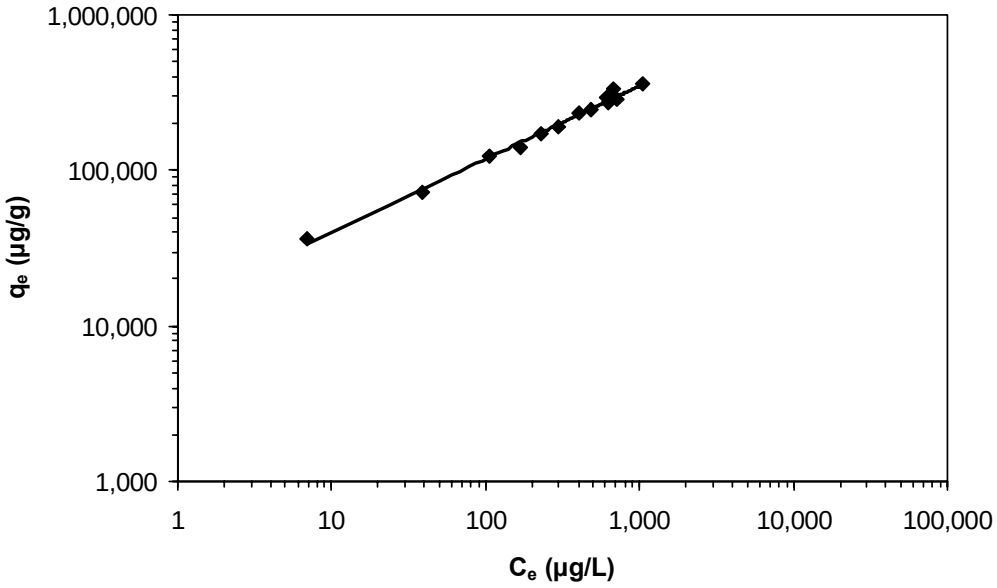

Figure 4.3 Individual Adsorption Isotherm for PCE, C_o = 26 mg/L

The equilibrium parameters from the single component isotherms were then used to predict competitive adsorption behavior for toluene and TCE as well as toluene and PCE, which were measured in dual-component competitive isotherm experiments. Duplicate dual-component isotherms were performed for toluene and TCE to ensure the accuracy of Ideal Adsorbed Solution Theory (IAST) predictions compared to measured data. The experimental data, corresponding single-component isotherms, and IAST predictions are plotted in Figures 4.4 through 4.6. Competition for adsorption sites was observed, as seen in the diminished adsorption capacity for each chemical relative to the single-component adsorption isotherms.

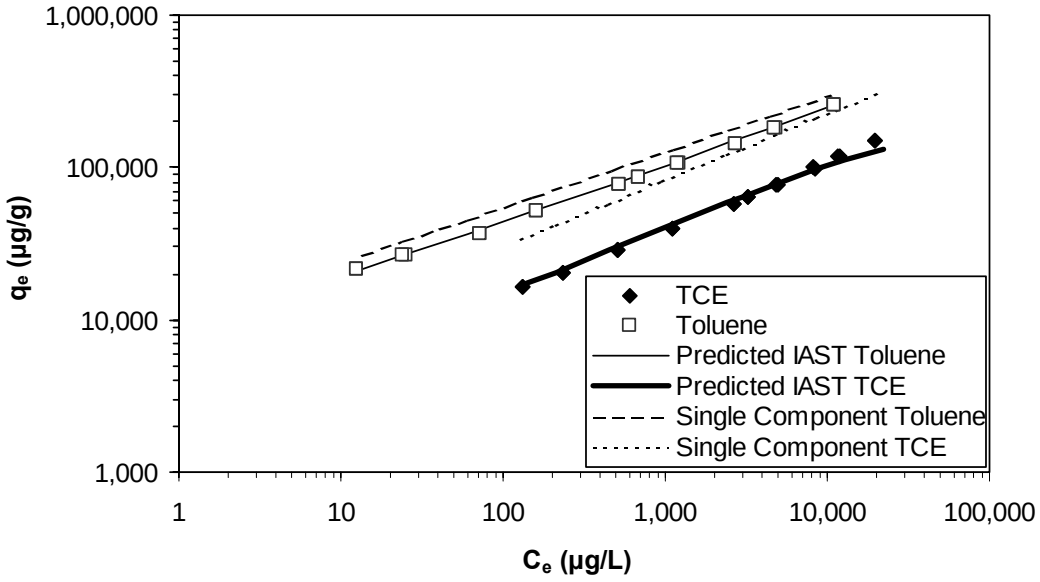

Figure 4.4 Toluene and TCE Competitive Isotherm 1, Toluene C_o = 61 mg/L, TCE C_o = 48 mg/L, P = 1 for both

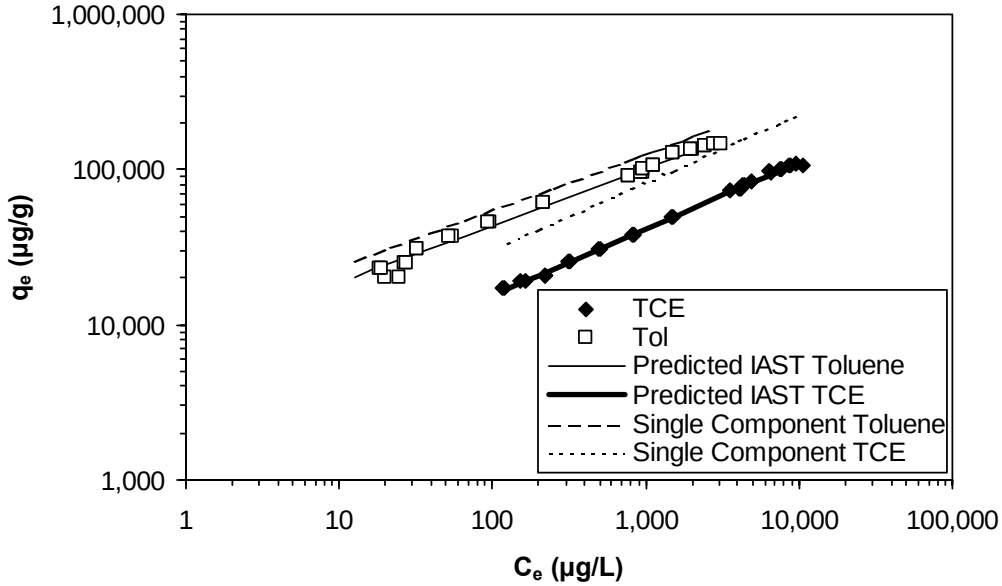

Figure 4.5 Toluene and TCE Competitive Isotherm 2, Toluene C_o = 62 mg/L, TCE C_o = 74 mg/L, P = 1 for both

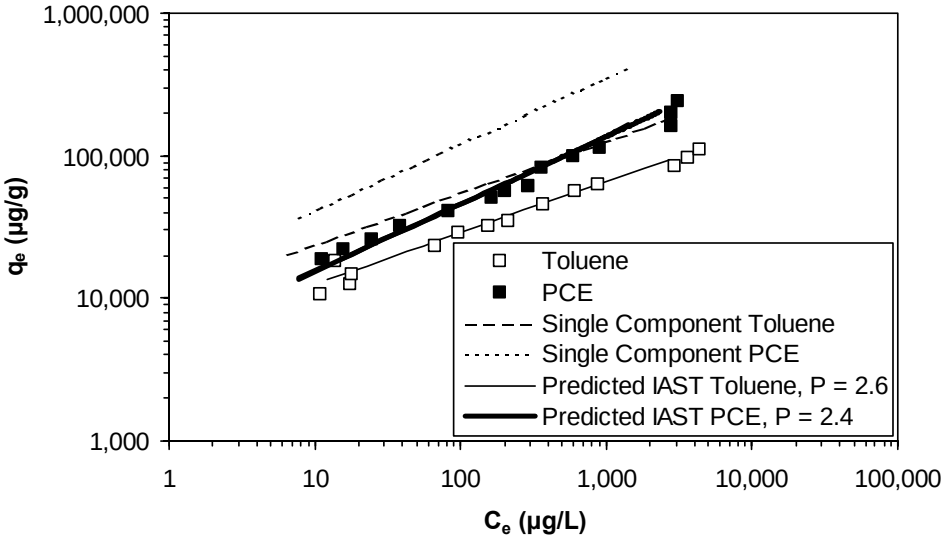

Figure 4.6 Toluene and PCE Competitive Isotherm, Toluene C_o = 15 mg/L, PCE C_o = 26 mg/L

The reduction in adsorption capacity experienced by toluene and TCE in a competitive environment fit very well with the IAST predictions. In Figure 4.4, the predicted toluene curve had an average percent error (APE) of 14% in C_e and 0.1% in q_e. Equations 4.1 and 4.2 show the method for calculating APE where the variable X represents the parameter for which the error is being estimated (*i.e.*, C_e or q_e for each SOC) and n is the number of measurements of variable X.

$$ErrorX_i = \left(\frac{Measured\ X_i - \Pr edicted\ X_i}{Measured\ X_i} \right) * 100 \ \ for\ i = 1\ to\ n \qquad \text{(Eq. 4.1)}$$

$$APE\ of\ X = \frac{\left(ErrorX_1 + ErrorX_2 \ldots + ErrorX_n\right)}{n} \qquad \text{(Eq. 4.2)}$$

Aziz *et al*. (1999) defined the quality of APE as good, fair, or poor for values <10%, 10-20%, or >20%, respectively. The predicted TCE curve had an APE of 5% in C_e and 0.3% in q_e. These APE values indicate fair and good agreement between the predicted and measured toluene and TCE isotherm curves, respectively. Crittenden *et al*. (1985b) found typical APE values for competitive adsorption to be 29% in C_e and 16% in q_e, which was similar to the precision of the single-solute data tested. In the replicate experiment (Figure 4.5), the predicted toluene curve had an APE of 7% in C_e and 0.2% in q_e. The predicted TCE curve had an APE of 9% in C_e and 1.6% in q_e. As in Figure 4.4, these APE values indicate good agreement between the predicted and measured isotherms.

Figure 4.6 shows toluene and PCE competitive adsorption was also described well by IAST, although it was necessary to use a correction factor, P, of 2.6 for toluene and 2.4 for PCE. P was applied to the IAST equation (as a multiplier to q_i) to account for differences between predicted and measured equilibrium due to nonideal mixing in real aqueous systems. The fitted toluene curve had an APE of 61% in C_e and 0.7% in q_e. The fitted PCE curve had an APE of 65% in C_e and 1.0% in q_e. These APE values indicated poorer agreement than with the toluene and TCE isotherms.

4.2 GAC COLUMN KINETICS

After the adsorption isotherms were completed, GAC column experiments were run to estimate adsorption and desorption kinetic parameters for toluene and TCE using adsorption equilibrium parameters as inputs to the Pore Surface

Diffusion Model (PSDM, see Section 2.4). Depending on the type of column experiment, the Freundlich adsorption parameters from either Table 2.3 (Speth and Miltner, 1990) or Table 4.1 (measured in this research) were used as a starting point for fitting. K values were then adjusted as necessary to fit the PSDM model to the data with respect to the breakthrough time. Smaller K and 1/n adsorption parameters were seen for all three SOCs in the Speth and Miltner (1990) results compared to those measured in this research, despite similar adsorption conditions. The difference in adsorption parameters probably occurred because of the order-of-magnitude differences in the initial concentrations used for the two isotherm sets, perhaps leading to some amount of irreversible adsorption in the case of the high initial concentrations. The equilibrium parameters from Speth and Miltner (1990) were used for modeling virgin GAC columns because the initial concentrations used for the isotherms were between 0.361 and 1.093 mg/L, which was closer to the influent toluene and TCE concentrations in the virgin columns. The measured equilibrium parameters were used for modeling exhausted GAC columns because the initial concentrations used for the isotherms performed in this research were between 58 and 62 mg/L for toluene and 79 and 85 for TCE. These initial concentrations were closer to the values used for pre-equilibrium in the exhausted GAC columns, which were usually near saturation for toluene (98 – 607 mg/L toluene, 2 – 75 mg/L TCE).

The dependence of adsorption capacity on initial concentration has been studied by past researchers with conflicting results. Crittenden and Weber (1978) and Van Vliet *et al*. (1980) found that higher initial concentrations resulted in

lower adsorption capacities. Peel and Benedek (1980) and Yonge *et al*. (1985), however, found no influence of initial concentration on adsorption capacity when the concentration was increased five-fold. Rather, they attributed conflicting results found by others to the increased time needed for equilibrium when large initial concentrations are used. This failure to attain equilibrium would result in artificially low adsorption capacities when large initial concentrations are used. In contrast, the very large initial concentrations used for the isotherms in this research resulted in an *increased* GAC adsorption capacity compared to that found by Speth and Miltner (1990). This increase may have occurred because the larger initial concentration created a stronger driving force for adsorption into pores deeper within the GAC, perhaps resulting in irreversible adsorption.

The experimental and fitted effluent concentrations from a toluene and TCE adsorption experiment are shown in Figure 4.7. The sterile virgin GAC column was used as a control in Experiment 7 as discussed in Section 5.3.1. The column was fed 1,570 µg/L of toluene and 87 µg/L of TCE and had a 0.93-min. empty bed contact time (EBCT). A short EBCT was used to minimize the amount of time required to achieve saturation of the entire column. Some variation occurred in the influent concentrations and thus the toluene and TCE concentrations near the end of the experiment decreased slightly instead of reaching a plateau at the average influent concentration. The fitted effluent concentrations were derived from the PSDM, and the calculated kinetic coefficients are shown in Table 4.2. AdDesignS© (Adsorption Design Software, CenCITT), an implementation of the PSDM described in Section 2.4, was used to

fit the toluene and TCE effluent concentration over time using a modification of the equilibrium parameters from Table 2.3. To minimize the average residual sum of squares (S^2) between the AdDesignS© fit and the measured data, the adsorption parameter K for toluene was decreased from 5010 to 4460 µg/g $(L/\mu g)^{1/n}$.

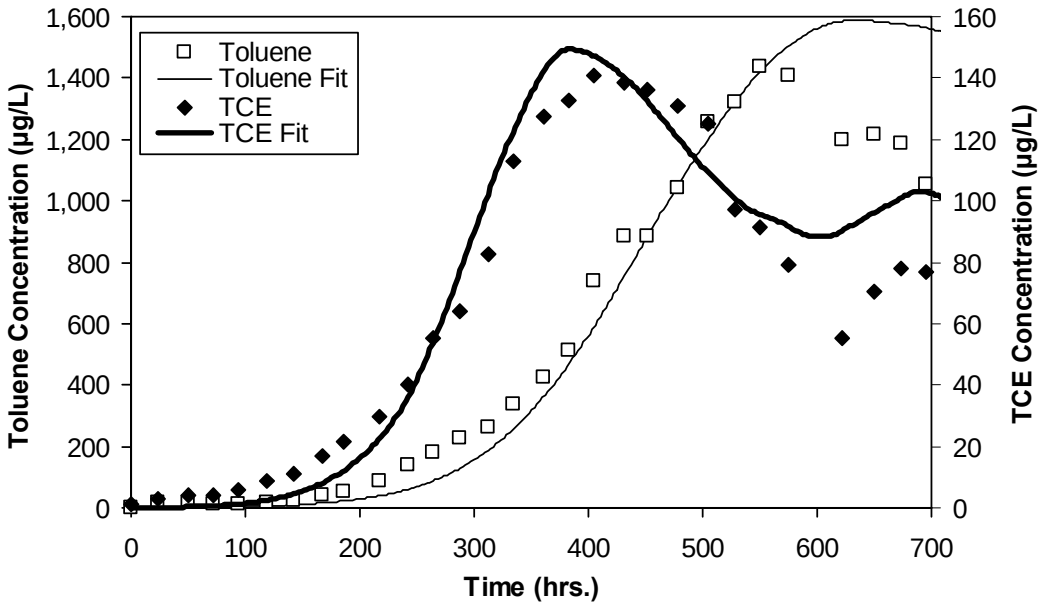

Figure 4.7 Measured and PSDM-Fitted Toluene and TCE Adsorption, Toluene C_o = 1570 µg/L, TCE C_o = 87 µg/L, 0.9-min. EBCT

Besides using the Freundlich equation, the PSDM also uses IAST to describe adsorption of multiple components; thus, it was important that IAST predicted the competitive isotherm data well, as shown in Section 4.1. Perturbing the kinetic parameters (k_f, D_p, and D_s in Table 4.2) from the calculated values in AdDesignS© did not appreciably decrease the S^2; therefore, the calculated kinetic values were used without change. The k_f and D_s values were calculated via the

Gnielinski correlation and the Sontheimer correlation, respectively (Sontheimer *et al*., 1988). The D_p values were calculated using the tortuosity (set at the default value of 1) and the liquid diffusivity. The liquid diffusivity was calculated via the Hayduk and Laudie correlation (Hayduk and Laudie, 1974). The surface to pore diffusion ratio (SPDFR) was set at the default value of 5 because Hand *et al*. (1989) and Dobrezelewski *et al*. (1985) found 2 – 8 to be typical values for the SPDFR (Surface to Pore Diffusion Flux Ratio) when using water free of natural organic matter. The toluene and TCE PSDM fits slightly underestimated the concentrations before the breakthrough and slightly overestimated the concentrations after the breakthrough. Given the variation in the influent, the PSDM fit the experimental data well.

Table 4.2 Calculated PSDM Kinetic Coefficients for Adsorption and Desorption

Coeff.	**Description**	**Desorption**		**Adsorption**	
		Toluene	**TCE**	**Toluene**	**TCE**
k_f (cm/s)	Liquid Film Transport Coefficient	3.00×10^{-3}	3.21×10^{-3}	1.90×10^{-3}	2.04×10^{-3}
D_p (cm^2/s)	Pore Diffusion Coefficient	8.87×10^{-6}	9.71×10^{-6}	8.87×10^{-6}	9.71×10^{-6}
D_s (cm^2/s)	Surface Diffusion Coefficient	2.08×10^{-10}	5.14×10^{-10}	6.33×10^{-10}	2.34×10^{-10}

Pore diffusion has not been found in the literature to be a major transport mechanism compared to surface diffusion for moderately and strongly adsorbed chemicals (Friedman, 1984). In addition, similar effluent concentrations were

predicted from PSDM modeling with a D_p of 1 x 10^{-10} cm^2/s (very little pore diffusion) and with the calculated D_p (~10^{-6} cm^2/s). Furthermore, the SPDFR was calculated for toluene and TCE as a function of concentration via the methods of Sontheimer *et al.* (1988). SPDFR values are typically around 5, and pore diffusion is considered to be insignificant above that value. From these SPDFR calculations, pore diffusion was determined to be insignificant below 1.5 mg/L for toluene and below 85 µg/L for TCE. Thus, the Homogeneous Surface Diffusion Model (HSDM), which ignores pore diffusion, was determined to be applicable. The HSDM is the basis for the adsorption and biodegradation model (MDBA Model, see Section 2.9 and Chapter 6) that was used to evaluate experimental results in BAC columns. Therefore, confirmation of the adsorption component of the model was an important step in building confidence in the more complicated adsorption and biodegradation model.

A toluene and TCE desorption experiment was also performed to compare the kinetics of adsorption and desorption in a continuous-flow column. To perform the desorption experiment, a GAC column was pre-equilibrated at a high initial concentration with toluene and TCE and then contaminant-free water was pumped through the 0.08-min. EBCT column. The resulting effluent concentrations are shown in Figure 4.8. AdDesignS© was used to predict the toluene and TCE effluent concentrations using the equilibrium parameters from Table 4.1 and the calculated kinetic coefficients shown in Table 4.2. Figure 4.8 shows that the predicted effluent concentrations were larger than the measured concentrations. This overprediction indicated that the predicted cumulative extent

of desorption was greater than that measured. The cumulative extent of desorption was defined as the integrated mass of SOC desorbed over time.

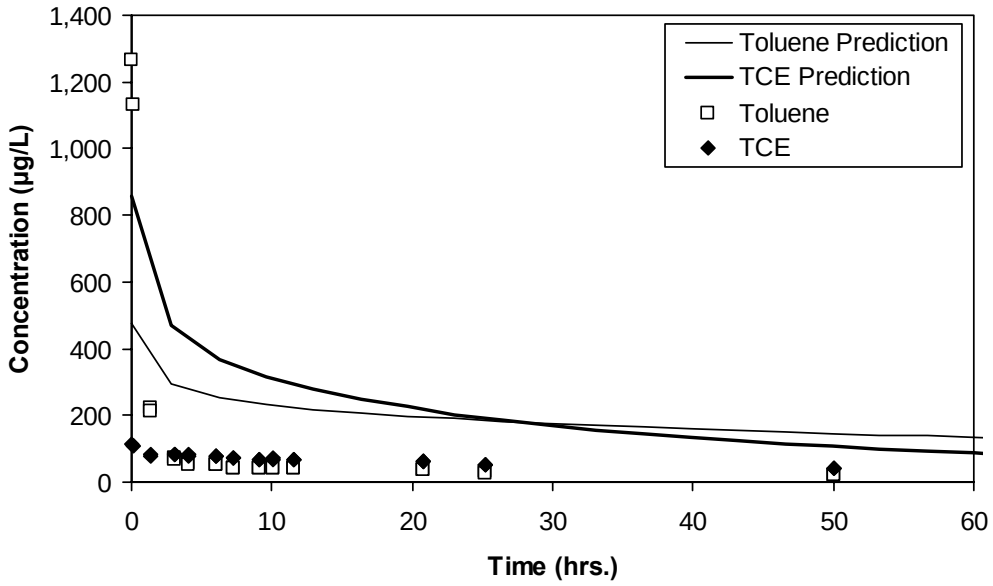

Figure 4.8 Measured and PSDM-Predicted Toluene and TCE Desorption, Toluene Equilibrium Conc. = 474 µg/L, TCE Equilibrium Conc. = 858 µg/L, 0.08-min. EBCT

The average residual sum of squares (S^2) for desorption was roughly ten times higher than that for adsorption (0.35 for toluene and 0.21 for TCE). The discrepancy between the measured and predicted effluent concentrations may be explained by the high initial concentrations that were used to pre-equilibrate the GAC. These high concentrations may have led to irreversible adsorption. Irreversible adsorption would result in a slower-than-expected desorption rate. Both underprediction and overprediction of the batch phenol desorption rate by the HSDM was reported by Speitel (1985). In addition, overprediction of the DCP desorption rate was observed by Speitel *et al*. (1989c) and attributed to

irreversible adsorption. Only drastic changes from the calculated kinetic parameters (k_f, D_p, and D_s) decreased the S^2; therefore, the calculated kinetic values in Table 4.2 were used without change to model the desorption experiment. The D_p values for the adsorption and desorption experiments were the same and the k_f values were similar. The D_s values, however, were more dissimilar than the k_f values.

4.3 BATCH BIODEGRADATION KINETICS

4.3.1 Enzyme Competition

To adequately describe bioregeneration in a biologically-active GAC column, microbial kinetic parameters are needed in addition to activated carbon adsorption parameters. Microbial kinetic parameters for toluene and TCE were determined via batch kinetic studies with a toluene-acclimated mixed culture. Toluene oxygenase enzymes produced via the toluene degradation pathway also degrade TCE (*i.e.*, cometabolism) along with the primary substrate, toluene. Figure 4.9 shows the simultaneous degradation of toluene and TCE in a headspace free reactor with oxygenated, buffered nutrient water where X_o is the initial biomass concentration. No regeneration of NADH occurs with the oxidation of the cometabolite, so the microorganism reaps no benefits from cometabolism. Furthermore, both toluene and TCE can compete for active sites on the oxygenase enzymes, possibly resulting in competitive inhibition of the degradation kinetics. Toluene has been shown to out-compete TCE for these sites (Robinson *et al.*, 1998). In some studies, competitive inhibition has been quite

significant, resulting in TCE not being cometabolized until toluene was nearly completely degraded (Robinson *et al*., 1998; Cox *et al*., 1998). Figure 4.9, however, shows no lag in the initiation of TCE cometabolism, thus indicating that little or no enzyme competition existed between toluene and TCE at the concentrations used in this experiment. This is an important finding because significant enzyme competition can minimize the usefulness of a cometabolism-based biologically active column.

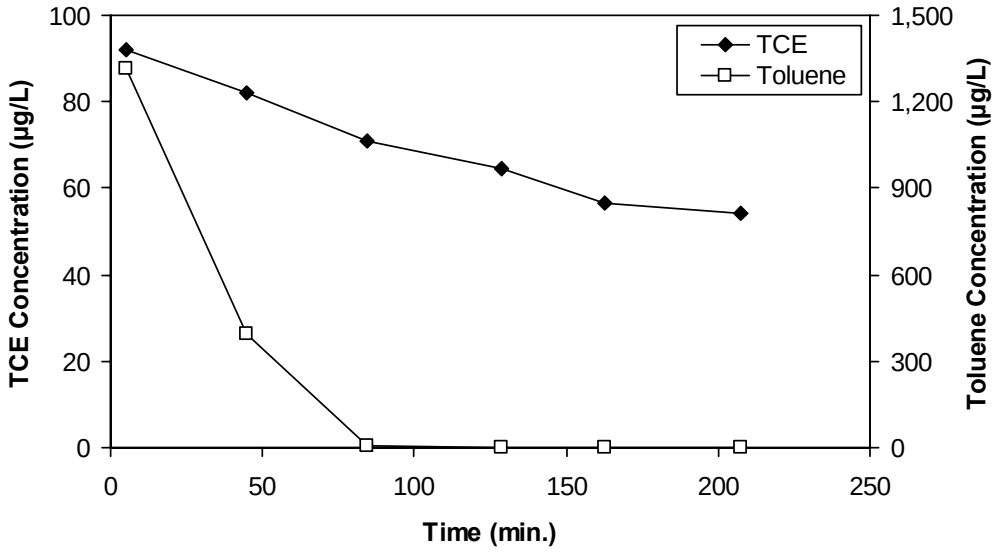

Figure 4.9 Simultaneous Toluene and TCE Batch Degradation, X_o = 36 mg/L

Figure 4.10 shows TCE cometabolism in the presence of varying concentrations of toluene. For these experiments, the culture was fed 15 mg/L toluene during growth but stripped of toluene before the kinetic test began; therefore, toluene dioxygenase enzymes were still present in solution. The appropriate amount of toluene was then added to attain the desired concentration.

With increasing toluene concentration, the rate of TCE degradation increased, presumably because of the increased production of toluene oxygenase enzymes. The toluene concentrations and toluene yield were small enough that the cell concentrations did not increase significantly by the end of the experiment. This result further supports the lack of enzyme competition, even in the presence of moderate concentrations of toluene.

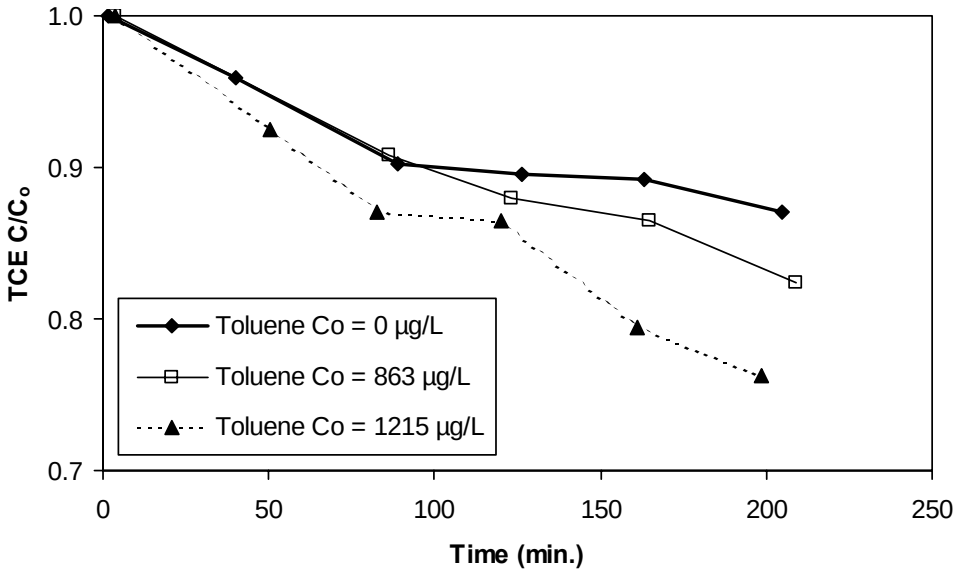

Figure 4.10 TCE Batch Cometabolism in the Presence of Increasing Initial Toluene Concentrations, X_o = 19 - 26 mg/L

4.3.2 Effect of Iron on Biodegradation

To increase the TCE cometabolism rate, iron was added to the culture during growth. Iron was added because it is part of the chemical make-up of the five-protein toluene oxygenase enzyme system. In addition, reduced iron is needed for the reaction of one of the five enzymes, the iron-sulfur protein, with

toluene and oxygen to form *cis*-toluene dihydrodiol (Wackett and Gibson, 1988). The results of simultaneous toluene and TCE degradation using cultures grown with and without iron are shown in Figure 4.11. In the presence of iron, the toluene degradation rate increased, as expected. The TCE cometabolism rate, however, was significantly faster in the presence of iron (4.5 times), essentially making iron an on-off switch for TCE cometabolism. This finding allowed for a control method to determine the contribution of cometabolism compared to that of metabolism in bioregeneration. Furthermore, the faster TCE cometabolism occurs, the faster additional adsorption sites on the GAC will be regenerated. Therefore, rapid onset of cometabolism may further increase the GAC column service life.

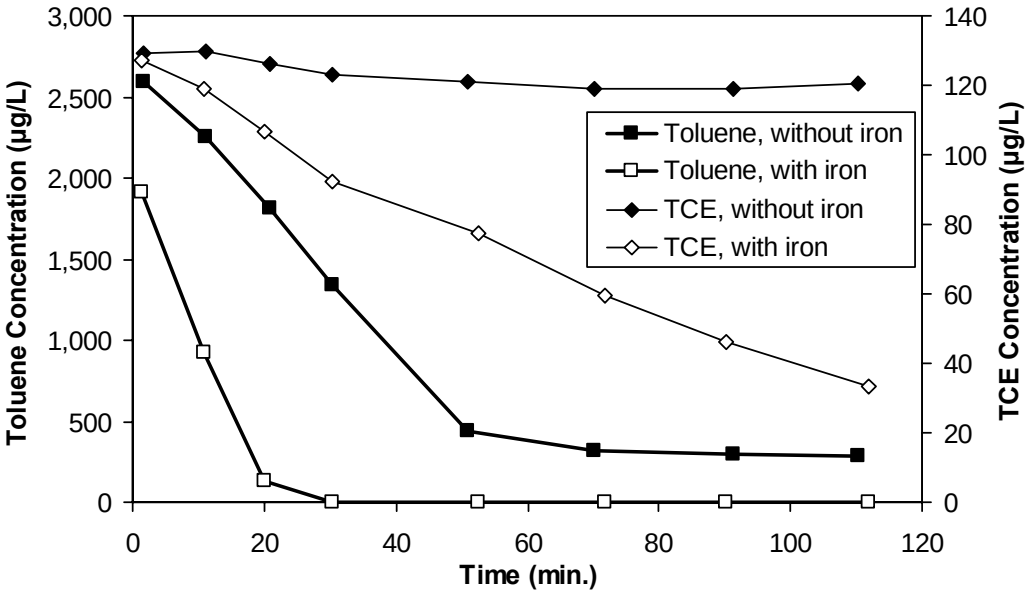

Figure 4.11 Toluene and TCE Batch Degradation With and Without Iron, X_o = 80 – 93 mg/L

4.3.3 Toluene Metabolism Kinetic Parameters

Separate experiments were undertaken for each chemical to determine individual metabolism or cometabolism kinetics because previous batch experiments had both toluene and TCE present. The batch metabolism rates for toluene were measured by ^{14}C-radiochemical techniques via the methods of Speitel (1985) and Speitel and DiGiano (1988). Figure 4.12 shows the typical increase in carbon dioxide, non-purgeable degradation products (NPPs), and cells as a result of the successful biodegradation of toluene. Radioactivity recovery was 93% by the end of batch experiment, indicating no significant toluene volatilization through the Teflon plunger. Endogenous decay tests were also performed (with and without iron) which monitored carbon dioxide production over time in the absence of any substrate. The biomass carbon fraction converted to CO_2, K_c, was determined from the slope of cumulative $^{14}CO_2$ formed versus ^{14}C-biomass remaining as shown in Figure 4.13. The endogenous decay coefficient, b, was determined from the slope of the natural log of the normalized biomass versus time as shown in Figure 4.14.

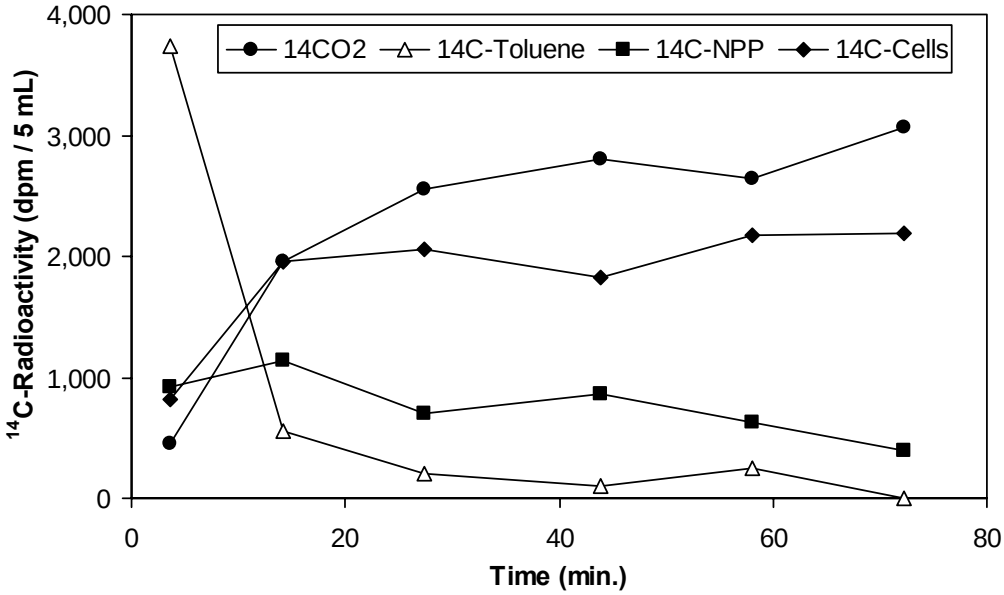

Figure 4.12 ^{14}C-Radiochemical Toluene Batch Metabolism With Iron, X_o = 40 mg/L

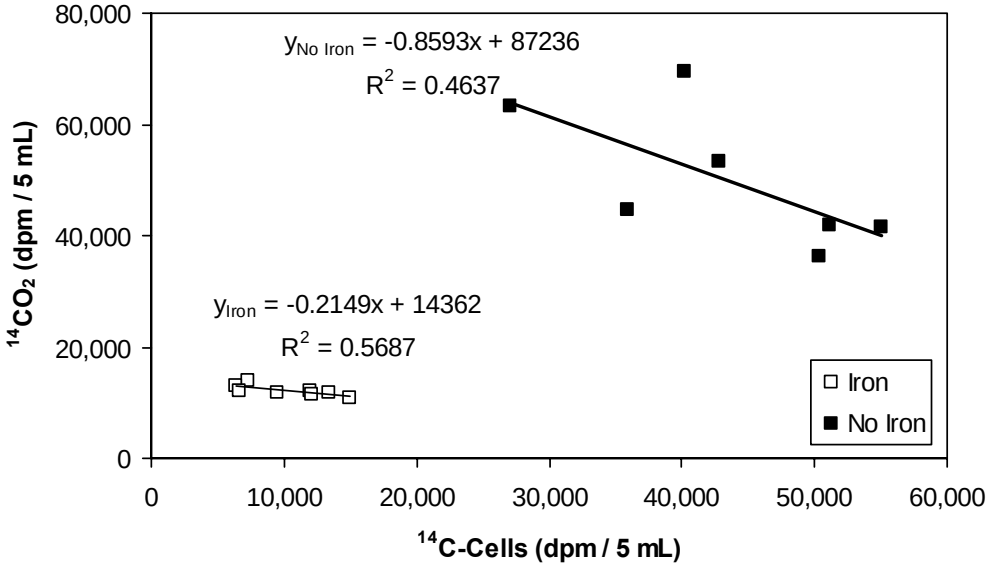

Figure 4.13 Determination of Biomass Carbon Fraction Converted to CO_2 (K_c) With and Without Iron

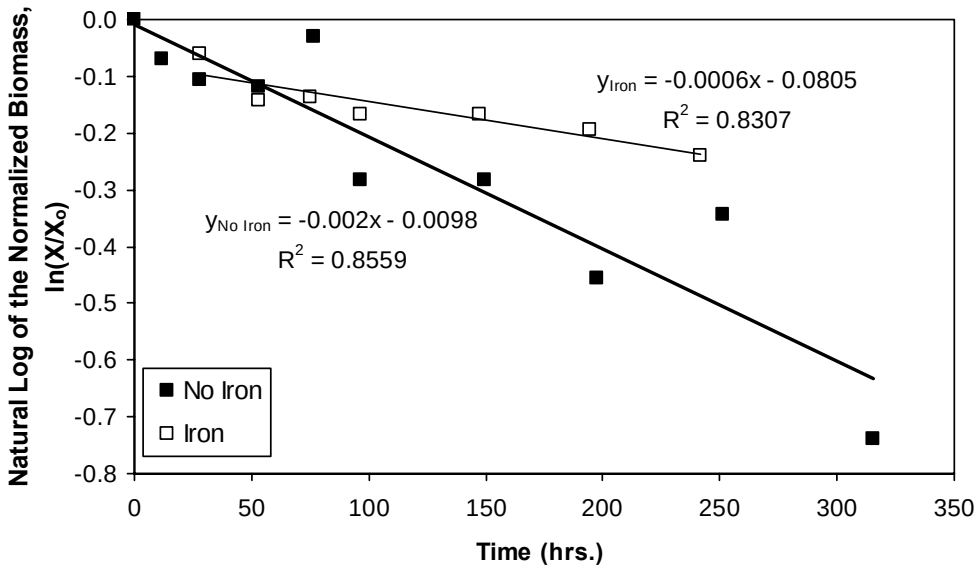

Figure 4.14 Determination of Endogenous Decay Coefficient (b) With and Without Iron

A 4th-order Runge-Kutta analysis was used to simultaneously fit the Monod equation to multiple data sets. Each batch kinetic data set varied in initial SOC concentration, biomass concentration, and in the presence or absence of iron. Multiple data sets were fit simultaneously to allow for experiments where the k could be estimated well but the K_s was difficult to ascertain with certainty and vice versa. One of the six iron-free data sets fit using this technique is shown in Figure 4.15 along with one of the seven iron-containing data sets. Parameters were estimated by minimizing the sum of the squares of the normalized error between predicted and measured concentrations using the Excel Solver function. The square of the error was normalized by the measured concentration. GC concentration data were used wherever possible due to the low accuracy of ^{14}C-toluene measurements at very small concentrations. The 95% joint confidence

interval for each parameter was then calculated using the sum of squares value that bounds the joint confidence region (S_c) as defined by Equation 4.1 (Berthouex and Brown, 1994):

$$S_c = S_r * [1 + F * (p /(n-p))] \quad \text{(Eq. 4.1)}$$

where S_r is the minimum sum of the normalized squares of the residual, F is the upper 5% value of the F distribution, p is the number of kinetic parameters, and n is the number of data points. Contour plots of 95% joint confidence regions were generated by varying the k and K_s values in the Monod equation and calculating the resulting sum of the normalized squares of the error between the measured and predicted concentrations. These joint confidence regions are shown in Figures 4.16 and 4.17 for toluene kinetic parameters without and with iron present, respectively. In these figures, the 95% joint confidence region is bounded by the S_c value. The kinetic parameters were determined by projecting the boundaries of the joint confidence region onto the k and K_s axes. The resulting parameters are listed in Table 4.3 (see Appendix C for the raw kinetic data).

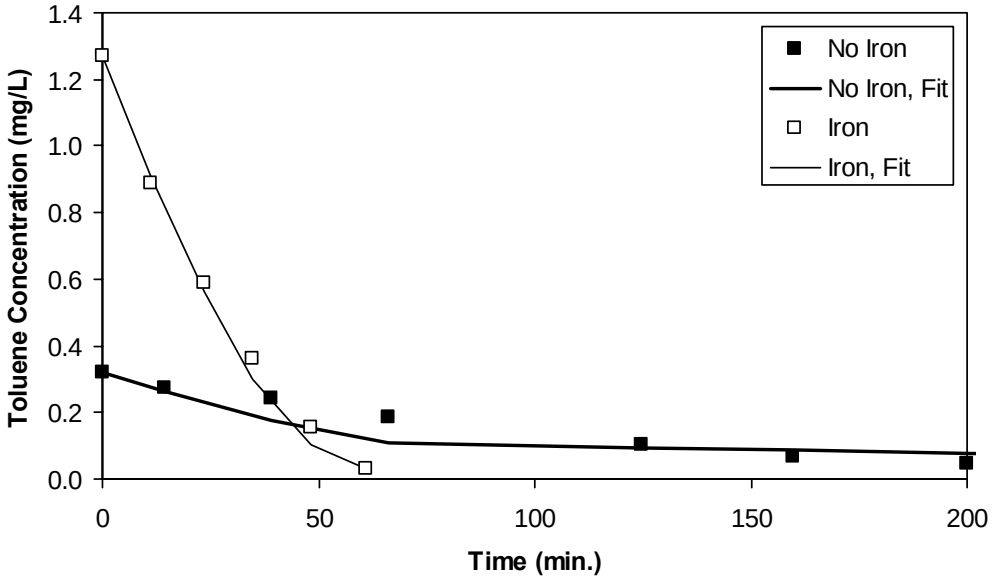

Figure 4.15 Example Runge-Kutta Monod Fits of Toluene Batch Degradation Data, X_o = 28 (iron) and 12 (no iron) mg/L

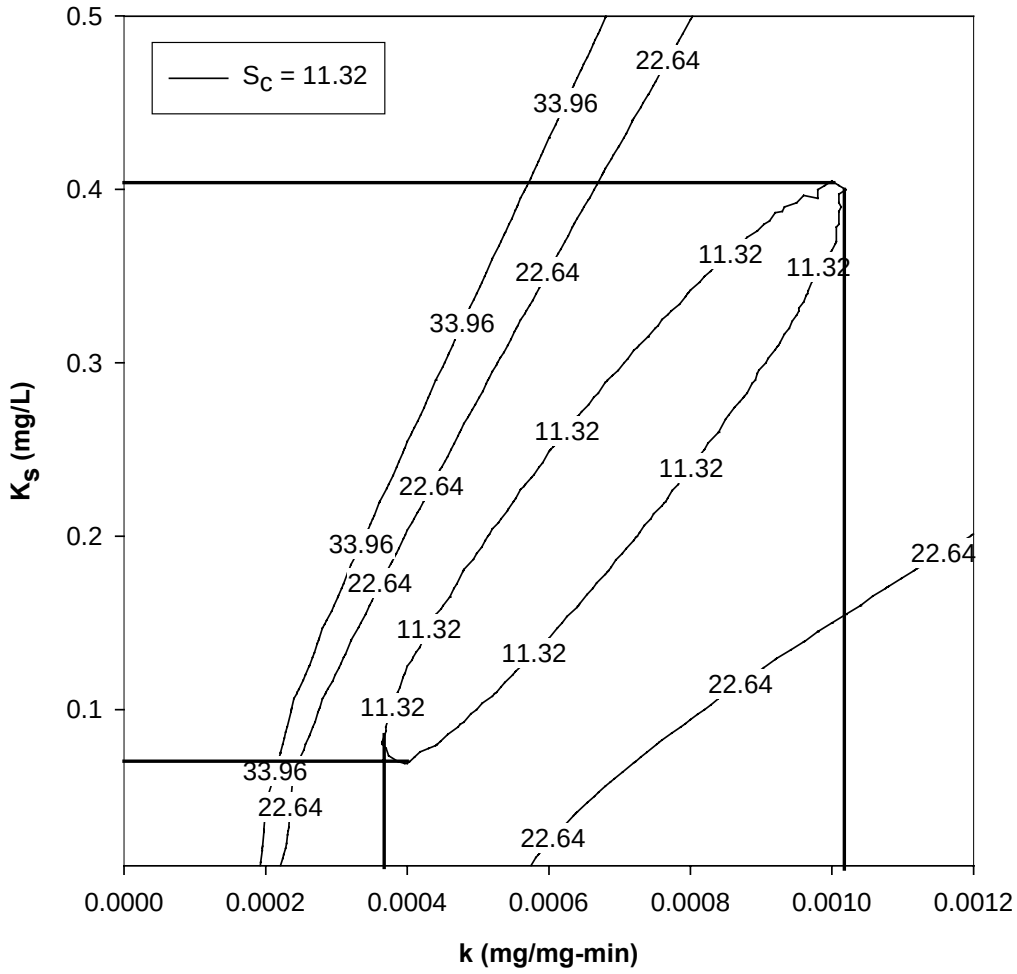

Figure 4.16 95% Joint Confidence Interval for Toluene Metabolism Without Iron

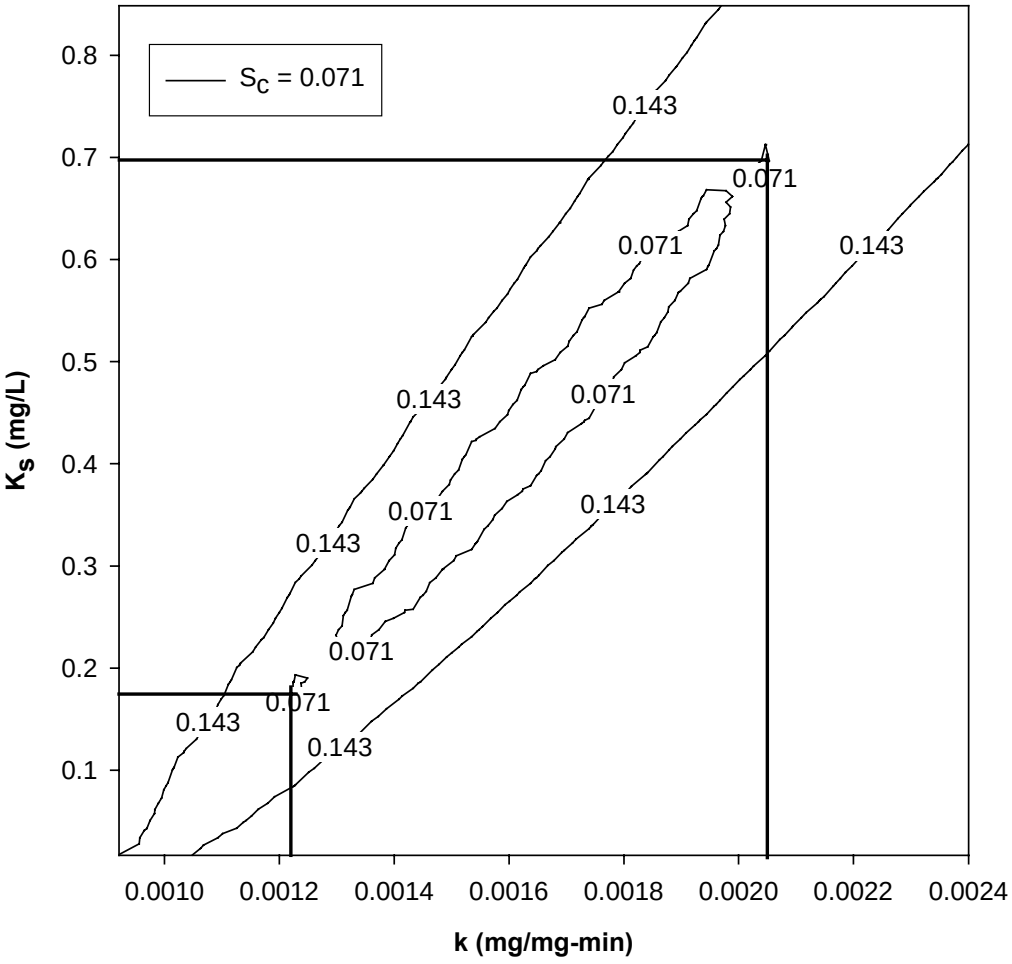

Figure 4.17 95% Joint Confidence Interval for Toluene Metabolism With Iron

Table 4.3 Monod Kinetic Parameters for Toluene

Parameter	**With Iron**	**Without Iron**	**Units**
Initial Conc. Range	105 to 1451	43 to 1400	µg/L
Avg. Yield	0.391	0.294	g C-cells/g C-toluene
Calculated Yield	0.201	0.201	g C-cells/g C-toluene
Maximum Substrate Utilization Rate, k	1.50×10^{-3}	5.40×10^{-4}	g toluene/g cells-min
95% Confidence Interval (CI) for k	1.23×10^{-3} to 2.05×10^{-3}	4.00×10^{-4} to 1.00×10^{-3}	g toluene/g cells-min
Half Saturation Coefficient, K_s	0.348	0.165	mg/L
95% CI for K_s	0.170 to 0.696	0.070 to 0.400	mg/L
Pseudo First Order Rate Constant, k_1	6.22	4.70	L/mg-d
95% CI for k_1	2.83 to 9.61	1.73 to 12.48	L/mg-d
Biomass Carbon Fraction Converted to CO_2, K_c	0.215	0.86	dpm CO_2/dpm cells
R^2 for K_c	0.569	0.46	
Endogenous Decay Coefficient, b	0.0006	0.002	1/hr
R^2 for b	0.83	0.86	

4.3.4 TCE Cometabolism Kinetic Parameters

Experiments also were undertaken with TCE alone to measure cometabolism kinetics. Figure 4.18 shows results from a ^{14}C-radiochemical kinetic test with TCE. The culture was fed 15 mg/L toluene during growth but stripped of toluene before the kinetic test began. The figure shows an increase in carbon dioxide as a result of the successful cometabolism of TCE. NPPs, or

degradation reaction intermediates, were also produced as TCE degradation occurred. Cometabolism rates are generally much slower than metabolism rates, thus explaining why the NPP concentration was larger than the CO_2 concentration, as contrasted by the large CO_2 production with toluene metabolism (Figure 4.12). There was also a slight increase in ^{14}C-cells over time in Figure 4.18. TCE and other chlorinated solvents are theorized to perturb the cell membrane thereby increasing cell cycling of fatty acids, but not actually increasing the transcription of toluene oxygenases (Heitzer *et al*., 1994). Thus, the increase in ^{14}C-cells may be due to the reaction of TCE with the cell membrane, not actual growth of cells, because no energy is provided to the microorganism from cometabolism. Furthermore, research has shown ^{14}C-TCE may be activated by toluene dioxygenase to produce radiolabeled reactive intermediates. These radioactive reactive intermediates can diffuse through the cell membrane and react with toluene dioxygenase and other proteins, resulting in the incorporation of ^{14}C and enzyme inactivation. (Wackett, 1992; Wackett and Householder, 1989). In addition, Newman and Wackett (1997) found after incubating a culture producing a toluene monooxygenase with ^{14}C-TCE, 12% of the remaining radioactivity was measured as radiolabeled proteins.

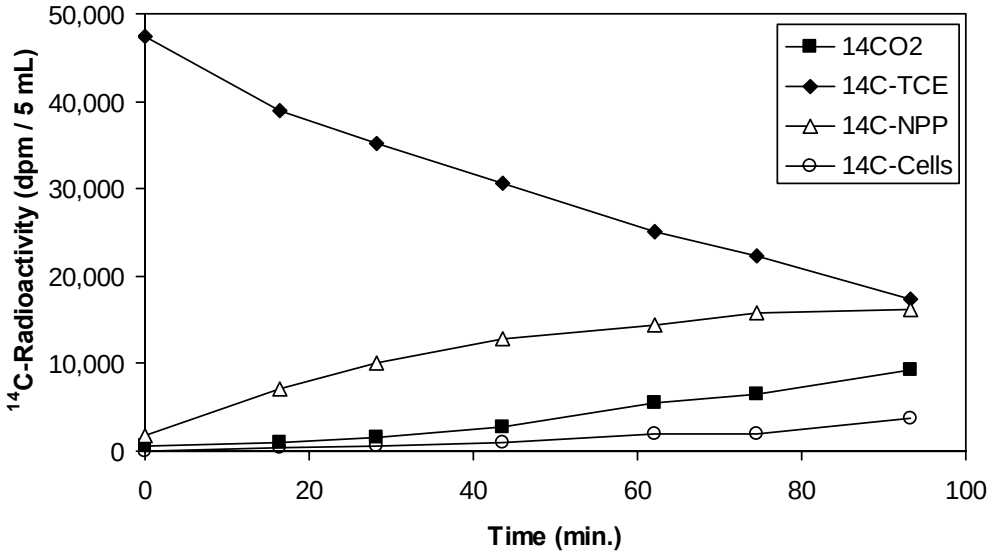

Figure 4.18 ^{14}C-Radiochemical TCE Batch Cometabolism With Iron, Xo = 105 mg/L

Transformation capacity experiments were also run for TCE with and without iron. The transformation capacity is a measure of the amount of a cometabolite that can be degraded before inactivation of the cells occurs due to intermediate toxicity. For experimental purposes, this translates to:

T_c = (Initial TCE Conc. – Final TCE Conc.)/ X. (Eq. 4.2)

where X is the cell concentration as measured by the average of the initial and final volatile suspended solids. Thus, the larger the transformation capacity, the less intermediate toxicity that occurred.

The resulting pseudo first order degradation rates (k_1), transformation capacities (T_c), and Monod parameters were estimated for cultures grown with and without iron and are shown in Table 4.4 (see Appendix C for the raw kinetic

data). Literature TCE T_c values range from 5.2 to 8.5 µg/mg for cultures using toluene as the primary substrate; however, some of these experiments were conducted with pure instead of mixed cultures and some had toluene present during the transformation capacity experiment (Chang & Alvarez-Cohen, 1996; Heald & Jenkins, 1994). Compared to these literature values, the T_c values in Table 4.4 are greater, indicating little intermediate toxicity at the concentrations tested. In addition, the T_c values shown in Table 4.4 were found to decrease with increasing microbial concentrations.

Table 4.4 Kinetic Parameters for TCE Cometabolism

Parameter	With Iron	Without Iron	Units
Initial (Non-T_c) Concentrations	13 to 325	90 to 1435	µg/L
Avg. Radioactive Yield	0.139	0.139*	g C-cells/g C-TCE
Calculated Yield	0	0	g C-cells/g C-TCE
Pseudo First Order Rate Constant, k_1	0.328	0.068	L/mg-d
95% Confidence Interval for k_1	0.173 to 0.483	0.031 to 0.105	L/mg-d
Avg. Transformation Capacity, T_c	16.2	27.1	µg TCE/mg cells
T_c Range**	9.5 to 23.0	14.2 to 48.3	µg TCE/mg cells

*estimated
**range of T_c values measured in all experiments

The average radioactive yield is also shown in Table 4.4. Due to the previously discussed slight increase in ^{14}C-cells over time when ^{14}C-TCE was used, a small radioactive yield was measured, despite a theoretical yield of zero

for cometabolism. Thus, in bioregeneration calculations for experiments where ^{14}C-TCE was used, a yield of 0.139g C-cells/g C-TCE was used; however, in MDBA modeling (see Chapter 6) of TCE cometabolism, a TCE yield of zero was used.

To estimate the TCE pseudo first order degradation rate (k_1), an exponential equation was fit to individual plots of TCE concentration versus time. The exponent from each equation was then divided by the biomass concentration to arrive at the estimate for k_1. These individual k_1 values were averaged to arrive at the overall k_1 presented in Table 4.4. For comparison, the Monod equation was also fitted to individual data sets using the solver function in Microsoft Excel to minimize the non-normalized error. The non-normalized error was used because more stable k_1 estimates resulted. The k_1 values for both of these methods were generally in agreement. The k_1 values found in this research were generally much larger (4 - 100 times) than those found in the literature (Segar et al., 1995; Folsom and Chapman, 1991).

For TCE, the combinations of substrate and biomass concentrations used in the batch kinetic tests were not sufficient to estimate the K_s. Thus, k could not be estimated because K_s and k are coupled parameters. For this reason, neither is listed in Table 4.4. Examples of TCE cometabolism data fit using the estimated pseudo first degradation order rate are shown in Figure 4.19 for experiments with and without iron. The K_c and b values are the same for both chemicals because the same culture was used to degrade both toluene and TCE.

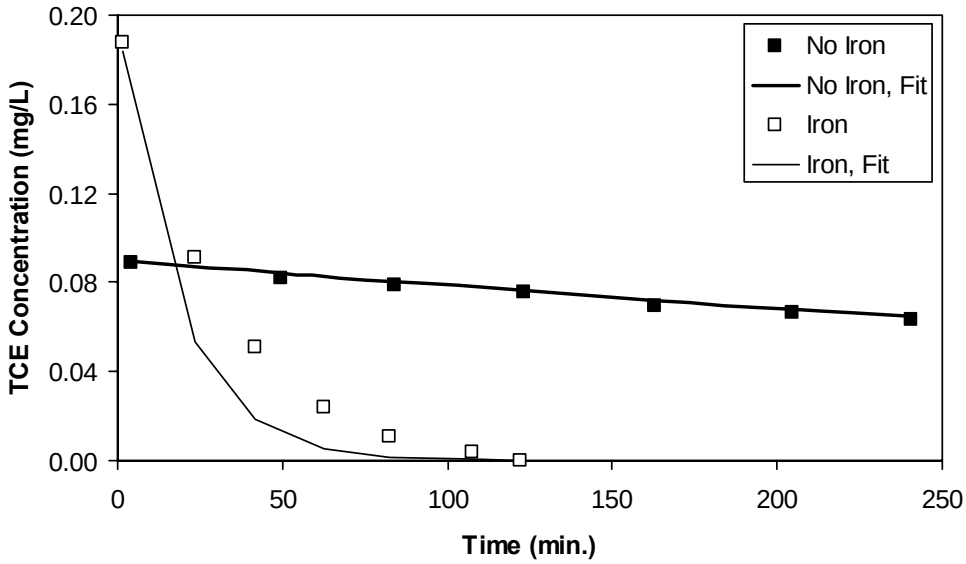

Figure 4.19 Example Pseudo First Order Equation Fits of TCE Batch Degradation Data, X_o = 249 (iron) and 29 (no iron) mg/L

4.3.5 Biological Activity Baseline

Baseline levels of biomass, protein, enzyme activity, and NADH were measured during growth of the mixed culture (grown with and without iron). These baseline levels provided a comparison for the levels measured during both batch biodegradation experiments and BAC column experiments. To measure the baseline levels, small samples of the mixed culture were taken over a four-day period (the feeding cycle). The raw data are shown in Appendix C. The resulting biomass, as measured by total suspended solids (TSS), and protein concentrations versus time are plotted in Figure 4.20. In Figure 4.20, the protein measurements over time were fairly similar, indicating consistency between the cultures. The TSS values (as estimated via optical density at 600 nm (OD_{600}), see Section 3.3.4)

for the iron-free culture were lower than that for the iron-fed culture, however. The protein only comprised an average of 11% of the cell mass, compared to the expected 50 to 65%. The protein measurement method used a combination of sodium hydroxide and heat to lyse the cells and solubilize the proteins before pelleting out the remaining insoluble material. Perhaps this lysing method was insufficient in lysing the cells, thereby resulting in the underestimation of the protein concentration.

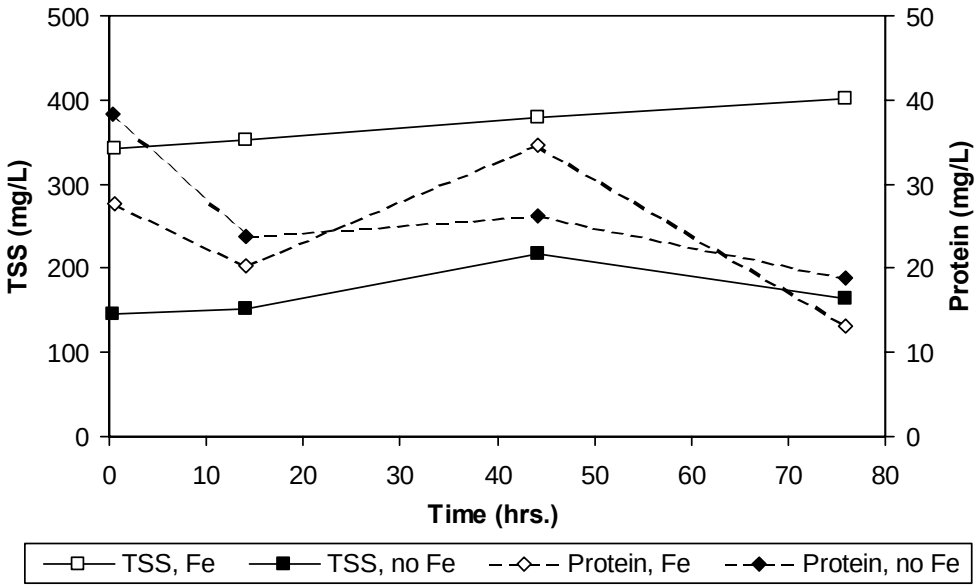

Figure 4.20 Baseline TSS and Protein Levels During Growth

The resulting TSS-normalized NADH and enzyme activity measurements are presented in Figure 4.21. The enzyme activity of the iron-free culture peaked then dropped off steeply compared to the iron-fed culture, indicating that the presence of iron may have added more stability to the enzyme activity in a batch environment. The relationship between the iron-containing and iron-free

measurements, however, was the opposite of what was expected given iron's beneficial effect on the TCE cometabolism rate: the iron-fed culture had lower NADH and enzyme activity levels than the iron-free culture. One possible explanation is that the OD_{600} measurement of the iron-free culture was artificially low due to aggregation of the cells into flocs, resulting in a low estimate of the TSS. In this case, the TSS-normalized NADH and enzyme activity measurements would have been artificially high. Another possible explanation is that the OD_{600} measurement of the iron-fed culture was artificially high due to the presence of iron precipitates ($Fe(OH)_{3(s)}$), resulting in a high TSS estimate. The growth culture had a pH of 6.8 and an iron concentration of 40 µM, resulting in a large concentration of iron precipitates. In this case, the TSS-normalized NADH and enzyme activity measurements would have been artificially low. These explanations are supported by the fact that the protein measurements were fairly similar, despite the large difference in TSS.

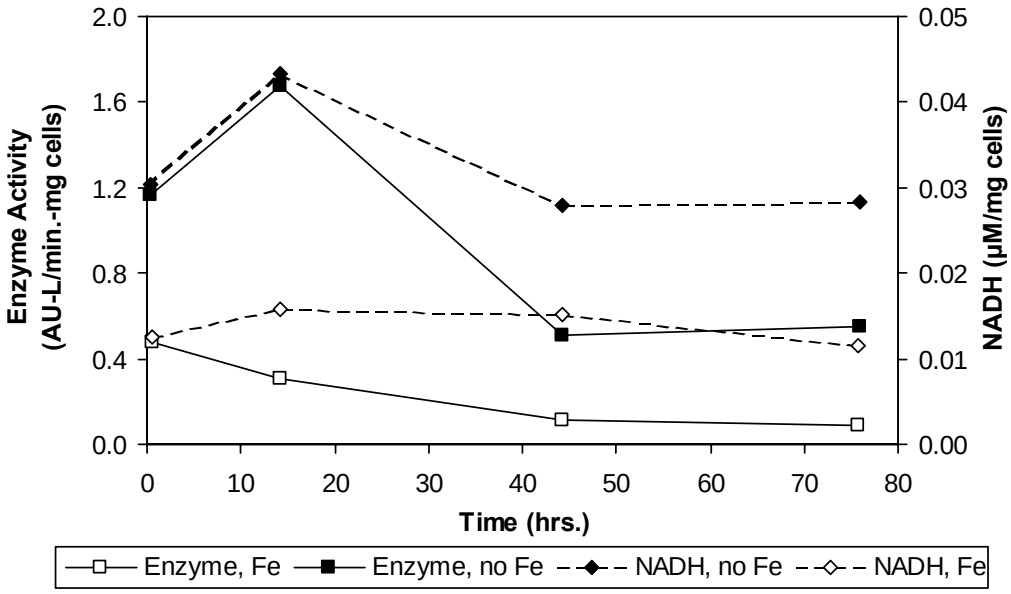

Figure 4.21 Baseline Enzyme Activity and NADH Levels During Growth

4.3.6 Enzyme Location

An experiment was also performed to verify that the toluene dioxygenase enzyme was located in the cytoplasm or periplasm of the cell rather than excreted or membrane-bound. Whether the enzyme is located within the cell or excreted is important because excreted enzymes may be washed out of a column, thus decreasing the amount of biodegradation that can occur within a column. Excreted enzymes may also adsorb to activated carbon, which would confound the modeling of BAC columns. The enzyme activity of an unfiltered culture sample was compared to a filtered sample as well as samples representing the enzyme concentration in the cytoplasm/periplasm and the cell membranes using the indole method described in Section 3.3.4. If the enzyme was located within

the cell, there would be a much larger enzyme activity measured in the unfiltered sample compared to the filtered one. If the enzyme was excreted, there would be little difference between the filtered and unfiltered samples. The raw enzyme activity (not TSS-normalized) data are shown in Appendix C. The results showed efficiency-normalized enzyme activities of near zero and 0.45 AU/min. in the filtered samples without and with iron present, respectively, and 178 and 63 AU/min. in the unfiltered samples without and with iron present, indicating the enzyme is not excreted, but contained within either the cytoplasm/periplasm or cell membrane.

4.4 SUMMARY

The adsorption equilibrium and kinetic results as well as the microbial kinetic results presented in this chapter were important in understanding and predicting the behavior of BAC columns treating toluene and TCE. The competition measured between toluene and TCE and the lack of significant enzyme competition or intermediate toxicity indicated the potential for significant cometabolism-based bioregeneration in BAC columns. The second phase of the research consisted of both exhausted and virgin BAC column experiments and is presented in Chapter 5.

Chapter 5: Bioregeneration Column Results

The main focus of this research was studying the relative effect of metabolism and cometabolism on GAC bioregeneration. To this end, there were two main research phases. The first phase, as discussed in Chapter 4, involved determining background equilibrium and kinetic parameters for each synthetic organic chemical (SOC). The second phase of this research, as discussed in this chapter, consisted of dual-component pre-exhausted and virgin biologically-active GAC (BAC) column experiments. The pre-exhausted BAC columns were both metabolism-only (toluene and PCE) and combined metabolism-cometabolism (toluene and TCE).

5.1 METABOLISM-ONLY EXHAUSTED COLUMN EXPERIMENTS

5.1.1 SOC Concentrations and Loadings

Once all the background adsorption and biological equilibrium and kinetic parameters were determined, continuous-flow, metabolism-only toluene (biodegradable) and PCE (nonbiodegradable) column experiments began. Depending upon the point in its service life, a GAC column contains three zones of varying length: exhausted GAC, partially exhausted GAC (also known as the mass transfer zone), and virgin GAC. Biological activity in the exhausted GAC zone has by far the most significant effect on process performance, and thus pre-exhausted GAC columns were the first of the two column types studied in this research (the other being virgin GAC columns).

The operating conditions for two BAC column experiments are presented in Table 5.1. Different influent concentrations and EBCTs were tested to observe their effect on the extent of bioregeneration. The first experiment examined the interaction between two moderately adsorbable chemicals, toluene and PCE. The columns were seeded with the toluene-acclimated mixed culture used in the batch kinetics and then fed toluene and PCE concentrations at or slightly above the equilibrium concentrations of the exhausted GAC to ensure that decreases in effluent concentration were due solely to biodegradation. The effluent concentrations for each chemical in the 6.9-min. EBCT column are shown in Figure 5.1. The effluent toluene concentration decreased over time and then remained very low over the second half of the experiment. The decreased toluene concentration in the aqueous phase stimulated desorption and biodegradation of sorbed toluene. As a result, the effluent PCE concentration also decreased because of both the increased availability of adsorption sites on the GAC and decreased competition for these sites by toluene. If this experiment had been run to equilibrium, the effluent PCE concentration would have eventually increased back to its influent concentration as the GAC adsorption sites again became saturated. These results illustrate the potential for increasing the GAC service life for nonbiodegradable SOCs through bioregeneration of GAC containing biodegradable SOCs.

Table 5.1 Summary of Toluene-PCE Bioregeneration Experimental Conditions

Exp.	SOC	Initial GAC Equilibrium Conc. (µg/L)	Influent Conc. (µg/L ± 95% CI[b])	Duration (hrs)	Avg. EBCT (min)
1	PCE Tol[a]	842 610	845 ± 20.3 607 ± 26.5	506	6.9, 11
2	PCE Tol	477 498	501 ± 14.0 1003 ± 292	355	2.5, 12

[a]Tol = Toluene
[b]CI = Confidence interval

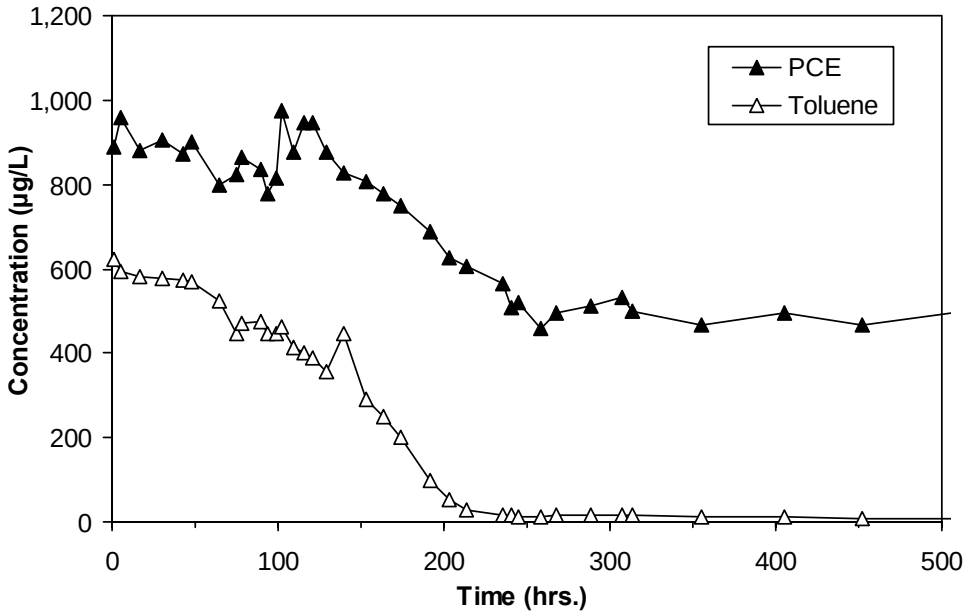

Figure 5.1 Effluent Toluene and PCE Concentrations, Exp. 1, 6.9-min. EBCT, No Iron, Avg. C_o = 610 (toluene) and 845 (PCE) µg/L

Some problems were encountered in maintaining aerobic conditions in the columns during vigorous bioregeneration (*i.e.*, biodegradation of sorbed toluene), as shown in Figure 5.2. The D.O. became limiting in the 11-min. EBCT column

at about 100 hours, resulting in a sharp decrease in biodegradation of toluene. The effluent D.O. before 100 hours was low as well, but was not limiting, as evidenced by a comparison of the shape of the initial toluene effluent curve in the low-D.O., 11-min. EBCT column and the higher-D.O., 6.9-min. EBCT column. This low effluent D.O. was not limiting because the initial bioregeneration rate was slow, as expected, resulting in a low D.O. demand. Had there been no interruption in oxygen supply at about 100 hrs, the effluent toluene concentration would probably have reached its low, steady-state value by about 150 hours instead of 250 hours based on the similarity of the slopes before and after oxygen interruption. The oxygen deficiency was corrected by adding small amounts of hydrogen peroxide to the influent, which was rapidly converted to oxygen when it came in contact with the GAC. Therefore, accurate estimation of oxygen consumption and provision of adequate oxygenation are important design considerations in BAC columns.

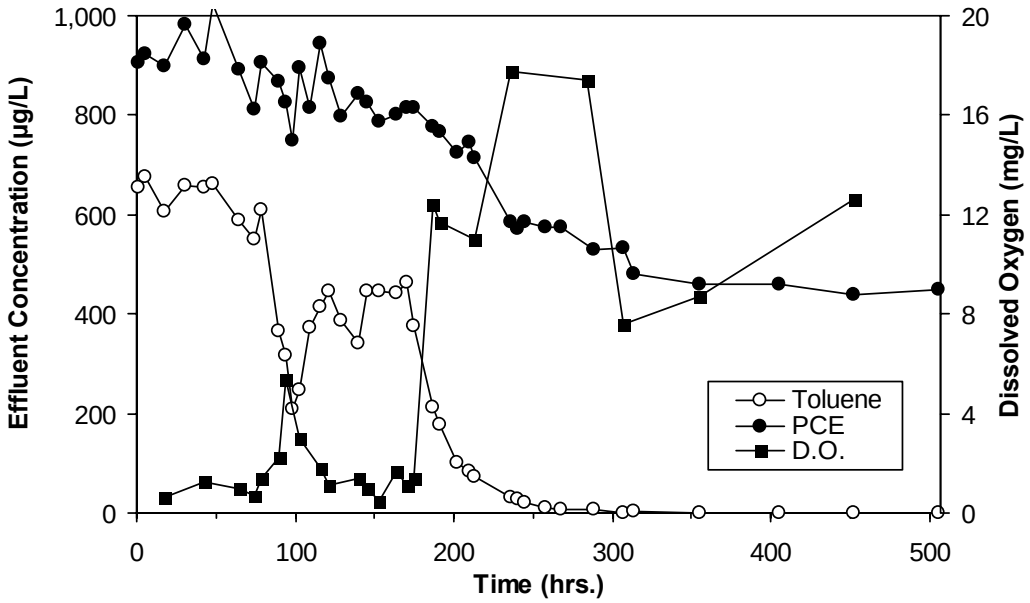

Figure 5.2 Effluent Toluene and PCE Concentrations and D.O., Exp. 1, 11-min. EBCT, No Iron, Avg. C_o = 610 (toluene) and 845 (PCE) µg/L

At the completion of Experiment 1, samples of GAC at the influent, middle, and effluent locations in each column were collected and extracted to determine the SOC loading (Figure 5.3). The ordinate shows the final GAC loading (q_f) normalized by the initial loading (q_o) for each SOC. The q_f/q_o ratio was less than one for toluene, and substantially so at the middle and effluent locations along the columns, providing further evidence of bioregeneration. In the case of the influent end of the column, very little contact time was available, so the toluene liquid phase concentration remained high, which provided little or no concentration gradient to drive desorption of toluene off the GAC. In contrast, the toluene concentration was very low at the effluent end, which caused a large driving force for toluene desorption and GAC bioregeneration.

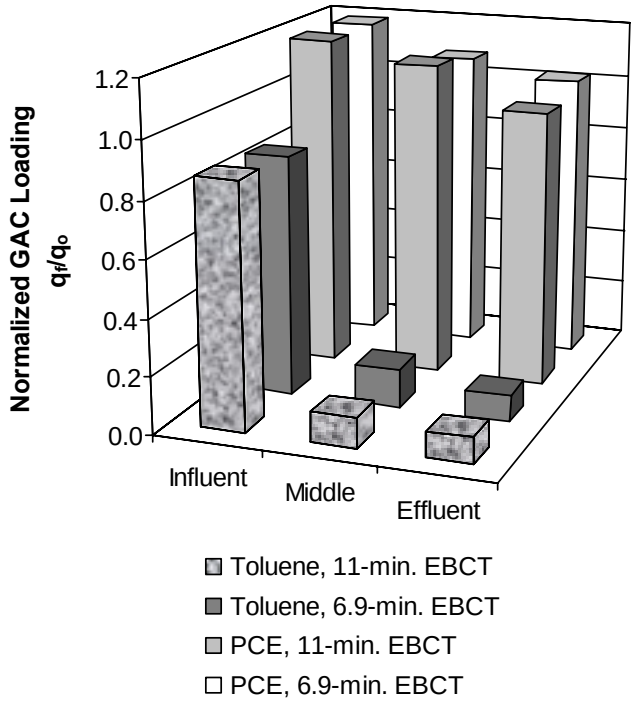

Figure 5.3 Final SOC Loading on GAC Column, Exp. 1, No Iron, Avg. C_o = 610 (toluene) and 845 (PCE) µg/L

The q_f/q_o ratio was greater than one for PCE, indicating that bioregeneration led to decreased competition for adsorption sites and further adsorption of PCE. The experiment also conclusively demonstrated that substantial additional adsorption capacity for nonbiodegradable chemicals can be realized through biodegradation of adsorbed chemicals. The q_f/q_o ratio for PCE decreased across the column, which is contrary to what would be expected if the entire GAC column had reached adsorptive equilibrium with respect to PCE, because the highest PCE q_f would be expected where the toluene q_f was lowest. This high PCE loading occurred where toluene was biodegraded because of the

decreased competition for adsorption sites. The typical duration of experiments in this research was several weeks, as opposed to the several months that would have been required to achieve equilibrium throughout the column. Thus, the shorter experiment time resulted in only the GAC near the beginning of the column becoming highly loaded with respect to PCE. Compared to the equilibrium loading expected for single-component adsorption, the PCE loading reached a maximum of 46% (at the influent end) for both columns in Experiment 1.

In Experiment 2, the EBCT in the shorter column was decreased from 6.9 to 2.5 minutes to more clearly observe the effect of EBCT on the extent of bioregeneration. Significant differences in the toluene effluent concentrations were observed between the two columns (Figure 5.4 vs. 5.5); the concentration was higher in the shorter EBCT column for a substantial portion of the experiment, as expected. This experiment also incorporated a small element of GAC at the effluent end of each column that had been equilibrated with ^{14}C-radiolabeled toluene prior to the start of the experiment. These radiolabeled elements were used to track bioregeneration over time. In Figures 5.4 and 5.5, the bioregeneration rate showed a peak corresponding to a large drop in toluene concentration, indicating that biodegradation of toluene in the liquid phase stimulated desorption and biodegradation of adsorbed toluene. In Figure 5.5, the D.O. level was limiting twice; therefore, the bioregeneration rate had two small peaks before the final large peak. The toluene in the outer portion of the GAC particles was readily available to microorganisms and was rapidly biodegraded. The bioregeneration rate probably decreased because diffusive transport

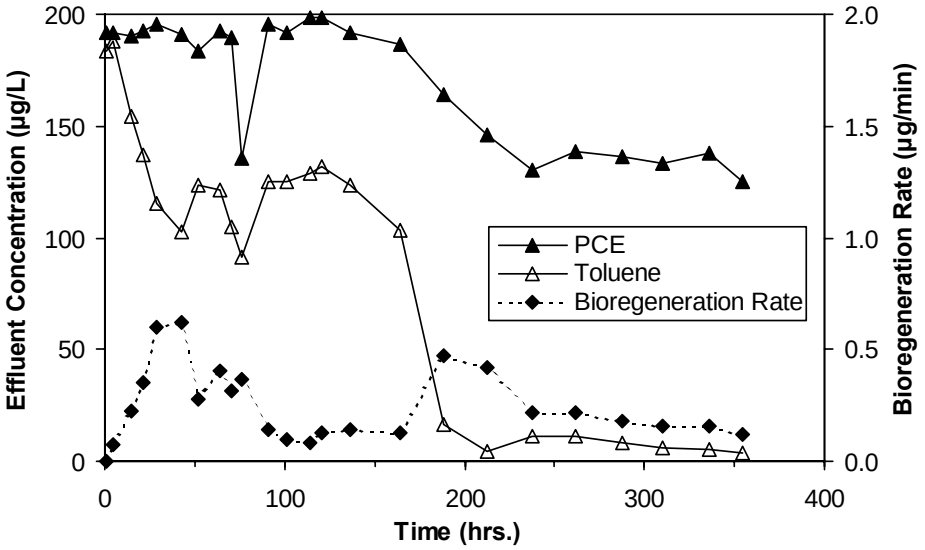

Figure 5.4 Effluent Concentrations and Toluene Bioregeneration Rate, Exp. 2, 2.5-min. EBCT, No Iron, Avg. C_o = 1000 (toluene) and 501 (PCE) µg/L

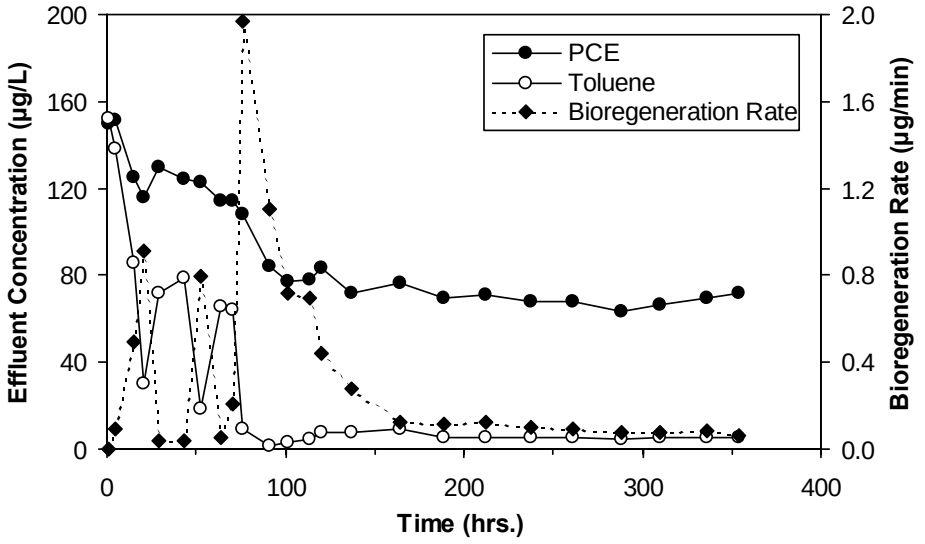

Figure 5.5 Effluent Concentrations and Toluene Bioregeneration Rate, Exp. 2, 12-min. EBCT, No Iron, Avg. C_o = 1000 (toluene) and 501 (PCE) µg/L

resistance in the GAC limited the bioregeneration of adsorption sites deeper inside the GAC, as reported by others (Speitel and DiGiano, 1987).

Again, a decrease in the effluent PCE concentration occurred after the onset of significant toluene biodegradation. This experiment further demonstrated the sequence of events for removal of nonbiodegradable SOCs: the onset of biodegradation drives the liquid phase concentration of the biodegradable SOC down, which in turn causes desorption and biodegradation of sorbed biodegradable SOC (bioregeneration); bioregeneration provides additional adsorption capacity for the nonbiodegradable SOC, which causes its liquid phase concentration to decrease and its GAC loading to increase.

This experiment also illustrated the important role of liquid phase concentration in this treatment process. More bioregeneration occurred at the effluent end of the 12-min. EBCT column than at the effluent end of the 2.5-min. column because the liquid phase concentration of the biodegradable SOC was substantially lower during the first half of the experiment. The effluent concentration of the shorter column was a representation of the liquid phase concentration that would have been measured about one-fifth of the way through the longer column. The effect of liquid phase concentration on bioregeneration was further illustrated by the relative size of the peak bioregeneration rates for both columns. The effluent end of the 12-min. EBCT column had a peak bioregeneration rate that was more than three times that of the effluent end of the 2.5-min. EBCT column. The larger bioregeneration rate led to a greater

availability of adsorption sites for the nonbiodegradable chemical, PCE, as evidenced by its lower effluent concentration in the 12-min. EBCT column.

5.1.2 Bioregeneration Calculations

With a detailed mass balance analysis of the radiochemical data, the rate and extent of bioregeneration over time can be estimated for the portion of the GAC column containing the radiolabeled element as explained in detail in Appendix A. The principal input to these calculations is $^{14}CO_2$ formation, but consideration of cell production, endogenous metabolism, and radiolabeled substrate leaving the GAC column is required to develop an accurate estimate of bioregeneration.

The extent of ^{14}C-based bioregeneration ranged from 39 to 46% in these experiments, which is larger than was seen in previous experiments with single chemical systems (Speitel 1985, Lu 1989, Speitel and DiGiano 1987, Speitel *et al*. 1989a). The larger extent of bioregeneration probably resulted from the higher concentrations used in this research. In addition, the greater the extent of bioregeneration, the greater the expected additional capacity for nonbiodegradable SOCs would be.

As shown in Table 5.2, bioregeneration was also measured via methanol extraction of the GAC at the end of the experiment. The toluene loading across the GAC was measured at the beginning and end of the experiment and the difference was attributed to toluene biodegradation. This loading difference was then divided by the initial loading to get a percent bioregeneration. There may have been a slight problem with this method, however, in that the methanol

extraction of the GAC may have only allowed for the SOC loadings within the outer, most easily desorbable portions of the GAC particles to desorb into the methanol solution. A slow desorption rate (and thus a reduced SOC recovery) would not have been a problem when performing extractions of GAC particles of uniform loading across the radius (*e.g.* GAC particles at equilibrium in an isotherm), but when substantial bioregeneration occurred, most of the toluene remaining on the GAC was likely to be deep in the micropores. Thus, this method may have underestimated the total toluene loading and overestimated the total PCE loading because it was assumed that the SOC loading was uniform across the GAC radius. In the case of a uniform SOC loading, the outer-diameter SOC loading could be extrapolated to the rest of the particle radius accurately. Because the total toluene loading on the GAC may have been underestimated, the resulting percent bioregeneration may have been overestimated compared to the ^{14}C-based bioregeneration in Table 5.2. Regardless, the methanol extraction technique for measuring bioregeneration was still a useful tool for relative comparison between experiments, especially when radioactive labeling of the SOC was not performed.

Table 5.2 Summary of Toluene-PCE Bioregeneration Experiment Results

Experiment	Avg. EBCT (min)	Toluene Bioregeneration (%)	
		^{14}C-Based	Extraction Based
1	6.9 11	—	90.8 90.8
2	2.5 12	39.4 45.5	61.0 67.8

It is also possible that the ^{14}C-based method for estimating bioregeneration may have underestimated the percent bioregeneration compared to the methanol extraction-based bioregeneration in Table 5.2. The measured parameters used in the detailed mass balance analysis of the radiochemical data had associated analytical and human error. It is possible, for example, that some $^{14}CO_2$ volatilized out of the column effluent samples during injection into the high or low-pH scintillation vials. This volatilization would result in a decreased estimate of ^{14}C-toluene metabolism and thus a decreased ^{14}C-based bioregeneration. It is also possible that the toluene Y or K_c was underestimated during batch measurement or was slightly larger in a column environment compared to a batch environment.

Figure 5.6 shows the methanol extraction-based bioregeneration near the effluent end of the column versus toluene equilibrium concentration and EBCT for Experiments 1 and 2. Two trends are suggested from this plot for moderately adsorbable SOCs: (1) a significantly shorter EBCT results in a smaller percent bioregeneration and (2) a lower equilibrium concentration results in a smaller percent bioregeneration. Both these findings have been suggested by previous research with single-component GAC columns (Speitel 1985, Lu 1989). A shorter EBCT implies a higher liquid phase concentration of the biodegradable SOC near the effluent end of the column, which in turn provides a smaller driving force for desorption and subsequent biodegradation of the sorbed SOC. The concentration dependence of bioregeneration is probably related to two phenomena. First, as concentration decreases the SOC loading on the GAC

surface decreases, which means that the SOCs on average are attached to higher energy adsorption sites. Desorption is more difficult from such sites and in the extreme may not occur at all (*i.e.*, irreversible adsorption). Second, lower concentrations inherently have a lower potential for establishing large concentration gradients within the GAC. Beyond the initial period of bioregeneration, the process tends to be diffusion limited, so the smaller concentration gradients associated with lower concentrations yield slower diffusion and thus slower bioregeneration rates.

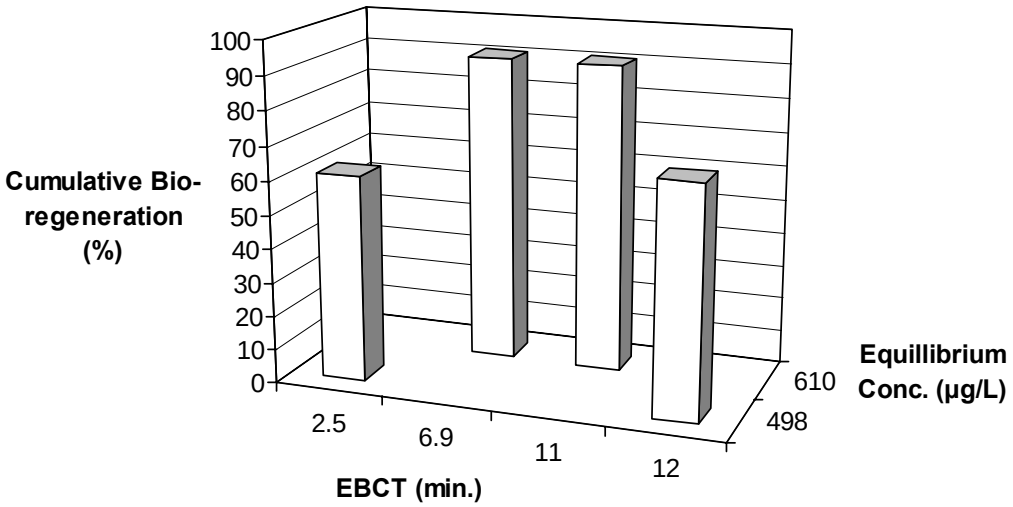

Figure 5.6 Effect of Toluene Equilibrium Concentration and EBCT on Toluene-Based Bioregeneration

5.2 COMBINED METABOLISM-COMETABOLISM EXHAUSTED COLUMN EXPERIMENTS

The operating conditions for four combined metabolism-cometabolism, exhausted BAC column experiments (Experiments 3 through 6) are presented in Table 5.3 (detailed data are provided in Appendix D). Different influent concentrations, EBCTs, iron loadings, and H_2O_2 concentrations were tested to observe their effect on the extent of metabolism- and cometabolism-based bioregeneration.

Table 5.3 Summary of Toluene-TCE Exhausted Bioregeneration Experimental Conditions

Exp.	SOC	GAC Equilibrium Concentration (µg/L)	Influent Conc. (µg/L)	Duration (hrs)	Avg. EBCT (min)	Iron[b] in Feed, H_2O_2
Sterile Column	TCE Tol[a]	569 556	916 1490	556	0.9	N, N
3	TCE Tol	181 1950	179 1740	671	A: 10.3 B: 10.4	N, Y Y, Y
4	TCE Tol	265 5680	266 6500	166	A: 3.4 B: 3.5	Y, Y Y, Y
5	TCE Tol	236 3270	200 3320	476	A: 2.3 B: 1.7	Y, Y Y, Y
6	TCE Tol	666 1240	721 1420	556	A: 3.0 B: 3.0	Y, N Y, N

[a]Tol = Toluene
[b]N = No, Y = Yes

5.2.1 Effect of Equilibrium Exchange on Bioregeneration

^{14}C-TCE was used in the toluene-TCE pre-equilibrated GAC columns to estimate the approximate onset and extent of TCE-based bioregeneration. One assumption of the ^{14}C-based method for estimating bioregeneration in pre-equilibrated GAC columns is that the only source of the ^{14}C-substrate is that

adsorbed onto the GAC (*i.e.*, there is no ^{14}C-substrate being fed in the influent). This assumption usually holds unless significant equilibrium exchange occurs between the ^{14}C-substrate and the non-radiolabeled ("cold") substrate. Equilibrium exchange leads to large concentrations of ^{14}C-substrate in the liquid phase and its replacement by "cold" substrate on the GAC. Equilibrium exchange confounds the interpretation of bioregeneration data because $^{14}CO_2$ formation can no longer be assured to be coming solely from the sorbed ^{14}C-TCE element. Instead, biodegradation of liquid-phase ^{14}C-substrate could overestimate the extent of ^{14}C-based bioregeneration. Thus, it was important to observe the extent of equilibrium exchange for all radiochemicals used in this research.

A 0.9-min. EBCT, sterile column consisting of only a ^{14}C-TCE radiolabeled element was run in parallel to the BAC columns in Experiment 6 to observe the amount of equilibrium exchange that occurred between the ^{14}C-TCE and the non-radiolabeled ("cold") TCE. Figure 5.7 shows the total effluent radioactivity over time for the sterile control column compared to Columns A and B of Experiment 6. The ^{14}C-toluene labeled column (Column A) was stable and then peaked as vigorous desorption and biodegradation of ^{14}C-toluene resulted in a high level of $^{14}CO_2$ in the effluent. In contrast, the ^{14}C-TCE labeled columns (Columns B and the sterile column) had large amounts of effluent radioactivity at the start of the experiment, which decreased nearly exponentially over time, and no radioactivity peak from bioregeneration was visible. This effluent radioactivity indicated that the amount of equilibrium exchange for ^{14}C-TCE was large.

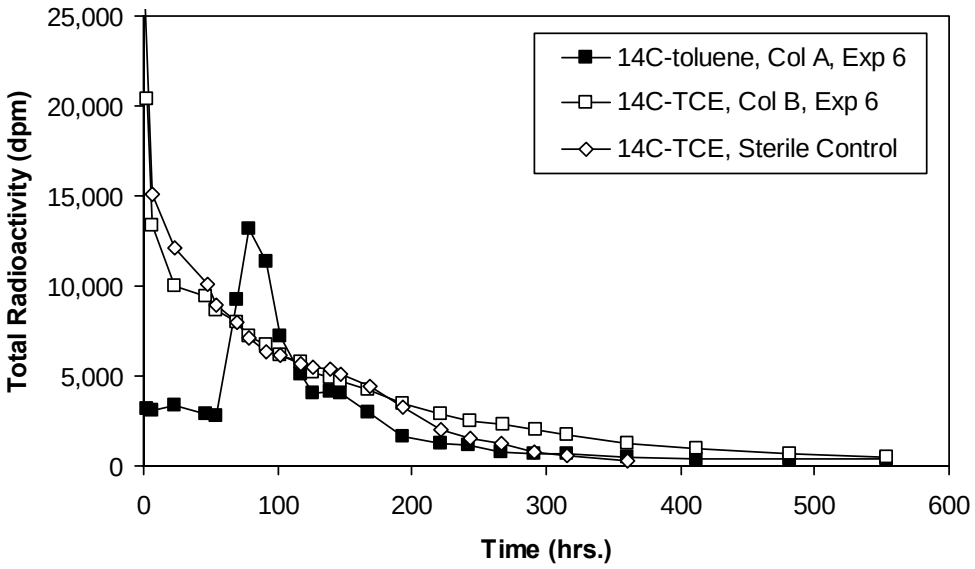

Figure 5.7 Total Radioactivity Profile for the Sterile Column (^{14}C-TCE, No Iron, 0.9-min. EBCT), Column A (biologically-active, ^{14}C-toluene, Iron, 3.0-min. EBCT), and Column B (biologically-active, ^{14}C-TCE, Iron, 3.0-min. EBCT) of Exp. 6

Figure 5.8 further demonstrates equilibrium exchange in the case of ^{14}C-TCE. The fraction of radioactivity desorbed off the GAC is plotted for the ^{14}C-TCE sterile column, both columns from Experiment 6, and a ^{14}C-toluene labeled column that was less biologically-active and was fed PCE. Figure 5.8 shows that significantly less ^{14}C-toluene desorption (and by correlation, equilibrium exchange) occurred than ^{14}C-TCE desorption, despite most of the ^{14}C-toluene desorption being due to toluene metabolism. Furthermore, the extent of toluene-based bioregeneration was essentially the same during the first 80 hours, regardless of the presence of TCE or PCE. In the case of the less biologically-active column, an un-acclimated culture was used to seed the column and thus

biodegradation was slow with the $^{14}CO_2$ peak occurring at 300 hrs. The less biologically-active column demonstrated the effect of small and large amounts of toluene metabolism on the amount of ^{14}C-toluene desorbed. As the amount of toluene metabolism increased, the amount of ^{14}C-toluene desorbed increased, as expected.

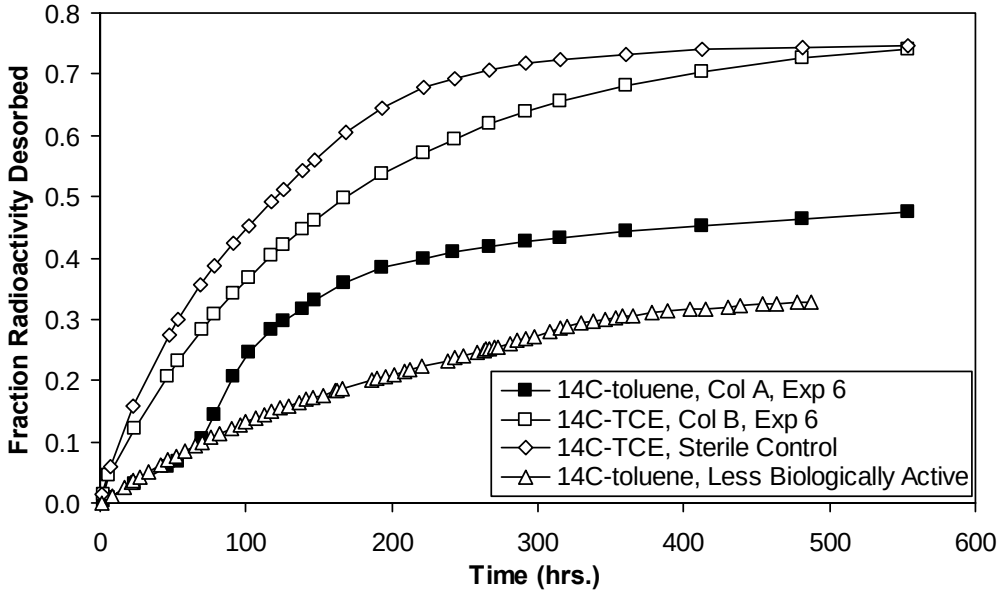

Figure 5.8 Fraction Radioactivity Desorbed for the Sterile Column (^{14}C-TCE, No Iron, 0.9-min. EBCT), Column A (biologically-active, ^{14}C-toluene, Iron, 3.0-min. EBCT), Column B (biologically-active, ^{14}C-TCE, Iron, 3.0-min. EBCT) of Exp. 6, and the Less Biologically Active Column (^{14}C-toluene, No Iron, 5.0-min. EBCT)

^{14}C-TCE was still used to track cometabolism in subsequent pre-exhausted column experiments despite problems with equilibrium exchange because information could still be gathered from the resulting data. Despite concerns of overestimation, the extent of the TCE-based bioregeneration measured with ^{14}C-TCE was estimated to be similar to the real value. This was evidenced by the

extent of TCE-based bioregeneration in Column B of Experiment 6,as shown in Table 5.4. Despite equilibrium exchange occurring in this column, the extent of bioregeneration was still estimated to be 0.0%. It is possible that the biofilm decreased the equilibrium exchange kinetics slightly, resulting in a closer estimate of the true extent of TCE-based bioregeneration than a sterile column would. Nevertheless, the most important information that comes from the TCE-based bioregeneration measurements is their values relative to each other as well as relative to the toluene-based measurements.

5.2.2 Effect of Fenton's Oxidation on Bioregeneration

In Experiment 3, two approximately 10.5-min. EBCT columns were run side by side. As with Experiments 1 and 2, the columns were seeded with either the iron- or non-iron acclimated, toluene-acclimated mixed culture used in the batch kinetic experiments. The columns were fed toluene and TCE concentrations at or slightly above the equilibrium concentrations. Due to difficulties controlling the toluene influent concentration, however, it was slightly lower than the equilibrium concentration. Each column contained the same GAC pre-equilibrated (exhausted) with toluene and TCE as well as identical plugs of ^{14}C-TCE-equilibrated GAC at the ends. One column was deprived of iron in its influent and thus only metabolism of toluene was expected (due to the need for iron to initiate significant cometabolism with this culture as described in Section 4.3). The other column, however, had a small amount of iron added to the influent stream shortly before the entrance to the column in order to "switch on" the cometabolism of TCE. The combined metabolism-cometabolism column was

also fed H_2O_2 to maintain the D.O. of the column and induce Fenton's oxidation. In the iron-fed column, an increase in the GAC bioregeneration and thus column performance was expected from a combination of (1) decreased competition for GAC adsorption sites through metabolism of the biodegradable SOC (toluene), (2) reduced demand for GAC adsorption sites by the traditionally nonbiodegradable SOC (TCE) due to cometabolism as well as Fenton's oxidation.

Fenton's oxidation has both positive and negative effects on the GAC column performance. Improvements in the column performance are seen because of (1) a D.O. increase within the column and (2) the production of hydroxyl radicals, which degrade TCE (and to a lesser degree toluene) to carbon dioxide, thereby reducing the demand for GAC adsorption sites. These same hydroxyl radicals, however, can inactivate or destroy the biofilm near the influent portion of the column. This cell destruction decreases the amount of bioregeneration that can occur, which in turn has negative effects on the GAC column performance. Thus, it was important in this research to find a balance between the positive and negative effects of hydrogen peroxide addition.

The resulting toluene and TCE effluent concentration profiles for Column A (iron-free influent) of Experiment 3 are shown in Figure 5.9. The toluene concentration in the column quickly decreased after a short lag period and was nondetectable by approximately 100 hrs, after which the effluent TCE concentration also decreased. The same toluene effluent concentration profile was found for Column B (iron-containing influent).

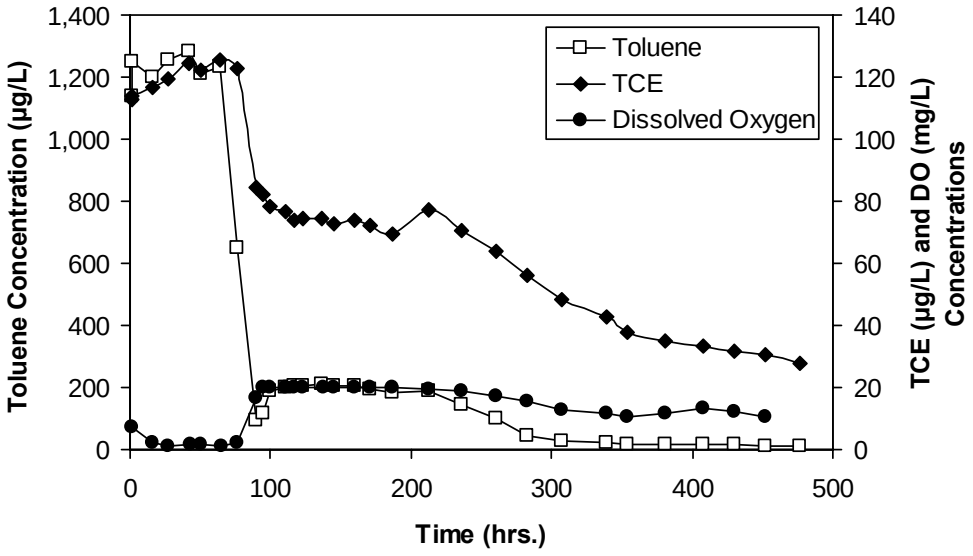

Figure 5.9 Effluent Toluene and TCE Concentrations and D.O., Exp. 3, Iron-Free Influent, 10.3-min. EBCT, Avg. C_o = 1740 (toluene) and 179 (TCE) µg/L

The iron-containing column, depending on the extent of cometabolism and Fenton's oxidation, should maintain a lower TCE effluent concentration for a longer period of time than a metabolism-only column and may never increase back to the influent concentration. Figure 5.10 shows the difference in TCE concentration between the iron-free and the iron-containing columns. For the first 100 hours, the effluent TCE concentrations were essentially identical. Then for the next 200 hours, the TCE concentration in the iron-containing column decreased more rapidly then the in the column with the iron-free influent. This difference was presumably due to increased Fenton's oxidation (due to an increase in the H_2O_2 influent concentration at 94 hrs.) and cometabolism in the

iron-fed column, thereby reducing competition as well as demand for adsorption sites.

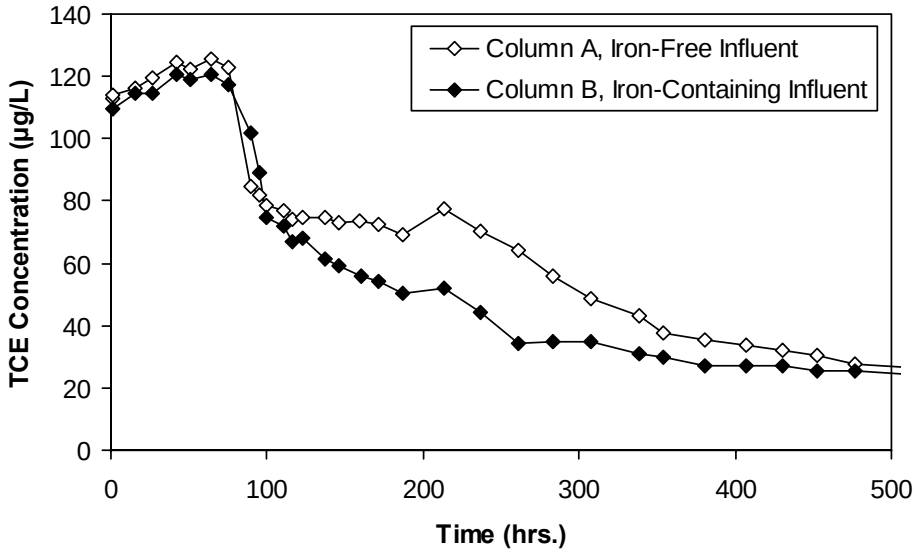

Figure 5.10 TCE Effluent Concentrations, Exp. 3, Avg. C_o = 1740 (toluene) and 179 (TCE) µg/L

By the end of the experiment, however, the TCE concentrations were nearly the same. This similarity probably occurred because a certain amount of iron is normally present in GAC. A fraction of this iron may have been available to the biofilm, thus allowing TCE cometabolism to take place in what would normally have been the "metabolism-only" column. If this was true, then the only real difference between the columns was that Fenton's oxidation and an iron-acclimated culture were present in the cometabolism column. Because the TCE effluent concentration difference between the two columns was small by the end of the experiment, this experiment indicated Fenton's oxidation did not have an

overall net positive effect on the reduction of the effluent TCE concentration. The large decrease in the TCE effluent concentrations from both columns, however, demonstrated the combined benefit of biological activity on the column performance.

The effect of Fenton's oxidation on TCE removal was also studied in the anthracite column experiments (Section 5.3.1). Fenton's oxidation was found to be insignificant as a TCE removal mechanism because little difference was seen between the influent and effluent TCE concentrations in a column where Fenton's oxidation was the only TCE removal mechanism present. Thus, Fenton's oxidation at the neutral pHs and the H_2O_2 concentrations used in this research was not deemed a worthwhile addition to the GAC column.

Elements of radiolabeled TCE GAC in Experiment 3 allowed for the contributions of cometabolism at the effluent ends of the columns to be measured by tracking the concentration of radiolabeled carbon dioxide that was produced as a result of any cometabolism. $^{14}CO_2$ production could only come from cometabolism at the effluent portion of the columns and not from direct Fenton's oxidation because hydroxyl radicals (and their precursor hydrogen peroxide) are unstable and highly reactive; thus, they were unlikely to reach the effluent portion of the column. This instability was evident in the measurement of enzyme activity, which was inhibited by the presence of oxidizers, across the column in Section 5.2.3. Figures 5.11 and 5.12 show the expected increase in metabolic products associated with cometabolism (CO_2 and NPPs) and lack of cell growth. $^{14}CO_2$ production showed a peak around 100 hours corresponding to the large

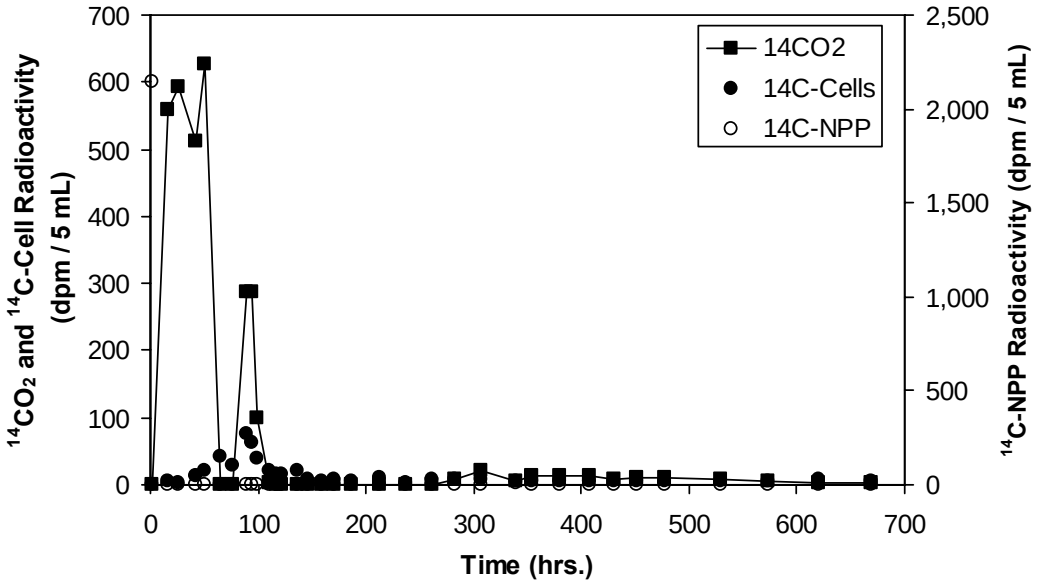

Figure 5.11 TCE Radioactivity Profile, Exp. 3, Iron-Free Influent, 10.3-min. EBCT, Avg. C_o = 1740 (toluene) and 179 (TCE) µg/L

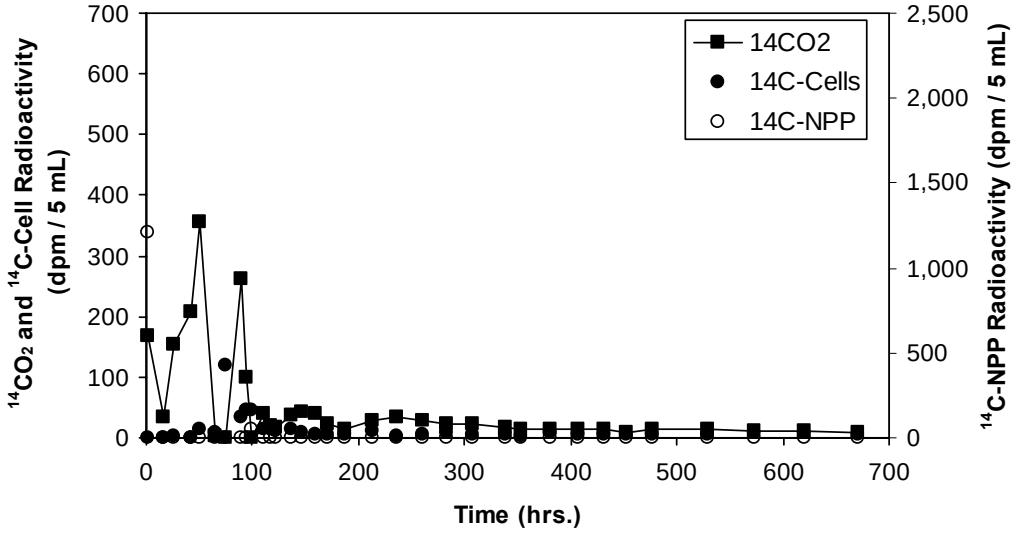

Figure 5.12 TCE Radioactivity Profile, Exp. 3, Iron-Containing Influent, 10.4-min. EBCT, Avg. C_o = 1740 (toluene) and 179 (TCE) µg/L

drop in toluene concentration as seen in Figure 5.9, indicating that the initial period of vigorous biodegradation of toluene produced toluene oxygenase enzymes that cometabolized the TCE. The peaks in Figures 5.11 and 5.12 prior to 100 hours are probably due to dynamic exchange of the ^{14}C-TCE during the initial phase of the experiment. This was corroborated by MDBA modeling of Column A (iron-free influent) in Figure 6.4.

Using a detailed mass balance analysis of the radiochemical data, the rate and extent of bioregeneration over time was estimated for the ^{14}C-TCE portion of the GAC column containing the radiolabeled element (Appendix A). Table 5.4 shows after 475 hours, the extent of cometabolism-based bioregeneration was 2.2% for the iron-fed column and 3.6% for the column with the iron-free influent. This TCE-based bioregeneration was in addition to the amount of GAC bioregenerated by toluene metabolism, which in Experiments 1 and 2 was between 39 and 46% for slightly lower influent toluene concentrations. The reported values for ^{14}C-TCE-based bioregeneration were most likely overestimated due to dynamic exchange of ^{14}C-TCE. Nevertheless, the cumulative fraction of cometabolism-based bioregeneration was smaller than that for toluene metabolism because of the difference between metabolism and cometabolism rates. The fact that the cometabolism-based bioregeneration was slightly larger in the column with the iron-free influent than the iron-containing influent further suggested that iron present in the GAC particles was utilized in the cometabolism of TCE.

5.2.3 Effect of EBCT and Enzyme Activity on TCE-based Bioregeneration

Experiment 4 was essentially the same as Experiment 3 except that it had a decreased EBCT and an increased toluene to TCE concentration ratio. Experiment 4 consisted of two approximately 3.5-min. EBCT columns run in parallel. The columns were both seeded and packed with the same GAC pre-equilibrated with toluene and TCE. One column (Column A) had a small element of ^{14}C-TCE at the end to track the end products of cometabolism whereas the other column (Column B) had a small element of ^{14}C-toluene to track the end products of metabolism. Both columns were fed iron and hydrogen peroxide to induce both cometabolism and Fenton's oxidation as well as to maintain the D.O. within the column. This experimental setup allowed for the simultaneous measurement of both toluene- and TCE-based bioregeneration.

Resulting toluene and TCE effluent concentrations are shown for Column B in Figure 5.13 (results were similar for Column A). The toluene concentration in the column quickly decreased down from the concentration of the influent, as did the effluent TCE concentration. The iron fed in the influent formed a hydroxide precipitate, however, which by around 140 hours clogged the influent section of the column. This clogging resulted in a quick increase in effluent toluene and TCE concentrations as the decrease in void spaces decreased the packed bed contact time and thus decreased the amount of biodegradation that could take place. Fluidized bed columns were considered as an alternate to packed bed columns in response to this iron clogging problem. It was determined, however, that a switch to fluidized beds would only delay the column

clogging, not stop it. In addition, the radiolabeled element method would not be usable for measuring bioregeneration, as the location of the radiolabeled element would not be permanent in a fluidized bed. Thus, the use of packed bed columns was continued and other measures for clogging abatement were employed.

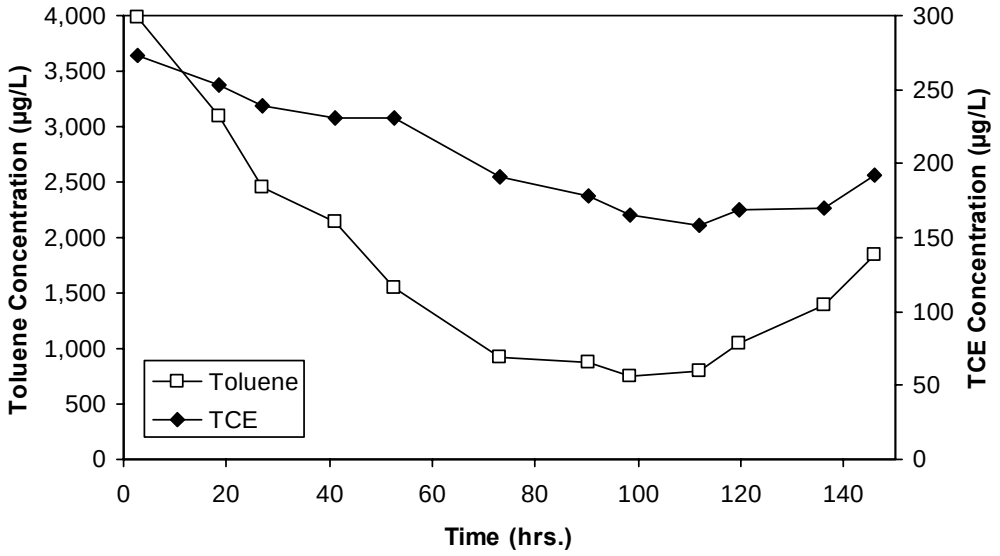

Figure 5.13 Effluent Concentrations, Exp. 4, Metabolism-Tracking Column, Iron, 3.4-min. EBCT, Avg. C_o = 6500 (toluene) and 266 (TCE) µg/L

At the completion of Experiment 4, the SOC loading was determined via methanol extraction at the influent, middle, and effluent ends of the columns (Figure 5.14). The ordinate shows the final GAC loading (q_f) normalized by the initial loading (q_o) for each SOC. The final SOC loadings between the columns were fairly replicable, as expected. The lines between data points are presented only to guide the eye, not to indicate knowledge of the SOC loading in those areas of the column. The q_f/q_o ratio was equal to or less than one for toluene and

decreased across the columns. This pattern was seen because the liquid phase toluene concentration decreased due to biodegradation across the column, providing an increased driving force for desorption of toluene off the GAC and thus GAC bioregeneration. The TCE loading increased across the column, presumably because of a high amount of TCE cometabolism at the influent and middle portions of the column.

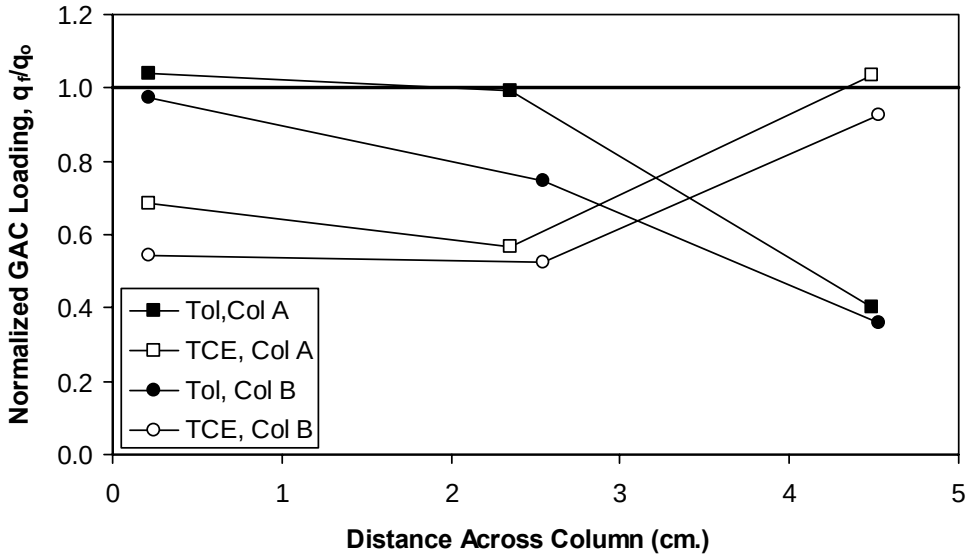

Figure 5.14 Final SOC Loadings, Exp. 4, Column A (metabolism-tracking, 3.4-min. EBCT) and Column B (cometabolism-tracking, 3.5-min. EBCT), Iron, Avg. C_o = 6500 (toluene) and 266 (TCE) µg/L

This TCE cometabolism rate was large near the influent end of the column because of the enzyme activity in that region. Figure 5.15 shows the enzyme activity across the column for Experiments 3 through 5, where for each experiment Column A is the metabolism-only or metabolism-tracking column and Column B is the cometabolism-tracking column. In addition, Figure 5.16 shows

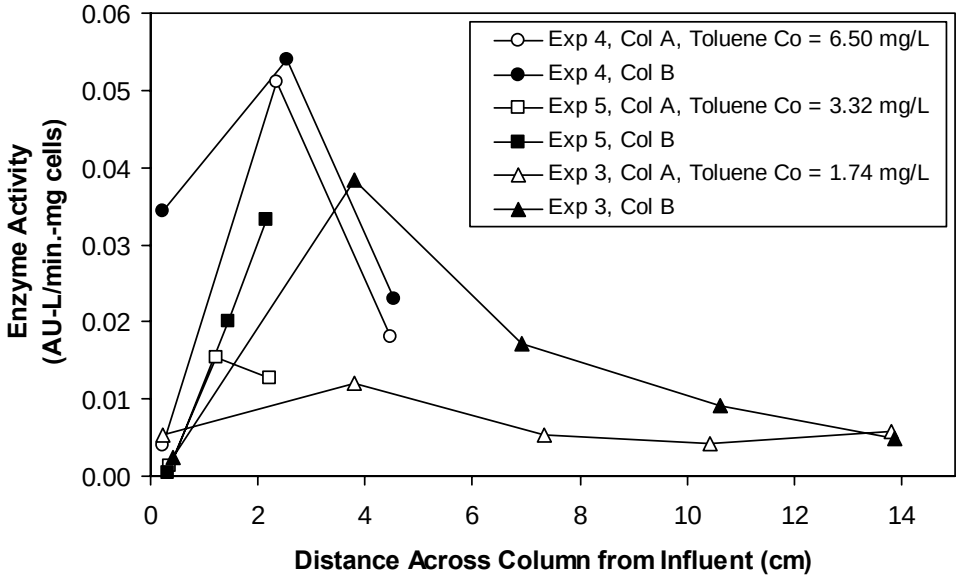

Figure 5.15 Enzyme Activity Across the Column, Exps. 3 – 5 (with H_2O_2)

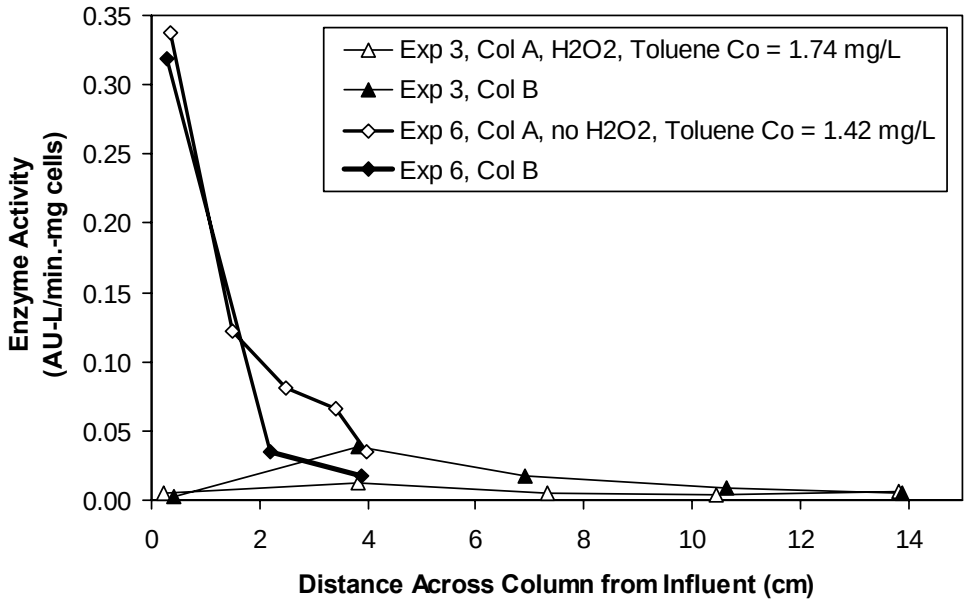

Figure 5.16 Enzyme Activity Across the Column, Exps. 3 (with H_2O_2) and 6 (very little H_2O_2)

the enzyme activity across the column for Experiment 3 in comparison to that for Experiment 6. In both figures, the biomass-normalized enzyme activity decreased across the columns. Experiments 3 through 5 involved feeding hydrogen peroxide, and its effect on the enzyme activity was clear compared to Experiment 6 where very little hydrogen peroxide was used. Any un-reacted hydrogen peroxide or hydroxyl radicals that reached the column inactivated or destroyed some of the biofilm. This inactivation significantly reduced the enzyme activity near the influent compared to that found in Experiment 6. However, the enzyme activity increased sharply beyond the influent region to a maximum in Experiments 3 through 5 before decreasing across the rest of the column.

The greatest amount of TCE cometabolism was expected to be in the location of the greatest enzyme activity. Thus, the extent of bioregeneration increased as the column length (and thereby EBCT) decreased, because the radiolabeled element moved closer to the influent, near where the enzyme activity was the highest. Furthermore, the NADH levels, which if low can limit the enzyme activity, were found to be fairly consistent across the length of the columns. In addition, they were found to be similar to the NADH levels found for the baseline culture (Section 4.3.5) and therefore not limiting. The enzyme activity was highest shortly beyond the influent region of the column because a constant supply of toluene was available for metabolism. Thus, it makes sense that Figure 5.15 shows that the overall enzyme activity generally increases with the toluene concentration.

The effect of shortening the EBCT to decrease the distance between the radiolabeled element and the area of maximum enzyme activity is further shown by a comparison of the cumulative TCE-based bioregeneration in Experiments 3 (10.4-min. EBCT) and 4 (3.5-min. EBCT) (Figure 5.17). The final percent of TCE-based bioregeneration for Experiment 4 was similar to that for Experiment 3; however, the longer-EBCT column (Exp. 3) had already reached its plateau value. The bioregeneration rate in the shorter-EBCT column (Exp. 4) had not yet finished its peak, as shown in Figure 5.17. Therefore, the plateau value of the cumulative bioregeneration in the shorter-EBCT column (Exp. 4) would most likely have been greater than that for the longer EBCT column (Exp. 3) if Experiment 4 had been operated for a longer period of time. The shorter EBCT and larger toluene to TCE concentration ratio used in Experiment 4 showed potential for a higher final percent bioregeneration if the experiment had run long enough. Table 5.4 shows that after 166 hours, the extent of metabolism (toluene)-based bioregeneration was 47%, which was similar to that for Experiments 1 and 2. The extent of cometabolism (TCE)-based bioregeneration was 3.0%, about 6% of that for toluene.

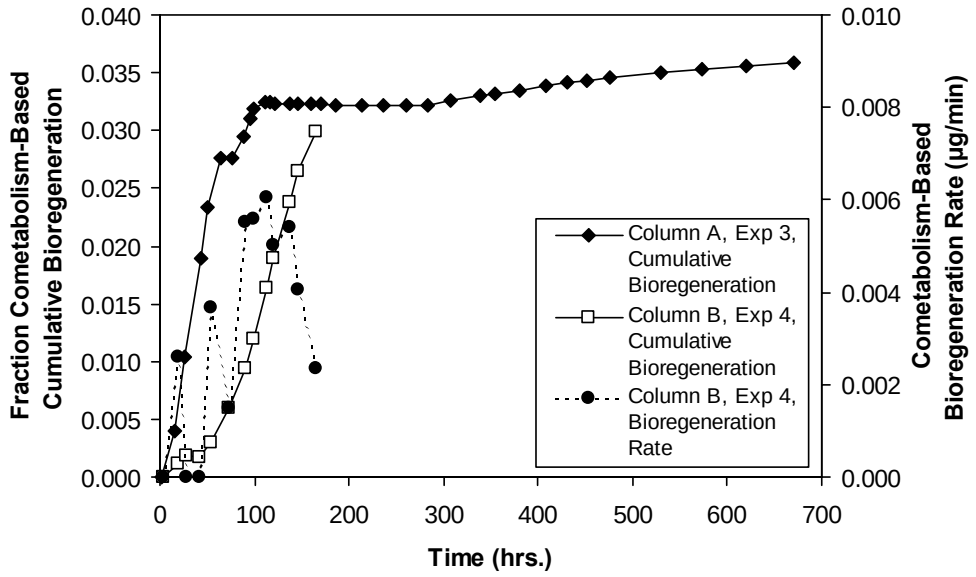

Figure 5.17 Cumulative Cometabolism-Based Bioregeneration and Bioregeneration Rate, Exps. 3 (10.4-min. EBCT, Iron, Avg. C_o = 1740 (toluene) and 179 (TCE) µg/L) and 4 (3.5-min. EBCT, Iron, Avg. C_o = 6500 (toluene) and 266 (TCE) µg/L)

5.2.4 Simultaineous Toluene- and TCE-based Bioregeneration

In Experiment 5, the EBCT was decreased to approximately 2 minutes from that of Experiment 4 (~3.5 min.) to allow for measurement of cometabolism-based bioregeneration as close as possible to the location of highest enzyme activity. In addition, Experiment 5 had a slightly smaller toluene to TCE ratio than Experiment 4 to observe its effect on the column performance. Again, both columns were packed with GAC pre-equilibrated with toluene and TCE, and one had a ^{14}C-TCE radiolabeled element, while the other had a ^{14}C-toluene radiolabeled element at the end of the column. In addition, both columns were fed hydrogen peroxide. Figure 5.18 shows the resulting toluene and TCE effluent

concentrations for the toluene-tracking column (results were similar for the TCE-tracking column). The toluene concentration quickly decreased from the influent concentration followed by a decrease in the TCE concentration, as seen previously. Eventually, iron clogging decreased the packed bed contact time and thus increased the effluent concentrations, as in Experiment 4.

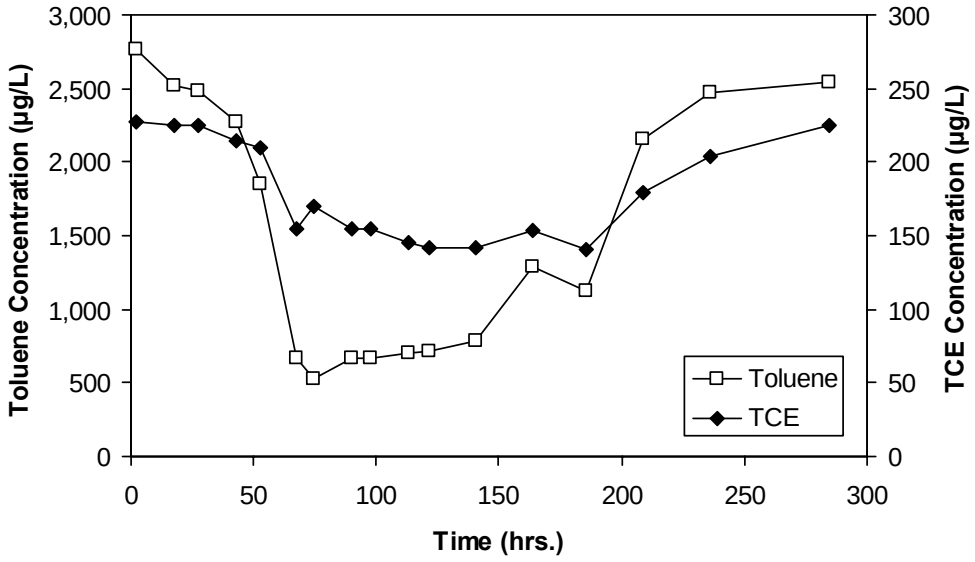

Figure 5.18 Effluent Toluene and TCE Concentrations, Exp. 5, ^{14}C-Toluene-Tracking Column, 2.3-min. EBCT, Iron, Avg. C_o = 3320 (toluene) and 200 (TCE) µg/L

The elements of radiolabeled GAC allowed for the contributions of metabolism and cometabolism at the effluent ends of the columns to be measured. Figure 5.19 shows the expected increase in metabolic products associated with metabolism (CO_2, cells, and NPPs). $^{14}CO_2$ production showed a peak corresponding to the large drop in toluene concentration. The CO_2 concentration

was much greater than the NPP concentration for the majority of the experiment, in contrast to that seen for cometabolism.

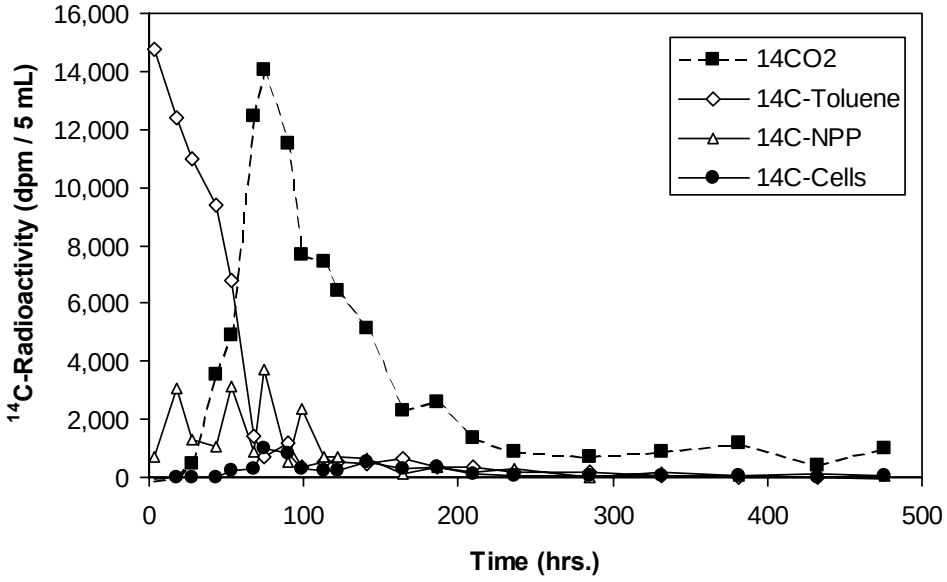

Figure 5.19 Toluene Radioactivity Profile, Exp. 5, ^{14}C-Toluene-Tracking Column, 2.3-min. EBCT, Iron, Avg. C_o = 3320 (toluene) and 200 (TCE) µg/L

Figure 5.20 shows the bioregeneration rate calculated from $^{14}CO_2$ production over time for both columns, with the large scale for toluene-based bioregeneration on the left axis and the small scale for TCE-based bioregeneration on the right axis. The bioregeneration peaks, which corresponded to time periods of vigorous desorption and biodegradation of the radiolabeled substrate followed by a time period of diffusion limited biodegradation, occurred virtually simultaneously for toluene and TCE. This time dependence indicated that little or no enzyme competition occurred between toluene and TCE in the column, as was found for the batch experiments reported in Section 4.3.1. This was an important

finding because enzyme competition can minimize the usefulness of a cometabolism-based biologically active column.

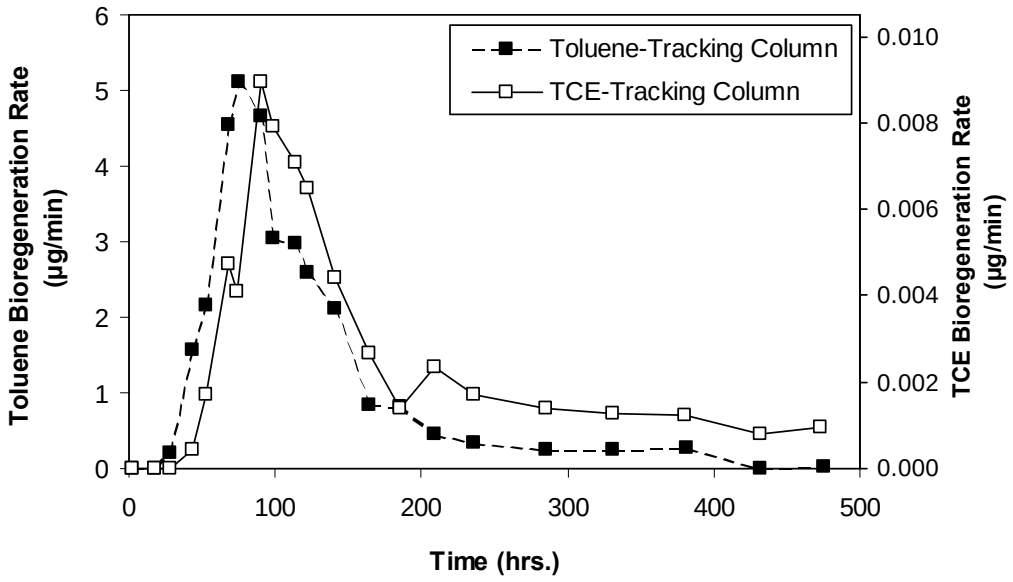

Figure 5.20 Toluene and TCE Bioregeneration Rates, Exp. 5, 2.3 (Toluene) and 1.7-min. (TCE) EBCTs, Iron, Avg. C_o = 3320 (toluene) and 200 (TCE) µg/L

The ^{14}C-radiochemical data from each column can be assumed to be representative of the other column because of their nearly identical setup. Further evidence of the close correlation between the two columns is presented in Figure 5.21, which shows that the SOC loadings as determined by methanol extraction at the end of the experiment were virtually identical. Furthermore, the toluene and TCE loading profiles were similar to that found in Figure 5.14 for Experiment 4. The toluene loading (q_f/q_o) was less than one and decreased across the column. The TCE loading increased across the column, presumably because of a high

amount of TCE degradation from cometabolism at the influent and middle portions of the column.

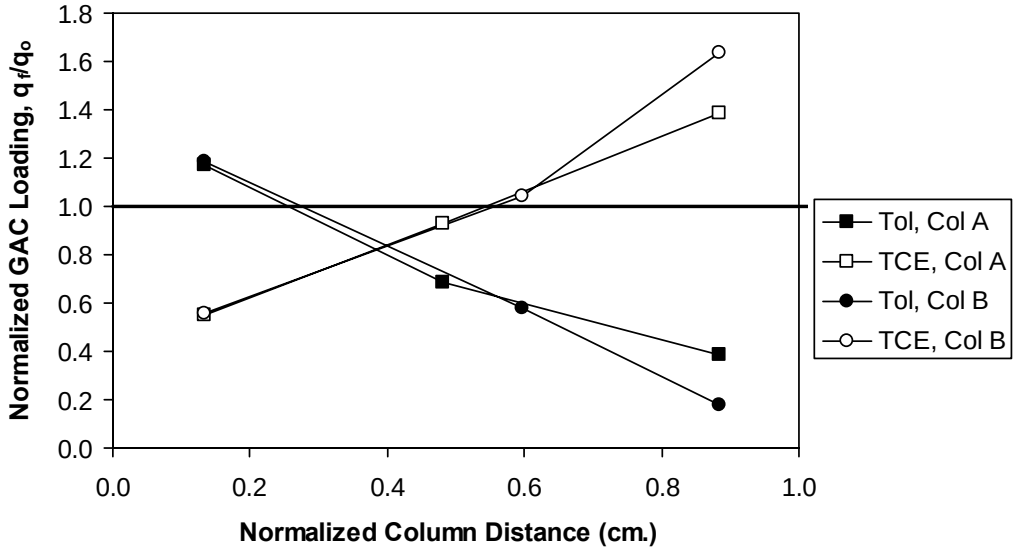

Figure 5.21 Final SOC Loadings, Exp. 5, 2.3 (Col A) and 1.7-min. (Col B) EBCTs, Iron, Avg. C_o = 3320 (toluene) and 200 (TCE) µg/L

5.2.5 Effect of Toluene to TCE Ratio on Bioregeneration

In Experiment 6, very little hydrogen peroxide was added to the columns, and the toluene to TCE ratio was very low. A low toluene to TCE ratio was used to aid in the identification of the minimum ratio at which cometabolism still occurred. Table 5.4 shows that the extent of metabolism (toluene)-based bioregeneration at the effluent end of the column was 47% for Experiment 6, which was the same as that found for Experiment 4. The extent of cometabolism (TCE)-based bioregeneration was 0.0%, indicating no difference compared to that expected from a toluene-PCE experiment. The lack of cometabolism-based

bioregeneration indicated the large effect that the toluene to TCE ratio had on cometabolism-based bioregeneration. The EBCTs and extents of toluene-based bioregeneration in Experiment 6 were very similar to those in Experiment 4, allowing for some comparison. Despite the removal of H_2O_2 and the longer duration in Experiment 6, the TCE-based bioregeneration was still less than the 3.0% found for Experiment 4. The removal of hydrogen peroxide and the longer duration should have increased the TCE-based bioregeneration in Experiment 6, but the key difference was that the toluene to TCE ratio was much lower than the 14 to 24 recommended in previous literature (Lu *et al*., 1998; see Section 2.5.2). Therefore, insufficient toluene may have been available in Experiment 6 to support TCE cometabolism.

Figure 5.22 shows the ^{14}C-TCE based bioregeneration near the effluent end of the columns versus the toluene to TCE equilibrium concentration ratio and EBCT for the iron-fed columns in Experiments 3 through 6. The extent of bioregeneration at the longest common operating time (166 hrs.) was used in Figure 5.22 to minimize differences due to experiment duration. In contrast to the trend found in Figure 5.6 with toluene-based bioregeneration, a shorter EBCT and a larger toluene:TCE ratio resulted in a larger percent TCE-based bioregeneration. Bioregeneration is dependent on the toluene:TCE ratio because enough toluene must be present to produce sufficient toluene dioxygenase enzymes for TCE cometabolism, while not so much that enzyme competition occurs. The more TCE present, the more toluene that is needed to produce the required toluene dioxygenase enzymes. Bioregeneration was dependent on the EBCT because of

the location of the ^{14}C-TCE element at the end of the column. Because the enzyme activity was the greatest near the influent region of the column (see Figures 5.15 & 5.16), the closer the ^{14}C-TCE element was to the influent and thus the shorter the column, the more bioregeneration that was measured. This indicates the EBCT, beyond a certain minimum, would have diminishing returns with respect to cometabolism-based bioregeneration. Figure 5.22 also shows that the abiotic removal of TCE due to the decrease in the liquid phase TCE concentration across the column (as seen with toluene) was not as important as the biotic removal of TCE (cometabolism in the influent region).

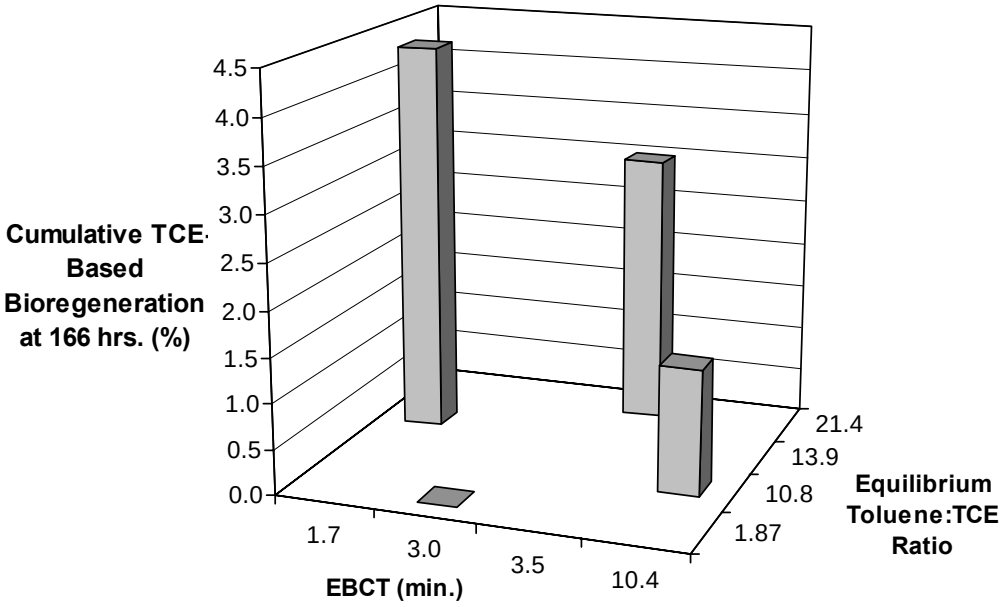

Figure 5.22 Effect of Equilibrium Toluene:TCE Concentration Ratio and EBCT on TCE-Based Bioregeneration

Figures 5.23 and 5.24 show the toluene and TCE effluent concentrations, respectively, from both columns in Experiment 6 along with the sterile control

column which was run in parallel with Experiment 6. As expected, the toluene concentration decreased quickly and remained low in the biologically active columns. During the first 80 hours of operation, the toluene and TCE effluent concentrations from Column B were lower than those of the other columns. These low effluent concentrations were due to slight differences in the pre-saturation loadings of the ^{14}C-TCE and ^{14}C-toluene radiolabeled elements.

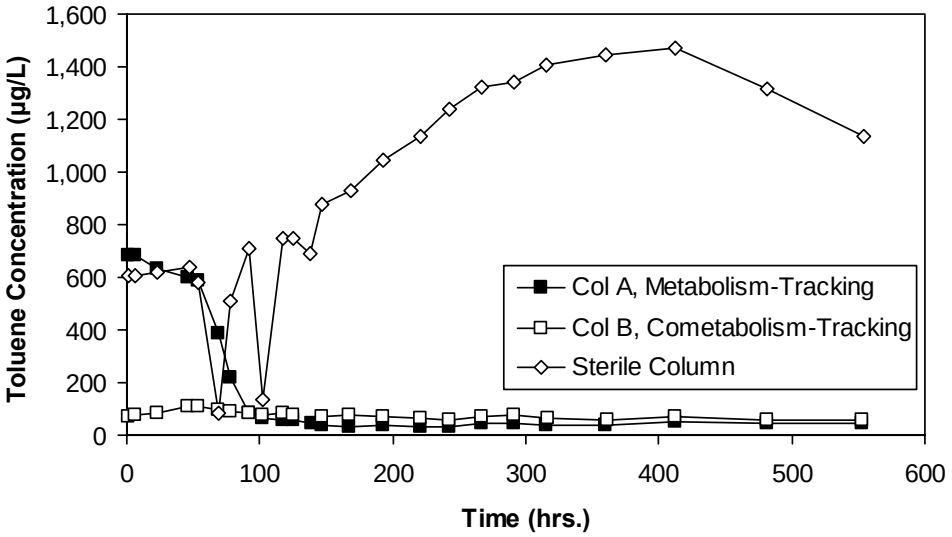

Figure 5.23 Effluent Toluene Concentrations, Exp. 6 (2.3 (A) and 1.7-min. (B) EBCTs, Iron, Avg. Toluene C_o = 1420 µg/L) and Sterile Column (0.9-min. EBCT, No Iron, Avg. Toluene C_o = 1490 µg/L)

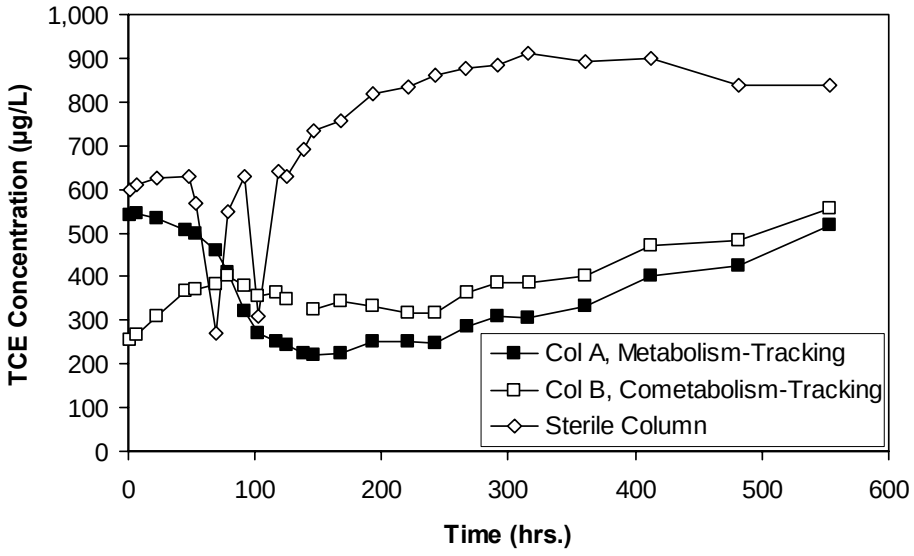

Figure 5.24 Effluent TCE Concentrations, Exp. 6 (2.3 (A) and 1.7-min. (B) EBCTs, Iron, Avg. TCE C_o = 721 µg/L) and Sterile Column (0.9-min. EBCT, No Iron, Avg. TCE C_o = 916 µg/L)

Beyond this initial period, the seeded metabolism and cometabolism-tracking columns behaved similarly (Columns A and B, respectively). The toluene and TCE effluent concentrations in the sterile column, however, were expected to stay the same (at the equilibrium level) over time. Instead, the effluent concentrations increased for two reasons. First, the influent concentrations were larger than the equilibrium concentrations (see Table 5.3). Second, to avoid the iron clogging that occurred in Experiments 4 and 5, Columns A and B in Experiment 6 were fed iron only intermittently. While the intermittent feeding of iron helped slow the rate of iron clogging, it did not completely stop it, resulting in a decreased packed bed contact time. Thus, the effluent TCE concentrations in Columns A and B increased after approximately 200 hours from both iron clogging and high influent concentrations. Nonetheless, the difference between the influent and effluent concentrations in Columns A and B demonstrated the large amount of toluene and TCE that was removed due to the combination of adsorption with metabolism and cometabolism. The metabolism and cometabolism in Columns A and B led to increased GAC adsorption capacity compared to the sterile column.

By the end of the experiment, GAC extractions showed that the SOC loadings were nearly identical between Columns A and B (Figure 5.25), further proving that Columns A and B sufficiently replicated each other. The normalized toluene loading was less than one and decreased across Columns A and B. The normalized TCE loading was greater than one near the influent region, peaked in the middle, and then decreased near the effluent region in Columns A and B.

Two issues were affecting the shape of the TCE loading profile. First, the potential for bioregeneration was lower at the influent end of the column, so the TCE loading was lower than the rest of the column at exhaustion. Second, the GAC was not re-equilibrated along the entire length of the column by the end of the experiment, so the TCE loading increased along the length of the column until the active mass transfer zone was reached. The increased toluene and TCE influent concentrations resulted in the normalized TCE loading in the sterile column being greater than one. The large difference in TCE loading between the biologically-active columns and the sterile columns shows the additional adsorption capacity afforded by the combination of metabolism and cometabolism.

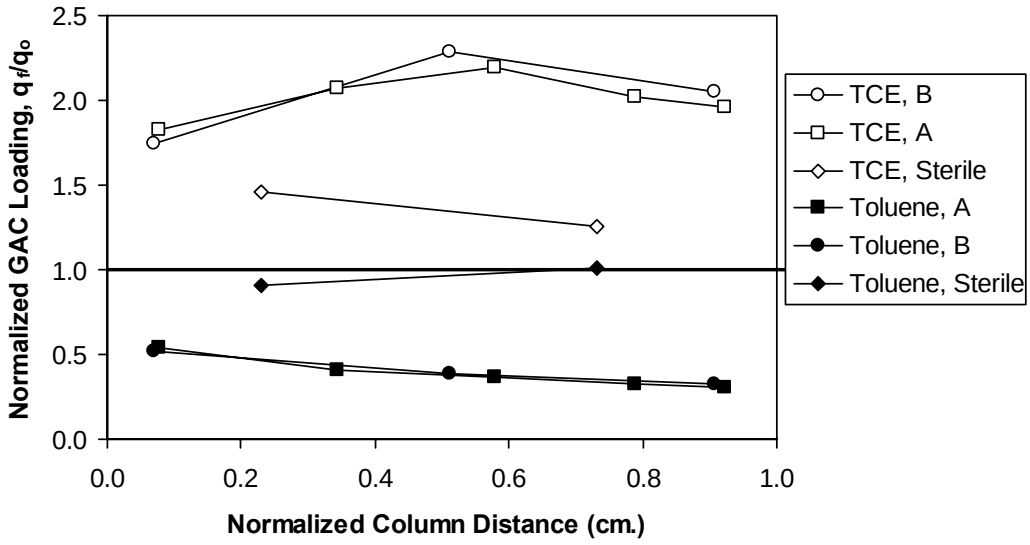

Figure 5.25 Final SOC Loadings, Exp. 6 (2.3 (A) and 1.7-min. (B) EBCTs, Iron, Avg. TCE C_o = 721 µg/L) and Sterile Column (0.9-min. EBCT, No Iron, Avg. TCE C_o = 916 µg/L)

Table 5.4 Summary of Toluene-TCE Exhausted Bioregeneration Experiment Results

Exp.	Avg. EBCT (min)	Iron[b] in Feed, H_2O_2	^{14}C-Based Bioregeneration (%)	
			Tol	TCE
Sterile Column	0.9	N, N	-	-
3	A: 10.3 B: 10.4	N, Y Y, Y	- -	3.6 2.2
4	A: 3.4 B: 3.5	Y, Y Y, Y	47 -	- 3.0
5	A: 2.3 B: 1.7	Y, Y Y, Y	53 -	- 7.4
6	A: 3.0 B: 3.0	Y, N Y, N	47 -	- 0.0

[a]Tol = Toluene
[b]N = No, Y = Yes

5.3 COMBINED METABOLISM-COMETABOLISM VIRGIN COLUMN EXPERIMENTS

The operating conditions for two combined metabolism-cometabolism, virgin BAC column experiments are presented in Table 5.5. The operating conditions for a sterile GAC control column and an anthracite column experiment are also presented in Table 5.5. Virgin BAC experiments are representative of all three adsorption zones within a column, whereas exhausted column experiments were representative of just the exhausted zone. Virgin columns allowed for a more direct measurement of service life than in the pre-equilibrated columns. EBCTs were all fairly short (~1 min.) to minimize the operation time needed to reach saturation. Different toluene to TCE ratios, iron loadings, and H_2O_2 concentrations were tested to observe their effect on the extent of metabolism- and cometabolism-based bioregeneration in virgin columns. SOC adsorption does

not occur to a significant degree on anthracite, yet biofilm formation should be similar to that in a GAC column, so the anthracite experiment served as an adsorption control for the GAC virgin experiments.

Table 5.5 Summary of Toluene-TCE Virgin Bioregeneration Experimental Conditions

Exp.	SOC	Avg. Influent Conc. (µg/L)	Duration (hrs)	Avg. EBCT (min)	Iron[c], H_2O_2
Anthracite Control	TCE Tol[a] Ratio[b]	62 623 10.1	168	A: 1.0 B: 0.9 C: 1.0	H, N P, N P, Y
Sterile Control	TCE Tol Ratio	88 1500 17.0	697	A: 0.9	N, N
7	TCE Tol Ratio	88 1500 17.0	697	B: 1.1 C: 1.2	N, N I, N
8	TCE Tol Ratio	65 741 11.4	617	A: 1.0 B: 1.0 C: 1.0	H, N P, N P, Y

[a]Tol = Toluene
[b]Ratio = Toluene to TCE influent concentration ratio
[c]I = Iron present in influent, P = Iron preloaded onto GAC, H = HCl desorption of iron off GAC, N = No, Y = Yes

5.3.1 Metabolism and Cometabolism without Adsorption

The exhausted BAC column experiments showed that biological activity produced two opposing driving forces: TCE adsorption onto the regenerated adsorption sites versus TCE desorption into the biofilm and subsequent cometabolism. These opposing driving forces indicated that a situation where the SOC was not very adsorbable would allow for the most SOC cometabolism. One way to test this hypothesis was to perform biologically-active column experiments

using anthracite instead of GAC. Anthracite does not have the extensive system of micropores that are present in GAC and thus has very little adsorption capacity. It still provides a surface for biofilm growth that is similar to GAC.

In the anthracite control experiment, three anthracite columns were run in parallel. Column A was HCl-washed to remove bio-available iron, seeded with the iron-free culture, and fed iron-free influent to ensure only metabolism occurred in the column. Column B was pre-loaded with iron to avoid clogging from iron precipitates, seeded with the iron-acclimated culture, and fed iron-free influent. Column C was setup the same as Column B, except hydrogen peroxide was added to the influent to induce Fenton's oxidation and maintain a sufficient D.O. level in the column. Radiolabeled SOCs could not be used with the anthracite because of the lack of adsorbability. The resulting effluent toluene and TCE concentrations from all three anthracite columns are shown in Figure 5.26 and 5.27, respectively. The influent SOC concentrations from Column C are shown for comparison to the effluent concentrations and are typical of the influent concentrations for Columns A and B. The toluene effluent concentrations in Columns A and B decreased quickly and stayed low. No toluene removal occurred in Column C. Unlike GAC, anthracite does not catalyze the reaction of hydrogen peroxide to oxygen, so the entirety of Column C was exposed to hydrogen peroxide instead of just the initial portion, which resulted in cell inactivation and hydrogen peroxide breakthrough. Thus, Column C was essentially sterile and served to measure the degradation due solely to Fenton's oxidation.

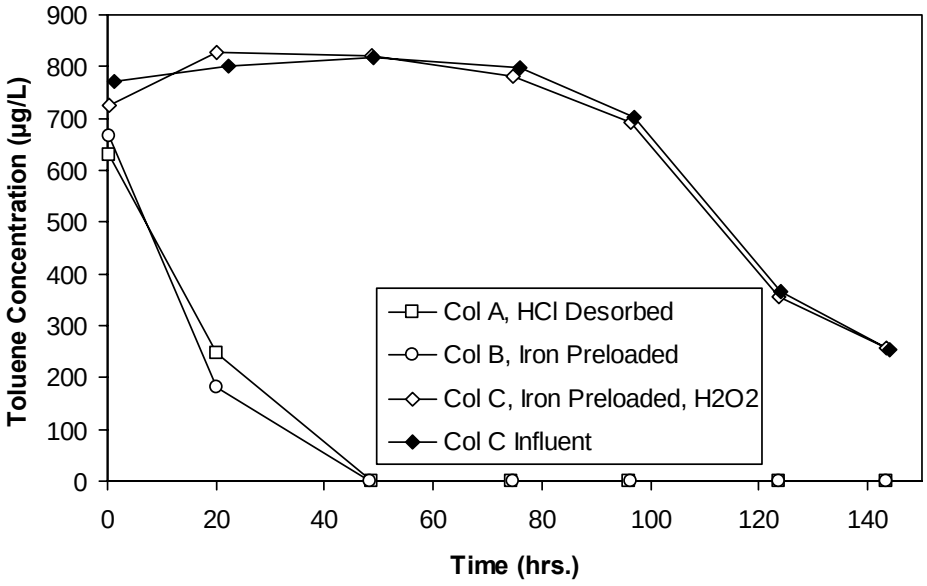

Figure 5.26 Toluene Effluent Concentrations, Anthracite Control Experiment, 1.0 (A), 0.9 (B), and 1.0-min. (C) EBCTs, Avg. Toluene C_o = 623 µg/L

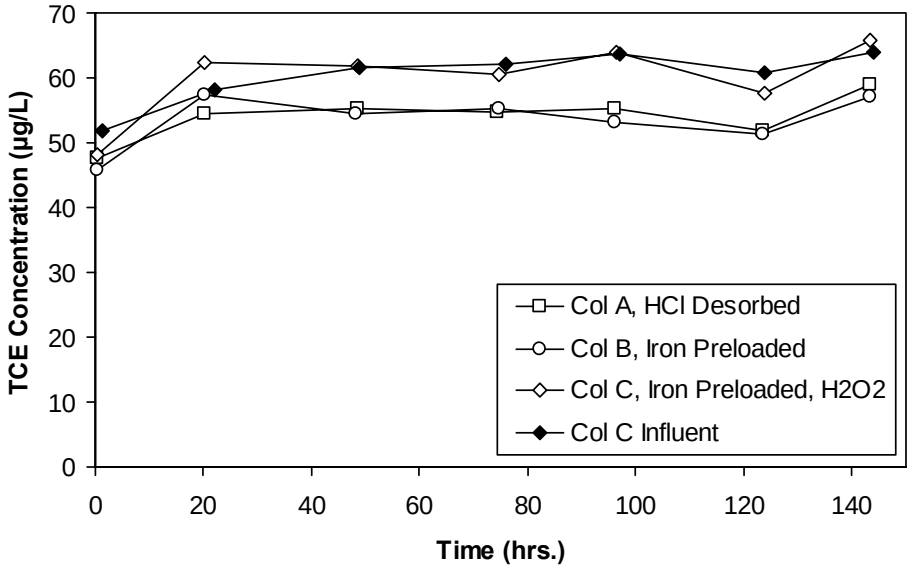

Figure 5.27 TCE Effluent Concentrations, Anthracite Control Experiment, 1.0 (A), 0.9 (B), and 1.0-min. (C) EBCTs, Avg. TCE C_o = 62 µg/L

TCE removal in Figure 5.27 was similar to that for toluene in Figure 5.26. In Columns A and B, the TCE effluent decreased from the influent between 0 to 50 hours, then stayed at a relatively fixed amount below the influent concentration for the rest of the experiment. This timing corresponded to the decrease in effluent toluene in Columns A and B between 0 and 50 hours. The maximum amount of TCE removal from cometabolism during the experiment was 11.4 µg/L, or 18% of the influent. The same amount of cometabolism occurred in both Columns A and B, despite the efforts to make Column A iron-free and thus keep cometabolism from occurring. Iron contamination may have been present in Column A or the kinetics of the iron-free culture may have changed to allow cometabolism without iron present. Furthermore, the difference between the TCE influent concentration and Column C effluent concentration was minimal (a maximum of 3.7 µg/L), indicating that Fenton's oxidation was unsuccessful at the H_2O_2 and iron concentrations tested.

Methanol extractions were performed at the end of the experiment to verify the lack of anthracite adsorbability. For the virgin experiments, q_o was defined as the multicomponent loading in equilibrium with the average influent concentrations as given by IAST. The q_f/q_o ratios for toluene and TCE were found to be around 0.001 and 0.03, respectively. These values indicated that, as expected, adsorption of toluene and TCE was minimal on the anthracite.

5.3.2 Adsorption without Metabolism or Cometabolism

A sterile virgin GAC column was run to observe adsorption in the absence of biological activity. The virgin column setup was the same as for the previous

pre-equilibrated columns except for the use of unused GAC. Figure 5.28 shows the resulting effluent concentrations. As expected, the toluene and TCE concentrations increased over time, as the mass transfer zone moved toward the effluent end of the column. Some variation occurred in the influent concentration, and thus the toluene and TCE concentrations near the end of the experiment decreased slightly instead of reaching a plateau at the average influent concentration. The chromatographic effect (see Section 2.4) is seen in Figure 5.28, where the TCE effluent concentration peaked above the average influent concentration of 88 µg/L. The TCE effluent concentration was greater than the influent concentration as the toluene started to break through because the TCE that had been adsorbed in the absence of toluene was displaced by the more adsorbable toluene.

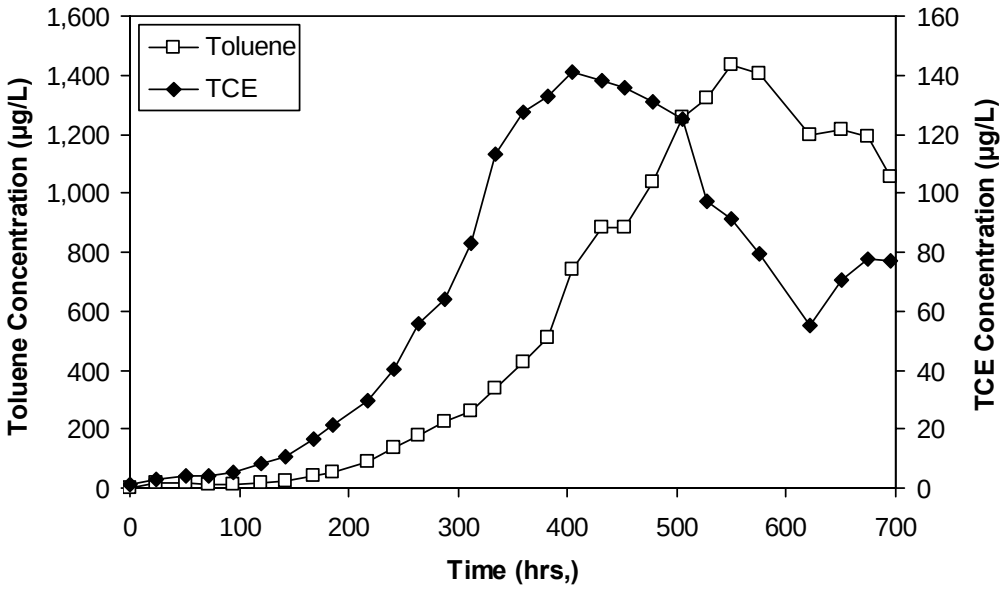

Figure 5.28 Toluene and TCE Effluent Concentrations, Sterile Column, No Iron, Toluene C_o = 1570 µg/L, TCE C_o = 87 µg/L, 0.9-min. EBCT

AdDesignS© (Adsorption Design Software, CenCITT), an implementation of the PSDM (see Section 2.4), was used to fit the toluene and TCE effluent concentrations over time in the sterile column using the adsorption equilibrium parameters listed in Table 2.3 from Speth and Miltner (1990) as inputs. To minimize the average residual sum of squares between the AdDesignS© fit and the measured data, the adsorption parameter K for toluene was decreased from 5010 to 4460 µg/g $(L/\mu g)^{1/n}$ in modeling all the virgin GAC columns. As discussed in Section 4.2, the equilibrium parameters in Table 2.3 were more appropriate for modeling of the virgin columns because the small initial concentrations were closer to the influent toluene and TCE concentrations in the virgin columns. The large initial concentrations used for the isotherms performed in this research (Table 4.1), however, were closer to the values used for pre-equilibrium in the exhausted GAC columns. The result of AdDesignS© modeling of Column A using the equilibrium parameters from Table 2.3 was shown in Figure 4.7 as part of the adsorption kinetics discussion but is repeated in Figure 5.29 for ease of comparison with other results presented in this section. The toluene and TCE PSDM fits slightly underestimated the concentrations before the breakthrough and slightly overestimated the concentrations after the breakthrough. Given the variation in the influent, the PSDM fit the experimental data well. Calibration of the AdDesignS© software was important as it negated the need for sterile GAC columns to be run as controls with subsequent experiments.

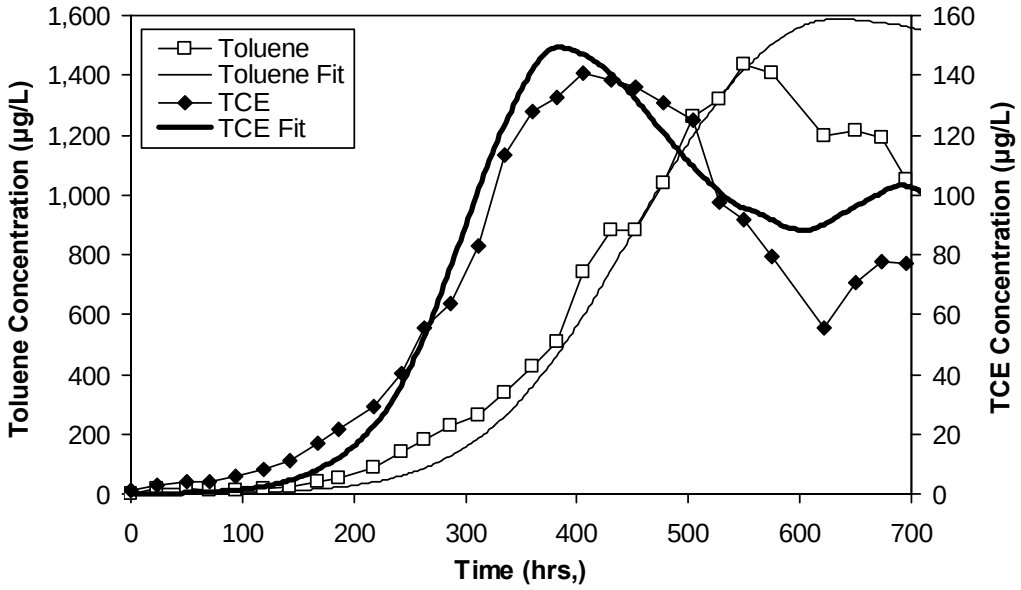

Figure 5.29 Measured and PSDM-Fitted Toluene and TCE Effluent Concentrations, Sterile Column, Toluene C_o = 1570 µg/L, TCE C_o = 87 µg/L, 0.9-min. EBCT

5.3.3 Effect of Biological Activity on Service Life

In Experiment 7, two columns were run in parallel along with the sterile column discussed in the previous section: (B) a column that was seeded with the iron-free culture and not fed iron, and (C) a column fed iron in the influent and seeded with the iron-acclimated culture. Running these columns in parallel allowed for a comparison of the individual effect of adsorption, metabolism, and cometabolism on column performance.

Figures 5.30 and 5.31 show the effluent concentrations from the seeded columns in comparison to the sterile column. Overall, the seeded columns (Cols

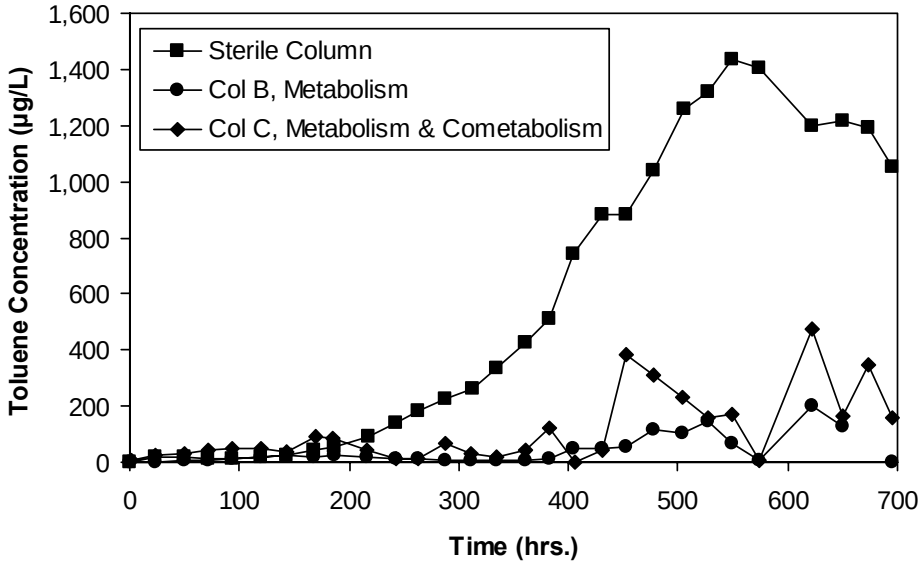

Figure 5.30 Toluene Effluent Concentrations, Exp. 7 Column B (No Iron, 1.1-min. EBCT), Exp. 7 Column C (Iron, 1.2-min. EBCT), and Sterile Column (No Iron, 0.9-min. EBCT), Avg. Toluene C_o = 1500 µg/L

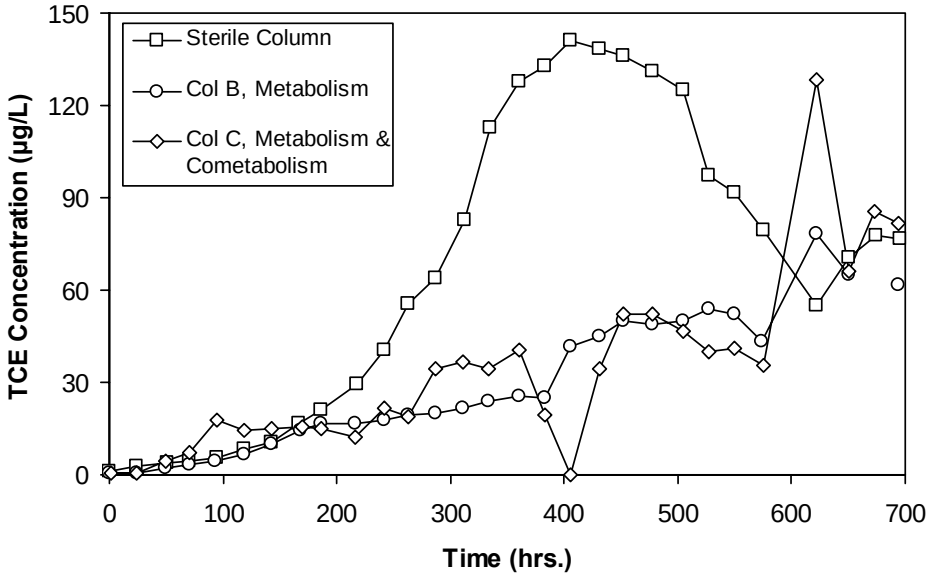

Figure 5.31 TCE Effluent Concentrations, Exp. 7 Column B (No Iron, 1.1-min. EBCT), Exp. 7 Column C (Iron, 1.2-min. EBCT), and Sterile Column (No Iron, 0.9-min. EBCT), Avg. TCE C_o = 88 µg/L

B and C) had much lower effluent concentrations than the sterile column (Col A). The large amount of toluene and TCE removal in the seeded columns showed the great effect biological activity had on the treatment capacity of the columns, which translated to an increased GAC column service life compared to the sterile column. The service life for Column B was double that for the sterile column when using 100 µg/L as the maximum allowed toluene concentration. The service life for Column B was 1.8 times that for the sterile column when using 50 µg/L as the maximum allowed TCE concentration. Due to the short EBCTs used in this experiment, the effect of biological activity on the effluent was not as pronounced during the first 200 hrs as it was at later operating times. Instead, during the first 200 hrs, adsorption was more important than metabolism or cometabolism.

Column C did not perform as well as Column B. The environmental conditions (*i.e.*, iron addition) used to promote cometabolism caused problems with the column performance. The more erratic nature of the effluent data from Column C was most likely due to slight clogging from iron precipitation. This clogging decreased the packed bed contact time, thereby decreasing the amount of time for biodegradation and adsorption to occur within the column. Thus, metabolism led to significant improvement in column performance whereas metabolism and cometabolism did not in this experiment.

5.3.4 Effect of Biological Activity on SOC Loading and Bioregeneration

Methanol extractions of the GAC were performed at the end of the Experiment 7 to compare the final SOC loading (q_f) to the multicomponent

loading in equilibrium with the average influent concentrations as given by IAST (q_o). The results are shown in Figure 5.32. The q_f/q_o values were not expected to be one, as in exhausted GAC experiments, because q_o was an equilibrium value, and the GAC did not start out pre-equilibrated. Thus, what Figure 5.32 shows is the relative benefit of biodegradation compared to the sterile column. The toluene loadings for Columns B and C were nearly the same and were lower than that for the sterile column because of toluene biodegradation. As expected, both the toluene and TCE loadings for the sterile column showed little change across the column, because the column had been run to saturation. The normalized TCE and toluene loadings in the sterile column were expected to be at one, but were slightly above and below one because of variations in the influent SOC concentrations.

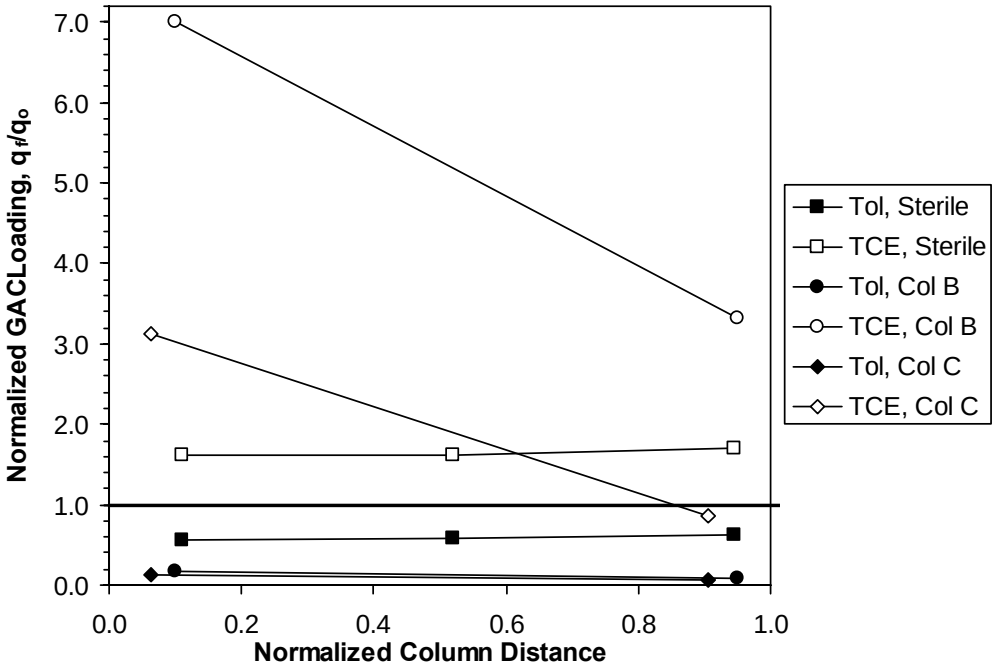

Figure 5.32 Final SOC Loadings for Exp. 7 Col B (No Iron, 1.1-min. EBCT), Exp. 7 Col C (Iron, 1.2-min. EBCT), and Sterile Column (No Iron, 0.9-min. EBCT)

The TCE loadings for Column B and C decreased across the column, because the mass transfer zone velocity was slow due to biological activity. The biological activity also resulted in an increase in the TCE loading in Column B to 7 times the calculated competitive equilibrium loading. Such a large increase in the TCE adsorption capacity occurred because of the great amount of competition between toluene and TCE. If all the toluene were desorbed from the GAC, the calculated TCE loading would be 17.6 times that of the calculated competitive loading. Column C had much lower TCE loadings than Column B presumably because of the effects of iron plugging: (1) a decreased contact time for

adsorption and (2) a slightly decreased flow rate to Column C, resulting in less mass of TCE being delivered to Column C.

In the virgin GAC column experiments (Experiments 7 & 8), ^{14}C-radiolabeled toluene could not be adsorbed to the GAC prior to the start of the experiments because the GAC started out unused instead of exhausted. Instead, radioactivity was fed to the columns using a syringe pump during only the first 27 to 50 hours of operation. During this period, the biofilm was still forming and thus, little biodegradation occurred. Instead, adsorption was the dominant removal mechanism; therefore, ^{14}C-toluene was adsorbed onto the GAC. This method allowed for adsorption of the radiolabeled toluene at only the influent end of the column. Therefore, the radioactive data gathered in these experiments represented bioregeneration at the influent end of the column instead of the effluent end of the column, as was the case in Experiments 1 through 6. Moving the radiolabeled element to the influent end of the column should slightly decrease the extent of toluene-based bioregeneration because the liquid phase concentration was not as low, resulting in a decreased driving force for ^{14}C-toluene desorption and subsequent metabolism. When compared at the same operating time (166 hrs.), the virgin columns had a slightly lower extent of toluene-based bioregeneration than the pre-exhausted column experiments. In addition, the extent of ^{14}C-toluene based bioregeneration ranged from 39.4 to 53% in the pre-exhausted column experiments and 26 to 48% in the virgin column experiments in 11 to 20 days. Both the virgin and the pre-exhausted values are

larger than was seen in previous experiments with single chemical systems (Speitel 1985, Lu 1989, Speitel and DiGiano 1987, Speitel *et al*. 1989a).

Figure 5.33 shows the resulting radioactivity profile for the column fed an iron-free influent (Column B). As found with the pre-equilibrated columns, a $^{14}CO_2$ peak occurred at 220 hours along with an increase in cells and a slight increase in non-purgeable products (NPPs). This $^{14}CO_2$ peak corresponded well with the point where the sterile and biologically-active column toluene effluent concentrations separated in Figure 5.30.

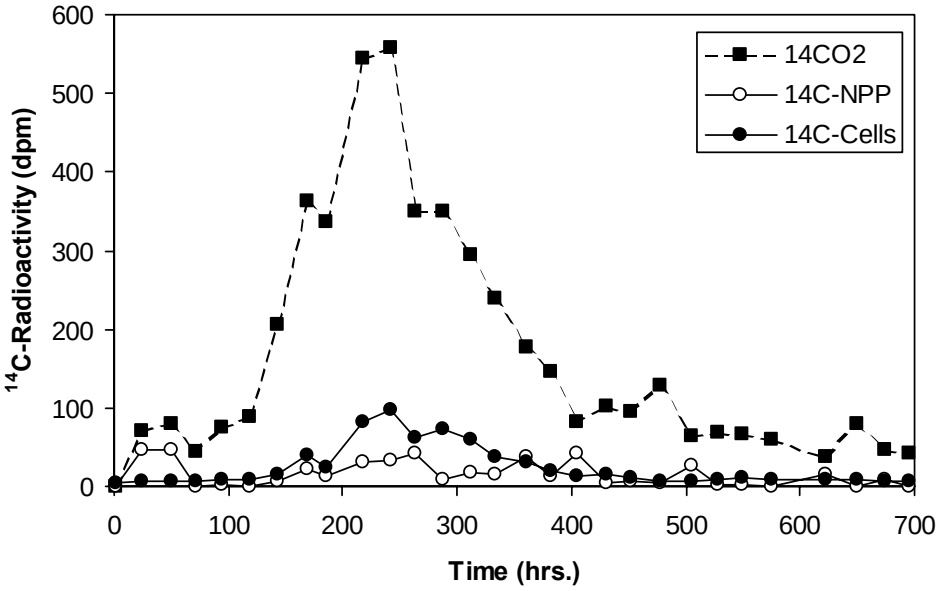

Figure 5.33 Radioactivity Profile, Exp. 7, Column B, Iron-Free Influent, 1.1-min. EBCT, Avg. C_o = 1500 (toluene) and 88 (TCE) µg/L

Figure 5.34 shows the bioregeneration rate for Columns B and C calculated from effluent $^{14}CO_2$ concentrations. The bioregeneration rate peak from the iron-fed column occurred earlier than that from the column with iron-

free influent. This time difference occurred because iron is part of the structural makeup of the toluene dioxygenase enzyme; therefore, toluene metabolism is slightly faster in the presence of iron. Slight iron dependence was also seen in metabolism batch experiments as shown in Figure 4.11 in Section 4.3.2.

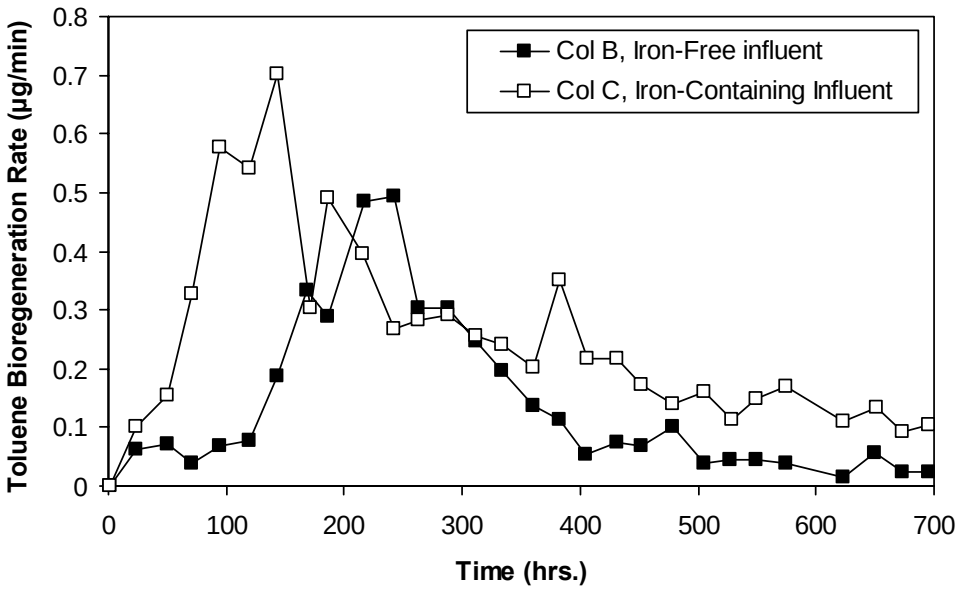

Figure 5.34 Bioregeneration Rate, Exp. 7, Column B (No Iron, 1.1-min. EBCT), and Exp. 7, Col C (Iron, 1.2-min. EBCT), Avg. C_o = 1500 (toluene) and 88 (TCE) µg/L

Despite the bioregeneration rate for the iron-fed column being greater than that for the column with the iron-free influent for most of the experiment, the iron-free column had a larger cumulative bioregeneration as shown in Figure 5.35 (48% compared with 43%). To calculate the cumulative bioregeneration, the bioregeneration rate was used to calculate the mass bioregenerated. Then this quantity was divided by the initial mass of ^{14}C-toluene on the GAC, which was

intended to be the same for each column. However, a leak occurred in the syringe pump that was feeding the ^{14}C-toluene to Column B; thus, a smaller amount of ^{14}C-toluene was adsorbed on to that column. This decreased denominator then increased the cumulative bioregeneration for Column B. The very large extent of toluene bioregeneration (48%) found in the iron-free column shows how such high TCE q_f/q_o values could be achieved in Figure 5.32. With almost half of the initial toluene desorbed off of the GAC, the adsorption capacity for TCE increased greatly.

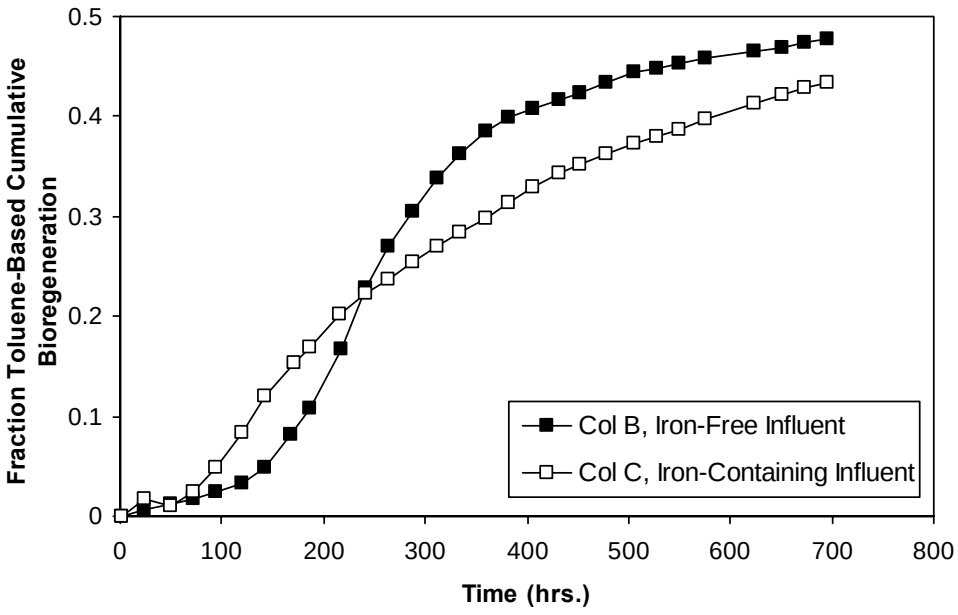

Figure 5.35 Cumulative Metabolism-Based Bioregeneration, Exp. 7, Col B (No Iron, 1.1-min. EBCT), and Exp. 7, Col C (Iron, 1.2-min. EBCT), Avg. C_o = 1500 (toluene) and 88 (TCE) µg/L

5.3.5 Effect of Fenton's Oxidation on Bioregeneration

Experiment 8 involved running three columns in parallel that had the same iron pre-loading setups as in the anthracite control experiment. Thus, only metabolism occurred in Column A, both metabolism and cometabolism occurred in Column B, and metabolism, cometabolism, and Fenton's oxidation occurred in Column C. The resulting effluent toluene and TCE concentrations from all three columns are shown in Figures 5.36 and 5.37. For comparison, the AdDesignS-predicted toluene and TCE effluents from a sterile column are also shown.

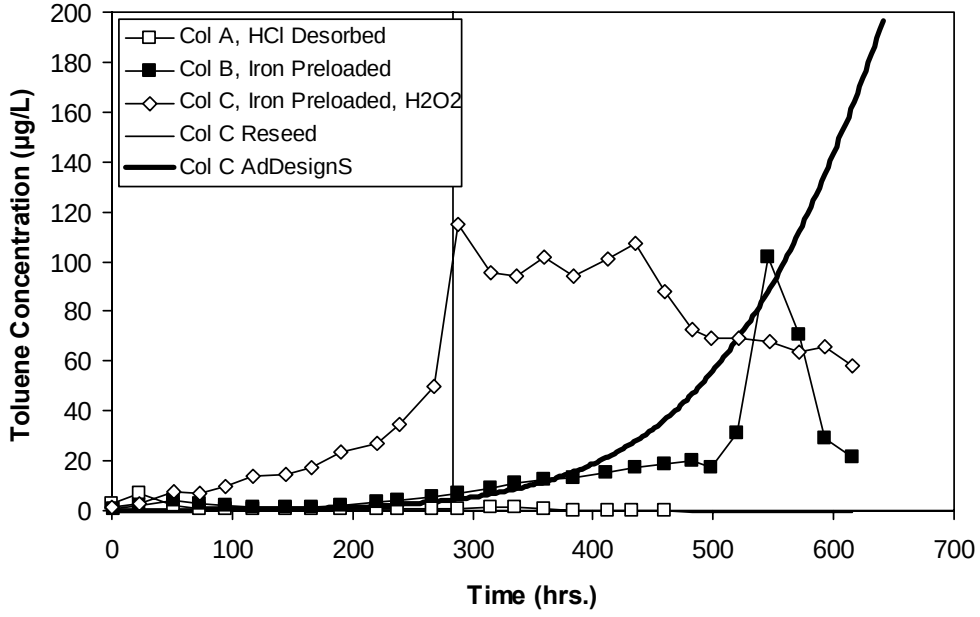

Figure 5.36 Toluene Effluent Concentrations, Exp. 8, 1.0-min. EBCTs, Avg. C_o = 741 (toluene) and 65 (TCE) µg/L

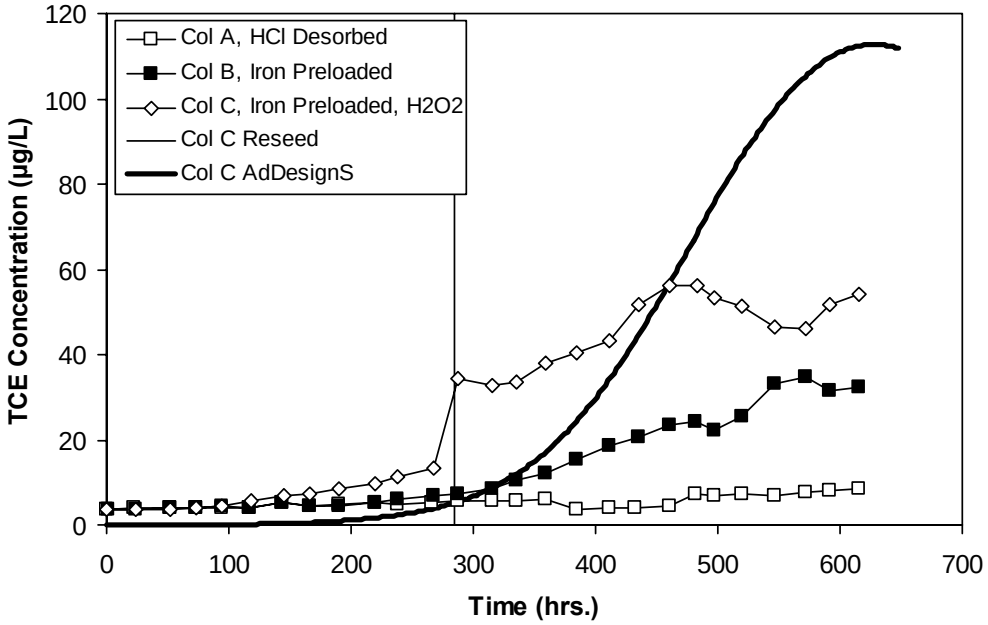

Figure 5.37 TCE Effluent Concentrations, Exp. 8, 1.0-min. EBCTs, Avg. C_o = 741 (toluene) and 65 (TCE) µg/L

Overall, the iron-free column performed well, maintaining low SOC effluent concentrations during the entire experiment and leading to an increased column service life compared to the other columns. The toluene effluent concentrations from Column A were not significantly different from those of the predicted sterile column until about 300 hours, when the predicted sterile effluent began to increase while Column A stayed low, due to metabolism. The TCE effluent concentrations from Column A were about 5 µg/L above those predicted for the sterile column until about 300 hours, when the predicted sterile effluent began to increase while Column A stayed low, due to biological activity. This 5-µg/L difference may have been a function of difficulties measuring low TCE concentrations on the GC-FID, instead of a realized concentration difference.

Column C did not perform as well. The attempt to induce Fenton's oxidation resulted in cell destruction. The influent hydrogen peroxide concentration was too high, and Column C was essentially sterile until a further decrease in hydrogen peroxide and re-seeding took place at 284 hours. The effect of re-seeding was evident in the toluene effluent concentrations, as the steep rise in toluene was quickly turned into a slow descent. An effect on the TCE effluent concentrations, however, was not realized. Furthermore, the SOC effluent concentrations from the iron pre-loaded columns (B & C) indicated that pre-loading iron onto the GAC had resulted in some decrease in the adsorption capacity which offset the benefit of cometabolism. This decrease in adsorption capacity occurred despite efforts to minimize redox reactions between the iron and GAC.

Figure 5.38 shows the bioregeneration rates for Experiment 8. In contrast to that found in Experiment 7, the column provided with iron had a later peak than the column kept iron-free. This unexpected result may have been due to some variability in the seeding of Columns A & B.

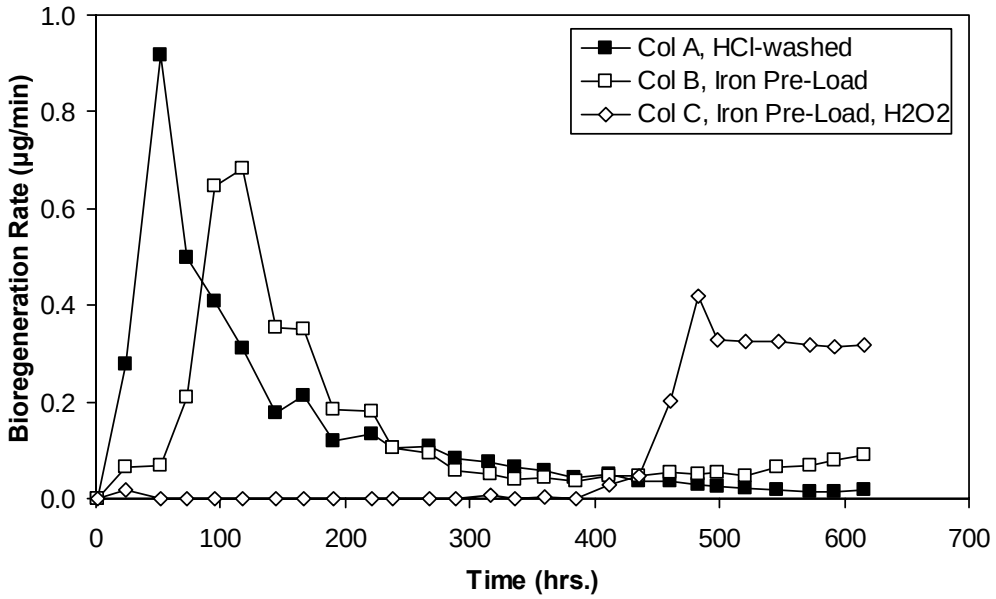

Figure 5.38 Toluene Bioregeneration Rate, Exp. 8, 1.0-min. EBCTs, Avg. C_o = 741 (toluene) and 65 (TCE) µg/L

The bioregeneration rates were used to calculate the cumulative fraction of metabolism-based bioregeneration over time for all three columns. The shapes of the cumulative bioregeneration curves for Columns A and B were similar to that seen with previous experiments: a steep increase corresponding to the peak in the bioregeneration rate followed by a slow increase corresponding to diffusion-limited bioregeneration. The cumulative bioregeneration after 617 hrs. for Columns A and B was 43 and 41%, respectively, as shown in Table 5.6. The extent of bioregeneration for these two columns were fairly close, but both were

larger than the 26% bioregeneration attained in Column C due to the problems with Fenton's oxidation and iron pre-loading.

Table 5.6 Summary of Toluene-TCE Virgin Bioregeneration Experiment Results

Experiment	Avg. EBCT (min)	Iron[a], H_2O_2	^{14}C-Tol Based Bioregeneration (%)
Anthracite Control	A: 1.0 B: 0.9 C: 1.0	H, N P, N P, Y	- - -
Sterile Control	A: 0.9	N, N	-
7	B: 1.1 C: 1.2	N, N I, N	48 43
8	A: 1.0 B: 1.0 C: 1.0	H, N P, N P, Y	43 41 26

[a]I = Iron present in influent, P = Iron preloaded onto GAC, H = HCl desorption of iron off GAC, N = No, Y = Yes

Figure 5.39 shows the ^{14}C-toluene based bioregeneration near either the influent (for virgin GAC columns) or the effluent (for the exhausted GAC columns) end of the columns versus toluene concentration and EBCT for Experiments 2 through 8. The extent of bioregeneration is shown at 166 hours of operation to allow comparison between experiments of different duration; therefore, the bioregeneration values are smaller than those listed in Tables 5.2, 5.4, and 5.6. For the virgin GAC columns, the influent toluene concentrations were used, whereas for the exhausted GAC columns, the equilibrium toluene concentrations were used. As suggested by Figure 5.6 (where bioregeneration was estimated via methanol extraction), a shorter EBCT and a lower equilibrium concentration resulted in a smaller percent toluene-based bioregeneration in both virgin and exhausted GAC column experiments.

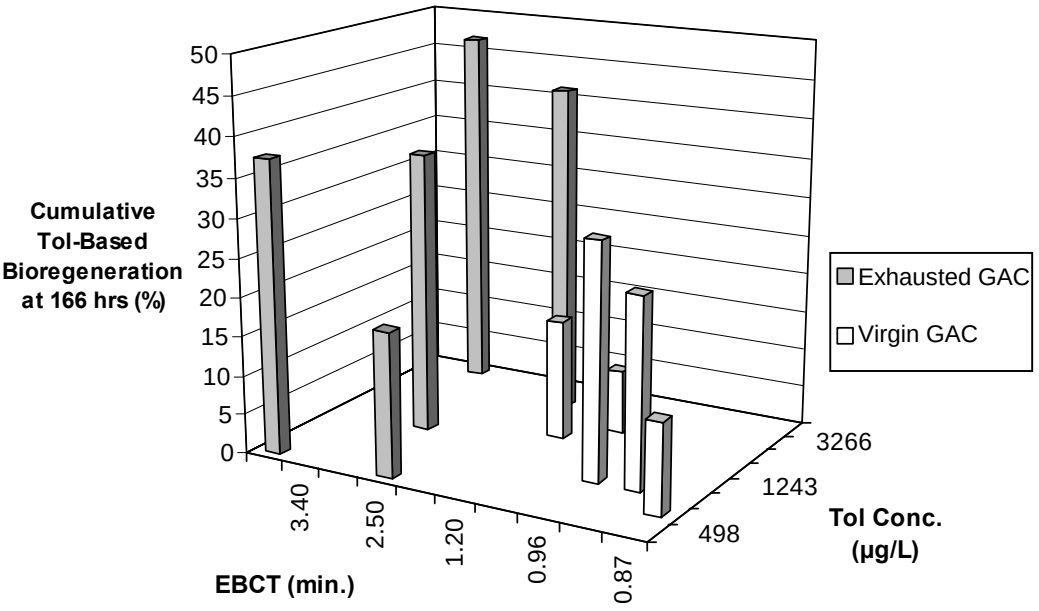

Figure 5.39 Effect of Toluene Concentration and EBCT on Toluene-Based Bioregeneration in both Exhausted and Virgin Column Exps.

5.4 SUMMARY

The toluene-PCE and toluene-TCE equilibrium GAC column experiments as well as the toluene-TCE virgin GAC column experiments (summarized in Table 5.7) presented in this chapter were necessary to understand the behavior of SOC mixtures in BAC columns. These experiments showed that with respect to toluene metabolism, higher toluene concentrations and longer EBCTs produced greater toluene-based bioregeneration. In contrast, the closer the radiolabeled TCE element was to the influent end, where the most enzyme activity was found, the greater the cometabolism-based bioregeneration. This indicated the column

length, beyond a certain minimum, had diminishing returns with respect to cometabolism. Overall, the extent of cometabolism-based bioregeneration was much smaller than that for metabolism-based bioregeneration due to slower degradation kinetics and a driving force for adsorption. In addition, the best performing column in most of the toluene-TCE experiments was the normal or HCl-washed GAC columns where only metabolism was expected to occur. The addition of Fenton's oxidation, iron in the influent, and iron pre-loading did not have a net beneficial effect on overall TCE removal in a column environment. The next part of the research, presented in Chapter 6, consisted of fitting experimental column data using the MDBA model to validate the model for cometabolism and to find the conditions under which cometabolism's contribution is significant.

Table 5.7 Summary of Bioregeneration Experiment Conditions and Results

Exp.	SOC	GAC Equil. Conc. (µg/L)	Avg. Influent Conc. (µg/L)	Time[b] (hrs)	Avg. EBCT (min)	Toluene Bioregeneration (%)	
						^{14}C-Based	Extraction Based
1	PCE Tol[a]	842 610	845 607	506	A: 6.9 B: 11	—	90.8 90.8
2	PCE Tol	477 498	501 1003	355	A: 2.5 B: 12	39.4 45.5	61.0 67.8

Exp.	SOC	GAC Equil. Conc. (µg/L)	Avg. Influent Conc. (µg/L)	Time (hrs)	Avg. EBCT (min)	Iron[c] in Feed, H_2O_2	^{14}C-Based Bioregen. (%)	
							Tol	TCE
Sterile Column	TCE Tol	569 556	916 1490	556	0.9	N, N	-	-
3	TCE Tol	181 1950	179 1740	671	A: 10.3 B: 10.4	N, Y Y, Y	- -	3.6 2.2
4	TCE Tol	265 5680	266 6500	166	A: 3.4 B: 3.5	Y, Y Y, Y	47 -	- 3.0
5	TCE Tol	236 3270	200 3320	476	A: 2.3 B: 1.7	Y, Y Y, Y	53 -	- 7.4
6	TCE Tol	666 1240	721 1420	556	A: 3.0 B: 3.0	Y, N Y, N	47 -	- 0.0
Anthra-cite Control	TCE Tol Ratio[d]	0 0	62 623 10.1	168	A: 1.0 B: 0.9 C: 1.0	H, N P, N P, Y	- - -	- - -
Sterile Control	TCE Tol Ratio	0 0	88 1500 17.0	697	A: 0.9	N, N	-	-
7	TCE Tol Ratio	0 0	88 1500 17.0	697	B: 1.1 C: 1.2	N, N I, N	48 43	- -
8	TCE Tol Ratio	0 0	65 741 11.4	617	A: 1.0 B: 1.0 C: 1.0	H, N P, N P, Y	43 41 26	- - -

[a]Tol = Toluene
[b]Time = Duration of experiment
[c]I = Iron present in influent, P = Iron preloaded onto GAC, H = HCl desorption of iron off GAC, N = No, Y = Yes
[d]Ratio = Toluene to TCE influent concentration ratio

Chapter 6: Mathematical Modeling Results

A kinetic model was developed by Speitel *et al*. (1989a) that describes both adsorption and biodegradation in multi-component GAC columns (see Section 2.9). This model is referred to as the MDBA (Multiple component, biofilm Diffusion, Biodegradation, and Adsorption) model. The MDBA model combines a single-component adsorption and biodegradation model developed by Speitel *et al*. (1987) with IAST to account for multi-component adsorption. The MDBA model simulations were compared with the measured column data in order to validate the model with respect to cometabolism and to assist in interpretation of the column data.

6.1 METABOLISM-ONLY EXHAUSTED COLUMN EXPERIMENT

The MDBA model was used to describe the results obtained in Experiment 1 using the parameters shown in Table 6.1 to further check the model's validity. The parameters were divided into three categories, (1) experimentally measured in this research, (2) calculated, and (3) assigned. The IAST correction factor, P, for toluene and PCE was measured in a competitive adsorption isotherm (see Figure 4.6) to adjust the IAST-predicted equilibrium concentrations to match those measured experimentally. The liquid film transfer coefficient (k_f) for each SOC was calculated via the Gnielinski correlation (Sontheimer *et al.*, 1988) and the b' (physical biofilm shearing coefficient) values were calculated via Rittmann (1982). The substrate diffusion coefficient in the

Table 6.1 MDBA Model Inputs for Exp. 1, 6.9-min. EBCT, Iron Free

Units	Toluene	PCE	Units	Toluene	PCE
Experimentally Measured			Calculated		
P (--)	2.6	2.4	k_f (10^{-3} cm/s)	2.38	2.38
1/n (--)	0.3641	0.4660	ρ_a (g GAC/cm^3)	0.7	
K (µg/g)(L/µg)$^{1/n}$	10,230	13,990	b' (day^{-1})	0.125	
L (cm)	8.8		D_f (10^{-5} cm^2/s)	0.8	0.8
R (cm)	0.026		D_s (10^{-10} cm^2/s)	2.43	1.10
D (cm)	1.5		*Assigned*		
W (g)	8.2		K_s (µg/L)	10.0	10.0
Wt1 (g)	0.409		L_{fo} (10^{-2} cm)	0.2	
Q (mL/min)	2.24		M_b (µg cells/ g GAC)	2000	
Y (µg cells/µg SOC)	0.505		q_e (µg SOC/g GAC)	47,410	157,400
k (µg SOC/ µg cells-hr)	0.032	0.0			
S_o (µg/L)	607	845			
b (day^{-1})	0.048				
b'_s (--)	0.368				

biofilm (D_f) for each SOC was estimated to be 80% of free-liquid diffusivity, where the free-liquid diffusivity was taken from McCarty (1983). The surface diffusion coefficient (D_s) for each SOC was calculated by the correlation proposed by Sontheimer *et al*. (1988). The toluene K_s was assigned as value of 10 µg/L instead of using the value measured from batch kinetics (165 µg/L) to better fit the slight variation in mixed-culture kinetics observed in this column. The initial biofilm thickness, L_{fo}, and initial biomass in the column, M_b, were unknown variables and thus assigned values to minimize the residual sum of squares between the measured and simulated effluent concentrations. Compared to values used by others (Speitel *et al*., 1989a), the L_{fo} value was smaller, and the M_b value was comparable. In addition, the equilibrium SOC loading, q_e, was increased from the calculated value of 43.11 to 47.41 mg/g for toluene and from 92.6 to 157.4 mg/g for PCE. This change was made to better match the initial measured effluent SOC concentrations. Some uncertainty was expected in the calculated q_e values because the initial SOC concentrations for the pre-equilibration of the GAC could not be measured, and the initial PCE concentration was expected to be slightly above the saturation concentration.

Figure 6.1 shows the result of the model simulations for the effluent toluene and PCE concentrations and toluene bioregeneration rate for Experiment 1. A reasonable fit was found between the measured and simulated values, particularly for toluene. The toluene bioregeneration rate increased as the toluene effluent concentration decreased, as expected. The bioregeneration rate then peaked and decreased over time, similar to that seen with measured data in

Figures 5.4 and 5.5. When the model was used to simulate the long term behavior of the column, the toluene concentration stayed low, while the PCE concentration dipped to a minimum followed by a long, diffusion-based increase back to the influent concentration. Even with a relatively short EBCT of 6.9 min., the model predicted an operating time of approximately 12,000 hours (500 days) for the PCE to re-saturate the GAC once biodegradation had begun.

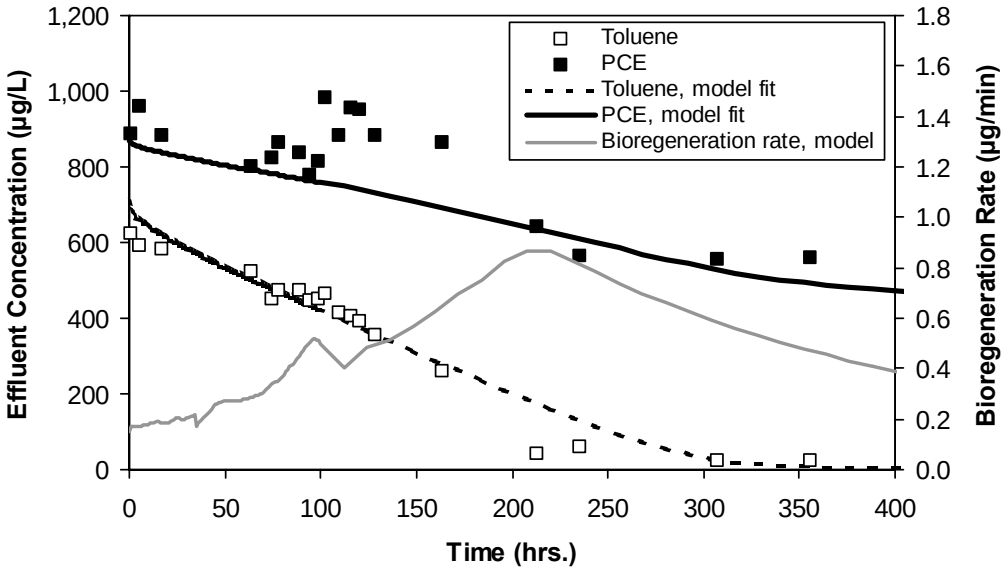

Figure 6.1 Effluent Toluene and PCE Concentration and Toluene Bioregeneration Rate Simulations for Exp. 1, 6.9-min. EBCT, No Iron, Avg. C_o = 607 (toluene) and 845 (PCE) µg/L

Toluene and PCE loadings along the GAC column at the end of the experiment were also simulated using the MDBA model. These simulations are compared in Figure 6.2 to the measured data from methanol extractions of the GAC. As explained in Chapter 5, GAC loadings less than one for the biodegradable SOC indicated bioregeneration, while GAC loadings greater than

one for the nonbiodegradable SOC indicated additional adsorption capacity as a result of bioregeneration. The measured and simulated loadings for PCE match reasonably well, with the model indicating a smaller PCE loading than the measurements. Both, nevertheless, indicated additional adsorption capacity for PCE at the influent and middle portions of the column as a result of bioregeneration. The PCE loading at the effluent end was relatively unchanged because the experiment was not run long enough to supply sufficient PCE to re-saturate the entire GAC column. The measured and simulated loadings for toluene had the largest discrepancy at the influent end, with the model predicting a smaller loading than the measurement. At the influent end, the boundary condition in the model caused some numerical instability in estimating the GAC loading, which may account for the difference between the measured and simulated toluene GAC loadings.

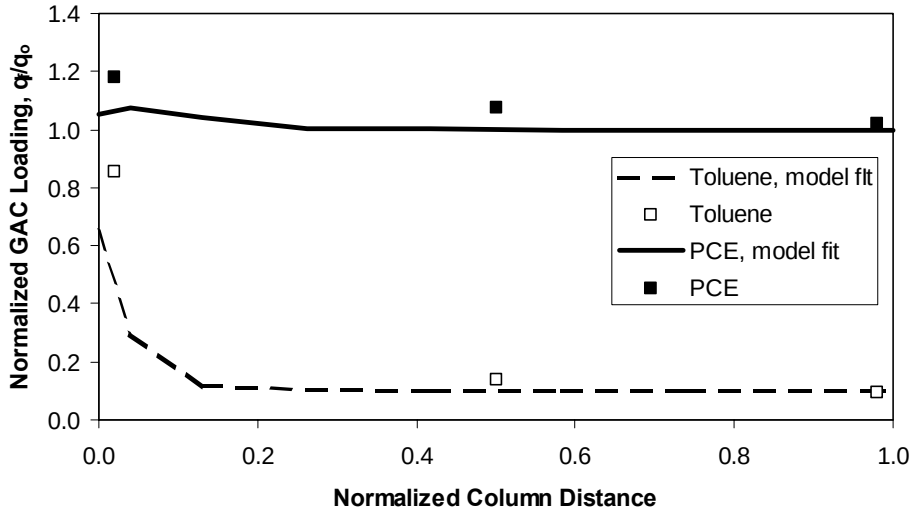

Figure 6.2 Measured and Simulated Final SOC Loadings for Exp. 1, 6.9-min. EBCT, No Iron, Avg. C_o = 607 (toluene) and 845 (PCE) µg/L

6.2 METABOLISM-COMETABOLISM EXHAUSTED COLUMN EXPERIMENT

MDBA modeling was also completed for combined metabolism-cometabolism BAC columns. Manipulation of the MDBA model was found to be unnecessary to account for cometabolism using the current SOCs and mixed culture. The lack of enzyme competition or significant intermediate toxicity indicated that TCE cometabolism could be modeled as a second simultaneous metabolism process with a cell yield of zero. The input parameters used to simulate Column A of Experiment 3 are shown in Table 6.2. No IAST correction factor was found to be necessary for toluene and TCE as measured in competitive adsorption isotherms (see Figures 4.4 and 4.5); thus, P was set to 1. The adsorption kinetic coefficients were calculated in the same manner as described in Section 6.1. Iron-fed biodegradation kinetic values modeled this column better than the iron-free values, despite being seeded with the iron-free culture, presumably because the small amount of iron present within the GAC "turned on" faster cometabolism kinetics. The TCE kinetics were best described by a pseudo-first-order rate equation; therefore, only a k_1 was measured to describe TCE cometabolism. The iron-free TCE k_1 was changed from 0.068 to 0.0028 L/mg-d to better fit the variation in mixed-culture kinetics observed in the columns. This variation in kinetics may have been caused by the iron concentration in the column being lower than that in the batch experiments. For the same reason, the iron-containing TCE k_1 was changed from 0.328 to 0.014 L/mg-d.

Table 6.2 MDBA Model Inputs for Exp. 3, 10.3-min. EBCT, Column A

Units	Toluene	TCE	Units	Toluene	TCE
Experimentally Measured			Experimentally Measured (Cont'd)		
q_e (µg SOC/g GAC)	128,000	2,044	b'_s (--)	0.368	
1/n (--)	0.3641	0.4375	P (--)	1.0	1.0
K $(\mu g/g)(L/\mu g)^{1/n}$	10,230	4,021	K_s (µg/L)	348	
L (cm)	14.3		Calculated		
R (cm)	0.026		k_f (10^{-3} cm/s)	2.10	2.25
D (cm)	1.5		ρ_a (g GAC/cm^3)	0.7	
W (g)	11.91		b' (day^{-1})	0.070	
Wt1 (g)	0.2434		D_f (10^{-5} cm^2/s)	0.80	0.88
Q (mL/min)	2.45		D_s (10^{-10} cm^2/s)	4.73	2.12
Y (µg cells/µg SOC)	0.672		Assigned		
k (µg SOC/µg cells-hr)	0.09	0.0046	K_s^* (µg/L)		8,000
S_o (µg/L)	1,730	178	L_{fo} (10^{-2} cm)	0.2	
b (day^{-1})	0.0144		M_b (µg cells/g GAC)	200	

*TCE k and K_s values were chosen to give a k_1 of 0.014 L/mg-d

Figure 6.3 shows the simulated effluent toluene and TCE concentrations from Experiment 3 where both metabolism and cometabolism occurred. The fit between the measured and simulated values was fair. Although the timing of the simulated sharp decrease in toluene concentration matched that of the measured well, the initial toluene effluent concentration was higher than predicted. The simulated TCE concentration was slightly high compared to the measured values.

When the model was used to simulate the long-term behavior of the column, the toluene concentration stayed low, while the TCE concentration dipped to a minimum of 22 µg/L by 3000 hrs. followed by a long, diffusion-based increase back to the influent concentration. With an EBCT of 10.3 min., the model predicted an operating time of approximately 9,000 hours (375 days) for the TCE to re-saturate the GAC once biodegradation had begun.

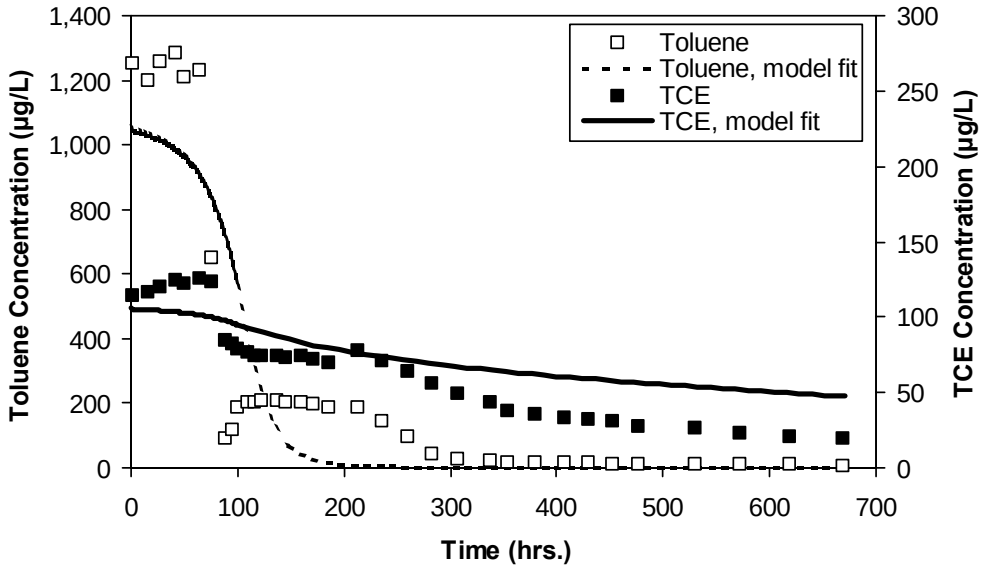

Figure 6.3 Effluent Toluene and TCE Concentration Simulations for Exp. 3, 10.3-min. EBCT, Column A, Iron-Free Influent, Avg. C_o = 1730 (toluene) and 179 (TCE) µg/L

The MDBA model was also used to estimate the TCE-based bioregeneration rate over time. The simulated bioregeneration rate had a similar profile compared to the measured rate except that it did not predict the large initial spike. This discrepancy was most likely due to the large amount of ^{14}C-TCE equilibrium exchange that occurred with the non-labeled bulk TCE during the

initial phase of the experiment. The MDBA model does not predict equilibrium exchange and thus represents the true bioregeneration rate. The experimental method for measuring the bioregeneration rate could not de-couple the effect of equilibrium exchange on the bioregeneration rate.

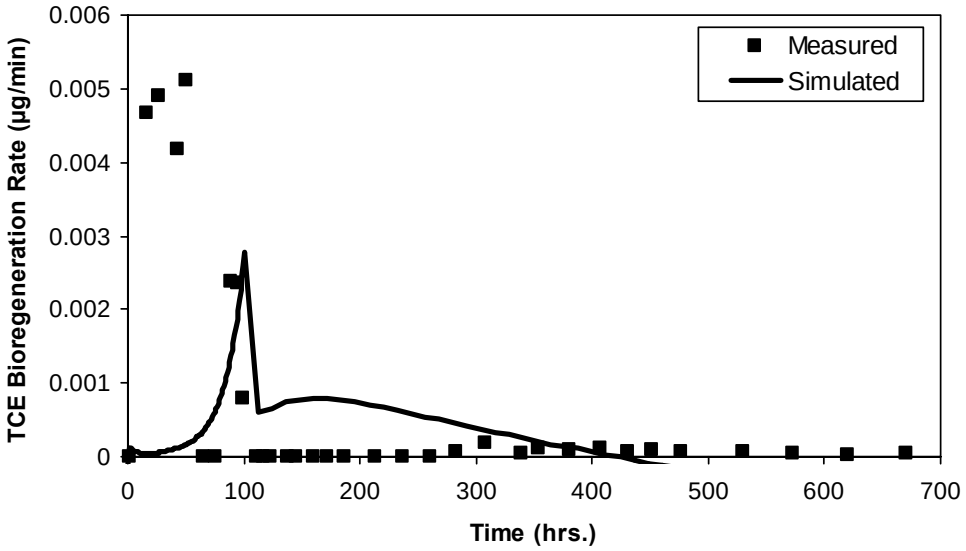

Figure 6.4 TCE Bioregeneration Rate Simulation for Exp. 3, 10.3-min. EBCT, Column A, Iron-Free Influent, Avg. C_o = 1730 (toluene) and 179 (TCE) µg/L

Toluene and TCE loadings along the GAC column at the end of the experiment were also simulated using the MDBA model. These simulations are compared in Figure 6.5 to the measured data from methanol extractions of the GAC. The simulated loadings for TCE had the same profile as the measured loadings except they appear shifted to the left, with the model indicating slightly larger TCE loadings than the measurements. Both, nevertheless, indicated additional adsorption capacity for TCE at the influent and middle portions of the

column as a result of bioregeneration. The extent to which additional TCE was adsorbed was greater in this experiment than the extent to which PCE was adsorbed in Figure 6.2, probably because of the increased toluene concentration used in this experiment. The toluene loading profiles were the same for Experiments 1 and 3: the toluene loading decreased shortly beyond the influent end and remained low (although only a small decrease was seen in Experiment 3). In addition, the TCE and PCE loading profiles were the same for Experiments 1 and 3: the loading had a peak near the influent end of the column and decreased across the rest of the column. The peaks in the TCE and PCE loading profiles represented the location where TCE or PCE re-saturation had already occurred at the new larger loading.

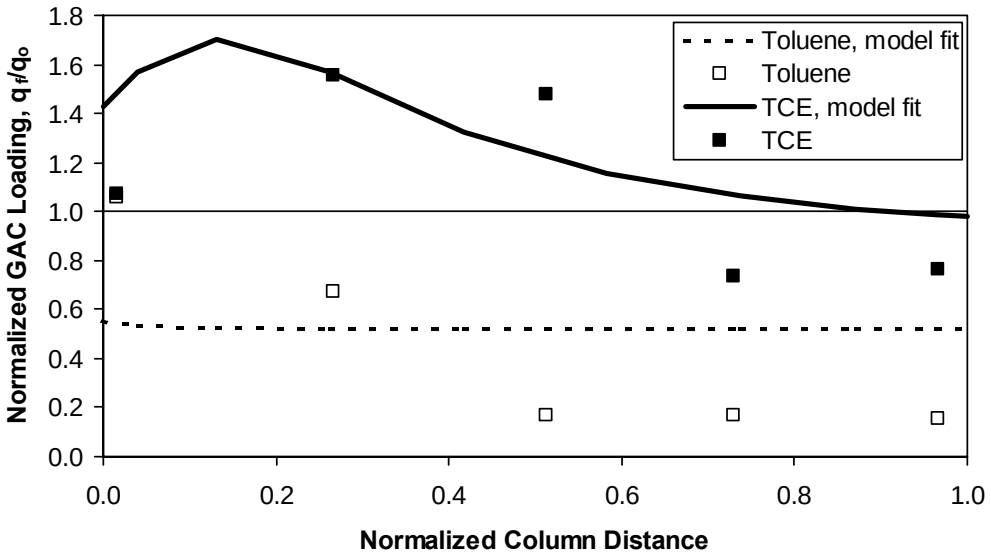

Figure 6.5 Measured and Simulated Final SOC Loadings for Exp. 3, 10.3-min. EBCT, Column A, Iron-Free Influent, Avg. C_o = 1730 (toluene) and 179 (TCE) µg/L

The TCE loading at the effluent end was estimated to be relatively unchanged because the experiment was not run long enough to supply sufficient TCE to re-saturate the entire GAC column; however, the measured normalized TCE loadings at the effluent end were lower than 1. These lower normalized loadings may be indicative of TCE-based bioregeneration at that location. The measured and simulated loadings for toluene did not agree as well as those for TCE, with the model predicting little variation across the column. This discrepancy was probably due to differences between the modeled and measured biomass concentrations.

Experiment 3 was also modeled at various operation times. In this case, however, the initial toluene and TCE loading were changed from that listed in Table 6.2 to 154,000 and 2,730 µg/g, respectively. This increase in the initial SOC loadings allowed for the average SOC influent concentrations and the initial SOC loadings to be in equilibrium as calculated by IAST. Figure 6.6 shows the toluene concentration across the column over time. As expected, the toluene concentration decreased across the column over time as toluene metabolism peaked. After 208 hours, though, toluene metabolism reached a steady, low rate and the toluene concentration across the column did not change. Figure 6.7 shows the TCE concentration for the same experiment, which also decreased across the column over time. The TCE concentration across the column is shown at 671 hours for a model run where cometabolism was “turned off”, which was similar to a toluene-PCE experiment. Without TCE cometabolism, the TCE concentration was approximately 20 µg/L higher across the column. However, no

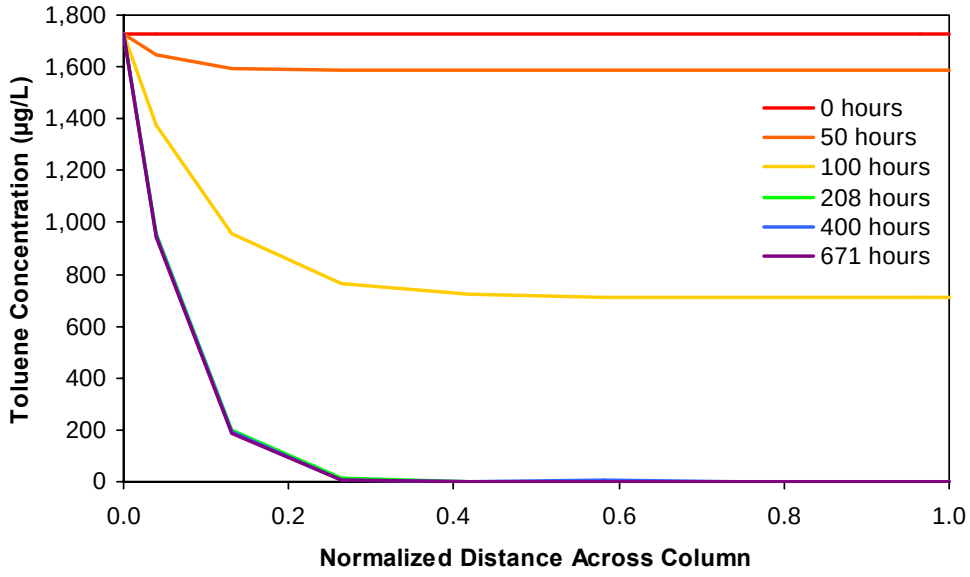

Figure 6.6 Bulk Toluene Concentration Simulations Over Time for a Variation of Exp. 3, 10.3-min. EBCT, Column A, Iron-Free Influent, Avg. C_o = 1730 (toluene) and 179 (TCE) µg/L

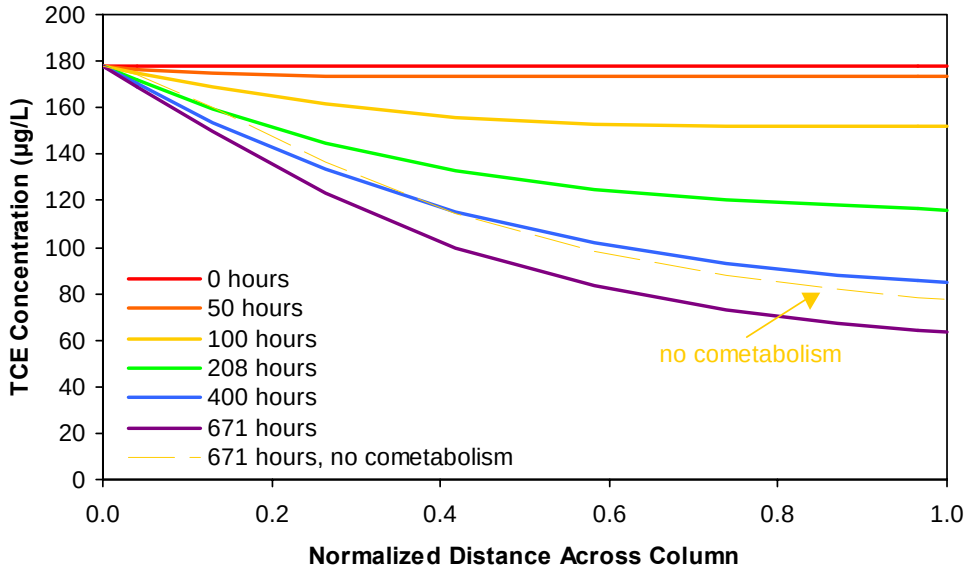

Figure 6.7 Bulk TCE Concentration Simulations Over Time for a Variation of Exp. 3, 10.3-min. EBCT, Column A, Iron-Free Influent, Avg. C_o = 1740 (toluene) and 179 (TCE) µg/L

difference in the toluene concentration was found when cometabolism did not occur.

Figure 6.8 shows the toluene loadings over time for the same experiment. As for the toluene concentration, the toluene loading decreased across the column over time as toluene metabolism peaked. Unlike the toluene concentration, however, the toluene loading continued to decrease after 208 hours. This loading continued to decrease because although the toluene concentration profile had stabilized, the low toluene concentration continued to create a driving force for desorption of toluene off the GAC, thereby lowering the toluene loading. Figure 6.9 shows the TCE loading for the same experiment. The TCE loadings peaked near the influent region and then decreased across the column, as also shown in Figure 6.5. The peaks in the TCE loading profiles represented the location where TCE re-saturation had already occurred at the new larger loading. Furthermore, the TCE loading increased in the influent region over time due to decreased competition from toluene for adsorption sites. Near the effluent end of the column, the TCE loading decreased slightly over time because of the driving force for desorption from the decreased liquid-phase TCE concentration. In addition, the TCE loading profile is shown at 671 hours for a model run where cometabolism was "turned off". Without TCE cometabolism, the TCE loading was approximately 4,000 µg/g higher across the column.

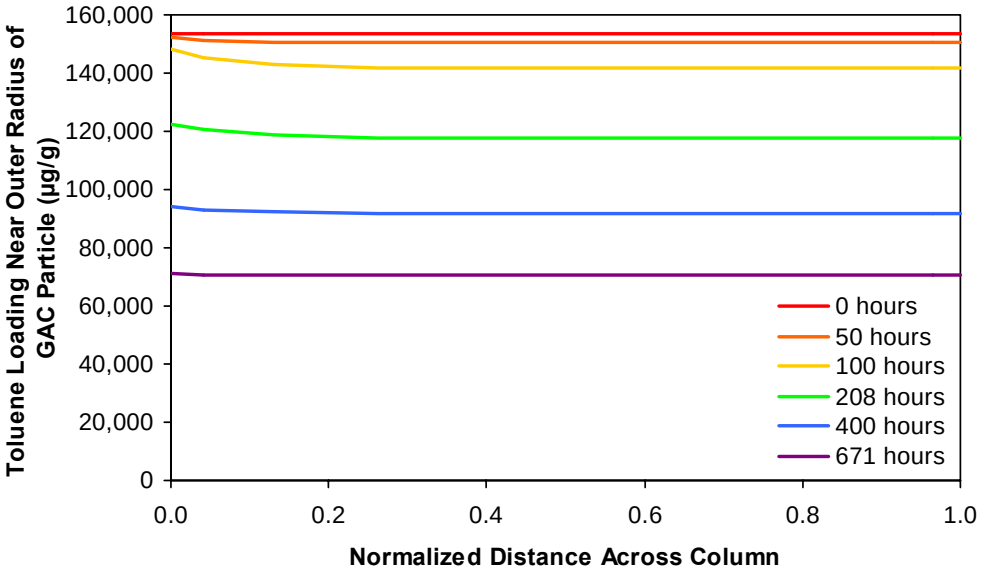

Figure 6.8 Toluene Loading Simulations Over Time for a Variation of Exp. 3, 10.3-min. EBCT, Column A, Iron-Free Influent, Avg. C_o = 1740 (toluene) and 179 (TCE) µg/L

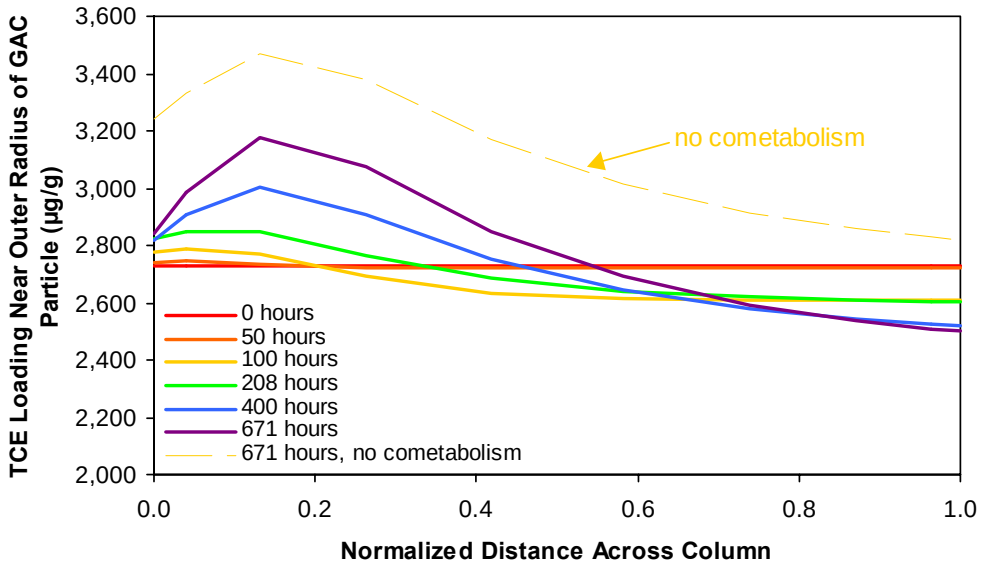

Figure 6.9 TCE Loading Simulations Over Time for a Variation of Exp. 3, 10.3-min. EBCT, Column A, Iron-Free Influent, Avg. C_o = 1740 (toluene) and 179 (TCE) µg/L

6.3 METABOLISM-COMETABOLISM VIRGIN COLUMN EXPERIMENTS

The exhausted zone is only part of a whole GAC column. Thus, the MDBA model was used to describe the results obtained in a 1.1-min. EBCT, iron-free, virgin column (Column B of Experiment 7) with toluene and TCE influent concentrations of 1540 and 91 µg/l, respectively. The parameters used to model Experiment 7 are shown in Table 6.3 and were similar to those used in Experiment 3, except the initial GAC loading was set to zero and the iron-free kinetic values were used. In addition, the adsorption equilibrium parameters were switched from those measured in this research to those from Speth and Miltner (1990) due to the large difference in SOC concentration between the pre-equilibrated and the virgin columns (see Section 4.2). The adsorption kinetic coefficients were calculated in the same manner as described in Section 6.1. In exhausted GAC column experiments, a portion of either the toluene or TCE adsorbed at the effluent end of the GAC column was ^{14}C-radiolabeled to allow measurement of bioregeneration of the adsorbed SOC; thus, the weight of the radiolabeled GAC, Wt1, was known. Since the GAC in the virgin columns was not pre-equilibrated, radiolabeled toluene was fed in the column influent for a short period at the beginning of the experiment until $^{14}CO_2$ was measurable in the effluent. Since the column was fed radiolabeled toluene at the beginning of the experiment, the main portion of the column that had radiolabeled toluene sorbed to the GAC was the influent end, not the effluent end as in the exhausted column experiments. Thus, in the virgin GAC experiments, Wt1 was not known and was assigned based on goodness-of-fit. In addition, the toluene maximum substrate

Table 6.3 MDBA Model Inputs for Exp. 7, 1.1-min. EBCT, Iron Free

Units	Toluene	TCE	Units	Toluene	TCE
Experimentally Measured			Calculated		
q_e (µg SOC/g GAC)	0	0	k_f (10^{-3} cm/s)	1.71	1.84
1/n (--)	0.429	0.482	ρ_a (g GAC/cm^3)	0.7	
K (µg/g)(L/µg)$^{1/n}$	4,460	2,000	b' (day^{-1})	0.031	
L (cm)	1.50		D_f (10^{-5} cm^2/s)	0.80	0.88
R (cm)	0.026		D_s (10^{-10} cm^2/s)	6.27	2.39
D (cm)	1.5		Assigned		
W (g)	1.01		Wt1 (g)	0.1500	
Q (mL/min)	2.50		K_s (µg/L)		100,000
Y (µg cells/µg SOC)	0.505		k (µg SOC/ µg cells-hr)	0.058	
S_o (µg/L)	1,540	90.8	L_{fo} (10^{-2} cm)	0.2	
k (µg SOC/ µg cells-hr)		0.0118	M_b (µg cells/g GAC)	2,800	
b (day^{-1})	0.048				
b'_s (--)	0.368				
P (--)	1.0	1.0			
K_s (µg/L)	165				

*TCE k and K_s values were chosen to give a k_1 of 0.0028 L/mg-d

utilization rate (k) was assigned a value of 0.058 mg/mg-hr, instead of using the value measured from batch kinetics (0.0324 mg/mg-hr) to better fit the slight variation in mixed-culture kinetics observed in this column.

Figure 6.10 shows the simulated effluent toluene and TCE concentrations from Experiment 7 where both metabolism and cometabolism occurred. For comparison with the biologically-active GAC (BAC) column, the simulation for a sterile column is shown. The fit between the measured and simulated values was good, although the TCE effluent was somewhat overestimated after 200 hours of operation. Compared to the sterile column, the BAC column simulation resulted in much lower effluent SOC concentrations and, thus, an increased service life. The BAC column simulation also lacked the chromatographic effect seen in the sterile column simulation because of the decreased competition for GAC adsorption sites as a result of biological activity.

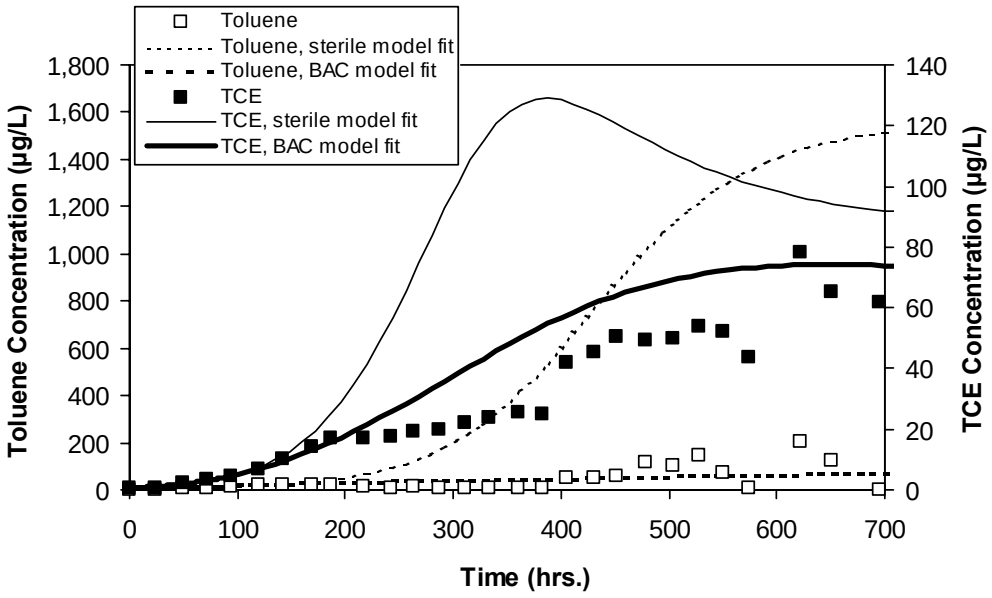

Figure 6.10 Effluent Toluene and TCE Concentration Simulations for Exp. 7, 1.1-min. EBCT, Iron-Free, Toluene C_o = 1540 µg/L, TCE C_o = 91 µg/L

The MDBA model was also used to simulate the toluene-based bioregeneration rate and the toluene adsorption rate over time. In the MDBA model, the adsorption rate is defined as being positive when the SOC is moving from the biofilm onto the GAC, whereas the bioregeneration rate is defined as being positive when the SOC is moving from the GAC into the biofilm. In the case of the virgin column, when the concentration difference between the biofilm and the GAC allows for rapid adsorption onto the GAC, bioregeneration, by definition, does not occur. This repression of bioregeneration is seen in Figure 6.11, where the simulated bioregeneration rate did not become significant until the simulated adsorption rate had decreased to zero. The bioregeneration rate was dependent on Wt1, which as explained previously could not be measured for

virgin GAC columns and thus was assigned based on goodness-of-fit. The simulated bioregeneration rate fit the measured rate well beyond the initial adsorption period where the measured bioregeneration rate was higher than that simulated by the model.

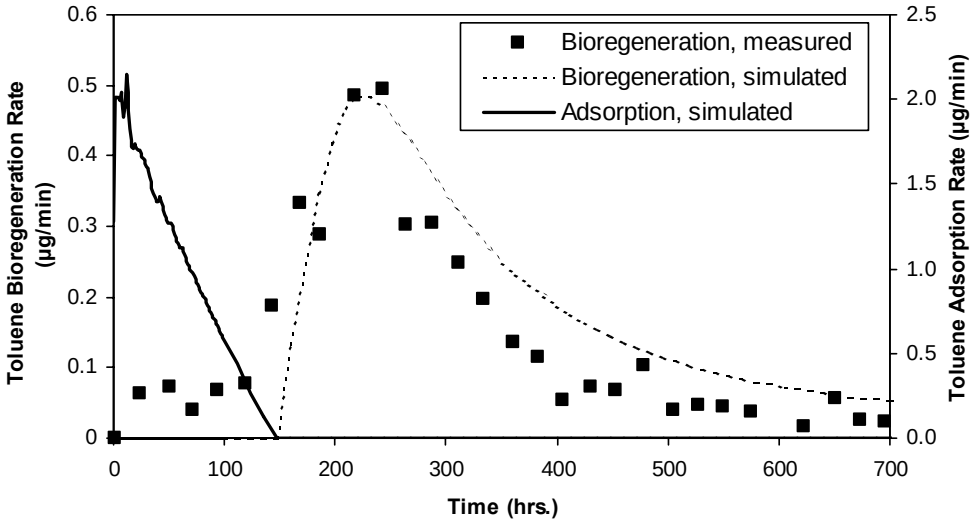

Figure 6.11 Toluene Adsorption and Bioregeneration Rate Simulation for Exp. 7, 1.1-min. EBCT, Iron-Free, Toluene C_o = 1540 µg/L, TCE C_o = 91 µg/L

Toluene and TCE loadings along the GAC column at the end of Experiment 7 were also simulated using the MDBA model. The results are shown in Figure 6.12. Only the final SOC loadings are presented because the initial SOC loadings were zero. Where the simulated TCE loadings were the lowest in Figure 6.12, the toluene loadings were the highest, showing the effect of SOC competition for adsorption sites. Due to the small EBCT and GAC mass necessary for reasonable experimental run times, only two samples could be taken

to measure the SOC loadings: one sample representing the average SOC loading for the first half of the column, and another sample representing that of the second half. The measured SOC loadings do not agree with the simulated loadings. The measured TCE loadings are greater than the simulated loadings. The toluene loadings are greater than the simulated loading in the first half of the column and smaller than the simulated loading in the second half. Errors in SOC loadings may have occurred due to the small GAC sample size used.

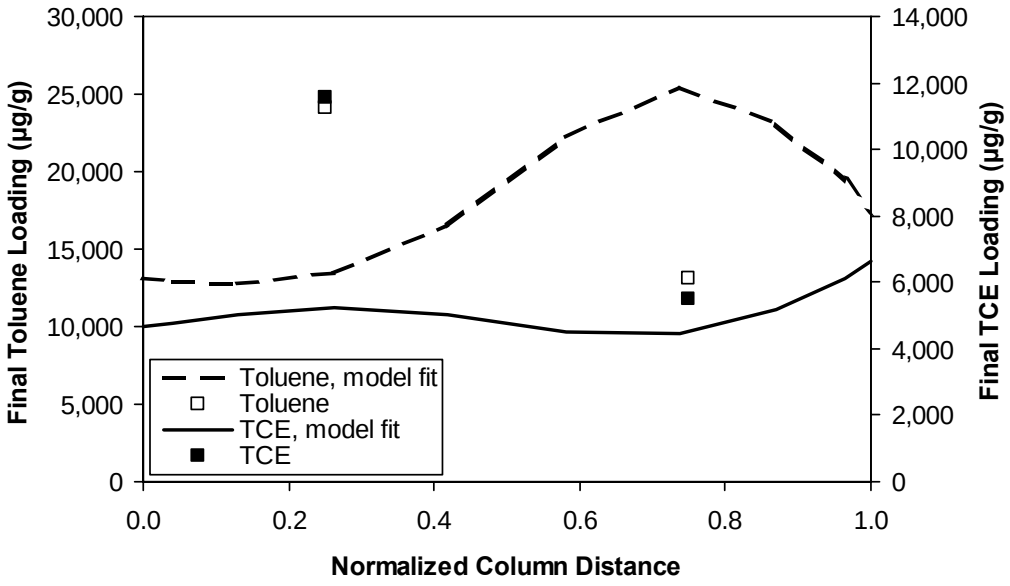

Figure 6.12 Simulated Final SOC Loadings (697 hrs.) for Exp. 7, 1.1-min. EBCT, Iron-Free, Toluene C_o = 1540 µg/L, TCE C_o = 91 µg/L

The SOC loading profile in Figure 6.12 looks very different from that seen with the pre-equilibrated columns in Figures 6.5 and 6.2. This difference is due to two opposing driving forces acting on both toluene and TCE in the virgin column: adsorption onto the GAC versus desorption into the biofilm and subsequent

metabolism or cometabolism. In the pre-equilibrated columns, SOC adsorption was only relevant for TCE or PCE. Toluene only underwent desorption and biodegradation (unless the toluene influent concentration increased beyond the equilibrium). To aid in the interpretation of the overall SOC loadings, the SOC loadings versus radial distance within the GAC particle were analyzed. When the SOC loadings at the outer GAC radius were smaller than those at other points within the GAC, desorption of the SOC off the GAC for subsequent biodegradation (*i.e.*, bioregeneration) was indicated. Conversely, when the profile was reversed, adsorption was indicated.

For TCE, adsorption was indicated in the first 60% of the column, whereas bioregeneration was indicated in the last 40% by 697 hours. For toluene, bioregeneration was indicated in the first 75% of the column, whereas adsorption was indicated in last 25% by 697 hours. Due to the short EBCT (1.1-min.) of this column, adsorption was the dominant mass transfer process early in the operation of the column (as shown in Figure 6.11 for toluene). By 697 hours, the biomass concentration had increased to the point where bioregeneration of the adsorbed toluene was occurring in the first 75% of the column, thereby decreasing the toluene loading in that location. Toluene bioregeneration in the first part of the column also decreased the amount of toluene that reached the last 25% of the column. The toluene bioregeneration in the first 75% of the column led to decreased competition for TCE adsorption in that location. The increased adsorption of TCE in the first 60% of the column led to a decreased TCE liquid

phase concentration downstream. This lower liquid phase concentration provided a driving force for desorption of TCE off the GAC into the biofilm.

Experiment 7 was also modeled at various operation times. Figure 6.13 shows the toluene concentration across the column over time. As expected, the toluene concentration decreased across the column due to adsorption. Until 208 hours, the toluene concentration across the column increased with time as adsorption occurred to a greater extent than metabolism. Around 208 hours, though, the toluene metabolism rate peaked (as shown in Figure 6.11) and began decreasing the toluene concentration within the column. This trend is also supported by the toluene loadings over time shown in Figure 6.14. The toluene loadings increased over time until 208 hours. After 208 hours, the toluene loading in the first section of the column decreased due to bioregeneration. The toluene loading in the second section of the column, however, increased over time. Toluene bioregeneration in the first part of the column decreased the amount of toluene that reached the last 25% of the column, as discussed previously regarding Figure 6.12.

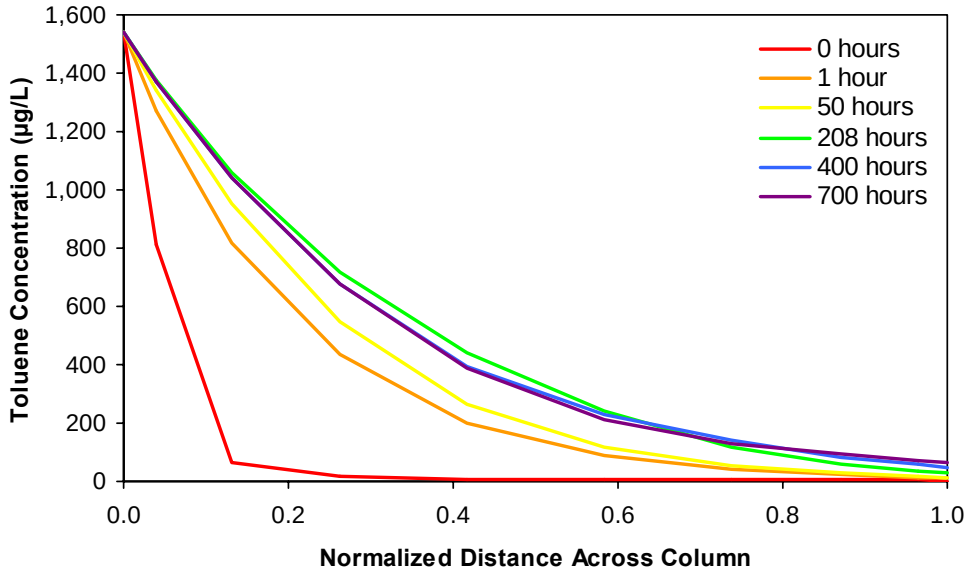

Figure 6.13 Toluene Concentration Simulations for Exp. 7, 1.1-min. EBCT, Iron-Free, Toluene C_o = 1540 µg/L, TCE C_o = 91 µg/L

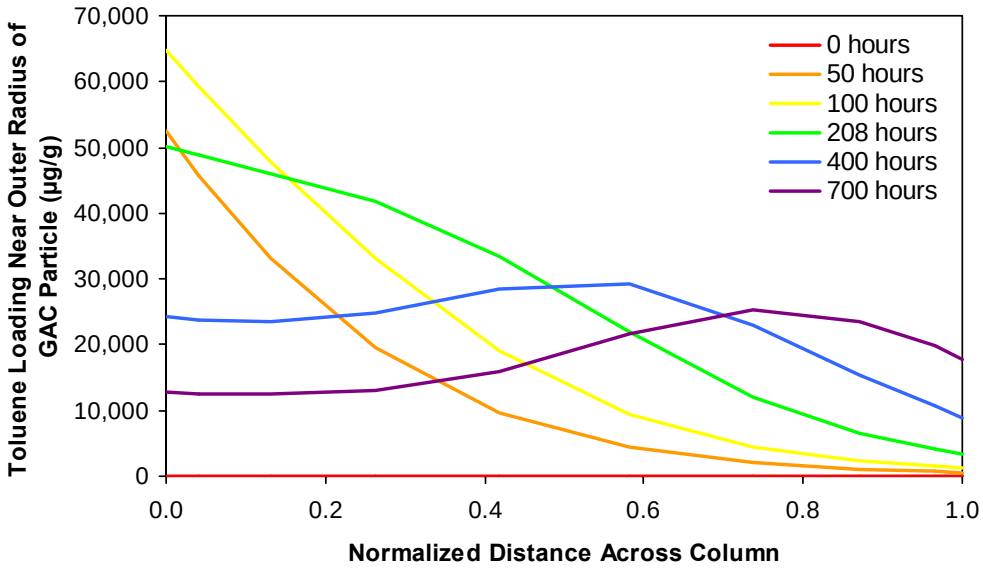

Figure 6.14 Toluene Loading Simulations Over Time for Exp. 7, 1.1-min. EBCT, Iron-Free, Toluene C_o = 1540 µg/L, TCE C_o = 91 µg/L

Figure 6.15 shows the TCE concentration across the column over time for Experiment 7. As was the case for toluene, the TCE concentration increased over time until 208 hours because the driving force for adsorption was greater than that for desorption and cometabolism. After 208 hours, the TCE concentration dipped in the middle region of the column due to toluene bioregeneration and subsequent increased TCE adsorption. Figure 6.16 shows the same trend with respect to time for the TCE loadings across the column. As discussed for Figure 6.12, by 700 hours for TCE, adsorption was indicated in the first 60% of the column, whereas desorption was indicated in the last 40%. The toluene bioregeneration in the first 75% of the column led to decreased competition for TCE adsorption in that region. The increased adsorption of TCE in the first 60% of the column led to a decreased TCE liquid phase concentration downstream. This lower liquid phase concentration provided a driving force for desorption of TCE off the GAC into the biofilm. In addition, the TCE concentration and loading across the column are shown at 700 hours for a model run where cometabolism was "turned off", which was similar to a toluene-PCE experiment. The TCE concentration and loading profiles were approximately the same with or without TCE cometabolism. No significant difference was observed because, unlike in the pre-exhausted columns, the driving force for adsorption in the virgin columns was too large to allow significant amounts of desorption and cometabolism until near saturation.

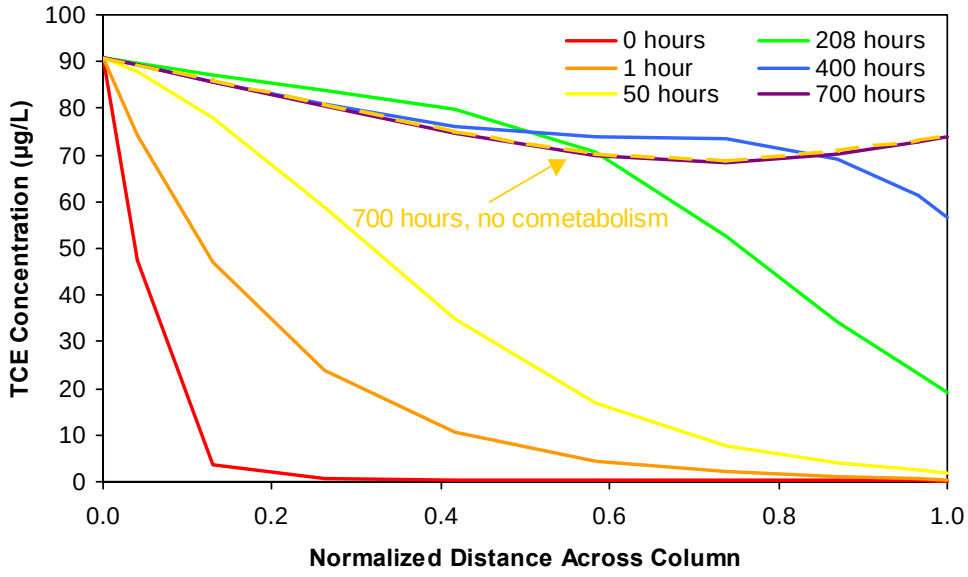

Figure 6.15 TCE Concentration Simulations for Exp. 7, 1.1-min. EBCT, Iron-Free, Toluene C_o = 1540 µg/L, TCE C_o = 91 µg/L

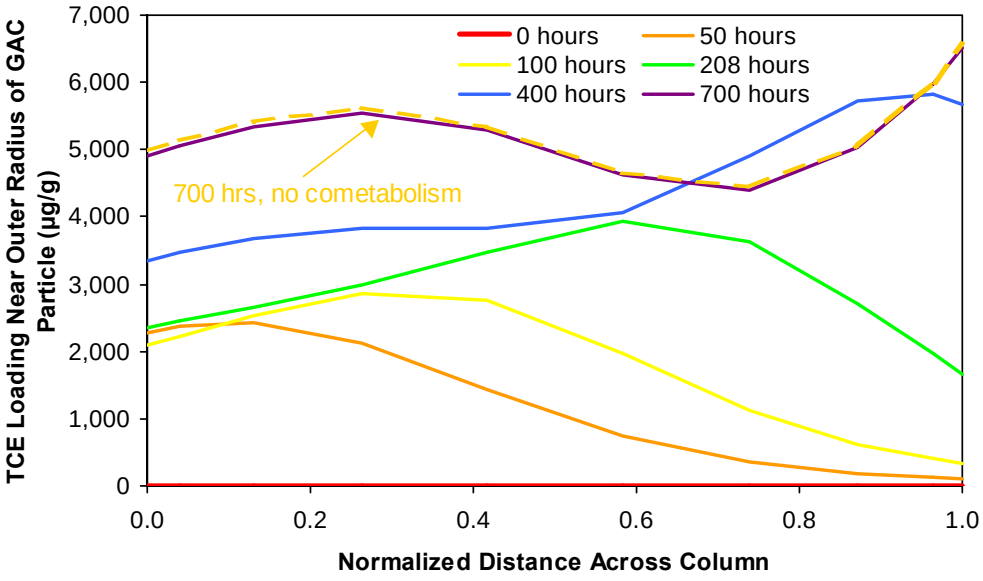

Figure 6.16 TCE Loading Simulations Over Time for Exp. 7, 1.1-min. EBCT, Iron-Free, Toluene C_o = 1540 µg/L, TCE C_o = 91 µg/L

6.4 FULL-SCALE MODEL PREDICTIONS

After validation and calibration of the MDBA model was completed using bench-scale columns, full-scale virgin BAC column performance was predicted. Table 6.4 shows the MDBA model inputs for a 1-min. EBCT virgin BAC column. Subsequent model runs involved variation of the following parameters: EBCT, influent concentration, K value, k value (to turn "on" or "off" metabolism or cometabolism), M_b, and TCE K_s. D_s values were re-calculated as described in Section 6.1 when influent SOC concentrations or adsorbabilities were changed. Table 6.5 shows the column dimensions for the each EBCT used. It was necessary to use short EBCTs to maintain numerical stability of the model.

Table 6.4 MDBA Model Inputs for Virgin BAC Column, 1.0-min. EBCT

Units	Toluene	TCE	Units	Toluene	TCE
Experimentally Measured			Experimentally Measured (Cont'd)		
q_e (µg SOC/g GAC)	0	0	b'_s (--)	0.368	
1/n (--)	0.429	0.482	P (--)	1.0	1.0
K $(\mu g/g)(L/\mu g)^{1/n}$	4,460	2,000	K_s (µg/L)	348	
L (cm)	32.4		Calculated		
R (cm)	0.053		k_f (10^{-3} cm/s)	3.56	3.79
D (cm)	122		ρ_a (g GAC/cm^3)	0.7	
W (g)	160,000		b' (day^{-1})	0.121	
Wt1 (g)	3271		D_f (10^{-5} cm^2/s)	0.80	0.88
Q (mL/min)	378,500		D_s (10^{-10} cm^2/s)	5.56	1.92
Y (µg cells/µg SOC)	0.672		Assigned		
k (µg SOC/µg cells-hr)	0.09	0.0046	K_s (µg/L)		8,000
S_o (µg/L)	2,000	100	L_{fo} (10^{-2} cm)	0.2	
b (day^{-1})	0.0144		M_b (µg cells/g GAC)	100	

*TCE k and K_s values were chosen to give a k_1 of 0.014 L/mg-d

Table 6.5 Column Dimensions for Virgin BAC Column Modeling

EBCT	0.5 min.	1.0 min.	1.5 min.
L (cm)	16.2	32.4	48.6
D (cm)	122	122	122
W (g)	80,000	160,000	240,000

6.4.1 Effect of EBCT on Column Performance

Virgin BAC column performance can be measured via an increase in the service life, the rate or extent of bioregeneration, or the reduction in effluent SOC concentrations. In most of the full-scale cases modeled, no discernible increase in the service lives of the columns resulted from biological activity. This lack of service life increase was due to the low amount of initial biomass and short EBCTs used to ensure the model was numerically stability. In this case, SOC adsorption occurred faster than biodegradation; therefore, the benefits of biological activity were not evident until the column had been run longer. Thus, the rate of bioregeneration and the reduction in effluent SOC concentration (at the plateau value around 2000 hrs.) were used instead to judge column performance.

The effect of EBCT on column performance was tested first. Figure 6.17 shows the effect of EBCT on the predicted effluent toluene concentration. As the EBCT increased, the toluene effluent plateau concentration decreased. This trend was expected because, with increased EBCTs, more time is available for adsorption and biodegradation to take place. In addition, Figure 6.18 shows the effect of EBCT on the predicted toluene bioregeneration rate at the influent and effluent ends of the same column. As the EBCT increased, the bioregeneration rate at the effluent end peaked higher and later. A similar trend was observed in Experiment 2 (Section 5.1.1) where the 12-min. EBCT column had a peak bioregeneration rate that was more than three times that of the effluent end of the 2.5-min. EBCT column. In both cases, more bioregeneration occurred at the effluent end of the longer column than at the effluent end of the shorter column

because the liquid phase concentration of the biodegradable SOC was substantially lower. The bioregeneration rate at the influent end of the columns in Figure 6.18, however, was independent of EBCT, because the liquid phase concentration at that point would be about the same in all of the columns regardless of EBCT.

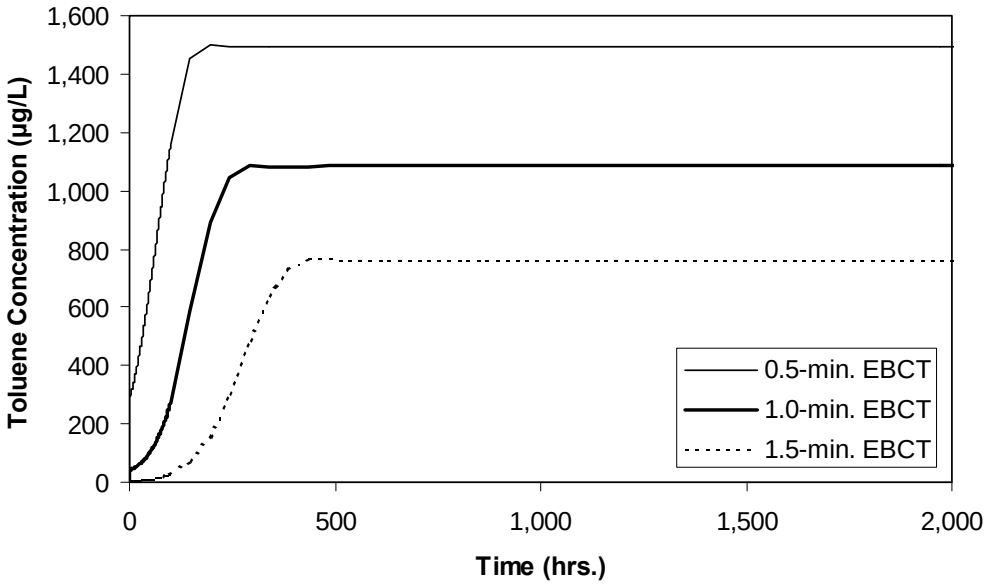

Figure 6.17 Predicted Effluent Toluene Concentration in Biologically-Active GAC Columns, Toluene C_o = 2000 µg/L, TCE C_o = 100 µg/L

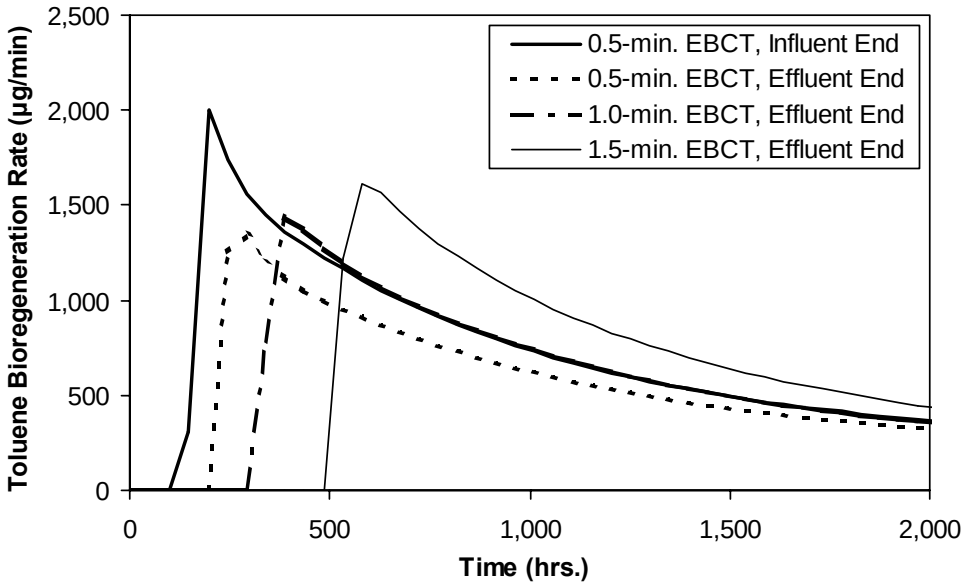

Figure 6.18 Predicted Biologically-Active Toluene Bioregeneration Rate at the Influent and Effluent Ends of the Column, Toluene C_o = 2000 µg/L, TCE C_o = 100 µg/L

Figure 6.19 shows the effect of EBCT on the predicted effluent TCE concentration from the same set of columns. As the EBCT increased, the TCE effluent plateau concentration decreased. The concentration decrease was not as great as it was in the case of toluene, however, because cometabolism kinetics are slower than metabolism kinetics.

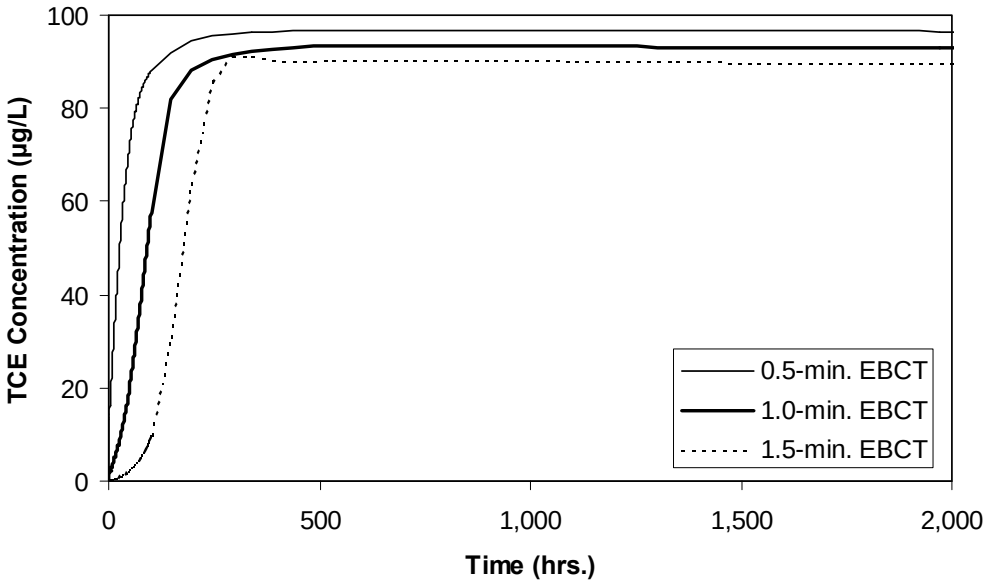

Figure 6.19 Predicted Biologically-Active Effluent TCE Concentrations, Toluene C_o = 2000 µg/L, TCE C_o = 100 µg/L

6.4.2 Effect of SOC Adsorbability and Concentration on Column Performance

In addition to the physical dimensions of the column, the adsorbability and concentration of the SOCs also affect the column performance. Large changes in the column service life were predicted by Erlanson *et al*. (1997) using the biodegradation/adsorption screening model (BASM) to model SOCs of variable adsorbability and concentration (see Section 2.9). The BASM model was based on equilibrium and thus ignored kinetics, whereas the MDBA model involved kinetics. Due to the stability issues encountered with the MDBA model at large EBCTs and high biomass concentrations (situations where the largest increase in service life would be expected) only small increases in service life could be

predicted. The short EBCTs did not allow sufficient time for biofilm development before breakthrough.

Figure 6.20 shows the effect of toluene concentration and EBCT on the reduction in normalized effluent toluene plateau concentration (compared to a sterile column), when both metabolism and cometabolism were occurring in the column. The most toluene was removed from the effluent in the case of 500 µg/L toluene and TCE. Toluene removal is dependent on both toluene concentration (by providing substrate for biofilm growth) and competition from TCE for adsorption sites (less of a driving force for adsorption). The 500 µg/L-toluene and TCE column was the combination that combined both a high toluene concentration and a large amount of competition with TCE.

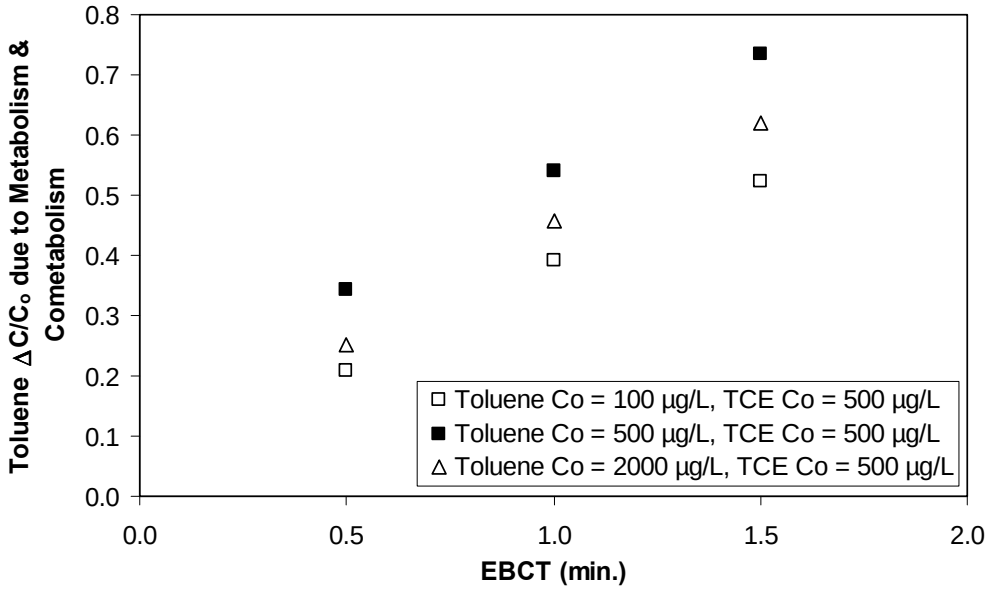

Figure 6.20 Predicted Reduction in Normalized Effluent Toluene Concentration due to Metabolism & Cometabolism

Figure 6.21 shows the effect of toluene adsorbability on the reduction in normalized effluent toluene plateau concentration (compared to a sterile column), when both metabolism and cometabolism were occurring in the column. The reduction in toluene effluent increased with increasing EBCT but was independent of the adsorbability of toluene. This independence was due to the low level of competition for adsorption sites that TCE presented in these runs. The TCE concentration was 100 µg/L whereas the toluene concentration was 2000 µg/L, so even when the toluene adsorbability was lower than that for TCE, toluene out-competed TCE for adsorption sites. Furthermore, by modeling the same columns with cometabolism "turned off" (TCE k set to zero), which would be similar to running a toluene-PCE experiment, it was found that metabolism-based removal of toluene accounted for 100% of the biological removal of toluene. Thus, cometabolism-based bioregeneration was not significant enough to allow for toluene re-adsorption onto the GAC.

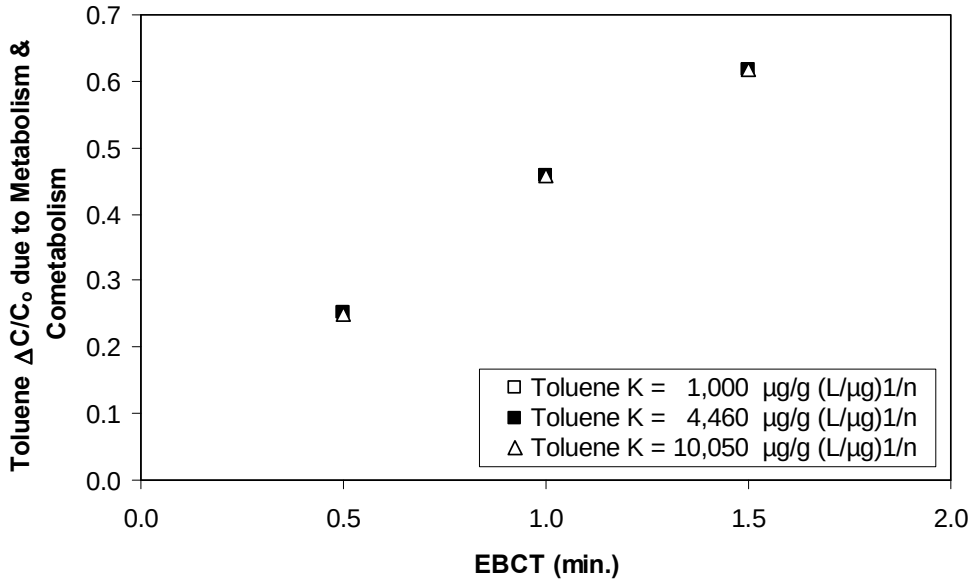

Figure 6.21 Predicted Reduction in Normalized Effluent Toluene Concentration due to Metabolism & Cometabolism, Toluene C_o = 2000 µg/L, TCE C_o = 100 µg/L

The same column was then modeled with changes in the TCE adsorbability while holding the toluene adsorbability constant. Figure 6.22 shows the effect on the reduction in the normalized effluent TCE plateau concentration (compared to a sterile column) when both metabolism and cometabolism were occurring in the column. TCE removal compared to a sterile column increased as both the EBCT and the TCE adsorbability increased. The increased removal of TCE with increased TCE adsorbability is explained by a comparison with Figure 6.23. There are two biologically-based removal mechanisms for TCE: (1) TCE cometabolism and (2) metabolism-based bioregeneration resulting in increased TCE adsorption. Figure 6.23 is the same as Figure 6.22 except that the TCE

effluent reduction due solely to cometabolism is shown. Cometabolism accounted for only 11 to 48% of the overall reduction in TCE effluent concentration, with the contribution decreasing as the TCE adsorbability increased. The rest of the reduction in TCE effluent was due to metabolism-based bioregeneration of GAC adsorption sites containing toluene. Thus, the combined metabolism plus cometabolism-based TCE effluent decreased with increasing TCE adsorbability because of the effect of the TCE adsorbability on toluene metabolism, not TCE cometabolism. An increase in the TCE adsorbability created more competition for adsorption sites, thus decreasing the driving force for toluene adsorption and allowing for increased toluene metabolism.

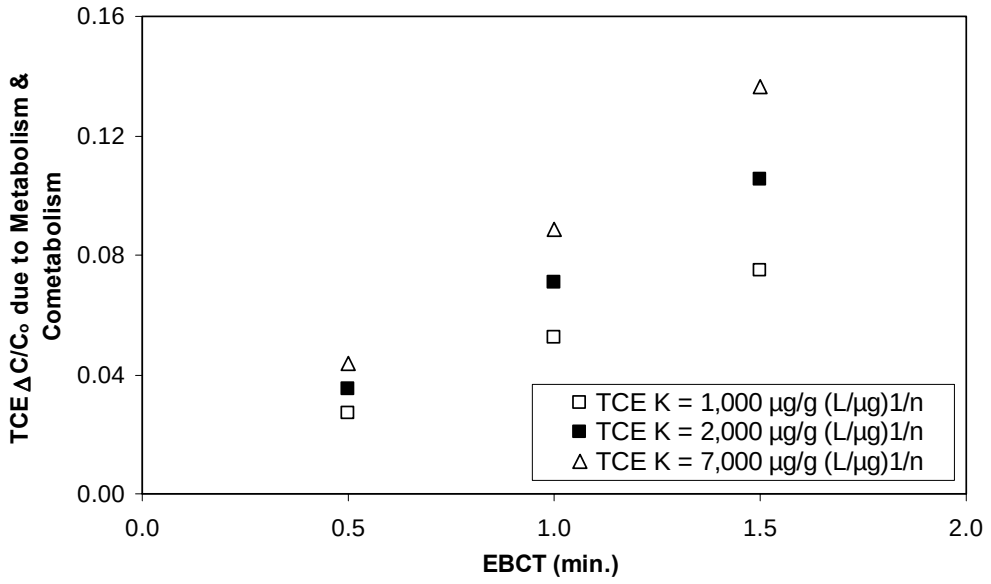

Figure 6.22 Predicted Reduction in Normalized Effluent TCE Concentration due to Metabolism & Cometabolism, Toluene C_o = 2000 µg/L, TCE C_o = 100 µg/L

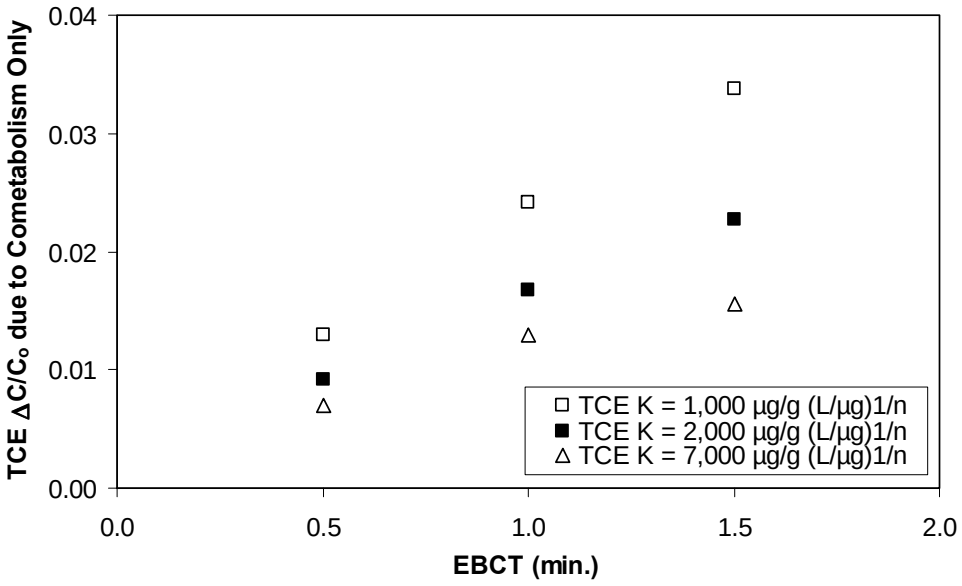

Figure 6.23 Predicted Reduction in Normalized Effluent TCE Concentration due to Cometabolism Only, Toluene C_o = 2000 µg/L, TCE C_o = 100 µg/L

6.4.3 Effect of Bacterial Seeding and Culture Kinetics on Column Performance

The properties of the seeding culture are critical to the performance of a BAC column. Figure 6.24 shows the effect of initial biomass concentration on the toluene effluent concentration when both metabolism and cometabolism were occurring. Varying the initial biomass concentration was a way of varying the onset time of bioregeneration. As the initial biomass concentration increased, or the onset time of bioregeneration decreased, the liquid phase toluene concentration decreased. The smallest amount of biomass used, 0.1 µg cells/g

GAC, resulted in a toluene concentration profile very close to that of a sterile column.

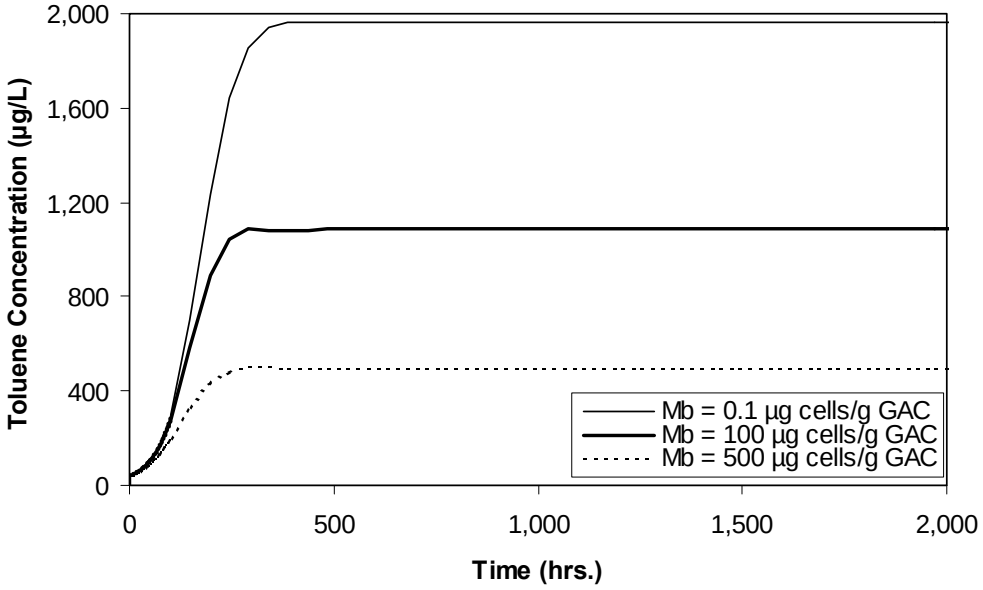

Figure 6.24 Predicted Biologically-Active Effluent Toluene Concentrations, 1-min. EBCT, Toluene C_o = 2000 µg/L, TCE C_o = 100 µg/L

TCE effluent concentration was also measured as a function of varying initial biomass concentrations (Figure 6.25). The same trend occurred with the TCE effluent concentration as with the toluene effluent concentration. The concentration effect was more subdued, however, due to the slower cometabolism kinetics.

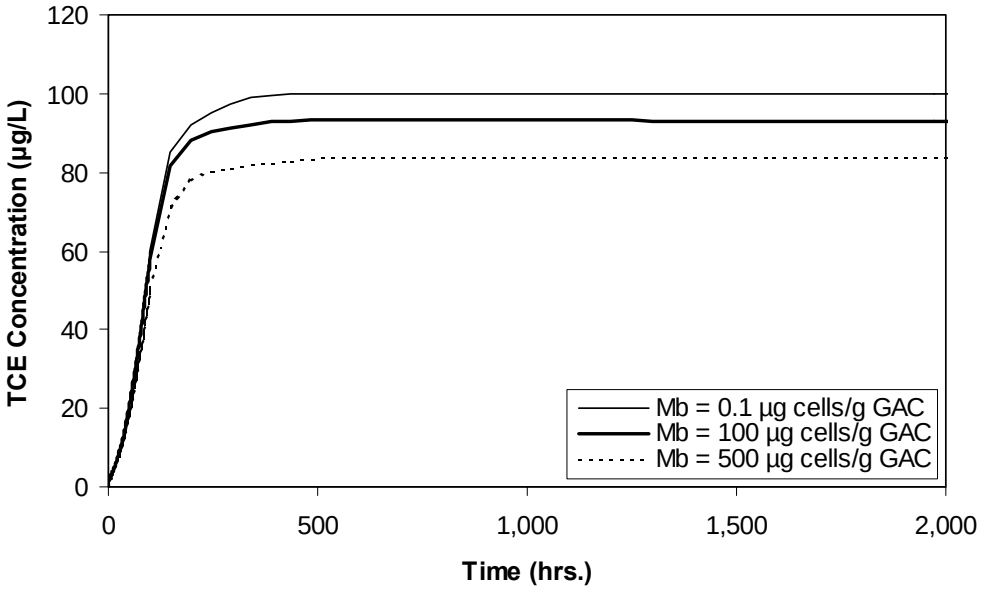

Figure 6.25 Predicted Biologically-Active Effluent TCE Concentrations, 1-min. EBCT, Toluene C_o = 2000 µg/L, TCE C_o = 100 µg/L

To observe the effect of more rapid cometabolism kinetics, the TCE k_1 was increased (from 0.014 to 0.328 L/mg-d) by decreasing the K_s from 8000 µg/L to 333 µg/L. The normalized reduction in the TCE effluent concentration (compared to a sterile column) due solely to TCE cometabolism was calculated for both the small ($\Delta C1/C_o$) and large ($\Delta C2/C_o$) k_1 values. Here, $\Delta C1$ is the TCE effluent plateau concentration from the sterile column minus that from the BAC column. The difference between these normalized TCE reduction values ($[\Delta C2/C_o]-[\Delta C1/C_o]$) was then calculated and referred to as "TCE ($\Delta C2-\Delta C1)/C_o$". As Figure 6.26 shows, the TCE removal as represented by TCE ($\Delta C2-\Delta C1)/C_o$ was found to increase as the EBCT and the toluene concentration increased. Thus, as the EBCT increased, the TCE k_1 became more important in

reducing the TCE effluent concentration because more extensive cometabolism kinetics resulted in a decreased liquid phase TCE concentration. In addition, the TCE k_1 became more important in reducing the TCE effluent concentration as the toluene concentration increased because toluene was the substrate for biofilm growth and thereby enzyme production. Thus the more enzymes were available, the more important cometabolism was as a mechanism of TCE removal.

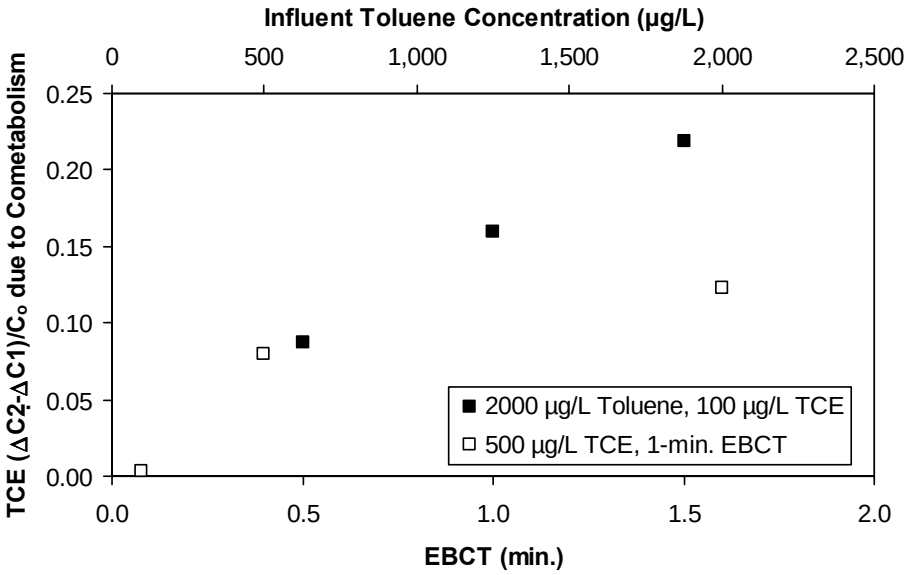

Figure 6.26 Predicted Reduction in Normalized Effluent TCE Concentration from Cometabolism due to an Increase in the TCE k_1

6.5 SUMMARY

Manipulation of the MDBA modeling code was found to be unnecessary to account for cometabolism using the current SOCs and mixed culture. The lack of enzyme competition or significant intermediate toxicity meant that the TCE

could be modeled as another biodegradable chemical with a yield of zero that was simultaneously biodegraded along with toluene. Overall, the MDBA model simulated the column data with moderate success and helped highlight the differences between the pre-equilibrated and virgin BAC columns.

Due to the ability of the MDBA model to capture the column data, its predictive ability was used to determine the effect of different physical, chemical, and biological parameters on virgin BAC performance. Model simulations showed that, as the EBCT increased, the metabolism-based bioregeneration rate at the effluent end peaked at a higher value and at a later time during the GAC service life. In addition, the MDBA model predicted toluene removal was dependent on both toluene concentration (by providing substrate for biofilm growth) and competition from TCE for adsorption sites (less of a driving force for adsorption). However, the MDBA-predicted normalized reduction in toluene effluent concentration increased with increasing EBCT but was independent of the adsorbability of toluene.

Furthermore, TCE removal compared to a sterile column was predicted to increase as both the EBCT and the TCE adsorbability increased. Cometabolism was predicted to account for only 11 to 48% of that removal, with the contribution decreasing as the TCE adsorbability increased. The rest of the TCE removal was due to metabolism-based bioregeneration of GAC adsorption sites containing toluene. MDBA model predictions also showed that as the EBCT increased or the toluene concentration increased, the TCE k_1 became more important in reducing the TCE effluent concentration. In addition, as the initial biomass concentration

used in the MDBA model increased, or the onset time of bioregeneration decreased, the liquid phase toluene and TCE concentrations decreased.

Chapter 7: Conclusions and Recommendations

This chapter presents the conclusions and recommendations for future research regarding the relative roles of metabolism and cometabolism in biologically-active GAC (BAC) columns. The conclusions are grouped according to their relationship to the objectives of this research and are followed by recommendations for future research.

7.1 CONCLUSIONS

Objective 1. Determine the relative significance of metabolism and cometabolism as mechanisms for increasing GAC service life.

i. Experiments with the toluene-PCE exhausted GAC columns demonstrated that bioregeneration of the GAC led to increased adsorption capacity for the nonbiodegradable SOC through decreased competition for adsorption sites.

ii. For a highly biodegradable and moderately adsorbable SOC (toluene), the extent of metabolism-based bioregeneration and the additional capacity for adsorption of the any remaining non-degraded SOC increased as the toluene concentration increased.

iii. The extent of metabolism-based bioregeneration at the effluent end of the column increased as the EBCT increased. MDBA model predictions also showed that as the EBCT increased, the metabolism-based bioregeneration rate at the effluent end peaked at a higher value and at a later time during the GAC service life.

iv. In the toluene-TCE column experiments, the extent of TCE-based cometabolism increased as the toluene to TCE influent concentration ratio increased. This concentration ratio was important because enough toluene had to be available for the production of enzymes through metabolism but not so much that enzyme competition occurred.

v. In contrast to the metabolism-based bioregeneration, the closer the radiolabeled TCE element was to the influent end (*i.e.*, the shorter the EBCT), near where the most enzyme activity was found, the more cometabolism-based bioregeneration was measured.

vi. Encouragement of biological activity in virgin toluene-TCE BAC columns led to decreased competition and demand for GAC adsorption sites, thereby increasing the GAC service life compared to adsorption-only columns.

vii. In batch experiments, the presence of iron significantly increased the TCE cometabolism rate but only slightly increased the toluene metabolism rate; thus iron served as an on-off switch for TCE cometabolism. In column experiments, however, iron fed in the influent precipitated and clogged the columns, thereby offsetting the benefit from cometabolism. Iron pre-loading in column experiments reduced the adsorption capacity of the GAC more than it increased the cometabolism rate. Iron-induced cometabolism, therefore, may be best utilized in a batch adsorption/biodegradation scenario.

viii. Overall, metabolism accounted for a much larger fraction of bioregeneration than cometabolism because of the relative difference in metabolism and cometabolism kinetics as well as the dependence of cometabolism on toluene (growth substrate) availability. The ^{14}C-toluene-based bioregeneration ranged from 26 - 53 % (for both equilibrated and virgin columns) whereas the ^{14}C-TCE-based bioregeneration ranged from 2.2 - 7.4 % (for equilibrated columns) in 11 - 20 days. Thus, the extent of TCE-based bioregeneration was much smaller than that for toluene.

Objective 2. Explore how relative chemical adsorbability and column penetration influence the extent of cometabolism.

i. Toluene, TCE, and PCE all had similar adsorption capacities as evidenced by Freundlich isotherm experiments. The IAST predicted competitive behavior between toluene and TCE well.

ii. The relative adsorbability of the two SOCs determined their mass transfer zone proximity within the GAC column. Cometabolism could only occur in the portion of the GAC column where both SOCs were present, because the presence of the biodegradable SOC was necessary to support microbial growth. Relative adsorbability determined the extent of the overlap between the two SOCs and, thus, was predicted to be an important indicator of the significance of cometabolism. Biological activity produced two opposing driving forces in the column experiments: TCE adsorption onto the regenerated GAC adsorption sites versus TCE

desorption into the biofilm and subsequent cometabolism. These opposing driving forces indicated that a situation where the SOC was not very adsorbable would allow for the most SOC cometabolism. TCE removal compared to a sterile column, however, was predicted to increase as both the EBCT and the TCE adsorbability increased. Cometabolism was predicted to account for only 11 to 48% of that removal, with the contribution increasing as the TCE adsorbability decreased. The rest of the TCE removal was due to metabolism-based bioregeneration of GAC adsorption sites containing toluene.

iii. The MDBA-predicted reduction in the toluene effluent concentration increased with increasing EBCT but was independent of the adsorbability of toluene. Instead, the MDBA model predicted toluene removal was dependent on both toluene concentration (by providing substrate for biofilm growth) and competition from TCE for adsorption sites (less of a driving force for toluene adsorption).

iv. The extent of SOC penetration into the GAC column prior to the onset of significant biodegradation was predicted to influence the extent of TCE removal. MDBA model runs showed encouragement of a rapid onset of biodegradation (by increasing the initial biomass concentration or the TCE k_1) decreased the liquid phase TCE effluent concentration. MDBA model predictions also showed that, as the EBCT increased or the toluene concentration increased, the TCE k_1 became more important in reducing the TCE effluent concentration.

Objective 3. Determine the significance of enzyme competition and intermediate toxicity in limiting the rate of cometabolism.

i. Little or no enzyme competition existed between toluene and TCE at the concentrations studied, as shown by both batch and column experiments. Furthermore, little or no intermediate toxicity existed at the TCE concentrations studied, as evidenced by the transformation capacities measured. These results show that for the chemicals studied, enzyme competition and intermediate toxicity do not need to be considered in the design and operation of BAC columns, unlike that found for other studies.

ii. The biomass-normalized enzyme activity (and thus the potential for cometabolism) was highest shortly beyond the influent region of the column because a constant supply of toluene was available for metabolism. Thus, it follows that the enzyme activity near the influent end of the column generally increased with the toluene concentration. Because little or no enzyme activity existed, as the toluene concentration increased, the potential for TCE cometabolism increased.

Objective 4. Determine the significance of adding Fenton's oxidation as a mechanism for increasing GAC service life.

i. Encouraging Fenton's oxidation in BAC columns increased the dissolved oxygen levels throughout the column, which was of great importance to successful operation of BAC columns. Attention to dissolved oxygen

levels was especially crucial at the onset of bioregeneration because a large amount of sorbed substrate very rapidly became available to the microorganisms.

ii. Fenton's oxidation was largely unsuccessful and did not have a net beneficial effect on TCE removal at the concentrations of H_2O_2 and iron tested. Fenton's oxidation was not found to increase the GAC service life in the virgin toluene-TCE column tested. Although Fenton's oxidation was not beneficial, some form of oxygenation, such as pure O_2 addition, may be essential.

iii. Any un-reacted hydrogen peroxide or hydroxyl radicals that reached the column inactivated or destroyed some of the biofilm, thus significantly reducing the enzyme activity near the influent compared to experiments without hydrogen peroxide.

Objective 5. Refine existing metabolism-based models of adsorption/biodegradation systems to account for cometabolism.

i. AdDesignS, an implementation of the PSDM, predicted adsorption of toluene and TCE well. Desorption of toluene and TCE, though, was overestimated.

ii. Manipulation of the MDBA model code was found to be unnecessary to account for cometabolism using the current SOCs and mixed culture. The lack of enzyme competition or significant intermediate toxicity meant that

TCE could be modeled as another biodegradable chemical with a yield of zero that was simultaneously biodegraded along with toluene.

iii. Good correlation was found between the MDBA model fits and the measured SOC effluent concentrations for the toluene-PCE experiment. The simulated and measured SOC loadings correlated as well. These results provide additional evidence that the MDBA model is a useful tool in improving our ability to predict the service life of BAC columns.

iv. In the case of the toluene-TCE experiments, a reasonable fit was found between the MDBA model fits and the measured SOC effluent concentrations and bioregeneration rate. It was necessary, however, to decrease the estimated TCE k_1 to attain this agreement. Less success was found with modeling the SOC loadings. This was demonstrated with both exhausted and virgin experiments.

v. The MDBA model proved numerically unstable when simulating full-scale, virgin GAC columns with long EBCTs or high biomass concentrations because the effluent SOC concentrations were near zero for long periods. Problems also occurred when simulating columns with very short EBCTs and low biomass concentrations such that the effluent SOC concentrations were near saturation for long periods. This instability was avoided by using relatively short EBCTs and moderate biomass concentrations; however this combination did not allow for differentiation between the predicted service lives of the sterile and biologically-active columns.

7.2 FUTURE RECOMMENDATIONS

Column Studies

In this research, only exhausted and virgin column experiments were studied. Depending upon the point in its service life, a GAC column contains three zones of varying length: exhausted GAC, partially exhausted GAC (the mass transfer zone (MTZ)), and virgin GAC. As time goes on, the constant length MTZ moves through the column at a constant velocity (assuming a constant influent concentration). Mass transfer zone column experiments should be performed to complement the existing virgin and pre-exhausted column experiments. Mass transfer zone column experiments would demonstrate the effect of biological activity on the length and velocity of the MTZ. In addition, BAC column experiments should be run with more than two SOCs or with background natural organic matter. The MDBA model should be tested for its ability to predict metabolism and cometabolism in such mixtures.

In a batch experiments, the presence of iron significantly increased the TCE cometabolism rate. In column experiments, however, iron fed in the influent precipitated and clogged the columns, thereby offsetting the benefit from cometabolism. Iron pre-loading in column experiments reduced the adsorption capacity of the GAC more than it increased the cometabolism rate. In order to benefit fully from cometabolism in BAC columns, alternative iron-introduction schemes should be investigated. A *very* low iron concentration in the influent should be used to avoid clogging. Perhaps a real groundwater sample with natural levels of iron and other metals present could be studied. These iron species may

be complexed with natural organic matter and thus be less likely to precipitate. Alternatively, GAC manufactured with iron already pre-loaded should be purchased to study the adsorption capacity of the manufactured iron pre-loaded GAC compared to that of the GAC pre-loaded under laboratory conditions.

For this research, two mixed cultures were maintained: one with iron and one without iron. The cultures were maintained in this manner for a long period of time (three years). The effects of long-term iron deprivation and long term exposure to high iron concentrations on the mixed culture should be studied. The iron-free and iron-containing cultures should be analyzed over time to see if morphological or population changes are induced.

Model Improvement

The MDBA model proved numerically unstable when simulating full-scale, virgin GAC columns with long EBCTs or high biomass concentrations because the effluent SOC concentrations were near zero for long periods. Problems also occurred when simulating columns with very short EBCTs and low biomass concentrations such that the effluent SOC concentrations were near saturation for long periods. Issues of numerical stability have been addressed in the adsorption only models (*i.e.*, AdDesignS) by breaking the GAC column up into a set of columns in series. Each column is then simulated sequentially. With this columns-in-series approach, the system of differential equations to be solved is less stiff and, therefore, more stable numerically. Although more complicated to implement with the MDBA model, a conversion to columns-in-series

nevertheless should be attempted to address the numerical stability problems observed in this research. In addition, the MDBA model only considers surface diffusion currently; however, the model would be more generally approachable if it also included pore diffusion as a transport mechanism within the GAC particle.

Appendix A – Bioregeneration Analysis Method

The bioregeneration calculation method presented here is from Speitel (1985), Speitel and DiGiano (1987), and Lu (1989). Radiochemical samples from BAC columns treating volatile organics contained radioactive substrate, carbon dioxide, biomass, and non-purgable products (NPPs, or reaction intermediates). In order to measure each one of these components, four effluent samples were taken: total, acid, base, and biomass (see Section 3.1.3). The "base" sample is a 5-mL sample that has been. The four radiochemical components of the BAC column effluent were therefore calculated as follows:

Substrate = total – base
CO_2 = base – acid
Biomass = biomass
NPP = acid - biomass

The radioactivity in the samples was measured by a liquid scintillation counter (Beckman LS 5000TD) in disintegrations per minute (dpm). After radiochemical samples had been taken over time for a BAC column, radioactivity concentrations (dpm/mL) were converted to mass rates (dpm/min) by incorporating the flow rate (mL/min) through the column at each sample time. The production rates of substrate, CO_2, and biomass are referred to as SE, CO, and BE, respectively, in subsequent calculations. Besides the radioactivity data, six other pieces of information are needed for the calculations:

SA = specific activity (dpm/μg) which is the total initial radioactivity divided by the total initial mass of substrate sorbed onto the radiolabeled GAC element.

Y = yield coefficient for the microorganisms (µg carbon from the biomass produced/µg carbon in the substrate biodegraded)

b = endogenous decay coefficient (1/min.)

K_c = fraction of CO_2 produced from endogenous decay (µg carbon from CO_2 produced/µg carbon from cells decayed)

IP = total initial mass of substrate sorbed onto the radiolabeled GAC element (µg)

MW = molecular weight of the substrate (g/mole)

Bioregeneration was calculated both with and without consideration of endogenous decay, which may or may not significantly affect the bioregeneration calculations. Without consideration of endogenous decay, the three main outputs from the bioregeneration calculations are the bioregeneration rate (µg/min, JIP), the extent of bioregeneration (µg, MI), and extent of bioregeneration compared to the initial substrate mass sorbed onto the GAC (dimensionless, BR). The calculations are as follows:

$$JIP(i) = \frac{CO(i)}{(1-Y)\,SA}$$

$$MI(i) = \int JIP(i) = MI_{(i-1)} + \frac{1}{2}\,(JIP_{(i)} + JIP_{(i-1)})\,(Time_{(i)} - Time_{(i-1)})$$

$$\mathrm{BR(i)} = \frac{\mathrm{MI(i)}}{\mathrm{IP}}$$

where MI (0) is zero and time is in minutes. In the case of bioregeneration calculations including endogenous decay, the equations change slightly to include the CO_2 produced from cell decay. To derive these equations, a mass balance was done on the biomass in the system:

$$JIP(i) = \frac{CO(i) - K_c * b * BM(i)}{(1 - Y)\, SA}$$

where JIP(i) in this case is in dpm/min instead of µg/min and BM(i) is the mass of radioactive biomass in the BAC column (dpm). BM(i) varied with time depending on the amount of growth from substrate degradation, the amount of endogenous decay, and the amount of detachment from fluid shear, as follows:

$$BM(i) = BM_{(i-1)} + \frac{1}{2}\left(Time_{(i)} - Time_{(i-1)}\right)\left[Y\left(JIP_{(i)} + JIP_{(i-1)}\right) - b\left(BM_{(i)} + BM_{(i-1)}\right) - \left(BE_{(i)} + BE_{(i-1)}\right)\right]$$

where JIP(0), BM(0) and BE(0) are equal to zero. BM(i) and JIP(i) can be solved for by combining the previous two equations to get:

$$JIP(i) = \frac{CO_{(i)}}{C2} - \frac{C1}{C2}\left[\left(C3 * BM_{(i-1)}\right) - \left(BE_{(i)} + BE_{(i-1)}\right) + \left(Y * JIP_{(i-1)}\right)\right]$$

where C1, C2, and C3 are constants:

$$C1 = \frac{K_c * b * \left(Time_{(i)} - Time_{(i-1)}\right)}{2 + b * \left(Time_{(i)} - Time_{(i-1)}\right)}$$

$$C2 = (1 - Y) + (Y * C1)$$

$$C3 = \frac{2}{Time_{(i)} - Time_{(i-1)}} - b$$

Using these constants and known variables, JIP(i) and BM(i) were calculated. The equations for MI(i) and BR(i) are the same as in the case of ignoring endogenous decay. Some extra calculations were done when considering endogenous decay. BF(i) is the cumulative biomass production (dpm) in the column if endogenous decay and detachment is ignored:

$$BF(i) = MI(i) * Y * SA$$

SBE(i) is the cumulative amount of biomass washed out of the column (dpm):

$$SBE(i) = SBE_{(i-1)} + \frac{1}{2}\left(BE_{(i)} + BE_{(i-1)}\right)\left(Time_{(i)} - Time_{(i-1)}\right)$$

where SBE(0) was equal to zero. FWO(i) is the ratio of biomass formation to biomass washout (dimensionless):

$$FWO(i) = \frac{SBE(i)}{BF(i)}$$

SSF(i) is the cumulative amount of initially sorbed substrate that desorbs but is not degraded and ends up in the column effluent (dpm):

$$\mathrm{SSF(i)} = \mathrm{SSF_{(i\text{-}1)}} + \frac{1}{2 * \mathrm{SA} * \mathrm{IP}}\left(SE_{(i)} + SE_{(i-1)}\right)\left(Time_{(i)} - Time_{(i-1)}\right)$$

Addition of SSF(i) and BR(i) allowed the determination of the total amount of initially sorbed substrate that desorbed off the GAC.

Appendix B – Additional Analytical Methods

Table B.1 Sequential Methanol Extraction Data, Toluene and PCE

	Units	Replicate								Avg.
		A	B	C	D	E	F	G	H	
q_{e1} from Mass Balance: Toluene	mg/g	75.8	75.8	75.2	75.2	4.1	74.1	74.1	74.1	
PCE		117	117	117	117	116	116	116	116	
1st Extraction: Tol Conc.	mg/L	505	434	741	661	780	982	1092	878	
PCE Conc.		1357	1193	1373	1248	1621	2032	2233	1788	
% of Total Mass Desorbed in 1st Extract: Toluene	%	80.4	79.2	79.0	80.4	79.3	76.2	75.3	77.4	**78.4**
PCE		87.8	86.9	84.5	85.8	85.7	82.8	81.6	84.0	**84.9**
2nd Extraction: Tol Conc.	mg/L	77	74	135	112	135	199	231	166	
PCE Conc.		143	141	203	168	212	329	393	268	
% of Total Mass Desorbed in 2nd Extract: Toluene	%	62.6	65.0	68.6	69.4	66.3	64.9	64.6	64.9	65.8
PCE		75.9	78.4	80.4	81.3	78.5	78.1	78.3	78.7	78.7
3rd Extraction: Tol Conc.	mg/L	25	23	36	29	37	56	65	46	
PCE Conc.		31	28	35	29	36	58	70	45	
% of Total Mass Desorbed in 3rd Extract: Toluene	%	55.1	56.9	58.6	59.3	53.3	52.4	51.5	51.4	54.8
PCE		67.7	71.7	71.5	74.9	62.1	63.1	64.3	61.6	67.1
4th Extraction: Tol Conc.	mg/L	11	9.1	14	11	18	27	31	23	
PCE Conc.		10	7.2	10	6.5	16	23	26	20	
% of Total Mass Desorbed in 4th Extract: Toluene	%	52.6	52.8	56.2	55.3	56.5	52.1	50.0	52.4	53.5
PCE		69.2	65.6	73.9	66.7	72.9	67.1	66.5	70.7	69.1
5th Extraction: Tol Conc.	mg/L	6.1	5.0	7.0	5.6	8.6	16	18	14	
PCE Conc.		2.9	2.7	2.3	2.3	4.0	7.4	8.8	5.3	
% of Total	%	62.0	62.3	62.2	61.7	61.5	64.4	58.5	64.9	62.2

Mass Desorbed in 5th Extract: Toluene										
PCE		64.3	70.5	63.5	71.5	66.6	66.4	67.5	65.5	67.0
6th Extraction: Tol Conc.	mg/L	3.7	3.1	4.3	3.5	5.4	8.7	13	7.3	
PCE Conc.		1.6	1.1	1.3	0.9	2.0	3.8	4.2	2.8	
GAC Mass in Bottle	g	0.20	0.18	0.21	0.18	0.23	0.34	0.31	0.27	
q_{e2} from Methanol Extraction, Toluene	mg/g	63.8	61.5	91.1	93.7	85.8	76.4	94.0	84.3	
PCE		157	154	158	166	165	145	177	158	
q_{e2}/q_{e1}, Toluene	-	0.84	0.81	1.21	1.25	1.16	1.03	1.27	1.14	**1.09**
q_{e2}/q_{e1}, PCE		1.34	1.31	1.35	1.41	1.43	1.26	1.53	1.37	**1.37**

Table B.2 Sequential Methanol Extraction Data, Toluene and TCE

	Units	Bottle A	Bottle B	Avg.
q_{e1} from Mass Balance: Toluene	mg/g	27.8	27.8	
TCE		54.3	54.3	
1st Extraction: Toluene Conc.	mg/L	263	293	
TCE Conc.		112	123	
% of Mass Desorbed in 1st Extraction: Toluene	%	80.1	78.8	**79.5**
TCE		96.6	96.3	**96.4**
2nd Extraction: Toluene Conc.	mg/L	42	50	
TCE Conc.		3.3	3.9	
% of Mass Desorbed in 2nd Extraction: Toluene	%	64.6	63.6	64.1
TCE		81.9	82.4	82.2
3rd Extraction: Toluene Conc.	mg/L	13	16	
TCE Conc.		0.39	0.35	
% of Mass Desorbed in 3rd Extraction: Toluene	%	55.1	55.0	55.0
TCE		53.8	42.0	47.9
4th Extraction: Toluene Conc.	mg/L	5.1	6.5	
TCE Conc.		0.0	0.0	
% of Mass Desorbed in 4th Extraction: Toluene	%	49.4	50.1	49.7
TCE		0.0	0.0	0.0
5th Extraction: Toluene Conc.	mg/L	2.6	3.2	
TCE Conc.		0.0	0.14	
% of Mass Desorbed in 5th Extraction: Toluene	%	50.3	50.1	50.2
TCE		0.0	29.6	14.8
6th Extraction: Toluene Conc.	mg/L	1.6	1.9	
TCE Conc.		0.16	0.16	
% of Mass Desorbed in 6th Extraction: Toluene	%	59.9	59.5	59.7
TCE		49.4	47.8	48.6
7th Extraction: Toluene Conc.	mg/L	1.0	1.3	
TCE Conc.		0.17	0.18	
GAC Mass in Bottle	g	0.103	0.116	
q_{e2} from Methanol Extraction: Toluene	mg/g	63.6	64.3	
TCE		22.5	22.1	
q_{e2}/q_{e1}, Toluene	-	2.29	2.31	**2.30**
q_{e2}/q_{e1}, TCE		0.41	0.41	**0.41**

Table B.3 Extraction Correction Factor Summary

Chemical	Efficiency Factor[1]	Mass Balance Factor[2]	Correction Factor[3]
Toluene, Trial 1	0.784	1.09	0.853
Toluene, Trial 2	0.795	2.30*	0.795
PCE	0.849	1.37	1.167
TCE	0.964	0.41*	0.964

[1]The fraction of the total mass of SOC desorbed during the 1st extraction
[2]The SOC loading determined via mass balance divided by the SOC loading determined via methanol extraction
[3]Actual factor applied to measured SOC loadings; = Efficiency Factor * Mass Balance Factor
*Uncharacteristically far from one, thus an error in measurement was suspected and values of 1 were used instead.
Note: Trial 1 Toluene Correction Factor was used in BAC Column Experiments 1 & 2; Trial 2 Toluene Correction Factor was used in BAC Column Experiments 3 through 10.

Table B.4 Headspace Analyzer User Program

Platen temperature	80°C
Sample equilibration time	15 min.
Vial size	22 mL
Mechanical mixing time	5 min.
Mixing power	7
Stabilizer time	0.10 min.
Vial pressurization time	1 min
Vial pressure equilibration time	0.25 min.
Sample loop fill time	1 min.
Sample loop equilibration time	0.25 min.
Sample injection time	1 min.
Sample loop temperature	170°C
Transfer line temperature	170°C
Vial pressurization	15 psi
Transfer line back pressure	12 psi

Table B.5 GC Peak Times

Chemical	FID, Toluene/PCE	FID, Toluene/TCE	ECD, PCE	ECD, TCE
Toluene	3.99 ± 0.12	6.26 ± 0.31		
PCE	4.33 ± 0.07		5.66 ± 0.02	
Benzene	2.81 ± 0.14	3.92 ± 0.20		
TCE		4.81 ± 0.20		4.19 ± 0.04
Bromoform			7.79 ± 0.01	11.02 ± 0.07

Table B.6 Standard Curve Preparation

Concentration (µg/L)	Volume of DDI (mL)	Vol. of 0.2 g/L Stock (µL)	Vol. of 1 g/L Stock (µL)	Vol. of 10 g/L Stock (µL)
0	50	0		
4.8	50	1.2		
10	50	2.5		
24.8	50	6.2		
68	50	17		
68	50		3.4	
100	50		5	
200	50		10	
500	50		25	
700	50		35	
700	50			3.5
1000	50			5

Table B.7 GC-FID Standard Curve Example, Toluene and PCE

Conc. (µg/L)	Benzene Peak Area	PCE Peak Area	Toluene Peak Area	PCE:Benz. Area Ratio	Toluene:Benz. Area Ratio
0	1322309	0	0	0.0000	0.0000
4.8	1379079	8606	7176	0.0062	0.0052
10	1425792	9742	12161	0.0068	0.0085
24.8	1421297	16340	33877	0.0115	0.0238
68	1457531	28781	84890	0.0197	0.0582
68	1439424	29887	87849	0.0208	0.0610
100	1450519	38830	130577	0.0268	0.0900
200	1454383	65928	247746	0.0453	0.1703
500	1474446	134644	554277	0.0913	0.3759
700	1467048	188224	821069	0.1283	0.5597
700	1479948	190552	844504	0.1288	0.5706
1000	1474193	304673	1234684	0.2067	0.8375

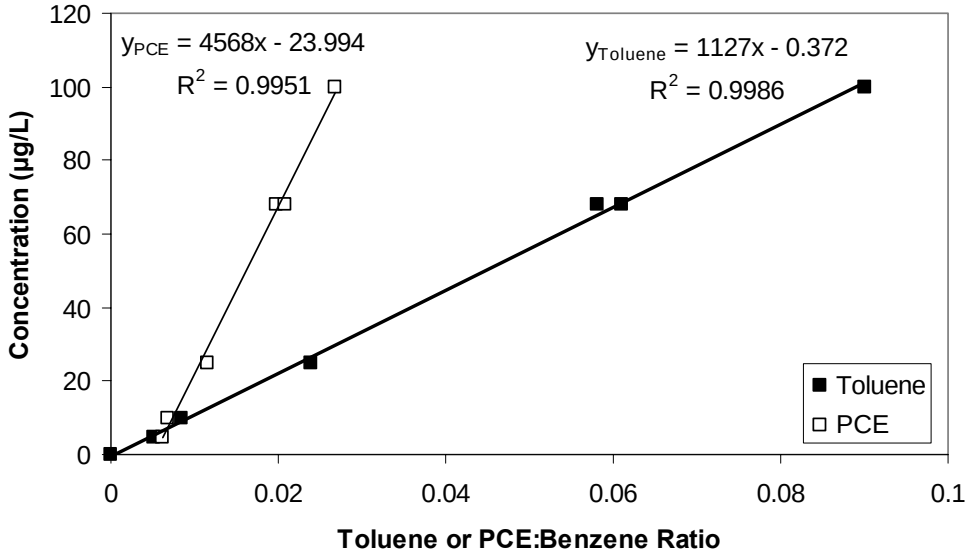

Figure B.1 0 – 100 µg/L Standard Curve Example, Toluene and PCE

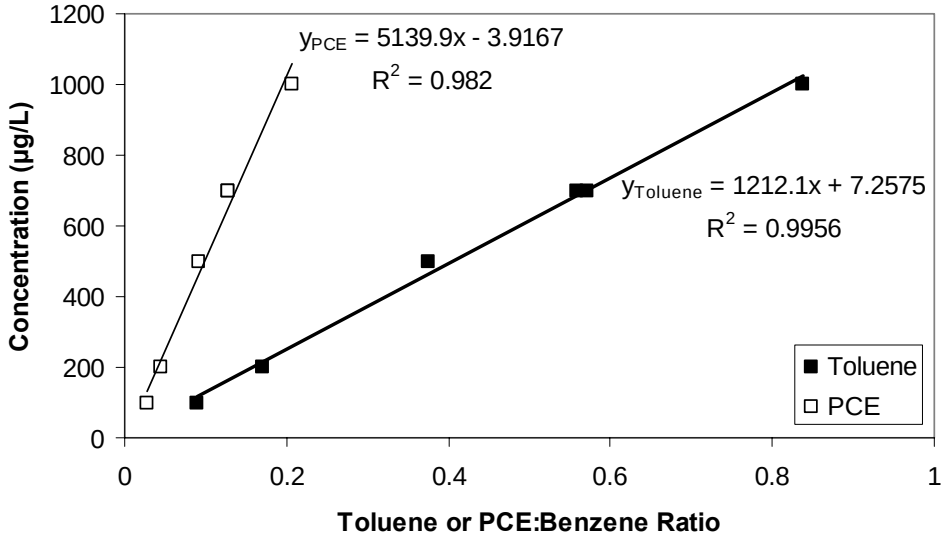

Figure B.2 100 – 1000 µg/L Standard Curve Example, Toluene and PCE

Table B.8 GC-FID Standard Curve Example, Toluene and TCE

Conc. (µg/L)	Benzene Peak Area	TCE Peak Area	Toluene Peak Area	TCE:Benz. Area Ratio	Toluene:Benz. Area Ratio
0	1938146	0	0	0.0000	0.0000
4.8	1938146	1558	9236	0.0008	0.0048
10	1922858	3703	17484	0.0019	0.0091
24.8	1856459	9545	41379	0.0051	0.0223
68	1952400	29745	123980	0.0152	0.0635
68	1871117	25516	110958	0.0136	0.0593
100	1968915	45409	184103	0.0231	0.0935
200	1867698	78486	318737	0.0420	0.1707
500	1888377	222505	868042	0.1178	0.4597
700	1860524	310946	1221390	0.1671	0.6565
700	1955540	342820	1320728	0.1753	0.6754
1000	1965956	458630	1812994	0.2333	0.9222

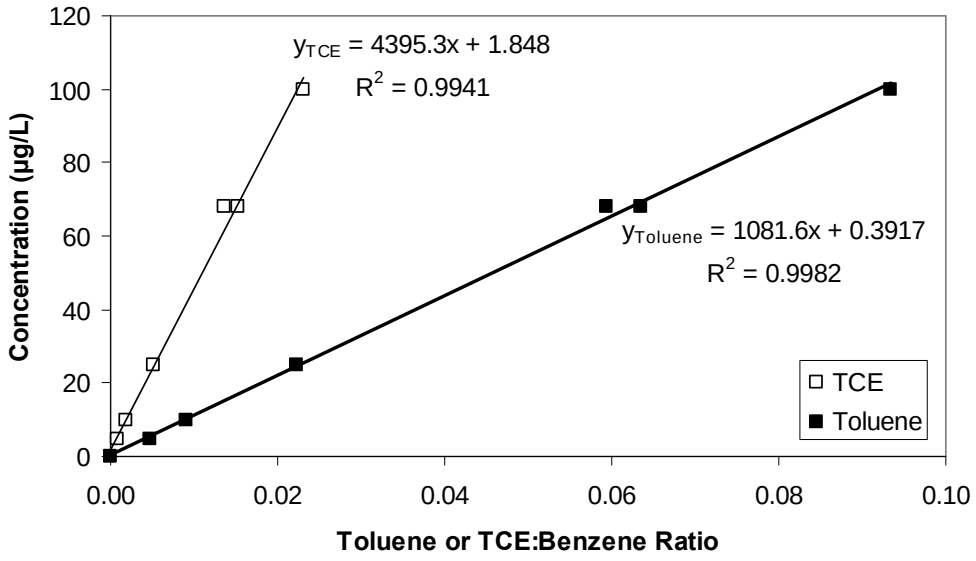

Figure B.3 0 – 100 µg/L Standard Curve Example, Toluene and TCE

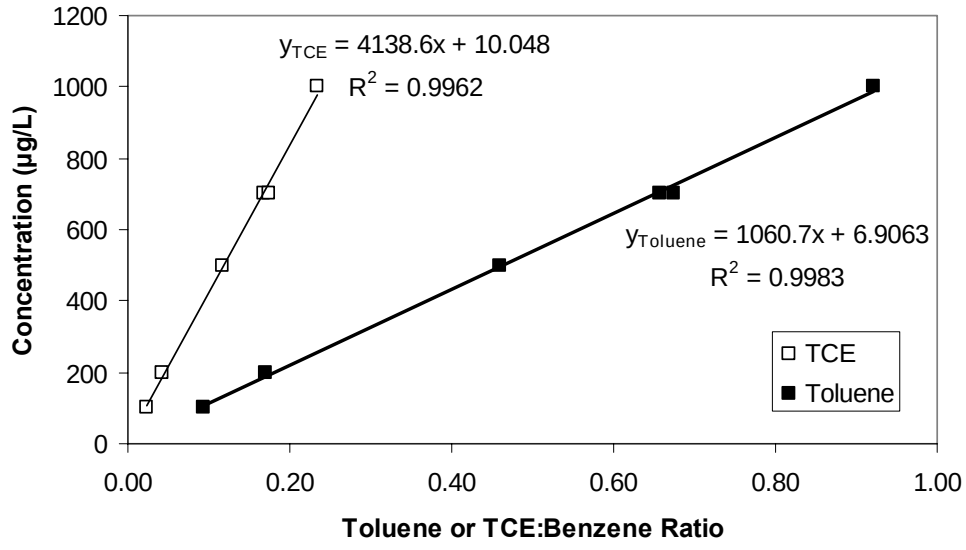

Figure B.4 100 – 1000 µg/L Standard Curve Example, Toluene and TCE

Table B.9 GC-ECD Standard Curve Example, PCE

	Peak Areas 1	Peak Areas 2	Peak Areas 3	PCE:Bromoform Ratio	Conc. (µg/L)
Bromoform	5684830	6031130	5764080	0.000	0
PCE					
Bromoform	6041484	6097284	6120514	0.080	4.8
PCE	8601	9703	8637		
Bromoform	6275531	6321631	6420111	0.178	10
PCE	11722	14289	11532		
Bromoform	6347783	6248213	6325753	0.486	24.8
PCE	08077	04493	07089		
Bromoform	6256868	6200008	6136688	1.387	68
PCE	61575	53335	62920		
Bromoform	6426321	6399055	6355458	1.796	100
PCE	147747	153478	142868		
Bromoform	6735842	6615902	6391772	3.535	200
PCE	361799	335678	280211		
Bromoform	7407685	7384933	7494755	7.321	500
PCE	417088	411000	488743		
Bromoform	7828637	7753437	7757255	9.248	700
PCE	230258	180011	173608		
Bromoform	8354629	8445029	8427669	11.477	1000
PCE	643007	657280	652788		

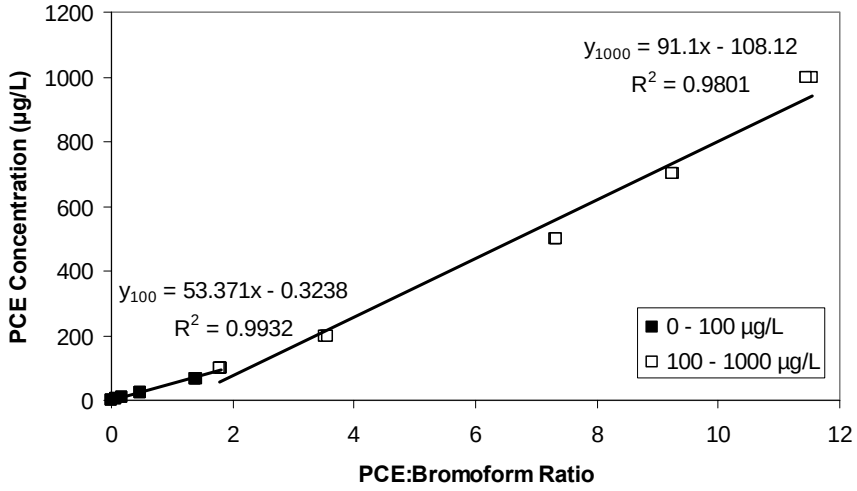

Figure B.5 Standard Curve Example, PCE

Table B.10 GC-ECD Standard Curve Example, TCE

	Peak Areas 1	Peak Areas 2	Peak Areas 3	TCE:Bromoform Ratio	Conc. (µg/L)
Bromoform	376807	388408	379285	0.0000	0
TCE	0	0	0		
Bromoform	392282	418505	414656	0.0457	4.8
TCE	18340	18634	18946		
Bromoform	399851	404658	408530	0.0740	10
TCE	29373	29957	30494		
Bromoform	408175	480212	402541	0.1658	24.8
TCE	68643	79408	65947		
Bromoform	426474	474832	401069	0.4491	68
TCE	194063	209820	180605		
Bromoform	417177	411309	417762	0.4253	68
TCE	178296	174784	176932		
Bromoform	432300	435334	427496	0.6089	100
TCE	263230	265322	260065		
Bromoform	425432	424824	426659	1.1194	200
TCE	477448	475136	476814		
Bromoform	435330	455549	442731	2.4252	500
TCE	1053601	1106103	1074634		
Bromoform	445255	446880	432891	3.1035	700
TCE	1376841	1387955	1347340		
Bromoform	430838	423533	407103	3.3067	700
TCE	1416518	1400227	1354074		
Bromoform	411489	408647	481436	4.3233	1000
TCE	1801851	1773742	2046348		

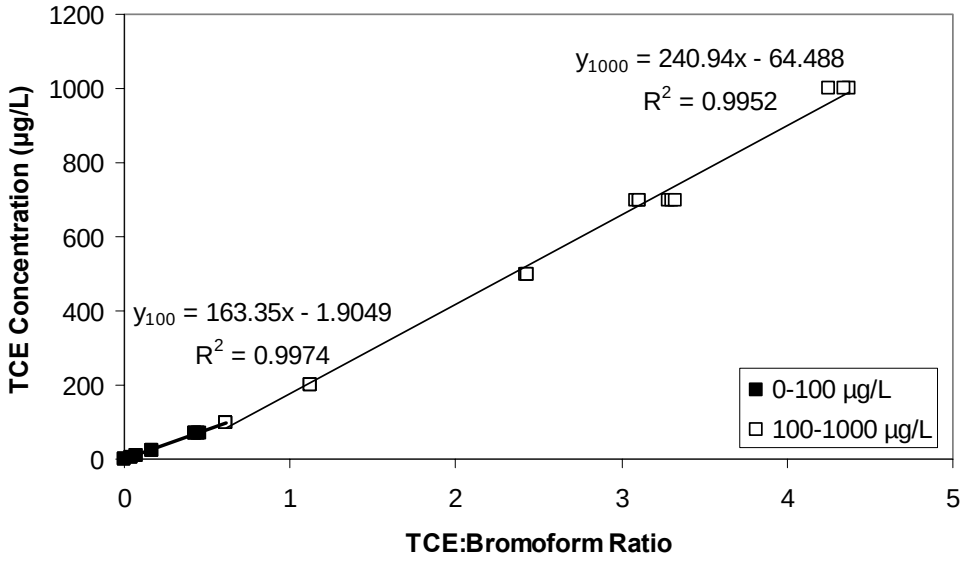

Figure B.6 Standard Curve Example, TCE

Table B.11 Liquid Scintillation Counter User Program

Preset Time: maximum amount of time that one sample is counted	30.00 min.
H#: the number of times H# determination is performed per sample	3
Sample Channels Ratio (SCR): a method of monitoring quench	N
Sample Repeat	1
Automatic Quench Compensation (AQC): with AQC, the channel lower and upper limits are automatically adjusted by an amount determined by the H# to correct for instrument counts affected by the sample quench	Y
Program Summary	Y
Cycle Repeat	1
Quench Compensation Factor (QCF): used when the samples all have the same level of quench	N
Low Sample Reject (LSR) Time: the count time used for testing for low activity, defined as samples counts per minute below the Channel LSR	0.10 min
LSR Interval (INT): interval between samples for low activity	999.95 min.

RS-232 Output: turns on or off the sending of results to an external computer	N
Random Coincidence Monitor (RCM): distinguishes between true radiation and other light-producing phenomenon such as photo-, chemi- or bioluminescence	Y
RCM Time: the count time used for calculating a % RCM	0.10 min.
RCM INT: interval between samples for RCM	999.95 min.
Count Channel: designates how many of the available channels to use	1
Channel Lower Limit	0
Channel Upper Limit	670
Channel 2 Sigma: statistical error to which a sample is measured as long as time is less than Preset Time	0.5
Channel Background Subtract	0
Channel Background 2 Sigma	0
Channel LSR: the net counts per minute minimum to avoid sample rejection	0
Data Calculation Program, Single Label Disintegrations per minute (dpm)	5
Print Format	1

Table B.12 ^{14}C-Toluene Radioactive Background Tests, Toluene/PCE Experiments

Experiment 1		
Sample Description	Net Radioactive Count (dpm)	% of 0-hr. Sample
1, pH of ~6.7, 0 hrs	Vial not measured correctly	
1.5 hrs	Not measured	
4.0 hrs	22152	100.0
12 hrs	21965	99.2
18 hrs	22197	100.2
24 hrs	21999	99.3
2. pH of 11, 0 hrs	32524	100.0
1.5 hrs	33192	102.1
4.0 hrs	32804	100.9
12 hrs	32573	100.2
18 hrs	32676	100.5
24 hrs	32555	100.1
Correction Factor: Little chemiluminescence seen, so stored samples for 24 hrs before running on scintillation counter.		
Experiment 2		
Sample Description	Net Radioactive Count (dpm)	% of Sample 1
1, 5-mL sample	54855	100
2, unrinsed filter	10309	18.8
3, ethanol rinsed filter	999.2	1.8
Correction Factor: 0.018 for “filter” samples		

Experiment 3				
Sample Description	Net $^{14}CO_2$ Count (dpm)	% of Sample 1	Net ^{14}C-Toluene Count (dpm)	% of Sample 1
1, 5-mL sample	2779*	100	60080	100
2, pH 1.54	3.3	0.1	2248	3.7
pH 1.7	2.5	0.1	2374	4.0
pH 1.9	1.8	0.1	2280	3.8
pH 2.17	4.6	0.2	2411	4.0
pH 6.65	1086	39	6250	10
3, pH 10.67	2908	105	2558	4.3
pH 11	3290	118	2715	4.5
pH 11.11	3086	111	2322	3.9
pH 11.2	3135	113	2715	4.5
pH 11.26	2974	107	2995	5.0
*Some sample spilled out of vial			Average:	4.8
Correction Factor: 0.048 for both “acid” and “base” samples				

Table B.13 ^{14}C-Toluene Radioactive Background Tests, Toluene/TCE Experiments

Experiment 1		
Sample Description	Net Radioactive Count (dpm)	% of Sample 1
1, pH of ~6.7, 0.5 hr	1057325	100.00
2. pH of ~11, 0.5 hr	1060024	100.26
Correction Factor: No significant chemiluminescence seen		
Experiment 2		
Sample Description	Net Radioactive Count (dpm)	% of Sample 1
1, 5-mL sample	985114	100.0
2, unrinsed filter	108947	11.1
3, ethanol rinsed filter	6186	0.63
Correction Factor: 0.0063 for “filter” samples		
Experiment 3		
Sample Description	Net ^{14}C-Toluene Count (dpm)	% of Sample 1
1, 5-mL sample	985114	100.0
2, pH 1.5	25013	2.54
3, pH 10.5	30273	3.07
Correction Factor: 0.0254 for “acid” samples; 0.0307 for “base” samples		

Table B.14 ^{14}C-TCE Radioactive Background Tests

Experiment 1		
Sample Description	Net Radioactive Count (dpm)	% of Sample 1
1, pH of ~6.7, 0.5 hr	89977	100.0
2. pH of ~11, 0.5 hr	91870	102.1
Correction Factor: Little chemiluminescence seen, so stored samples for 24 hrs before running on scintillation counter.		
Experiment 2		
Sample Description	Net Radioactive Count (dpm)	% of Sample 1
1, 5-mL sample	89977	100
2, unrinsed filter	8366	9.3
3, ethanol rinsed filter	341	0.38
Correction Factor: 0.0038 for “filter” samples		
Experiment 3		
Sample Description	Net ^{14}C-Toluene Count (dpm)	% of Sample 1
1, 5-mL sample	89977	100
2, pH 1.5	30000	33.3
3, pH 10.5	30638	34.0
Correction Factor: 0.333 for “acid” samples; 0.340 for “base” samples		

Table B.15 Phenanthroline Iron Standard Data Example

Iron Concentration (mg/L)	Absorbance (-)
0	0.0051
0.5	0.1051
1.0	0.2041
5.0	0.9548

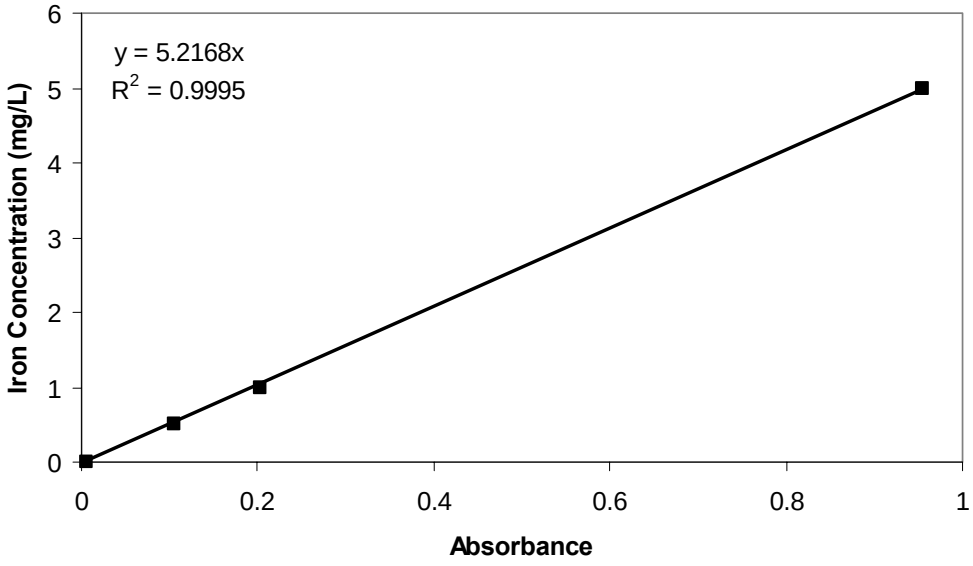

Figure B.7 Phenanthroline Iron Standard Curve Example

Table B.16 OD_{600}/TSS/VSS Standard Data

OD_{600} (-)	Sample Volume (mL)	Initial Filter (g)	100°C Filter (g)	550°C Filter (g)	TSS (mg/L)	VSS (mg/L)
0.0050	50	1.0804	1.0806	1.0803	4.2	5.8
0.0577	100	1.0753	1.0770	1.0762	17.2	8.2
0.1392	90	1.0962	1.0995	1.0979	36.8	17.0
0.1879	70	1.0804	1.0847	1.0828	60.7	26.7
0.3889	45	1.0843	1.0911	1.0879	152.0	70.9

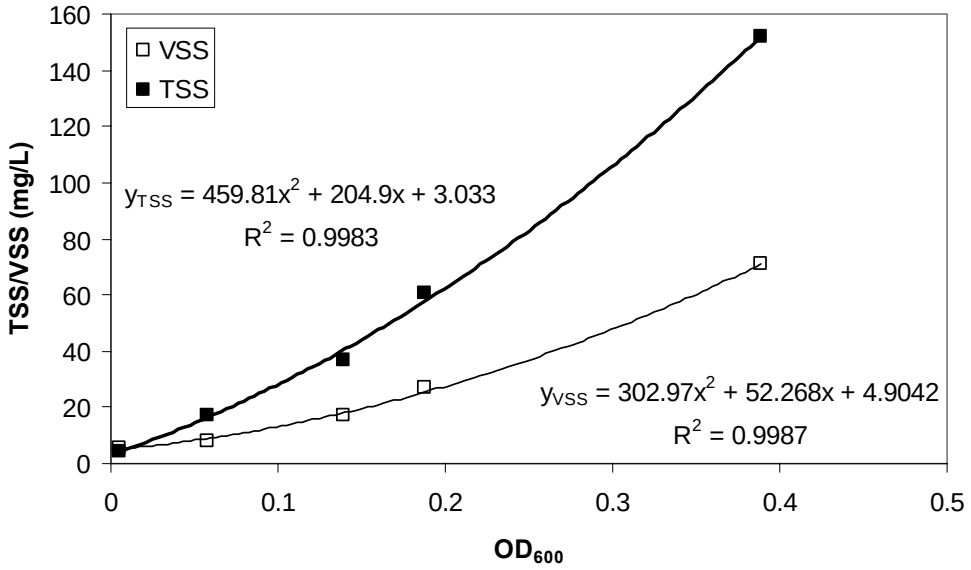

Figure B.8 OD_{600}/TSS/VSS Standard Curve

Table B.17 Protein Standard Data Example

Protein Concentration (mg/L)	Protein Stock Volume (µL)	3 M NaOH Volume (mL)	Absorbance (-)
0	0	0.20	0.0000
0	0	0.20	0.0000
0	0	0.20	0.0000
25	50	3.95	0.0274
25	50	3.95	0.0273
25	50	3.95	0.0256
50	100	3.90	0.0595
50	100	3.90	0.0562
125	100	1.50	0.1370
125	100	1.50	0.1350
125	100	1.50	0.1410
250	200	1.40	0.2781
250	200	1.40	0.2820
250	200	1.40	0.2792

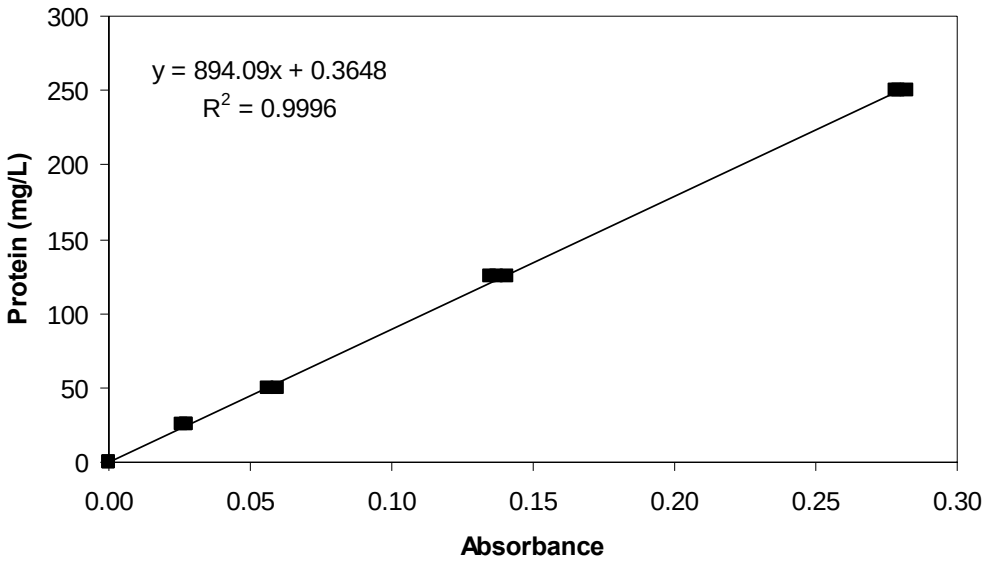

Figure B.9 Protein Standard Curve Example

Table B.18 NADH Standard Data Example

NADH Concentration	Absorbance			Average Absorbance
	1	2	3	
(µM)	(-)	(-)	(-)	(-)
0	0	0.2	0	0.1
0.43	9.2	9.4	9.3	9.3
1.08	17.6	17.6	17.6	17.6
5.42	70.9	70.7	70.3	70.6
10.84	131.5	131.3	131.4	131.4
54.18	621.7	620.6	620.9	621.1

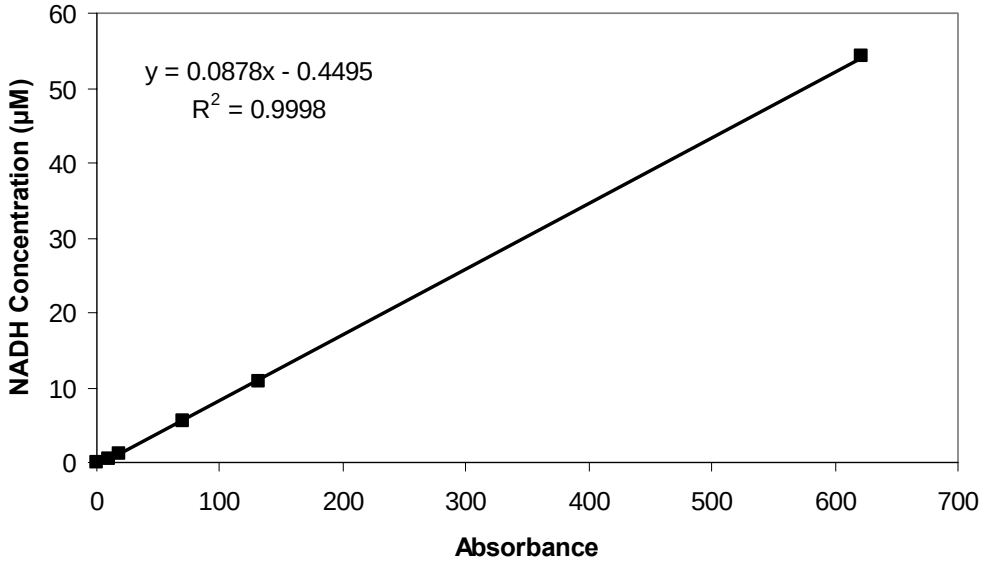

Figure B.10 NADH Standard Curve Example

Table B.19 Enzyme Activity Analysis Example

Influent End of Column		Middle of Column		Effluent End of Column	
Time (min.)	Abs. (-)	Time (min.)	Abs. (-)	Time (min.)	Abs. (-)
1.87	154.5	1.87	8.3	2.25	10.4
3.65	305.8	5.17	28.0	6.17	28.5
5.48	463.0	8.23	50.4	10.50	16.3
7.37	622.9	12.00	64.1	16.50	31.4
9.10	773.5			20.08	24.9

Table B.20 Enzyme Activity Slope Example

GAC Column Location	Slope (AU/min-g GAC)	TSS Normalized Slope (AU-L/min.-mg cells)	Protein Normalized Slope (AU-L/min.-mg protein)	r^2 (-)
Influent	220.2	0.337	4.459	1.00
Middle	14.6	0.081	0.350	0.98
Effluent	2.9	0.035	0.154	0.35

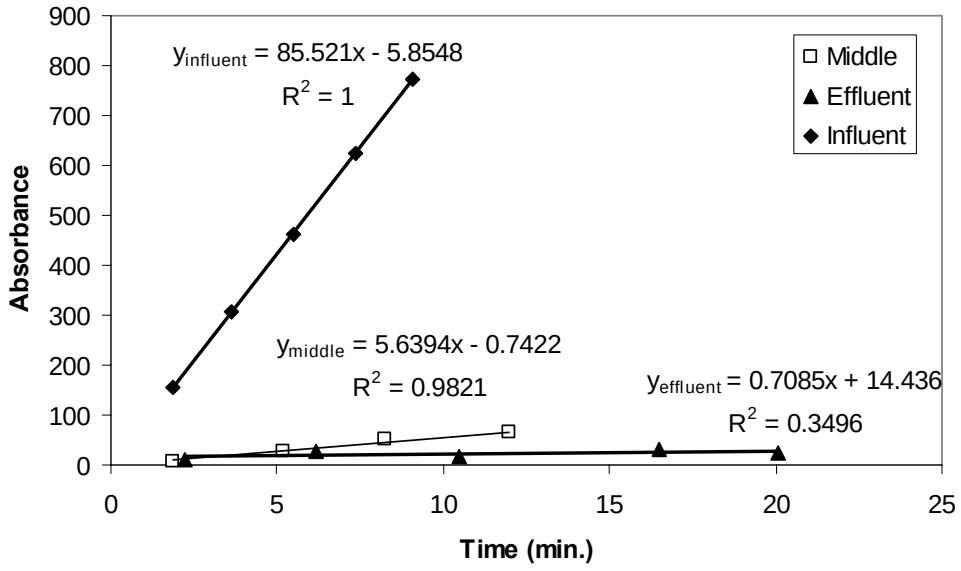

Figure B.11 Enzyme Activity Curve Example

Appendix C - Raw Batch Kinetic Data

Table C.1 Data for Toluene Monod Kinetic Parameter Determination with and without Iron Present

Toluene without iron present				Toluene with iron present			
Data Set	Time (min.)	Tol. Conc. (mg/L)	X (VSS, mg/L)	Data Set	Time (min.)	Tol. Conc. (mg/L)	X (VSS, mg/L)
1	0	0.835*	29.10	1	0	1.451*	34.73
	3.7	0.826			1.5	1.400	
	40.0	0.654			4.0	1.325	
	57.0	0.474			16.5	0.791	
	73.5	0.452			34.9	0.247	
	91.5	0.370			48.9	0.054	
	124.0	0.204			62.6	0.003	
	150.0	0.000			92.0	0.000	
2	0	0.549	27.63	2	0	0.751*	29.50
	34.5	0.442			1.7	0.687	
	66.0	0.424			4.4	0.640	
	97.0	0.311			20.7	0.324	
	143.5	0.193			36.8	0.047	
	191.0	0.088			70.4	0.000	
3	0	0.0430	13.07	3	0	0.105*	29.80
	32.4	0.0237			1.5	0.095	
	71.0	0.0107			3.7	0.082	
	101.3	0.0057			14.1	0.012	
	145.8	0.0042			25.0	0.000	
	176.5	0.0048			55.7	0.000	
4	0	0.322*	11.92	4	0	0.748	46.38
	14.3	0.274			13.7	0.331	
	39.0	0.245			24.8	0.018	
	66.0	0.186			47.5	0.000	
	124.6	0.103		5	0	0.245	50.31
	159.7	0.068			12.9	0.060	
	199.9	0.048			22.1	0.003	
	253.9	0.036			44.7	0.0002	
5	0	1.100*	90.30		77.0	0.0002	
	6.2	0.935		6	0.0	1.272	28.26
	41.9	0.052			11.3	0.890	
	80.4	0.055			23.5	0.591	
	165.0	0.015			34.8	0.363	
6	0	1.400*	97.20		48.1	0.155	
	5.3	1.312			61.1	0.032	
	22.2	0.954		7	0	0.107	37.40
	43.3	0.540			11.3	0.048	
	62.6	0.169			23.0	0.014	
	81.0	0.124			33.9	0.003	
	119.4	0.106			49.3	0.001	
* estimated					61.2	0.000	

Table C.2 Data for TCE Monod Kinetic Parameter Determ. with & without Iron

TCE without iron present				TCE with iron present			
Data Set	Time (min.)	TCE Conc. (mg/L)	X (VSS, mg/L)	Data Set	Time (min.)	TCE Conc. (mg/L)	X (VSS, mg/L)
1	0.0	0.730*	28.00	1	0.0	0.139	105.07
	1.4	0.729			13.6	0.102	
	39.9	0.699			30.1	0.085	
	88.9	0.657			40.8	0.073	
	126.3	0.652			59.2	0.057	
	163.1	0.649			72.1	0.045	
	204.6	0.634		2	0.0	0.200*	248.99
2	0.0	0.090*	28.94		1.5	0.187	
	4.3	0.089			23.4	0.091	
	49.4	0.082			41.8	0.051	
	84.1	0.079			62.6	0.024	
	123.1	0.076			82.6	0.011	
	162.6	0.069			107.5	0.004	
	204.5	0.066			122.0	0.000	
	240.5	0.063		3	0.0	0.325*	161.70
3	0.0	1.435*	21.13		4.2	0.291	
	2.9	1.429			30.3	0.142	
	41.6	1.351			63.6	0.064	
	82.6	1.333			97.6	0.032	
	121.0	1.298		4	0.0	0.013*	123.90
	167.7	1.284			2.3	0.012	
	204.1	1.226			15.8	0.007	
4	0.0	0.119	147.40		30.6	0.004	
	15.4	0.098			46.4	0.003	
	30.6	0.085			61.7	0.002	
	45.3	0.076			76.4	0.002	
	59.6	0.065			90.0	0.002	
	75.0	0.054		5	0.0	0.070*	82.90
	89.3	0.046			2.3	0.063	
					14.7	0.038	
					29.6	0.026	
					44.3	0.018	
					59.5	0.011	
					75.4	0.007	
*estimated					89.7	0.006	

Table C.3 Data for Toluene Endogenous Decay Coefficients Determination

Toluene without iron present											
Time (hrs.)	Total (dpm)	Acid (dpm)	Base (dpm)	Filter (dpm)	CO_2 (dpm)	Tol. (dpm)	NPP (dpm)	Cells (dpm)	$\ln(X/X_o)$	D.O. (mg/L)	pH
0.1	117151	53192	71874	56770	18682	45278	-3578	56770	0	N/A	N/A
11.9	111360	85016	108344	52995	23328	3017	32021	52995	-0.0688		
28.2	121605	66250	108198	51107	41948	13408	15143	51107	-0.1051		
52.8	121120	63246	99597	50388	36351	21523	12859	50388	-0.1193		
76.6	119767	61331	102982	55041	41651	16786	6290	55041	-0.0309		
96.2	122389	57122	110483	42757	53361	11906	14365	42757	-0.2835		
149.7	107649	41934	50718	42749	8783	56931	-814	42749	-0.2837		
197.5	110911	37474	82079	35939	44606	28832	1534	35939	-0.4572		
251.3	108094	37033	106469	40242	69437	1625	-3209	40242	-0.3441		
315.1	102642	33385	96648	27123	63263	5994	6262	27123	-0.7386		
Toluene with iron present											
0.3	36603	27845	35165	13917	7321	1438	13927	13917		8.9	6.72
28.0	34313	27573	33906	13110	6333	407	14463	13110	-0.0598		
53.3	34549	27708	34298	12064	6590	252	15644	12064	-0.1430		
75.2	33879	22097	34096	12144	11999	-217	9954	12144	-0.1363	6.7	6.75
96.2	34922	24590	34123	11787	9532	800	12803	11787	-0.1661		
147.0	34416	21181	34561	11789	13380	-145	9392	11789	-0.1660		
194.8	34416	21662	33748	11459	12086	668	10203	11459	-0.1944		
241.9	34416	18474	33492	10948	15018	923	7526	10948	-0.2400	4.1	6.77

CO_2 = Base – Acid
Tol. = Toluene = Total – Base
NPP = Acid – Filter
Cells = Filter

Table C.4 Data for TCE Transformation Capacity Determination

TCE without iron present							
Data Set	Time (min.)	TCE Conc. (mg/L)	VSS (mg/L)	D.O. (mg/L)	pH	Protein (mg/L)	NADH (μM)
1	2.4	8.923	199.5	8.2	6.87	-	-
	313.3	7.485					
	1304.4	5.439					
	1744.1	4.493		5.8	6.84		
	2684.1	4.735					
	3240.6	4.344	218.5	4.2	6.71		
2	1.8	2.101		9.1	6.85	26.6	5.5
	1354.8	1.020					
	2896.2	0.669		3.7	6.76	39.6	5.7
	3257.0	0.599	144.9				
	4432.6	0.472	97.1				
TCE with iron present							
1	2.2	7.878	119.6	14.0		34.3	0.4
	42.5	5.436					
	66.4	6.064				33.8	1.3
	99.2	5.931					
	175.2	5.268				32.1	-0.2
	321.6	4.991		12.0	6.79		
	446.3	4.517					
	1500.1	2.770		10.3			
	1874.6	2.471					
	2993.2	2.137	182.4				
	3249.5	2.103					
2	1.8	8.025	201.3	8.4	6.84		
	309.6	6.364					
	1312.7	4.741					
	1740.7	4.737		3.6	6.81		
	2680.7	4.648					
	3238.7	4.266	222.0	1.5	6.80		
3	3.6	5.350	281.1	7.8	6.77	42.6	
	300.5	4.149					
	1221.3	2.630					
	2637.1	1.975	224.9	1.1	6.83	53.3	
	4094.2	1.622	281.7	1.0	6.82	60.4	

Table C.5 Data for Culture Baseline Determination

Time	Norm. Enzyme Activity		TSS	Protein	Normalized NADH	
hrs.	AU-L/ min.-mg cells	AU-L/ min.-mg protein	mg/L	mg/mg cells	µM/mg cells	µM/mg protein
Without iron present						
0.4	1.170	4.435	145	0.264	0.030	0.115
14.1	1.675	10.624	151	0.158	0.043	0.275
44.2	0.508	4.226	218	0.120	0.028	0.232
75.9	0.547	4.728	163	0.116	0.028	0.246
With iron present						
0.5	0.480	5.954	343	0.081	0.013	0.156
14.2	0.306	5.351	353	0.057	0.016	0.277
44.2	0.111	1.215	380	0.091	0.015	0.168
75.9	0.087	2.657	401	0.033	0.012	0.352

Table C.6 Data for Toluene Dioxygenase Enzyme Location Determination

	Without iron present		With iron present	
Cell Fraction	Enzyme Activity (AU/min)	Normalized* Enzyme Activity (AU/min)	Enzyme Activity (AU/min)	Normalized* Enzyme Activity (AU/min)
Unfiltered	178.4	178.4	63.1	63.1
Filtered	-0.29	-0.29	0.45	0.45
Cyto/Periplasm	3.2	5.5	0.90	1.4
Membrane	16.8	9.9	9.2	5.8

	Plate count without iron present			Plate count with iron present		
	Sonicated & Ground	Sonicated	Unfilt.	Sonicated & Ground	Sonicated	Unfilt.
Avg. 1/10 Dilution, CFU/cm^2	41	71	98	73	96	200
St. Dev.	11	31	40	35	35	45
Avg. 1/10 Dilution, CFU/plate	2408	4221	5826	4355	5677	11905
No Dilution, 10^5 CFU/mL	2.4	4.2	5.8	4.4	5.7	11.9
% of Unfiltered	41%	72%	100%	37%	48%	100%

*Norm. Enzyme Activity, Cyto/Periplasm = Enzyme Activity/(100-% of Unfiltered for the sonicated & ground sample)

Norm. Enzyme Activity, Membrane = Enzyme Activity(100-% of Unfiltered for the sonicated and ground sample)

The enzyme activity was normalized to account for any intact cells that were left in solution after the sonication and grinding processes. Any remaining intact cells would decrease the enzyme activity in the cytoplasm fraction and increase the enzyme activity in the membrane fraction (because the heavy intact cells would spin out during centrifugation and become part of the cell membrane pellet).

Appendix D – Raw Column Experiment Data

D.1 Effluent SOC and DO Concentrations

Table D.1 Effluent SOC and DO Concentrations, Experiment 1

Influent						Effluent									
6.9-min. EBCT			11-min. EBCT			6.9-min. EBCT					11-min. EBCT				
Time (hrs)	Toluene (µg/L)	PCE (µg/L)	Time (hrs)	Toluene (µg/L)	PCE (µg/L)	Time (hrs)	Toluene (µg/L)	PCE (µg/L)	DO (mg/L)	Q (mL/min)	Time (hrs)	Toluene (µg/L)	PCE (µg/L)	DO (mg/L)	Q (mL/min)
1.2	647	848	1.1	657	854	0.8	623	888		2.00	0.8	653	906		2.20
5.5	645	861	5.5	646	848	5.3	592	958		2.40	5.3	674	925		2.33
17.6	690	915	17.5	667	882	17.0	583	880			17.0	606	898		
64.6	680	884	30.8	684	887	23.7			2.4		23.7			0.7	
75.4	722	951	48.6	779	1044	30.3	577	903		2.33	30.3	660	982		2.30
91.0	588	819	64.6	696	912	42.6	574	872	0.8		42.6	655	913	1.3	
99.1	684	940	75.4	697	913	48.3	569	899			48.3	663	1023		
117	660	910	91.0	636	842	64.2	523	798	1.4		64.1	589	891	1.0	
129	626	856	99.1	666	919	74.8	448	823	3.9		74.8	551	812	0.7	
154	550	699	117	672	935	78.5	471	865	7.1		78.5	608	906	1.4	
164	596	744	129	652	892	89.2	475	835	>10	2.40	89.2	367	869	2.2	2.40
175	601	778	146	622	851	94.0	446	777	14.8		93.9	318	827	5.4	
192	611	769	154	543	693	98.8	448	814		2.10	98.8	208	749		2.35
203	632	786	164	561	692	102	462	974			102	246	897	3.0	
213	610	780	175	618	804	110	413	877			110	374	814		
236	712	824	192	635	759	116	403	948	13.4		116	416	944	1.8	
246	560	767	203	653	828	121	388	944	11.8		121	446	874	1.1	
268	452	803	213	619	800	129	355	875			129	386	798		
289	428	808	236	704	802	139	448	826	10.2		139	340	843	1.4	
308	432	837	245	550	759	146			9.5		146	444	825	1.0	
314	434	861	268	456	806	154	289	805	7.1		154	447	788	0.5	
334	538	784	289	406	746	164	249	777	9.5	2.35	164	441	802	1.7	2.35
356	697	813	308	438	851	171			6.8		171	462	816	1.1	
406	1108	941	314	456	893	174	200	748	6.2		174	377	816	1.4	
452	2892	929	334	525	747	187			19.6		187	213	778	12.4	
506	4324	918	356	710	857	191	100	686	13.2		191	179	767	11.7	
			406	1105	956	203	54	625			203	101	723		
			452	2853	914	213	30	607	>20	2.30	210	83	747		
			506	4525	946	236	17	567	>20		213	73	714	11.0	2.00
						241	15	507			236	32	584	17.8	
						245	14	519			241	27	572		
						259	12	459			245	21	586		
						268	17	497			258	11	576		
						284			>20		268	8	575		
						289	18	510			284			17.4	
						307	14	531	13.0		289	5	528		
						314	18	500			307	1	532	7.6	
						355	13	465	11.3	2.10	314	3	479		
						406	11	497			355	0	460	8.7	2.40
						452	9	468	14.7		406	0	461		
						506	8	495		2.30	452	0	440	12.6	
											506	0	448		2.30

Table D.2 Effluent SOC and DO Concentrations, Experiment 2

Influent						Effluent									
2.5-min. EBCT			12-min. EBCT			2.5-min. EBCT					12-min. EBCT				
Time (hrs)	Toluene (µg/L)	PCE (µg/L)	Time (hrs)	Toluene (µg/L)	PCE (µg/L)	Time (hrs)	Toluene (µg/L)	PCE (µg/L)	DO (mg/L)	Q (mL/min)	Time (hrs)	Toluene (µg/L)	PCE (µg/L)	DO (mg/L)	Q (mL/min)
1.3	1052	494	1.3	1159	506	0.8	183	192		2.00	0.8	152	150		2.10
5.1	826	495	5.1	935	495	4.8	188	192	17.8		4.8	138	151	16.0	
15.6	577	516	15.5	456	416	14.9	154	190	>20		14.9	85	125	14.2	
21.6	3198	535	21.6	3371	522	21.0	137	193		2.20	21.0	30	116		2.00
29.2	2736	553	29.2	2572	518	28.9	116	195	18.6		28.9	72	129	1.4	
43.4	2045	521	43.6	1770	528	42.9	102	191			42.9	79	125	0.6	
52.8	745	581	52.8	859	549	52.3	124	184	>20		52.3	18	122	1.2	
64.8	623	494	64.8	608	491	64.2	122	193			64.2	65	115	1.4	
70.6	2147	559	70.6	1648	505	70.3	105	189	>20		70.3	64	114	0.9	
76.8	2677	535	76.8	2689	511	76.5	91	136	>20		76.5	9	108	2.0	
91.2	484	464	91.3	511	438	90.7	125	195		2.10	90.7	2	84	17.1	2.10
101	76	487	101	195	513	101	125	192	>20		101	3	77	>20	
114	216	489	114	167	376	114	129	198			114	5	78		
121	12	367	121	157	544	121	132	198			121	8	83	>20	
137	426	496	137	508	498	137	123	191			137	8	72		
165	58	384	165	518	463	165	103	187	12.2		165	9	76	10.5	
189	1436	536	189	1271	488	189	17	164	7.5		189	5	69	4.5	
213	470	516	213	382	498	212	5	146	6.6		212	6	71	4.4	
238	205	459	238	366	525	237	11	130			237	5	68		
262	178	479	262	146	458	261	11	139	9.1		261	6	68	7.0	
289	348	577	289	312	533	288	9	137			288	5	64		
311	197	476	311	73	442	310	6	134			310	6	66		
336	325	535	336	354	556	336	5	138	7.7	2.10	336	5	70	6.1	2.10
355	2920	537	355	3139	564	354	4	125			354	5	72		

Table D.3 Effluent SOC and DO Concentrations, ^{14}C-TCE Pre-Equilibrated Sterile Column

Influent			Effluent				
Time (hrs)	**Toluene (µg/L)**	**TCE (µg/L)**	**Time (hrs)**	**Toluene (µg/L)**	**TCE (µg/L)**	**DO (mg/L)**	**Q (mL/min)**
2.4	1569	723	1.5	607	598	8.4	
23.8	1522	561	6.3	606	609		2.56
48.3	1258	479	22.9	622	624		
54.3	1399	566	47.8	641	630	8.8	2.50
69.8	1456	708	53.6	582	569		
79.1	1345	741	69.0	85	270	12.7	2.53
93.6	1549	65	78.3	507	548		
103	1551	547	91.6	707	630		
119	1489	586	102.0	137	311		
126	1565	822	117.8	748	640		
139	1525	833	125.6	745	627	8.5	2.53
147	1576	825	138	688	691		
171	1581	990	147	876	732		
194	1564	828	168	931	757		
222	1530	889	193	1046	819		2.54
243	1501	902	220	1134	834	7.8	2.54
268	1524	795	243	1236	861	8.1	2.46
293	1453	850	267	1320	876	15.2	2.47
316	1681	1002	291	1342	884	9.1	2.43
362	1549	795	315	1407	911	8.6	2.52
413	1561	929	361	1447	892	13.5	
482	1592	944	412	1474	898	10.2	
554	1401	1109	481	1315	837	6.9	
			554	1137	838	6.5	

Table D.4 Effluent SOC and DO Concentrations, Experiment 3

Influent						Effluent									
10.3-min. EBCT			10.4-min. EBCT			10.3-min. EBCT					10.4-min. EBCT				
Time (hrs)	Toluene (µg/L)	TCE (µg/L)	Time (hrs)	Toluene (µg/L)	TCE (µg/L)	Time (hrs)	Toluene (µg/L)	TCE (µg/L)	DO (mg/L)	Q (mL/min)	Time (hrs)	Toluene (µg/L)	TCE (µg/L)	DO (mg/L)	Q (mL/min)
1.6	1735	164	1.6	1809	165	0.9	1250	114	7.1	2.44	0.9	1199	109	7.5	2.37
16.1	1819	193	16.2	1680	179	15.4	1199	116	2.1	2.47	15.4	1089	115	2.4	2.38
27.3	1852	186	27.3	1718	171	26.7	1258	120	1.3		26.7	1154	115	1.7	
43.1	1832	175	43.1	1806	175	42.4	1283	125	1.4	2.43	42.4	1203	121	1.6	2.38
51.1	1801	183	51.1	1737	180	50.5	1211	122	1.7		50.5	1026	119	1.1	
65.2	1803	183	65.3	1786	179	64.5	1231	126	0.9	2.45	64.5	1118	120	1.2	2.37
75.8	1872	206	76.0	1871	204	75.6	649	123	2.4		75.7	411	117	1.8	
89.9	1861	219	90.1	1884	229	89.1	93	85	16.8	2.47	89.3	354	102	4.9	2.28
99.8	1876	207	99.9	1853	203	94.9	117	82	>20		94.9	15	89	9.6	
117	1853	196	117	1813	197	99.5	189	78	>20	2.45	99.6	44	75	19.8	2.32
137	1684	193	137	1663	188	111	200	77	>20		111	101	72	>20	
160	1821	184	160	1679	178	116	203	74	>20		116	131	67	>20	
187	1790	191	187	1534	187	122	205	75	>20	2.37	123	118	68	>20	2.35
213	964	139	213	1480	167	137	210	75	>20	2.43	137	94	61	>20	2.33
237	1609	184	237	1629	182	146	204	73	>20		146	84	59	>20	
261	660	144	261	1339	202	160	203	74	>20	2.47	160	82	56	>20	2.34
283	437	116	283	2353	213	171	196	72	>20	2.44	171	75	54	>20	2.40
308	2195	205	308	1606	191	187	185	69	>20	2.44	187	71	51	>20	2.42
339	1796	163	339	1891	173	213	188	77	19.7		213	77	52	18.3	
354	2192	195	354	1638	180	236	146	70	18.8	2.47	237	42	44	15.2	2.46
381	1296	161	381	1764	180	261	98	64	17.2	2.43	261	21	34	16.0	2.43
408	1575	197	408	1725	207	283	44	56	15.6		283	23	35	16.8	
431	2297	209	431	2463	213	307	28	49	13.0	2.47	308	21	35	14.1	2.45
452	1448	163	452	2608	197	339	22	43	11.6		339	15	31	12.8	
477	1567	164	477	385	104	354	18	38	10.3		354	13	30	11.4	
530	1585	145	530	1948	153	380	17	35	11.9	2.42	381	10	27	12.3	2.46
573	2186	175	573	2329	178	407	16	34	13.5		408	9	27	13.2	
620	2586	174	620	2597	176	430	14	32	12.1		430	9	27	11.4	
670	2138	159	670	206	76	452	13	31	10.6	2.41	452	7	25	9.5	2.50
						477	12	28		2.40	477	7	25		2.47
						530	13	26			530	8	24		
						573	9	23		2.47	573	5	22		2.51
						620	8	21			620	4	19		
						670	7	19		2.52	670	3	18		2.51

Table D.5 Effluent SOC and DO Concentrations, Experiment 4

Influent						Effluent									
3.4-min. EBCT			3.5-min. EBCT			3.4-min. EBCT					3.5-min. EBCT				
Time (hrs)	Toluene (µg/L)	TCE (µg/L)	Time (hrs)	Toluene (µg/L)	TCE (µg/L)	Time (hrs)	Toluene (µg/L)	TCE (µg/L)	DO (mg/L)	Q (mL/min)	Time (hrs)	Toluene (µg/L)	TCE (µg/L)	DO (mg/L)	Q (mL/min)
3.2	6285	282	3.3	6578	292	2.7	3977	273	13.0	2.56	2.7	2038	187	12.8	2.47
19.0	6610	282	19.1	6695	280	18.6	3087	253	9.5	2.53	18.7	2345	217	9.2	2.48
27.3	6878	287	27.3	6794	283	26.9	2453	239	2.3	2.48	26.9	2195	213	2.1	2.43
41.6	6571	273	41.7	6478	260	41.1	2148	231	>20	2.48	41.1	1963	211	>20	2.44
53.3	6959	281	53.3	6635	274	52.6	1548	231	12.6	2.50	52.7	1800	215	12.1	2.43
73.7	6284	229	73.8	6145	235	73.1	924	191	8.8		73.2	787	173	7.2	
90.9	2081	186	91.0	6686	270	90.4	874	178	7.5	2.46	90.5	368	133	4.7	2.43
99.0	7004	250	99.1	6757	247	98.4	754	166	6.3		98.5	177	114	3.2	
115	6620	265	115	6456	263	112	800	158	7.9	2.45	112	228	110	4.7	2.43
120	6841	267	120	6624	253	120	1051	169	9.4		120	288	108	6.0	
137	6647	270	137	6971	274	136	1383	170	10.8	2.33	136	266	104	7.2	2.45
147	6720	283	147	6992	283	146	1843	192	13.4		146	1559	178	11.8	
166	6790	267	166	6786	267	165	878	162	4.7	2.53	165	3553	237	7.7	2.50

Table D.6 Effluent SOC and DO Concentrations, Experiment 5

Influent						Effluent									
2.3-min. EBCT			1.7-min. EBCT			2.3-min. EBCT					1.7-min. EBCT				
Time (hrs)	Toluene (µg/L)	TCE (µg/L)	Time (hrs)	Toluene (µg/L)	TCE (µg/L)	Time (hrs)	Toluene (µg/L)	TCE (µg/L)	DO (mg/L)	Q (mL/min)	Time (hrs)	Toluene (µg/L)	TCE (µg/L)	DO (mg/L)	Q (mL/min)
3.3	3113	218	3.1	3120	223	2.4	2768	227	12.8	2.50	2.3	2521	188	12.7	2.53
18.3	3041	208	18.4	2487	194	17.8	2524	224	12.4	2.50	17.8	2143	184	11.8	2.53
28.0	3163	210	28.1	3489	223	27.5	2480	225	12.2	2.51	27.5	2256	192	12.0	2.53
43.7	3289	195	43.7	3275	195	43.0	2271	215	11.2		43.0	1973	187	10.5	
53.6	3228	206	53.6	3296	213	53.0	1849	210	10.1	2.48	53.0	1720	186	9.2	2.50
68.2	3187	170	68.2	3313	174	67.6	663	155	7.1	2.07	67.6	803	157	6.4	2.57
74.9	3044	148	74.8	3004	145	74.4	528	170	4.9	2.06	74.3	478	147	4.9	2.57
90.6	3260	178	90.4	2987	167	89.8	663	155	12.4	2.30	89.8	479	129	11.8	2.49
98.4	3183	180	98.5	2950	179	98.0	666	155	12.7	2.26	98.0	423	117	12.5	2.50
114	3171	163	114	3252	168	113	697	145	12.8	2.29	113	461	122	12.0	2.52
122	3264	180	122	3252	181	122	710	142		2.30	122	481	122		2.52
141	2775	148	141	2702	147	140	785	142	12.4	2.37	140	587	122	12.6	2.54
164	3160	170	164	3207	166	164	1285	153	13.8	2.15	164	1033	142	13.2	2.53
186	2691	121	186	3138	133	186	1121	141	13.2	1.86	185	1622	145	13.6	2.53
209	4381	443	209	4442	460	209	2160	179	13.8	2.06	209	1552	171	12.6	2.53
236	4336	231	236	3952	231	236	2471	204	13.2	2.29	236	1666	183	11.6	2.53
285	4553	208	285	4664	216	285	2542	226	13.1	2.25	285	1907	192	12.0	2.74

Table D.7 Effluent SOC and DO Concentrations, Experiment 6

Influent						Effluent									
3.0-min. EBCT, Col A			3.0-min. EBCT, Col B			3.0-min. EBCT, Col A					3.0-min. EBCT, Col B				
Time (hrs)	Toluene (µg/L)	TCE (µg/L)	Time (hrs)	Toluene (µg/L)	TCE (µg/L)	Time (hrs)	Toluene (µg/L)	TCE (µg/L)	DO (mg/L)	Q (mL/min)	Time (hrs)	Toluene (µg/L)	TCE (µg/L)	DO (mg/L)	Q (mL/min)
2.3	1525	681	2.3	1547	668	1.8	687	540	7.0	2.50	1.8	74	253	7.2	2.48
23.9	1314	517	23.9	1395	534	6.2	682	546	6.9	2.50	6.2	77	265	7.2	2.47
47.6	1202	458	47.7	1172	461	23.3	632	531	1.2	2.51	23.3	85	307	2.5	
54.1	787	448	54.2	1184	530	45.9	603	508	0.7	2.52	45.9	107	365	0.8	2.45
70.1	1024	636	70.1	677	520	53.5	589	498	0.9	2.50	53.6	110	369	0.8	2.45
79.0	1502	763	79.1	1326	743	69.2	386	461	4.9	2.48	69.3	95	382	5.6	2.43
93.3	1551	69	93.3	1577	70	78.2	222	408	3.9		78.2	93	401	6.7	
102	1171	484	102	1617	566	91.4	87	320	5.7	2.45	91.4	85	378	9.4	2.45
119	1074	497	119	1506	578	102	64	270	8.4		102	79	355	10.4	
126	1375	770	126	1486	800	117	57	252	10.3	2.50	117	82	362	11.2	2.50
139	1462	814	139	1490	801	126	57	242	4.5		126	79	347	5.8	
147	1448	777	147	1563	810	139	45	225	2.5	2.48	139			3.8	2.48
168	1550	685	168	1288	630	146	38	221	2.5	2.47	146	70	326	4.0	2.50
194	1390	760	194	1430	790	167	35	224	3.2	2.51	167	74	342	4.2	2.50
222	1478	903	222	1526	888	193	38	251	3.6	2.52	193	68	332	4.2	2.50
243	1520	932	243	1457	895	220	35	251	4.0	2.43	221	62	319	4.4	2.50
267	1482	772	268	1550	800	242	32	246	3.9	2.53	243	58	315	6.2	2.53
293	1551	863	293	1531	853	267	47	284	14.2	2.47	267	74	365	14.2	2.53
316	1502	909	316	1516	941	291	46	310	7.9	2.52	292	74	386	7.7	2.50
361	1564	805	361	1546	790	316	39	305	5.3	2.53	316	67	386	5.3	2.53
413	1553	932	413	1592	954	361	42	331	10.8	2.53	361	61	400	10.8	2.53
482	1730	934	482	1614	900	412	49	400	8.5	2.53	412	69	470	8.2	2.53
554	1435	1128	554	1390	1122	481	46	423	4.9	2.53	482	60	482	4.8	2.51
						553	48	516	4.9	2.52	553	59	555	5.0	2.49

Table D.8 Effluent SOC and DO Concentrations, Anthracite Control Experiment

Influent									Effluent															
1.0-min. EBCT, Col A			0.9-min. EBCT, Col B			1.0-min. EBCT, Col C			1.0-min. EBCT, Col A					0.9-min. EBCT, Col B					1.0-min. EBCT, Col C				
Time (hrs)	Toluene (µg/L)	TCE (µg/L)	Time (hrs)	Toluene (µg/L)	TCE (µg/L)	Time (hrs)	Toluene (µg/L)	TCE (µg/L)	Time (hrs)	Toluene (µg/L)	TCE (µg/L)	DO (mg/L)	Q (mL/min)	Time (hrs)	Toluene (µg/L)	TCE (µg/L)	DO (mg/L)	Q (mL/min)	Time (hrs)	Toluene (µg/L)	TCE (µg/L)	DO (mg/L)	Q (mL/min)
1.0	829	57	1.2	836	57	1.3	771	52	0.4	630	48	8.2	2.32	0.3	665	46	8.4	2.57	0.3	725	48	8.5	2.37
20.3	866	66	20.3	859	64	22.1	800	58	20.1	246	55		2.30	20.1	181	57		2.53	20.1	829	62		2.37
49.0	847	64	48.9	829	62	49.0	818	62	48.6	1.6	55	7.2	2.28	48.4	1.1	54	7.0	2.53	48.6	822	62	8.3	2.33
76.2	791	64	76.2	802	65	76.1	799	62	74.5	0.7	55		2.28	74.6	0.8	55		2.52	74.7	781	61		2.37
96.4	610	66	96.5	578	64	97.0	701	64	96.2	0.1	55	7.0	2.28	96.2	0.1	53	6.9	2.50	96.5	694	64	8.1	2.37
124	199	58	124	233	61	124	368	61	124	0.1	52			124	0.1	51			124	356	58		
144	140	66	144	162	66	144	255	64	143	0.1	59		2.30	143	0.1	57		2.52	143	258	66	10.6	2.15

Table D.9 Effluent SOC and DO Concentrations, Virgin Sterile Column

Influent			Effluent				
0.9-min. EBCT			0.9-min. EBCT				
Time (hrs)	Toluene (µg/L)	TCE (µg/L)	Time (hrs)	Toluene (µg/L)	TCE (µg/L)	DO (mg/L)	Q (mL/min)
1.8	1561	74	0.7	1	1	14.0	2.51
23.8	1592	77	23.3	17	3	13.6	2.52
50.8	1575	112	50.5	16	4	13.2	2.50
71.7	1522	83	71.2	11	4	10.6	2.53
94.4	1520	81	93.9	13	6	9.3	2.51
120	1588	66	119	19	8	10.5	2.56
143	1657	80	142	25	11	8.2	2.57
168	1529	74	167	40	17	8.1	2.60
186	1608	43	186	55	21	11.5	2.55
218	1676	44	217	90	29	8.8	2.57
242	1577	119	242	138	40	8.1	2.57
264	1563	124	264	180	56	11.1	2.57
288	1449	116	287	227	64	8.5	2.55
312	1367	104	312	263	83	10.4	2.53
335	1391	104	334	337	113	10.5	2.47
361	1522	113	360	424	128	8.3	2.43
383	1520	25	382	511	133	11.6	2.57
405	1858	74	405	740	141	13.6	2.57
431	1871	77	431	884	138	10.1	2.57
478	1736	73	452	884	136		2.63
505	1912	74	478	1039	131	10.1	2.60
528	2006	71	505	1259	125	8.5	2.66
550	1436	108	528	1320	97	11.4	2.63
575	1709	65	550	1436	91	8.2	2.57
623	1064	143	575	1407	79	6.6	2.63
651	1199	123	622	1197	55	8.1	2.45
674	1616	127	650	1214	70	12.0	2.55
695	1299	71	674	1190	78	8.0	2.53
			695	1053	77	6.4	2.55

Table D.10 Effluent SOC and DO Concentrations, Experiment 7

Influent						Effluent									
1.1-min. EBCT			1.2-min. EBCT			1.1-min. EBCT					1.2-min. EBCT				
Time (hrs)	Toluene (µg/L)	TCE (µg/L)	Time (hrs)	Toluene (µg/L)	TCE (µg/L)	Time (hrs)	Toluene (µg/L)	TCE (µg/L)	DO (mg/L)	Q (mL/min)	Time (hrs)	Toluene (µg/L)	TCE (µg/L)	DO (mg/L)	Q (mL/min)
2.1	1707	79	2.3	1498	73	0.7	0	0	16	2.42	0.8	4	0	16.2	2.60
24.4	1723	83	24.4	1591	81	23.4	2	1	13.2	2.40	23.6	24	1	13.4	2.60
50.7	1735	121	50.5	1671	118	49.9	5	2	13.2	2.40	49.7	31	5	13.5	2.57
71.8	1631	92	72.3	1633	86	71.0	9	3	10.6	2.42	71.0	45	7	10.7	2.62
95.4	1503	80	95.4	1446	78	93.9	12	4	9.2	2.43	94.0	46	18	7.5	2.60
120	1608	69	120	1579	68	119	19	7	10.2	2.43	119	48	14	9.0	2.61
143	1693	83	143	1616	80	143	23	10	7.8	2.47	143	34	15	6.3	2.61
169	1602	76	169	1422	73	168	21	14	7.9	2.48	170	91	15	5.0	1.51
187	1564	41	187	1579	42	186	24	17	11.1	2.34	186	85	15	11.0	2.60
218	1516	41	218	1426	42	216	16	17	7.3	2.43	216	41	12	8.5	2.60
243	1552	117	243	1215	115	242	10	18	6.4	2.44	242	11	22	6.8	2.28
264	1610	126	264	1176	118	263	12	20	9.9	2.45	263	13	19	10.2	2.23
288	1448	122	288	1433	118	287	9	20	6.6	2.47	287	65	34	7.4	2.67
313	1385	109	312	1410	110	312	7	22	6.3	2.45	312	29	37	7.1	2.50
335	1500	110	335	1273	103	334	9	24	9.4	2.47	334	19	35	10.2	2.45
363	1438	113	363	1352	111	360	7	26	6.5	2.44	360	44	41	6.9	2.35
383	1410	24	383	1305	24	382	9	25	10.3	2.52	382	120	20	10.7	2.43
405	1639	72	406	1798	71	405	51	42	12.5	2.57	406			11.6	2.32
431	1886	79	432	1858	77	431	50	45	9.7	2.57	431	44	34	9.75	2.40
478	1769	75	479	1831	79	452	57	50			452	383	52		2.65
505	1756	71	505	1810	71	478	115	49	8.1	2.60	478	309	52	8.4	2.70
528	1956	71	528	1952	71	504	103	50	6.7	2.62	504	231	47	6.6	2.72
550	1749	67	550	1197	67	528	147	54	10.7	2.62	528	161	40	10.6	1.81
625	974	147	576	264	58	549	69	52	6.9	2.63	549	171	41	7.1	2.41
651	1198	124	625	914	136	575	5	43	6.2	2.66	575	6	35	5.9	1.93
674	1603	137	651	1206	135	622	202	78	7.7	2.52	622	477	128	8	2.62
695	538	122	673	1095	126	650	125	65	11.5	2.55	650	162	66	11.8	2.11
			696	453	117	674			7.5	2.55	673	346	86	7.9	2.20
						695	3	62	6.3	2.57	695	160	82	6.3	2.76

Table D.11 Effluent SOC and DO Concentrations, Experiment 8

Influent									Effluent														
1.0-min. EBCT, Col A			1.0-min. EBCT, Col B			1.0-min. EBCT, Col C			1.0-min. EBCT, Col A					1.0-min. EBCT, Col B					1.0-min. EBCT, Col C				
Time (hrs)	Toluene (µg/L)	TCE (µg/L)	Time (hrs)	Toluene (µg/L)	TCE (µg/L)	Time (hrs)	Toluene (µg/L)	TCE (µg/L)	Time (hrs)	Toluene (µg/L)	TCE (µg/L)	DO (mg/L)	Q (mL/min)	Time (hrs)	Toluene (µg/L)	TCE (µg/L)	DO (mg/L)	Q (mL/min)	Time (hrs)	Toluene (µg/L)	TCE (µg/L)	DO (mg/L)	Q (mL/min)
0.0	739	80	0.0	742	71	0.0	941	63	0.7	3	4	8.6	2.30	0.9	0	4	8.7	2.47	0.5	1	4	11.3	2.44
24.1	822	59	24.3	798	58	24.3	780	56	23.2	7	4	8.5	2.27	23.3	2	4	8.7	2.43	23.3	3	4	11.4	2.42
52.6	765	54	52.6	756	53	52.9	730	50	51.9	2	4		2.27	52.0	4	4		2.43	52.0	8	4		2.43
73.7	776	59	73.7	758	58	73.8	766	60	72.8	0	4	7.8	2.30	72.8	3	4	8.1	2.43	72.9	7	4	10.9	2.43
95.4	795	68	95.5	790	69	95.3	761	65	94.5	1	4		2.27	94.8	2	4		2.43	94.7	10	5		2.43
118	803	65	118	769	63	118	772	63	118	0	4		2.31	118	1	4		2.45	118	14	6		2.46
145	785	71	145	806	73	145	766	69	144	1	5	7.8	2.30	144	1	5	7.5	2.43	144	14	7	10.6	2.46
168	812	80	167	804	77	167	774	73	167	1	5		2.30	167	1	4		2.43	166	17	7		2.43
191	795	82	192	816	84	191	784	80	190	1	5	7.4	2.30	190	2	5	7.4	2.43	190	24	8	9.3	2.43
221	758	68	221	776	71	221	770	71	220	1	5		2.30	220	3	5		2.43	220	27	10		2.43
239	795	80	239	781	79	239	758	77	238	1	5			238	4	6			238	34	11		
268	809	69	267	814	71	268	783	68	267	1	5	7.9	2.29	267	6	7	8.4	2.43	267	50	13	10.3	2.43
288	828	73	289	833	74	289	791	69	287	1	6		2.29	288	7	7		2.40	288	115	34		2.42
316	845	74	316	802	71	316	801	70	315	1	6			315	9	8			316	96	33		
336	772	72	337	748	69	336	736	67	336	1	6	7.7	2.30	336	11	11	8.0	2.40	336	94	34	9.1	2.37
360	748	72	360	738	71	360	720	66	359	1	6		2.26	359	12	12		2.37	359	102	38		2.40
385	728	65	385	725	64	385	696	58	384	0	4		2.30	384	13	16			384	94	40		
412	705	66	412	688	64	412	666	58	412	0	4	7.8	2.30	411	15	19	8.4	2.37	412	101	43	10.4	2.40
436	714	65	436	719	66	436	689	60	432	0	4		2.30	435	17	21		2.37	435	107	52		2.28
461	730	61	461	716	60	461	684	55	460	0	4		2.27	460	19	24		2.38	460	88	56		2.26
483	763	57	484	744	58	484	725	56	482	0	7		2.33	482	20	24		2.46	483	73	56		2.33
499	653	60	499	635	60	499	615	57	497	0	7		2.33	497	17	22		2.41	498	69	53		2.38
521	682	56	521	648	56	521	566	48	520	0	7		2.28	520	31	26		2.40	520	69	51		2.37
547	620	54	547	665	64	547	651	60	546	0	7		2.33	546	102	33		2.32	546	68	46		2.36
572	696	58	572	641	56	573	644	55	572	0	8		2.35	572	71	35		2.40	572	63	46		2.35
593	665	62	593	695	68	593	649	61	592	0	8		2.36	592	29	31		2.38	592	66	52		2.30
616	654	54	617	682	64	617	621	54	616	0	9		2.35	616	21	32		2.43	616	58	54		2.25

D.2 BIOREGENERATION RATE AND EXTENT

Table D.12 Bioregeneration Rate and Extent, Experiment 2

2.5-min. EBCT, ^{14}C-Toluene			12-min. EBCT, ^{14}C-Toluene		
Time (hrs)	**Bioregeneration Rate (µg/min)**	**Cumulative Bioregeneration**	**Time (hrs)**	**Bioregeneration Rate (µg/min)**	**Cumulative Bioregeneration**
0.8	0.000	0.000	0.8	0.000	0.000
4.8	0.077	0.001	4.8	0.092	0.001
14.9	0.227	0.008	14.9	0.498	0.014
21.0	0.353	0.016	21.0	0.910	0.033
28.9	0.596	0.032	28.9	0.037	0.050
42.9	0.624	0.071	42.9	0.037	0.052
52.3	0.280	0.090	52.3	0.794	0.070
64.2	0.406	0.108	64.2	0.056	0.092
70.3	0.314	0.118	70.3	0.210	0.096
76.5	0.364	0.128	76.5	1.967	0.126
90.7	0.146	0.144	90.7	1.104	0.224
101	0.095	0.150	101	0.717	0.266
114	0.083	0.155	114	0.695	0.306
121	0.125	0.158	121	0.439	0.323
137	0.139	0.167	137	0.281	0.349
165	0.127	0.184	165	0.121	0.374
189	0.470	0.216	189	0.112	0.387
212	0.420	0.264	212	0.125	0.399
237	0.217	0.300	237	0.097	0.412
261	0.221	0.323	261	0.091	0.422
288	0.181	0.348	288	0.078	0.432
310	0.156	0.364	310	0.075	0.440
336	0.155	0.382	336	0.088	0.449
354	0.116	0.394	354	0.064	0.455

Specific Activity (dpm/µg) = 2836 (2.5-min. EBCT), 2678 (12-min. EBCT)
Yield Coefficient (µg C-cells/µg C-substrate) = 0.301
Fraction of Biomass Converted to CO_2 (µg C-CO_2/µg C-cells) = 0.8593
Endogenous Decay Coefficient (1/min) = 3.33×10^{-5}
Initial Substrate in Element (µg) = 13340 (2.5-min. EBCT), 13422 (12-min. EBCT)

Table D.13 Bioregeneration Rate and Extent, ^{14}C-TCE Pre-Equilibrated Sterile Column

0.9-min. EBCT, ^{14}C-TCE		
Time (hrs)	**Bioregeneration Rate (µg/min)**	**Cumulative Bioregeneration**
1.2	0.000	0.000
6.6	0.000	0.000
23.1	0.000	0.000
48.0	0.000	0.000
53.8	0.000	0.000
69.4	0.000	0.000
78.8	0.000	0.000
91.8	0.000	0.000
102	0.000	0.000
117	0.068	0.003
126	0.000	0.005
139	0.000	0.005
146	0.067	0.007
168	-0.001	0.011
193	-0.001	0.011
221	0.002	0.011
243	-0.001	0.011
267	0.000	0.011
291	0.000	0.011
316	0.000	0.011
361	0.000	0.011
413	0.000	0.011
482	0.001	0.011
554	0.000	0.012

Specific Activity (dpm/µg) = 7497
Yield Coefficient (µg C-cells/µg C-substrate) = 0.139
Fraction of Biomass Converted to CO_2 (µg C-CO_2/µg C-cells) = 0.8593
Endogenous Decay Coefficient (1/min) = 3.33×10^{-5}
Initial Substrate in Element (µg) = 9395

Table D.14 Bioregeneration Rate and Extent, Experiment 3

10.3-min. EBCT, ^{14}C-TCE, Col A			10.4-min. EBCT, ^{14}C-TCE, Col B		
Time (hrs)	**Bioregeneration Rate (µg/min)**	**Cumulative Bioregeneration**	**Time (hrs)**	**Bioregeneration Rate (µg/min)**	**Cumulative Bioregeneration**
1.1	0.000	0.000	1.4	0.000	0.000
15.7	0.005	0.004	15.7	0.000	0.000
26.7	0.005	0.010	26.7	0.001	0.001
42.6	0.004	0.019	42.6	0.002	0.004
50.5	0.005	0.023	50.5	0.003	0.006
64.7	0.000	0.028	64.8	0.000	0.009
75.6	0.000	0.028	75.7	0.000	0.009
89.4	0.002	0.029	89.6	0.002	0.011
94.9	0.002	0.031	94.9	0.001	0.011
99.5	0.001	0.032	99.6	0.000	0.012
111	0.000	0.032	111	0.000	0.012
116	0.000	0.032	117	0.000	0.012
122	0.000	0.032	123	0.000	0.012
137	0.000	0.032	137	0.000	0.013
146	0.000	0.032	146	0.000	0.013
160	0.000	0.032	160	0.000	0.013
171	0.000	0.032	171	0.000	0.014
187	0.000	0.032	187	0.000	0.014
213	0.000	0.032	213	0.000	0.015
236	0.000	0.032	237	0.000	0.015
261	0.000	0.032	261	0.000	0.016
283	0.000	0.032	283	0.000	0.017
307	0.000	0.033	308	0.000	0.017
339	0.000	0.033	339	0.000	0.018
354	0.000	0.033	354	0.000	0.018
380	0.000	0.034	381	0.000	0.019
407	0.000	0.034	408	0.000	0.019
431	0.000	0.034	431	0.000	0.019
452	0.000	0.034	452	0.000	0.020
477	0.000	0.035	477	0.000	0.020
530	0.000	0.035	530	0.000	0.021
573	0.000	0.035	573	0.000	0.021
620	0.000	0.036	620	0.000	0.022
670	0.000	0.036	670	0.000	0.022

Specific Activity (dpm/µg) = 68547
Yield Coefficient (µg C-cells/µg C-substrate) = 0.139
Fraction of Biomass Converted to CO_2 (µg C-CO_2/µg C-cells) = 0.8593 (Col A), 0.2149 (Col B)
Endogenous Decay Coefficient (1/min) = 3.33×10^{-5} (Col A), 1.0×10^{-5} (Col B)
Initial Substrate in Element (µg) = 504 (Col A), 492 (Col B)

Table D.15 Bioregeneration Rate and Extent, Experiment 4

3.4-min. EBCT, ^{14}C-Toluene, Col A			3.5-min. EBCT, ^{14}C-TCE, Col B		
Time (hrs)	**Bioregeneration Rate (µg/min)**	**Cumulative Bioregeneration**	**Time (hrs)**	**Bioregeneration Rate (µg/min)**	**Cumulative Bioregeneration**
3.0	0.000	0.000	3.1	0.000	0.000
18.6	1.680	0.012	18.7	0.003	0.001
27.0	4.968	0.038	27.1	0.000	0.002
41.2	1.253	0.079	41.3	0.000	0.002
52.9	3.694	0.105	53.0	0.004	0.003
73.4	5.074	0.188	73.5	0.001	0.006
90.6	4.751	0.266	90.7	0.006	0.009
98.7	5.076	0.302	98.7	0.006	0.012
112	4.665	0.362	112	0.006	0.016
120	3.208	0.391	120	0.005	0.019
136	2.362	0.433	136	0.005	0.024
146	1.211	0.449	147	0.004	0.026
165	0.854	0.467	165	0.002	0.030

Specific Activity (dpm/µg) = 1315 (Col A), 61389 (Col B)
Yield Coefficient (µg C-cells/µg C-substrate) = 0.391 (Col A), 0.139 (Col B)
Fraction of Biomass Converted to CO_2 (µg C-CO_2/µg C-cells) = 0.2149
Endogenous Decay Coefficient (1/min) = 1.0×10^{-5}
Initial Substrate in Element (µg) = 65218 (Col A), 1055 (Col B)

Table D.16 Bioregeneration Rate and Extent, Experiment 5

2.3-min. EBCT, ^{14}C-Toluene			1.7-min. EBCT, ^{14}C-TCE		
Time (hrs)	**Bioregeneration Rate (µg/min)**	**Cumulative Bioregeneration**	**Time (hrs)**	**Bioregeneration Rate (µg/min)**	**Cumulative Bioregeneration**
2.8	0.000	0.000	2.6	0.000	0.000
18.0	0.000	0.000	18.1	0.000	0.000
27.7	0.202	0.001	27.7	0.000	0.000
43.3	1.558	0.017	43.3	0.000	0.000
53.0	2.153	0.037	53.0	0.002	0.001
67.8	4.537	0.094	67.8	0.005	0.004
74.7	5.107	0.132	74.5	0.004	0.006
90.1	4.656	0.218	90.0	0.009	0.014
98.2	3.041	0.253	98.2	0.008	0.018
113	2.978	0.306	113	0.007	0.026
122	2.599	0.332	122	0.007	0.030
141	2.120	0.383	141	0.004	0.038
164	0.845	0.423	164	0.003	0.043
186	0.819	0.444	185	0.001	0.046
209	0.460	0.461	209	0.002	0.049
236	0.339	0.473	236	0.002	0.053
285	0.261	0.490	285	0.001	0.059
331	0.249	0.503	330	0.001	0.063
381	0.272	0.518	381	0.001	0.067
432	-0.003	0.526	432	0.001	0.071
475	0.026	0.526	473	0.001	0.074

Specific Activity (dpm/µg) = 1860 (Col A), 73526 (Col B)
Yield Coefficient (µg C-cells/µg C-substrate) = 0.391 (Col A), 0.139 (Col B)
Fraction of Biomass Converted to CO_2 (µg C-CO_2/µg C-cells) = 0.2149
Endogenous Decay Coefficient (1/min) = 1.0×10^{-5}
Initial Substrate in Element (µg) = 52507 (Col A), 854 (Col B)

Table D.17 Bioregeneration Rate and Extent, Experiment 6

3.0-min. EBCT, ^{14}C-Toluene, Col A			3.0-min. EBCT, ^{14}C-TCE, Col B		
Time (hrs)	**Bioregeneration Rate (µg/min)**	**Cumulative Bioregeneration**	**Time (hrs)**	**Bioregeneration Rate (µg/min)**	**Cumulative Bioregeneration**
2.0	0.000	0.000	2.0	0.000	0.000
6.4	0.015	0.000	6.4	0.000	0.000
23.5	0.000	0.000	23.5	0.000	0.000
46.1	0.001	0.000	46.2	0.000	0.000
53.7	0.035	0.000	53.8	0.000	0.000
69.7	2.814	0.035	69.8	0.000	0.000
78.6	4.861	0.087	78.8	0.000	0.000
91.6	3.647	0.172	91.7	0.000	0.000
102	2.680	0.223	102	0.000	0.000
117	1.837	0.275	117	0.000	0.000
126	1.178	0.295	126	0.000	0.000
139	1.000	0.316	139	0.000	0.000
147	1.088	0.329	147	0.000	0.000
167	0.786	0.358	168	0.000	0.000
193	0.420	0.382	193	0.000	0.000
221	0.370	0.399	221	0.000	0.000
242	0.343	0.411	243	0.000	0.000
267	0.197	0.421	267	0.000	0.000
292	0.144	0.427	292	0.000	0.000
316	0.174	0.433	316	0.000	0.000
361	0.119	0.443	361	0.000	0.000
412	0.076	0.451	413	0.000	0.000
482	0.065	0.458	482	0.000	0.000
554	0.059	0.465	554	0.000	0.000

Specific Activity (dpm/µg) = 1919 (Col A), 15985 (Col B)
Yield Coefficient (µg C-cells/µg C-substrate) = 0.391 (Col A), 0.139 (Col B)
Fraction of Biomass Converted to CO_2 (µg C-CO_2/µg C-cells) = 0.2149
Endogenous Decay Coefficient (1/min) = 1.0×10^{-5}
Initial Substrate in Element (µg) = 39314 (Col A), 4788 (Col B)

Table D.18 Bioregeneration Rate and Extent, Experiment 7

1.1-min. EBCT, ^{14}C-Toluene, Col B			1.2-min. EBCT, ^{14}C-Toluene, Col C		
Time (hrs)	**Bioregeneration Rate (µg/min)**	**Cumulative Bioregeneration**	**Time (hrs)**	**Bioregeneration Rate (µg/min)**	**Cumulative Bioregeneration**
1.0	0.000	0.000	1.1	0.000	0.000
23.6	0.064	0.007	23.8	0.102	0.017
50.1	0.072	0.012	49.9	0.156	0.011
71.3	0.039	0.018	71.4	0.326	0.024
94.1	0.067	0.024	94.2	0.577	0.049
119	0.077	0.033	120	0.542	0.084
143	0.187	0.048	143	0.701	0.119
169	0.333	0.082	171	0.303	0.154
186	0.288	0.109	186	0.490	0.169
217	0.485	0.167	216	0.395	0.201
242	0.495	0.228	242	0.267	0.223
263	0.302	0.270	264	0.281	0.237
287	0.304	0.305	288	0.291	0.254
312	0.247	0.339	312	0.256	0.270
334	0.197	0.363	334	0.241	0.284
361	0.136	0.385	360	0.203	0.298
383	0.114	0.398	383	0.352	0.313
405	0.053	0.408	406	0.217	0.329
431	0.074	0.416	431	0.217	0.343
452	0.069	0.423	452	0.171	0.353
478	0.102	0.434	478	0.139	0.363
505	0.040	0.443	505	0.160	0.372
528	0.046	0.448	528	0.112	0.380
550	0.044	0.453	550	0.150	0.387
574.8	0.037	0.458	575	0.169	0.397
623	0.015	0.464	623	0.110	0.413
650.5	0.057	0.469	651	0.134	0.422
673.7	0.025	0.474	674	0.091	0.428
694.8	0.022	0.477	695	0.105	0.433

Specific Activity (dpm/µg) = 748 (Col B), 76.8 (Col C)
Yield Coefficient (µg C-cells/µg C-substrate) = 0.294 (Col B), 0.391 (Col C)
Fraction of Biomass Converted to CO_2 (µg C-CO_2/µg C-cells) = 0.8593 (Col B), 0.2149 (Col C)
Endogenous Decay Coefficient (1/min) = 3.33×10^{-5} (Col B), 1.0×10^{-5} (Col C)
Substrate Sorbed by 50 hrs. (µg) = 12172 (Col B), 24451 (Col C)

Table D.19 Bioregeneration Rate and Extent, Experiment 8

1.0-min. EBCT, ^{14}C-Toluene, Col A			1.0-min. EBCT, ^{14}C-Toluene, Col B			1.0-min. EBCT, ^{14}C-Toluene, Col C		
Time (hrs)	Bioregeneration Rate (µg/min)	Cumulative Bioregeneration	Time (hrs)	Bioregeneration Rate (µg/min)	Cumulative Bioregeneration	Time (hrs)	Bioregeneration Rate (µg/min)	Cumulative Bioregeneration
1.7	0.000	0.000	1.6	0.000	0.000	1.3	0.000	0.000
23.6	0.279	0.024	23.7	0.064	0.005	23.7	0.017	0.001
52.2	0.919	0.106	52.2	0.068	0.012	52.4	0.000	0.002
73.0	0.499	0.164	73.0	0.210	0.026	73.2	0.000	0.002
94.7	0.409	0.210	95.0	0.644	0.070	94.9	0.001	0.002
118	0.312	0.249	118	0.683	0.141	118	0.000	0.002
144	0.178	0.279	144	0.355	0.205	145	0.000	0.002
167	0.212	0.300	167	0.351	0.242	167	0.001	0.002
191	0.119	0.318	191	0.184	0.272	191	0.000	0.002
221	0.135	0.336	221	0.179	0.297	221	0.000	0.002
238	0.104	0.346	239	0.104	0.309	239	0.000	0.002
267	0.107	0.361	268	0.094	0.323	268	0.000	0.002
288	0.083	0.370	288	0.059	0.330	289	0.000	0.002
316	0.078	0.380	316	0.050	0.337	316	0.008	0.003
336	0.066	0.387	336	0.040	0.341	336	0.002	0.003
359	0.057	0.394	359	0.044	0.346	360	0.004	0.003
384	0.043	0.400	384	0.037	0.351	384	0.001	0.004
412	0.050	0.406	412	0.045	0.356	412	0.030	0.006
435	0.037	0.410	435	0.045	0.361	436	0.048	0.010
460	0.035	0.415	461	0.053	0.367	461	0.204	0.025
483	0.030	0.418	483	0.051	0.372	483	0.419	0.057
498	0.027	0.420	498	0.054	0.376	498	0.327	0.084
521	0.021	0.422	521	0.048	0.381	521	0.324	0.119
546	0.017	0.425	546	0.065	0.388	547	0.324	0.158
572.1	0.015	0.427	572	0.068	0.396	572	0.318	0.196
592.4	0.016	0.428	592	0.081	0.403	593	0.315	0.227
616.2	0.017	0.430	616	0.089	0.413	617	0.316	0.262

Specific Activity (dpm/µg) = 1204 (A), 1224 (B), 1199 (C)
Yield Coefficient (µg C-cells/µg C-substrate) = 0.294 (A), 0.391 (B, C)
Fraction of Biomass Converted to CO_2 (µg C-CO_2/µg C-cells) = 0.8593 (A), 0.2149 (B, C)
Endogenous Decay Coefficient (1/min) = 3.33×10^{-5} (A), 1.0×10^{-5} (B, C)
Substrate Sorbed by 50 hrs. (µg) = 10472 (A), 12688 (B), 12802 (C)

D.3 GAC LOADINGS

In these tables the initial GAC loadings were determined via mass balance and the final GAC loadings from the end of the experiment were determined via methanol extraction. For the virgin columns, the initial GAC loadings were zero; therefore, the calculated equilibrium GAC loadings were used for normalization.

Table D.20 GAC Loadings, Experiment 1

6.9-min. EBCT, 8.8-cm. Length			11-min. EBCT, 14.0-cm. Length		
Distance Across Column from Influent (cm)	**Toluene (mg/g)**	**PCE (mg/g)**	**Distance Across Column from Influent (cm)**	**Toluene (mg/g)**	**PCE (mg/g)**
Initial	43.1	92.6	Initial	43.1	92.6
0.2	36.7	109	0.3	37.3	109
4.4	5.95	99.6	7.0	4.58	103
8.6	3.96	94.2	13.7	3.96	90.5

Table D.21 GAC Loadings, Experiment 2

2.5-min. EBCT, 3.0-cm. Length			12-min. EBCT, 14.15-cm. Length		
Distance Across Column from Influent (cm)	**Toluene (mg/g)**	**PCE (mg/g)**	**Distance Across Column from Influent (cm)**	**Toluene (mg/g)**	**PCE (mg/g)**
Initial	32.6	46.6	Initial	32.6	46.6
0.1	58.5	53.5	0.3	47.0	50.7
1.5	24.9	53.4	7.1	10.1	44.4
2.9	12.7	49.6	13.9	10.5	34.7

Table D.22 GAC Loadings, ^{14}C-TCE Pre-Equilibrated Sterile Column

0.9-min. EBCT, 1.3-cm. Length		
Distance Across Column from Influent (cm)	**Toluene (mg/g)**	**TCE (mg/g)**
Initial	79.1	9.67
0.30	71.5	14.1
0.95	79.5	12.1

Table D.23 GAC Loadings, Experiment 3

10.3-min. EBCT, 15-cm. Length, Col A			10.4-min. EBCT, 15-cm. Length, Col B		
Distance Across Column from Influent (cm)	**Toluene (mg/g)**	**TCE (mg/g)**	**Distance Across Column from Influent (cm)**	**Toluene (mg/g)**	**TCE (mg/g)**
Initial	128	2.04	Initial	128	2.04
0.25	135	2.19	0.45	139	2.20
4.00	86.1	3.18	4.00	35.6	4.12
7.70	21.1	3.02	7.25	23.0	2.14
11.0	21.6	1.51	11.2	20.6	1.40
14.5	19.3	1.56	14.6	17.4	1.48

Table D.24 GAC Loadings, Experiment 4

3.4-min. EBCT, 4.8-cm. Length, Col A			3.5-min. EBCT, 4.8-cm. Length, Col B		
Distance Across Column from Influent (cm)	**Toluene (mg/g)**	**TCE (mg/g)**	**Distance Across Column from Influent (cm)**	**Toluene (mg/g)**	**TCE (mg/g)**
Initial	150	2.37	Initial	150	2.37
0.22	156	1.62	0.22	146	1.28
2.35	149	1.34	2.55	112	1.24
4.49	60.7	2.45	4.53	54.0	2.19

Table D.25 GAC Loadings, Experiment 5

2.3-min. EBCT, 2.6-cm. Length, Col A			1.7-min. EBCT, 2.6-cm. Length, Col B		
Distance Across Column from Influent (cm)	**Toluene (mg/g)**	**TCE (mg/g)**	**Distance Across Column from Influent (cm)**	**Toluene (mg/g)**	**TCE (mg/g)**
Initial	123	1.98	Initial	123	1.98
0.35	145	1.09	0.35	146	1.10
1.25	85.1	1.85	1.55	71.2	2.06
2.30	47.4	2.75	2.30	21.8	3.24

Table D.26 GAC Loadings, Experiment 6

3.0-min. EBCT, 4.5-cm. Length, Col A			3.0-min. EBCT, 4.3-cm. Length, Col B		
Distance Across Column from Influent (cm)	Toluene (mg/g)	TCE (mg/g)	Distance Across Column from Influent (cm)	Toluene (mg/g)	TCE (mg/g)
Initial	79.1	9.67	Initial	79.1	9.67
0.35	42.9	17.6	0.30	41.5	16.9
1.55	32.2	20.1			
2.60	29.2	21.2	2.20	30.7	22.2
3.55	26.2	19.6			
4.15	24.4	19.0	3.90	25.9	19.9

Table D.27 GAC Loadings, Anthracite Control Experiment

1.0-min. EBCT, 1.25-cm. Length, Col A			0.9-min. EBCT, 1.25-cm. Length, Col B			1.0-min. EBCT, 1.25-cm. Length, Col C		
Distance Across Column from Influent (cm)	Toluene (mg/g)	TCE (mg/g)	Distance Across Column from Influent (cm)	Toluene (mg/g)	TCE (mg/g)	Distance Across Column from Influent (cm)	Toluene (mg/g)	TCE (mg/g)
Equilibrium (for GAC)	113	1.50	Equilibrium (for GAC)	113	1.51	Equilibrium (for GAC)	112	1.44
0.13	0.14	0.05	0.13	0.08	0.04	0.13	0.09	0.04
1.15	0.21	0.07	1.20	0.15	0.06	1.20	0.10	0.05

Table D.28 GAC Loadings, Virgin Sterile Control

0.9-min. EBCT, 1.35-cm. Length, Col A		
Distance Across Column from Influent (cm)	Toluene (mg/g)	TCE (mg/g)
Equilibrium	145	1.57
0.15	81.3	2.55
0.70	82.6	2.54
1.28	90.6	2.69

Table D.29 GAC Loadings, Experiment 7

1.1-min. EBCT, 1.5-cm. Length, Col B			1.2-min. EBCT, 1.6-cm. Length, Col C*		
Distance Across Column from Influent (cm)	Toluene (mg/g)	TCE (mg/g)	Distance Across Column from Influent (cm)	Toluene (mg/g)	TCE (mg/g)
Equilibrium	144	1.65	Equilibrium	139	1.65
0.15	24.1	11.5	0.10	16.5	5.18
1.43	13.1	5.49	1.45	9.34	1.42

*Sample broke, had to re-fill with methanol

Table D.30 GAC Loadings, Experiment 8

1.0-min. EBCT, 1.25-cm. Length, Col A			1.0-min. EBCT, 1.3-cm. Length, Col B			1.0-min. EBCT, 1.5-cm. Length, Col C		
Distance Across Column from Influent (cm)	**Toluene (mg/g)**	**TCE (mg/g)**	**Distance Across Column from Influent (cm)**	**Toluene (mg/g)**	**TCE (mg/g)**	**Distance Across Column from Influent (cm)**	**Toluene (mg/g)**	**TCE (mg/g)**
Equilibrium	113	1.50	Equilibrium	113	1.51	Equilibrium	112	1.44
0.13	14.5	3.83	0.10	43.7	2.32	0.05	74.9	1.48
1.20	0.40	2.00	1.25	8.41	2.91	1.45	38.4	3.48

D.4 BIOLOGICAL MEASUREMENTS AT END OF EXPERIMENT

Table D.31 Biological Measurements, Experiment 3

10.3-min. EBCT, 15-cm. Length, Col A					10.4-min. EBCT, 15-cm. Length, Col B				
Distance Across Column from Influent (cm)	Enzyme Activity (Abs/min-g GAC)	TSS (mg/L-g GAC)	Protein (mg/L-g GAC)	NADH (µM/g GAC)	Distance Across Column from Influent (cm)	Enzyme Activity (Abs/min-g GAC)	TSS (mg/L-g GAC)	Protein (mg/L-g GAC)	NADH (µM/g GAC)
0.25	1.39	262	-	2.05	0.45	0.93	367	-	5.79
4.00	7.58	627	-	3.29	4.00	17.2	448	-	4.05
7.70	2.38	445	-	2.85	7.25	6.07	355	-	3.77
11.0	0.75	175	-	1.63	11.2	1.64	180	-	2.45
14.5	1.12	195	-	1.15	14.6	1.45	298	-	1.37

Table D.32 Biological Measurements, Experiment 4

3.4-min. EBCT, 4.8-cm. Length, Col A					3.5-min. EBCT, 4.8-cm. Length, Col B				
Distance Across Column from Influent (cm)	Enzyme Activity (Abs/min-g GAC)	TSS (mg/L-g GAC)	Protein (mg/L-g GAC)	NADH (µM/g GAC)	Distance Across Column from Influent (cm)	Enzyme Activity (Abs/min-g GAC)	TSS (mg/L-g GAC)	Protein (mg/L-g GAC)	NADH (µM/g GAC)
0.22	0.54	134	401	1.76	0.22	3.33	96.7	426	9.88
2.35	12.9	253	459	4.03	2.55	20.9	387	558	7.61
4.49	22.5	1250	817	14.1	4.53	27.9	1209	679	17.1

Table D.33 Biological Measurements, Experiment 5

2.3-min. EBCT, 2.6-cm. Length, Col A					1.7-min. EBCT, 2.6-cm. Length, Col B				
Distance Across Column from Influent (cm)	Enzyme Activity (Abs/min-g GAC)	TSS (mg/L-g GAC)	Protein (mg/L-g GAC)	NADH (µM/g GAC)	Distance Across Column from Influent (cm)	Enzyme Activity (Abs/min-g GAC)	TSS (mg/L-g GAC)	Protein (mg/L-g GAC)	NADH (µM/g GAC)
0.35	2.03	1414	12.9	5.22	0.35	2.87	5578	39.1	5.28
1.25	35.2	2287	213	12.3	1.55	42.2	2105	186	16.8
2.30	37.6	2954	236	20.0	2.30	77.8	2336	197	22.3

Table D.34 Biological Measurements, Experiment 6

3.0-min. EBCT, 4.5-cm. Length, Col A					3.0-min. EBCT, 4.3-cm. Length, Col B				
Distance Across Column from Influent (cm)	Enzyme Activity (Abs/min-g GAC)	TSS (mg/L-g GAC)	Protein (mg/L-g GAC)	NADH (µM/g GAC)	Distance Across Column from Influent (cm)	Enzyme Activity (Abs/min-g GAC)	TSS (mg/L-g GAC)	Protein (mg/L-g GAC)	NADH (µM/g GAC)
0.35	220	653	49.4	225	0.30	187	586	49.0	17.4
1.55	47.3	387	49.4	6.48					
2.60	14.6	181	41.8	5.40	2.20	3.36	97.2	19.2	16.8
3.55	6.33	95.6	30.8	1.71					
4.15	2.93	84.7	19.1	7.38	3.90	3.25	192	36.1	124

Table D.35 Biological Measurements, Anthracite Control Experiment

1.0-min. EBCT, 1.25-cm. Length, Col A					0.9-min. EBCT, 1.25-cm. Length, Col B				
Distance Across Column from Influent (cm)	Enzyme Activity (Abs/min-g GAC)	TSS (mg/L-g GAC)	Protein (mg/L-g GAC)	NADH (µM/g GAC)	Distance Across Column from Influent (cm)	Enzyme Activity (Abs/min-g GAC)	TSS (mg/L-g GAC)	Protein (mg/L-g GAC)	NADH (µM/g GAC)
0.23	4.48	96.2	18.4	18.7	0.18	4.30	83.0	10.9	2.73
0.90	5.35	134	15.1	22.4	1.00	3.09	42.7	5.56	0.97
1.0-min. EBCT, 1.25-cm. Length, Col C									
Distance Across Column from Influent (cm)	Enzyme Activity (Abs/min-g GAC)	TSS (mg/L-g GAC)	Protein (mg/L-g GAC)	NADH (µM/g GAC)					
0.23	1.60	27.2	0.28	3.39					
0.95	0.19	22.4	10.2	0.77					

Table D.36 Biological Measurements, Experiment 7

1.1-min. EBCT, 1.5-cm. Length, Col B					1.2-min. EBCT, 1.6-cm. Length, Col C				
Distance Across Column from Influent (cm)	Enzyme Activity (Abs/min-g GAC)	TSS (mg/L-g GAC)	Protein (mg/L-g GAC)	NADH (µM/g GAC)	Distance Across Column from Influent (cm)	Enzyme Activity (Abs/min-g GAC)	TSS (mg/L-g GAC)	Protein (mg/L-g GAC)	NADH (µM/g GAC)
0.30	5.33	105	-	0.70	0.30	32.9	344	-	5.25
1.15	3.88	120	-	1.13	1.25	9.14	109	-	5.38

Table D.37 Biological Measurements, Experiment 8

1.0-min. EBCT, 1.25-cm. Length, Col A				
Distance Across Column from Influent (cm)	Enzyme Activity (Abs/min-g GAC)	TSS (mg/L-g GAC)	Protein (mg/L-g GAC)	NADH (µM/g GAC)
0.28	21.6	261	50.8	4.94
1.05	0.00	60.2	5.30	2.40

1.0-min. EBCT, 1.3-cm. Length, Col B				
Distance Across Column from Influent (cm)	Enzyme Activity (Abs/min-g GAC)	TSS (mg/L-g GAC)	Protein (mg/L-g GAC)	NADH (µM/g GAC)
0.25	24.6	409	50.3	6.36
1.05	3.93	221	17.2	4.65

1.0-min. EBCT, 1.5-cm. Length, Col C				
Distance Across Column from Influent (cm)	Enzyme Activity (Abs/min-g GAC)	TSS (mg/L-g GAC)	Protein (mg/L-g GAC)	NADH (µM/g GAC)
0.25	8.05	96.9	9.34	3.50
1.25	0.00	69.4	0.00	5.50

Glossary

The following symbols are used in this dissertation:

A	surface area available for adsorption
b	endogenous biofilm decay coefficient
b'	physical biofilm shearing coefficient
b'_s	biological biofilm shearing coefficient
C_o	initial concentration
D	column diameter
D_f	substrate diffusion coefficient in biofilm
D_s	surface diffusion coefficient
K	Freundlich isotherm adsorption capacity at unit concentration
k	Maximum specific substrate utilization rate
k_d	overall biofilm loss coefficient
k_f	liquid film transfer coefficient
K_s	Monod half saturation coefficient
k_1	pseudo first-order rate coefficient
L	length of column
L_{fo}	initial biofilm thickness
M_b	initial biomass in GAC column
1/n	Freundlich isotherm adsorption intensity
P	empirical coefficient for non-ideal adsorption in IAST
Q	flow rate
q_c	competitive GAC loading
q_e	equilibrium GAC loading
q_f	final GAC loading
q_o	initial GAC loading
q_s	single component GAC loading
R	radius of GAC particle or the ideal gas constant
S_o	influent substrate concentration
T	temperature
t	time
T_c	transformation capacity
W	total dry weight of GAC in column
Wt1	dry weight of radiolabeled GAC at end of column
X	biomass concentration
Y	microbial yield coefficient
ε_b	column porosity
π	spreading pressure
ρ_a	apparent density of GAC
υ	interstitial fluid velocity

References

Ahumada, E., Lizama, H., Orellana, F., Suárez, C., Huidobro, A., Sepúlveda-Escribano, A., and Rodríguez-Reinozo, F. Catalytic oxidation of Fe(II) by Activated Carbon in the Presence of Oxygen. Effect of the Surface Oxidation Degree on the Catalytic Activity. *Carbon*, 40: 2827-2834, 2002.

Alvarez-Cohen, L., and McCarty, P.L. A Cometabolic Biotransformation Model for Halogenated Aliphatic Compounds Exhibiting Product Toxicity. *Environmental Science and Technology*, 25 (8): 1381-1387, 1991.

Anderson, J.E., and McCarty, P.L. Model for Treatment of Trichloroethylene by Methanotrophic Biofilms. *Journal of Environmental Engineering*, 120 (2): 379-400, 1994.

Applegate, B.M., Kelly, C., Lackey, L., McPherson, J., Kehrmeyer, S., Menn, F.-M., Bienkowski, P., and Saylor, G.S. *Pseudomonas putida* B2: A *tod-lux* Bioluminescent Reporter for Toluene and Trichloroethylene Co-metabolism. *Journal of Industrial Microbiology and Biotechnology*, 18: 4-9, 1997.

Arvin, E. Biodegradation Kinetics of Chlorinated Aliphatic Hydrocarbons with Methane Oxidizing Bacteria in an Aerobic Fixed Biofilm Reactor. *Water Research*, 25 (7): 873-881, 1991.

ATSDR (Agency for Toxic Substances and Disease Registry). Public Health Statement for Toluene. Division of Toxicology, accessed 17 Nov. 2003. http://www.atsdr.cdc.gov/ToxProfiles/phs8923.html, 1994.

ATSDR. Public Health Statement for Trichloroethylene. Division of Toxicology, accessed 17 Nov. 2003. http://www.atsdr.cdc.gov/ToxProfiles/phs8824.html, 1997.

Augusti, R., Dias, A. O., Rocha, L. L., and Lago, R. M. Kinetics and Mechanism of Benzene Derivative Degradation with Fenton's Reagent in Aqueous Medium Studied by MIMS. *Journal of Physical Chemistry A*, 102 (52): 10723-10727, 1998.

Aziz, C.E., Georgiou, G., and Speitel, G.E., Jr. Cometabolism of Chlorinated Solvents and Binary Chlorinated Solvent Mixtures Using M.

trichosporium OB3b PP358. *Biotechnology and Bioengineering*, 65 (1): 100-107, 1999.

Bae, W. and Rittmann, B.E. Accelerating the Rate of Cometabolic Degradations Requiring an Intracellular Electron Source-Model and Biofilm Application. *Water Science and Technology*, 31 (1): 29-39, 1995.

Belhateche, D. and Symons, J.M. Using Cobalt-Ultraviolet Spectrophotometry to Measure Hydrogen Peroxide Concentration in Organically Laden Groundwaters. *Journal American Water Works Association*, 83 (8): 70-73, 1991.

Ben Abderrazik, N., Al Momani, F., Rodriguez, M., Azmani, A., Sans, C., and Esplugas, S. Biodegradability Improvement by Photo Fenton Reaction. *Afinidad*, 59 (500): 391-398, 2002.

Berthouex P.M. and Brown, L.C. *Statistics for Engineers*. CRC Press, Inc., Boca Raton, FL, 1994.

Bin, A. K., Zielinski, J., Jakobczyk-Baraniecka, J., Ostrowska, J., and Ptak, A. Chemical and Biological Methods for Oxidation of Toxic Pollutants in Industrial Wastewater. *Technologia Chemiczna na Przelomie Wiekow*, Wydawnictwo Stalego Komitetu Kongresow Technologii Chemicznej, Gliwice, Poland, 683-686, 2000. Conference written in Polish.

Champagne, P., Van Geel, P.J., and Parker, W.J. A Proposed Transient Model for Cometabolism in Biofilm Systems. *Biotechnology and Bioengineering*, 60 (5): 541-550, 1998.

Chang, H.-L. and Alvarez-Cohen, L. Model for the Cometabolic Biodegradation of Chlorinated Organics. *Environmental Science and Technology*, 29 (9): 2357-2367, 1995a.

Chang, H.-L. and Alvarez-Cohen, L. Transformation Capacities of Chlorinated Organics by Mixed Cultures Enriched on Methane, Propane, Toluene, or Phenol. *Biotechnology and Bioengineering*, 45 (5): 440-449, 1995b.

Chang, H.-L. and Alvarez-Cohen, L. Biodegradation of individual and multiple chlorinated aliphatic hydrocarbons by methane-oxidizing cultures. *Applied and Environmental Microbiology*, 62 (9): 3371-3377, 1996.

Chang, M.-K., Voice, T.C., and Criddle, C.S. Kinetics of Competitive Inhibition and Cometabolism in the Biodegradation of Benzene, Toluene, and p-

Xylene by Two Pseudomonas Isolates. *Biotechnology and Bioengineering*, 41 (11): 1057-1065, 1993.

Chang, W. and Criddle, C.S. Experimental Evaluation of a Model for Cometabolism: Prediction of Simultaneous Degradation of Trichloroethylene and Methane by a Methanotrophic Mixed Culture. *Biotechnology and Bioengineering*, 56 (5): 492-501, 1997.

Chen, G., Hoag, G. E., Chedda, P., Nadim, F., Woody, B. A., and Dobbs, G. M. The Mechanism and Applicability of In Situ Oxidation of Trichloroethylene with Fenton's Reagent. *Journal of Hazardous Materials B*, 87 (2): 171-186, 2001.

Chudyk, W. and Snoeyink, V.L. Bioregeneration of Activated Carbon Saturated with Phenol. *Environmental Science and Technology*, 18 (1): 1-5, 1984.

Clark, R.M and Lykins, B.W., Jr. *Granular Activated Carbon: Design, Operation and Cost*. Lewis Publishers, Inc., Chelsea, MI, 1989.

Cobb, G.D., and Bouwer, E.J. Effects of Electron Acceptors on Halogenated Organic Compound Biotransformations in a Biofilm Column. *Environmental Science and Technol*ogy, 25 (6): 1068-1074, 1991.

Cox, C.D., Woo, H., and Robinson, K.G. Cometabolic Biodegradation of Trichloroethylene (TCE) in the Gas Phase. *Water Science and Technology*, 37 (8): 97-104, 1998.

Criddle, C.S. The Kinetics of Cometabolism. *Biotechnology and Bioengineering*, 41 (11): 1048-1056, 1993.

Crittenden, J.C., Hand, D.W., Arora, H., and Lykins, B.W., Jr. Design Considerations for GAC Treatment of Organic Chemicals. *Journal American Water Works Association*, 79 (1): 74-82, 1987.

Crittenden, J.C., Luft, P., and Hand, D.W. Prediction of Multicomponent Adsorption Equilibria in Background Mixtures of Unknown Composition. *Water Research*, 9 (12): 1537-1548, 1985a.

Crittenden, J.C., Luft, P., Hand, D.W., Oravitz, J.L., Loper, S.W., and Ari, M. Prediction of Multicomponent Adsorption Equilibria Using Ideal Adsorbed Solution Theory. *Environmental Science and Technology*, 19 (11): 1037-1043, 1985b.

Crittenden, J.C., and Weber, W.J., Jr. Predictive Model for Design of Fixed-Bed Adsorbers: Parameter Estimation and Model Development. *Journal of Environmental Engineering*, 104 (4): 185-197, 1978.

De Laat, J., Bouanga, F., Dore, M., and Mallevialle, J. Influence of Bacterial Growth in Granular Activated Carbon Filters on the Removal of Biodegradable and of Non-Biodegradable Organic Compounds. *Water Research*, 19 (12): 1565-1578, 1985. Paper written in French and English.

DeWaters, Jan E. Biological Activity on Granular Activated Carbon in the Presence of Ozonated Naturally Occurring Humic Substances. Technical Report, University of North Carolina at Chapel Hill, 1987.

Dobrezelewski, M. *et al.* Determination and Prediction of Surface Diffusivities of Volatile Organic Compounds Found in Drinking Water. National Technology Information Service, Springfield, Virginia, 1985.

Edwards, M. and Benjamin, M.M. Adsorptive Filtration Using Coated Sand: A New Approach for Treatment of Metal-Bearing Wastes. *Journal Water Pollution Control Federation*, 61 (9): 1523-1533, 1989.

Ely, R.L., Hyman, M.R., Arp, D.J., Guenther, R.B., and Williamson, K.J. A Cometabolic Kinetics Model Incorporating Enzyme Inhibition, Inactivation, and Recovery: II. Trichloroethylene Degradation Experiments. *Biotechnology and Bioengineering*, 46 (3): 232-245, 1995.

Ensley, B.D. Biochemical Diversity of Trichloroethylene Metabolism. *Annual Review of Microbiology*, 45: 283-299, 1991.

Environmental Defense. Chemical Profile for Toluene, accessed 17 Nov. 2003. http://www.scorecard.org/chemical-profiles/summary.tcl?edf_substance_id=+108-88-3, 2003a.

Environmental Defense. Chemical Profile for Trichloroethylene, accessed 17 Nov. 2003. http://www.scorecard.org/chemical-profiles/summary.tcl?edf_substance_id=+79-01-6, 2003b.

Erlanson, B.C., Dvorak, B.I., Lawler, D.F., and Speitel, G.E. Jr. Equilibrium Model for Biodegradation and Adsorption of Mixtures in GAC Columns. *Journal of Environmental Engineering, ASCE*, 123 (5): 469-478, 1997.

Fan, S. and Scow, K.M. Biodegradation of Trichloroethylene and Toluene by Indigenous Microbial Populations in Soil. *Applied and Environmental Microbiology*, 59 (6): 1911-1918, 1993.

Folsom, B.R. and Chapman, P.J. Performance Characterization of a Model Bioreactor for the Biodegradation of Trichloroethylene by Pseudomonas cepacia G4. *Applied and Environmental Microbiology*, 57 (6): 1602-1608, 1991.

Folsom, B.R., Chapman, P.J., and Pritchard, P.H. Phenol and Trichloroethylene Degradation by Pseudomonas cepacia G4: Kinetics and Interactions between Substrates. *Applied and Environmental Microbiology*, 56 (5): 1279-1285, 1990.

Freundlich, H. *The Elements of Colloidal Chemistry*. Methuen, London, 1926.

Friedman, G. Mathematical Modeling of Multicomponent Adsorption in Batch and Fixed-Bed Reactors. M.S. Thesis, Department of Chemical Engineering, Michigan Technological University, 1984.

Hand, D.W., Crittenden, J.C., Arora, H., Miller, J.M., and Lykins, B.W. Designing Fixed Bed Adsorbers to Remove Mixtures of Organics. *Journal American Water Works Association*, 81 (1): 67-77, 1989.

Hayduk, W., and Laudie, H. Prediction of Diffusion Coefficients for Non-Electrolytes in Dilute Aqueous Solutions. *American Institute of Chemical Engineers Journal*, 20 (3): 611-615, 1974.

Heald, S., and Jenkins, R.O. Trichloroethylene Removal and Oxidation Toxicity Mediated by Toluene Dioxygenase of *Pseudomonas putida. Applied and Environmental Microbiology*, 60: 4634-4637, 1994.

Heitzer, A., Malachowsky, K., Thonnard, J.E., Bienkowski, P.R., White, D.C., and Sayler, G.S. Optical Biosensor for Environmental On-line Monitoring of Naphthalene and Salicylate Bioavailability with an Immobilized Bioluminescent Catabolic Reporter Bacterium. *Applied and Environmental Microbiology*, 60: 1487-1494, 1994.

HSIA (Halogenated Solvents Industry Alliance, Inc.). Trichloroethylene-White Paper, accessed 17 Nov. 2003. http://www.hsia.org/white_papers/tri%20wp.htm, 2001.

Huling, S. G., Arnold, R. G., Jones, P. K., and Sierka, R. A. Predicting Fenton-Driven Degradation Using Contaminant Analog. *Journal of Environmental Engineering*, 126 (4): 348-353, 2000.

Hutchinson, D. H. and Robinson, C. W. A Microbial Regeneration Process for Granular Activated Carbon—II. Regeneration Studies. *Water Research*, 24 (10): 1217-1223, 1990.

Jenkins, R.O. and Dalton, H. The use of indole as a spectrophotometric assay substrate for toluene dioxygenase. *FEMS Microbiology Letters*, 30: 227-231, 1985.

Kastner, J. R., Domingo, J. S., Denham, M., Molina, M., and Brigmon, R. Effect of Chemical Oxidation on Subsurface Microbiology and Trichloroethylene (TCE) Biodegradation. *Bioremediation Journal*, 4 (3): 219-236, 2000.

Kuo, W. G. Decolorizing Dye Wastewater with Fenton's Reagent. *Water Research*, 26 (7): 881-886, 1992.

Leahy, J.G., Byrne, A.M., and Olsen, R.H. Comparison of Factors Influencing Trichloroethylene Degradation by Toluene-Oxidizing Bacteria. *Applied and Environmental Microbiology*, 62 (3): 825-833, 1996.

Lee, S. H. and Carberry, J. B. Aerobic Biodegradation of Trichloroethylene Enhanced by Chemical Oxidants. *Hazardous and Industrial Wastes*, 23: 198-210, 1991.

Li, A.Y.L and DiGiano, F.A. Availability of sorbed substrate for microbial degradation on granular activated carbon. *Journal Water Pollution Control Federation*, 55 (4): 392-399, 1983.

Lin, B., Yamaguchi, R., Hosomi, M., and Murakami, A. A New Treatment Process for Photo-Processing Waste Using a Sulfur-Oxidizing Bacteria/Granular Activated Carbon System Followed by Fenton Oxidation. *Water Science and Technology*, 38 (4-5): 163-170, 1998.

Losh, D.E. The Role of Bioregeneration in Treating Mixtures of Biodegradable and Non-Biodegradable Chemicals in Granular Activated Carbon Columns. M.S. Thesis, Department of Civil Engineering, University of Texas at Austin, 2001.

Lu, C.-J. Biodegradation of Synthetic Organic Chemicals in Granular Activated Carbon Columns: Effect of Analogous Enrichment, Concentration, and

Adsorbability. Ph.D. Dissertation, Department of Civil and Environmental Engineering, University of Houston, 1989.

Lu, C.-J., Chang, C.Y., and Lee, C.M. Aerobic Biodegradation of Trichloroethylene by Microorganisms that Degrade Aromatic Compounds. In: *Bioremediation of Chlorinated Solvents*, R.E. Hinchee *et al.* (eds.). Battelle Press, Columbus, OH, 1-7, 1995.

Lu, C.-J., Lee, C.M., and Chung, M.-S. The Comparison of Trichloroethylene Removal Rates by Methane- and Aromatic-Utilizing Microorganisms. *Water Science and Technology*, 38 (7): 19-24, 1998.

McCarty, P.L. Removal of Organic Substances from Water by Air Stripping, in *Control of Organic Substances in Water and Wastewater*, Berger, B.B., ed. USEPA Report No. EPA-600/8-83-011, 1983.

McClay, K., Streger, S.H., and Steffan, R.J. Induction of Toluene Oxidation Activity in *Pseudomonas mendocina* KR1 and *Pseudomonas* sp. Strain ENVPC5 by Chlorinated Solvents and Alkanes. *Applied and Environmental Microbiology,* 61: 3479-3481, 1995.

Myers, A.L. and Prausnitz, J.M. Thermodynamics of Mixed-Gas Adsorption. *American Institute of Chemical Engineers Journal*, 11 (1): 121-127, 1965.

Na, C., Cannon, F.S., and Hagerup, B. Perchlorate Removal via Iron-Preloaded GAC and Borohydride Regeneration. *Journal American Water Works Association*, 94 (11): 90-102, 2002.

Nelson, M.J.K, Montgomery, S.O., Mahaffey, W.R., and Pritchard, P.H. Biodegradation of Trichloroethylene and Involvement of an Aromatic Biodegradative Pathway. *Applied and Environmental Microbiology*, 53 (5): 949-954, 1987.

Newman, L.M. and Wackett, L.P. Trichloroethylene Oxidation by Purified Toluene 2-Monooxygenase: Products, Kinetics, and Turnover-Dependent Inactivation. *Journal of Bacteriology*, 179 (1): 90-96, 1997.

Oh, D. J., Whittaker, M., and Monroe, D. TCE Graphical Pathway Map, accessed 1 Apr. 2001. http://umbbd.ahc.umn.edu/tce/tce_image_map.html. University of Minnesota, 2001.

Olmstead, K. P. Microbial Interference with the Adsorption of Target Organic Contaminants by Granular Activated Carbon. Ph.D. Dissertation, University of Michigan at Ann Arbor, 1989.

Peel, R.G. and Benedek, A. Attainment of Equilibrium in Activated Carbon Isotherm Studies. *Environmental Science and Technology*, 14 (1): 66-71, 1980.

Pontius, F.W. New Horizons in Federal Regulation. *Journal American Water Works Association*, 90 (3): 38-50, 1998.

Putz, A.R.H., Losh, D.E., and Speitel, G.E. Jr. Biological Activated Carbon: Understanding the Role of Metabolism in Extending Service Life and Improving Process Performance. *Proceedings American Water Works Association Annual Conference*, Washington, D.C., 2001.

Radke, C.J. and Prausnitz, J.M. Thermodynamics of Multi-Solute Adsorption from Dilute Liquid Solutions. *American Institute of Chemical Engineering Journal*, 18 (4): 761-768, 1972.

Randtke, S.J. and Snoeyink, V.L. Evaluating GAC Adsorptive Capacity. *Journal American Water Works Association*, 75 (8): 406-413, 1983.

Reddy, K.P. Recovery and Recycle of Copper from Wastewater using Iron Coated GAC. *Critical Issues in Water and Wastewater Treatment, Proceedings of the National Conference on Environmental Engineering -- Boulder, CO*, American Society of Civil Engineers, 1994.

Rittmann, B.E. The Effect of Shear Stress on Biofilm Loss Rate. *Biotechnology and Bioengineering*, 24(2): 501-506, 1982.

Rittmann, B.E. and McCarty, P.L. Model of Steady-State-Biofilm Kinetics. *Biotechnology and Bioengineering*, 22: 2343-2357, 1980.

Robinson, K.G., Pieters, J.G., Sanseverino, J., Cox, C.D., Wright, C.L., Cheng, C.L., and Sayler, G.S. Microbial Oxidation and Bioluminescence Response for Toluene and Trichloroethylene. *Water Science and Technology*, 38 (7): 1-8, 1998.

Rose, H. E. Fluid Flow Through Beds of Granular Media. *Some Aspects of Fluid Flow: Papers Presented at a Conference of the Institute of Physics, October, 1950*. Edward Arnold & Co., London, 136-162, 1951.

Schultz, J. R. and Keinath, T. M. Powdered Activated Carbon Treatment Process Mechanisms. *Journal Water Pollution Control Federation*, 56 (2): 143-151, 1984.

Segar, R.L. Jr., De Wys, S.L., and Speitel, G.E. Jr. Sustained Trichloroethylene Cometabolism by Phenol-Degrading Bacteria in Sequencing Biofilm Reactors. *Water Environment Research*, 67(5): 764-774, 1995.

Shi, J., Zhao, X., Hickey, R.F., and Voice, T.C. Role of Adsorption in Granular Activated Carbon-Fluidized Bed Reactors. *Water Environment Research*, 67(3): 302-309, 1995.

Shingleton, J.T., Applegate, B.M., Nagel, A.C., Bienkowski, P.R., and Sayler, G.S. Induction of the *tod* Operon by Trichloroethylene in *Pseudomonas putida* TVA8. *Applied and Environmental Microbiology*, 64 (12): 5049-5052, 1998.

Smith, E.H. and Weber, W.J., Jr. Modeling Activated Carbon Adsorption of Target Organic Compounds from Leachate-Contaminated Ground Waters. *Environmental Science and Technology*, 22(3): 313-321, 1988.

Snoeyink, V.L., Weber, W.J., and Mark, H.B. Sorption of Phenol and Nitrophenol by Active Carbon. *Environmental Science and Technology*, 3 (10): 918-926, 1969.

Sontheimer, H., Crittenden, J.C., and Summers, R.S. *Activated Carbon for Water Treatment*. DVGW-Forschungsstelle, Germany, 1988.

Speitel, G.E. Jr. Bioregeneration of Granular Activated Carbon: Quantification at Low Substrate Concentrations by Radiochemical Techniques. Ph.D. Dissertation, Department of Environmental Sciences and Engineering, University of North Carolina at Chapel Hill, 1985.

Speitel, G.E. Jr. and DiGiano, F.A. The Bioregeneration of GAC Used to Treat Micropollutants. *Journal American Water Works Association*, 79(1): 64-73, 1987.

Speitel, G.E. Jr. and DiGiano, F.A. Determination of Microbial Kinetic Coefficients Through Measurement of Initial Rates by Radiochemical Techniques. *Water Research*, 22(7): 829-835, 1988.

Speitel. G.E. Jr., Dovantzis, K., and DiGiano, F.A. Mathematical Modeling of Bioregeneration in GAC Columns. *Journal of Environmental Engineering*, 113 (1): 32-48, 1987.

Speitel, G.E. Jr., Lu, C.-J., Zhu, X.J., and Turakhia, M.H. Biodegradation and Adsorption of a Bisolute Mixture in GAC Columns. *Journal Water Pollution Control Federation*, 61 (2): 221-229, 1989a.

Speitel, G.E. Jr., Lu, C.-J., and Turakhia, M.H. Biodegradation of Trace Concentrations of Substituted Phenols in GAC Columns. *Environmental Science and Technology*, 23 (1): 68-74, 1989b.

Spetiel, G.E. Jr., Turakhia, M.H., and Lu, C.-J. Initiation of Micropollutant Biodegradation in Virgin GAC Columns. *Journal American Water Works Association*, 81 (4): 168-176, 1989c.

Speitel, G.E. Jr. and Segar, R.L. Jr. Cometabolism in Biofilm Reactors. *Water Science and Technology*, 31 (1): 215-225, 1995.

Speth, T.F. and Miltner, R.J. Adsorption Capacity of GAC for Synthetic Organics. *Journal American Water Works Association*, 82 (2): 72-75, 1990.

Standard Methods for the Examination of Water and Wastewater, 18th Edition. Greenberg, A.E., Clescen, L.S., and Eaton, A.D., eds. American Public Health Association, Washington, DC, 1992.

Stein, L.Y. Effects of Ammonia, pH, and Nitrite on the Physiology of *Nitrosomonas europaea*, an Obligate Ammonia-Oxidizing Bacterium. Ph.D. Dissertation, Oregon State University, 1998.

Tang, W. Z. and Huang, C. P. An Oxidation Kinetic Model of Unsaturated Chlorinated Aliphatic Compounds by Fenton's Reagent. *Journal of Environmental Science and Health, Part A: Environmental Science and Engineering & Toxic and Hazardous Substance Control*, A31 (10): 2755-2775, 1996.

Tekin, H., Gulkaya, I., Bilkay, O., Ataberk, S. S., Balta, T. H., Ceribasi, I. H., and Yetis, U. Treatment of Pharmaceutical Wastewaters by Fenton's Oxidation Followed by Activated Sludge: A Case Study. *Proceedings Water Environment Federation WEFTEC 2002 Conference*, Chicago, IL, 2002.

Thacker, W.E., Crittenden, J.C., and Snoeyink, V.L. Modeling of Adsorber Performance: Variable Influent Concentration and Comparison of Adsorbents. *Journal of the Water Pollution Control Federation*, 56 (3): 243-250, 1984.

Turney, T. A. *Oxidation Mechanisms*. Butterworths, Washington, 1965.

Uchida, M., Shinohara, O., Ito, S., Kawasaki, N., Nakamura, T., and Tanada, S. Reduction of Iron (III) Ion by Activated Carbon Fiber. *Journal of Colloid and Interface Science*, 224 (2): 347-350, 2000.

Uranowski, L. J., Tessmer, C.H., and Vidic, R. D. The Effect of Surface Metal Oxides on Activated Carbon Adsorption of Phenolics. *Water Research*, 32: 6, 1841-1851, 1998.

USEPA. Chemicals in the Environment: Toluene. Office of Pollution Prevention and Toxics, accessed 1 Apr. 2001. http://www.epa.gov/opptintr/chemfact/f_toluen.txt, 1994.

USEPA. Drinking Water and Health, Technical Factsheet on: Toluene. Office of Ground Water and Drinking Water, accessed 1 Apr. 2001. http://www.epa.gov/OGWDW/dwh/t-voc/toluene.html, 1998.

USEPA. Drinking Water and Health, Technical Factsheet on: Trichloroethylene. Office of Ground Water and Drinking Water, accessed 1 Apr. 2001. http://www.epa.gov/OGWDW/dwh/t-voc/trichlor.html, 1999.

Vanderberg, L.A., Krieger-Grumbine, R., and Taylor, M.N. Evidence for diverse oxidations in the catabolism of toluene by *Rhodococcus rhodochrous* strain OFS. *Applied Microbiology and Biotechnology*, 53 (4): 447-452, 2000.

Van Vliet, B.M., Weber, W.J., Jr., and Hozumi, H. Modeling and Prediction of Specific Compound Adsorption by Activated Carbon and Synthetic Adsorbents. *Water Research*, 14 (12): 1719-1728, 1980.

Verschueren, K. *Handbook of Environmental Data on Organic Chemicals*. Van Nostrand Reinhold, New York, NY, 1983.

Voice, T.C., Pak, D., Zhao, X., Shi, J., and Hickey, R.F. Biological Activated Carbon in Fluidized Bed Reactors for the Treatment of Groundwater Contaminated with Volatile Aromatic Hydrocarbons. *Water Research*, 26 (10): 1389-1401, 1992.

Wackett, L.P. Mechanism of Trichloroethylene Oxidation by Toluene Dioxygenase: Implications for Bioremediation. Available from the National Technical Information Service (NTIS) of the U.S. Department of Commerce as report # AD-A247757. *Gov. Rep. Announce. Index (U. S.)*, 92 (13), 11 pgs, 1992.

Wackett, L.P. Toluene (Methylbenzene) Degradation Pathway. University of Minnesota, accessed 14 Mar. 2001. http://umbbd.ahc.umn.edu/tol/tol_image_map2.html, 2000.

Wackett, L.P., and Gibson, D.T. Degradation of Trichloroethylene by Toluene Dioxygenase in Whole-Cell Studies with *Pseudomonas putida* F1. *Applied and Environmental Microbiology*, 54 (7): 1703-1708, 1988.

Wackett, L.P., and Householder, S.R. Toxicity of Trichloroethylene *to Pseudomonas putida* F1 Is Mediated by Toluene Dioxygenase. *Applied and Environmental Microbiology*, 55 (10): 2723-2725, 1989.

Walling, C. Fenton's Reagent Revisited. *Accounts of Chemical Research*, 8 (4): 125-131, 1975.

Weber, W.J. and DiGiano, F.A. *Process Dynamics in Environmental Systems*. John Wiley and Sons, Inc., New York, NY, 1996.

Weber, W.J. Jr., Pirbazari, M., and Melson, G.L. Biological Growth on Activated Carbon: An Investigation by Scanning Electron Microscopy. *Environmental Science and Technology*, 12 (7): 817-819, 1978.

Weber, W.J. Jr. and Smith, E.H. Simulation and Design Models for Adsorption Processes. *Environmental Science and Technology*, 21 (11): 1040-1050, 1987.

Woo, H., Sanseverino, J., Cox, C.D., Robinson, K.G., and Sayler, G.S. The Measurement of Toluene Dioxygenase Activity in Biofilm Culture of *Pseudomonas putida* F1. *Journal of Microbiological Methods*, 40: 181-191, 2000.

Yonge, D.R., Keinath, T.M., Poznanska, K., and Jiang, Z.P. Single-Solute Irreversible Adsorption on Granular Activated Carbon. *Environmental Science and Technology*, 19 (8): 690-694, 1985.

Zhao, X., Hickey, R. F., and Voice, T. C. Long-Term Evaluation of Adsorption Capacity in a Biological Activated Carbon Fluidized Bed Reactor System. *Water Research*, 33 (13): 2983-2991, 1999.

Zhu, X.-J. Mathematical Modeling of Biodegradation and Adsorption for Single and Multiple Substrates in Granular Activated Carbon Beds. Masters Thesis, Environmental Engineering Program, University of Houston, 1987.

Zylstra, G.J. and Gibson, D.T. Toluene Degradation by *Pseudomonas putida* F1: Nucleotide Sequence of the TODC1C2BADE Genes and Their Expression in *Escherichia coli*. *Journal of Biological Chemistry*, 264 (25): 14940-14946, 1989.

Vita

Andrea Robin Holthouse Putz was born in Park Ridge, Illinois on July 28, 1976, the daughter of JoAnn (Holthouse) Schindler and the late Frank Lawrence Holthouse. After receiving her diploma from Maine West Township High School in Des Plaines, Illinois in 1994, she entered the University of Illinois at Urbana-Champaign. During her university breaks, she worked as an Engineer Trainee at the Metropolitan Water Reclamation District of Greater Chicago in Chicago, Illinois. She received her Bachelor of Science with Honors in Civil (Environmental) Engineering in May 1998. In September 1998 she entered the Environmental and Water Resources Engineering program at the University of Texas at Austin. Andrea received her Masters of Science in May 2001 and continued on at the University of Texas at Austin to pursue her doctorate.

Permanent address: 1366 Van Buren, Des Plaines, IL 60018

This dissertation was typed by the author.